Identifying regulators of cytotoxic T cell function through molecular and genetic screening

Katharina Strege

University of Cambridge

This dissertation is submitted for the degree of
Doctor of Philosophy

Downing College

December 2018

For Mama, Papa, Isabell, Charlotte and Annette

Declaration

This thesis is the result of my own work and includes nothing which is the outcome of work done in collaboration except as declared here and specified in the text. The RNA-sequencing study described in chapter 4 was analysed in collaboration with Martin Del Castillo Velasco-Herrera.

This thesis is not substantially the same as any that I have submitted, or, is being concurrently submitted for a degree or diploma or other qualification at the University of Cambridge or any other University or similar institution. I further state that no substantial part of my dissertation has already been submitted, or, is being concurrently submitted for any such degree, diploma or other qualification at the University of Cambridge or any other University or similar institution.

This dissertation contains less than 60,000 words as prescribed by the Degree Committee for the Faculty of Biology.

Katharina Strege
December 2018

Abstract

Identifying regulators of cytotoxic T cell function through molecular and genetic screening
Katharina Strege

Cytotoxic T lymphocytes (CTL) are crucial components of the adaptive immune system that kill infected and tumourigenic cells. CTL killing requires focused secretion of cytotoxic compounds from lytic granules. This process is known as degranulation. In this study, I aimed to establish the CRISPR-Cas9 gene editing technology in primary T cells and to optimise screening approaches to identify regulators of CTL killing.

The first half of the thesis focuses on primary mouse CTL. The CRISPR technology was successfully optimised in CTL using Cas9-ribonucleoprotein complexes resulting in efficient CRISPR-mediated loss of target proteins. Genes encoding known mediators of CTL cytotoxicity, *Rab27a*, *Munc13-4* and *Prf1*, were targeted using CRISPR. The resulting samples were used to establish a flow cytometry-based assay that simultaneously measures CTL degranulation and target cell death.

This assay enabled me to screen for mediators of CTL killing, while providing mechanistic insight by detecting degranulation. The screen was informed by a transcriptomic study that compared naive and effector CD8 T cells. 1803 significantly upregulated differentially expressed genes [log2(fold change)>2] were identified. Functional annotation analysis and literature research were used to select genes for the targeted CRISPR screen, which highlighted the importance of HIF-1α and NFIL3 in CTL killing.

The second half of the thesis focuses on primary human CTL. The combined degranulation and killing assay was further validated using patient-derived CTL, indicating its potential as a diagnostic test. I showed that the assay is suitable for mid-sized screens using a library of 64 compounds targeting the NF-κB signalling pathway. Further opportunities for increasing the scale of this screening technique are discussed.

Finally, I successfully tested CRISPR using Cas9-ribonucleoprotein complexes in the human system. Additionally, stable Cas9 expression through lentiviral transduction was explored in primary CTL and related cell lines. This has the potential to allow selection of cells expressing the CRISPR machinery, providing a cleaner experimental system and the possibility of large-scale screening approaches.

In summary, the techniques established in this thesis will be valuable for studying the genetics underlying CTL killing and the combined degranulation and killing assay furthermore shows great potential for diagnostic purposes.

Acknowledgements

First of all, I would like to thank my supervisors Professor Gillian Griffiths and Dr David Adams for their guidance and enthusiasm throughout my PhD. I am grateful for the opportunity to work on such an interesting and timely topic. Furthermore, I am thankful that Gillian and Dave encouraged me to pursue my interests inside and outside of the lab, such as an internship in science policy. I would also like to thank the Medical Research Council and the Wellcome Sanger Institute for funding this PhD.

I feel very lucky to have worked with two great teams. There was never a shortage of entertaining conversations or cake in either lab. Thank you to all members, past and present, of the Griffiths lab and Team 113. I would like to particularly highlight the contributions of Chris, Arianne, Sandra and Martin. I will always fondly remember the hours spent with Chris (aka Doctor Uncle) during long tissue culture sessions and train journeys. I really appreciate all his help and his proofreading of several chapters. I would like to thank Arianne for explaining various bioinformatic concepts, giving advice on statistics, and for her excellent proofreading skills. Sandra contributed hugely through her seemingly infinite knowledge of growing human T cells and I thank her for adding a healthy dose of Germanness to my PhD experience. A huge thank you to Martin for having the patience to explain thousands of lines of code to me, and thank you to Pip, Lyra and Nele who initially taught me all the fundamental techniques in the lab.

Special thanks go to Jake for bringing a bit of York to Cambridge and for even making thesis writing fun (at least at the start). Thank you to the friends who kept me sane along the way, particularly Fernando for our weekly walks and fierce fitbit battles, Audrey and Ayiba for so many entertaining Wednesday nights, as well as Izzy, Lizi, Aravind and Sofia for all the happy memories.

Anyone who needs to write a thesis should really have someone like Ben, who always knew just what to say when I needed cheering up and has an impressive skill of putting things

into perspective. His support has meant so much to me, especially over the last few months.

A huge thank you goes to my parents, Marlies and Frank, and sisters, Isabell, Charlotte and Annette. All of them have contributed through supportive phone calls, passing on the family tradition of the thesis bar graph and very important wine drinking breaks. I dedicate this thesis to my family for their collective encouragement and always believing in me.

Table of contents

List of figures

List of tables

Abbreviations

AF488	- Alexa Fluor 488
APC	- Allophycocyanin
APCs	- Antigen presenting cells
B2M	- $\beta 2$ microglobulin
BFP	- Blue fluorescent protein
BGP	- β-glycerol phosphate
bp	- Base pairs
BV421	- Brilliant Violet 421
BV711	- Brilliant Violet 711
CARs	- Chimeric antigen receptors
Cas	- CRISPR-associated proteins
CCR5	- C-C motif chemokine receptor 5
CD	- Cluster of differentiation
CER1	- Cytoplasmic extraction reagent 1
CER2	- Cytoplasmic extraction reagent 2
CHS	- Chediak-Higashi Syndrome
CRISPR	- Clustered regularly interspaced short palindromic repeats
crRNA	- CRISPR RNA

cSMAC - Central supramolecular activation complex

CTL - Cytotoxic T lymphocytes

CTLA-4 - Cytotoxic T-lymphocyte-associated antigen 4

DAG - Diacylglycerol

DAPI - 4',6-diamidino-2-phenylindole

DAVID - Database for Annotation, Visualization and Integrated Discovery

DMEM - Dulbecco's Modified Eagle Medium

DMSO - Dimethyl sulfoxide

DPBS - Dulbecco's Phosphate-Buffered Saline

dSMAC - Distal supramolecular activation complex

DTT - DL-Dithiotheitol

E:T - Effector-to-target

EDTA - Ethylene-Diamine Tetraacetic acid

ERK - Extracellular signal-regulated kinase

FACS - Fluorescence-activated cell sorting

FasL - Fas ligand

FBS - Fetal bovine serum

FDR - False discovery rate

FHL - Familial hemophagocytic lymphohistiocytosis

FIDEA - Functional Interpretation of Differential Expression Analysis

FITC - Fluorescein isothiocyanate

FPKM - Fragments per kilobase per million

FSC - Forward scatter

GAPs - GTPase-activation proteins

GDP - Guanosine diphosphate

GEFs - Guanine nucleotide exchange factors

GO - Gene ontology

GS - Griscelli syndrome

GTP - Guanosine triphosphate

h - Hours

hCTL - Human CTL

HDR - Homology-directed repair

HDs - Healthy donors

HEK - Human embryonic kidney

het - Heterozygous

HIF - Hypoxia-inducible factor

HIV - Human immunodeficiency virus

HLH - Hemophagocytic lymphohistiocytosis

HNTC - Highest non-toxic concentrations

hom - Homozygous

HPS - Hermansky-Pudlak Syndrome

HRP - Horseradish peroxidase

hTCM - Human T cell media

IκB - Inhibitor of κB

IFNs - Interferons

IKK - IκB kinase

IL - Interleukin

indels - Insertions or deletions

IP_3 - Inositol-(1,4,5)-triphosphate

IS - Immunological synapse

ITAM - Immunoreceptor tyrosine-based activation motifs

ITK - Interleukin-2-inducible T cell kinase

kDa - Kilodalton

KEGG - Kyoto Encyclopaedia of Genes and Genomes

KO - Knockout

LAG-3 - Lymphocyte activation gene 3

LAMP1 - Lysosomal-associated membrane protein 1

LAT - Linker for activation of T cells

LB - Luria-Bertani

Lck - Lymphocyte-specific protein tyrosine kinase

LDH - Lactate dehydrogenase

MAPK - Mitogen-activated protein kinase

mCTL - Mouse CTL

$MgCl_2$ - Magnesium chloride

MHC - Major histocompatibility complex

min - Minutes

MOI - Multiplicity of infection

mRNA - Messenger RNA

mTCM - Mouse T cell media

MW - Molecular weight

NaCl - Sodium chloride

NaF - Sodium fluoride

NaOV - Sodium orthovanadate

NaPPi - Sodium pyrophosphate

NER - Nuclear extraction reagent

NF-κB - Nuclear factor-κB

NFAT - Nuclear factor of activated T cells

NFIL3 - Nuclear factor, interleukin 3 regulated

NHEJ - Non-homologous end-joining

NK - Natural killer

NP40 - Nonidet P40

NT - Non-targeting

OVA - Ovalbumin

padj - Adjusted p-value

PAM - Protospacer adjacent motif

PBMCs - Peripheral blood mononuclear cells

PCA - Principal component analysis

PD-1 - Programmed cell death 1

PE - Phycoerythrin

Pen - Penicillin

PHA - Phytohaemagglutinin

pHRSIN-mCh - pHRSIN-mCherry

PI(4,5)P_2 - Phosphatidylinositol-(4,5)-biphosphate

PIP5K - Phosphatidylinositol 4-phosphate 5-kinase type I

PKC - Protein kinase C

PKD - Protein kinase D

PLCγ1 - Phospholipase Cγ1

PMA - Phorbol 12-myristate 13-acetate

PMSF - Phenylmethylsulfonyl fluoride

pSMAC - Peripheral supramolecular activation complex

RAS-GRP1 - Guanine nucleotide exchange factor RAS guanyl-releasing protein 1

RE - Restriction enzyme

RIN - RNA integrity number

RISC - RNA-induced silencing complex

RNA-seq - RNA-sequencing

RNPs - Ribonucleoprotein complexes

RPMI - Roswell Park Memorial Institute

RT - Room temperature

SD - Standard deviation

SDS - Sodium dodecyl sulfate

sec - Seconds

sgRNA - Single guide RNA

siRNA - Small interfering RNA

SLACs - Synaptotagmin-like protein lacking C2 domains

SLP76 - Src homology 2 domain-containing leukocyte protein of 76 kDa

SLPs - Synaptotagmin-like proteins

SNAP - Synaptosome associated protein

SNARE - Soluble NSF attachment protein receptor

SOC - Super optimal broth with catabolite repression

SSC - Side scatter

Strep	- Streptomycin
STX11	- Syntaxin-11
TAE	- Tris-acetate-EDTA
TALENs	- Transcription activator-like effector nucleases
TBS-T	- Tris buffered saline-Tween
TCR	- T cell receptor
TIGIT	- T Cell ITIM Domain
TNF	- Tumour necrosis factor
tracrRNA	- Trans-activating crRNA
Tris-HCl	- Tris(hydroxymethyl)aminomethane hydrochloride
TU	- Transducing units
VAMP	- Vesicle-associated membrane protein
VAV1	- Vav Guanine Nucleotide Exchange Factor 1
WB	- Western blotting
WT	- Wild-type
Zap70	- ζ-chain-associated protein kinase of 70 kDa
ZFNs	- Zinc finger nucleases

Chapter 1

Introduction

1.1 Cytotoxic cells in the immune system

Our immune system protects us from disease and fights infections. It can broadly be separated into two arms, the innate and the adaptive immune system. The innate immune system immediately responds to defend the host, while the adaptive immune system launches a highly specific and long-lasting response that takes several days to develop (Lowry and Zehring, 2017; Pennock et al., 2013). Cytotoxic lymphocytes are found across the innate and adaptive arms of the immune system (Russell and Ley, 2002). Natural killer (NK) cells are part of the innate immune system, while cytotoxic T lymphocytes (CTL) are part of the adaptive immune system (Russell and Ley, 2002; Topham and Hewitt, 2009). Activated T cells that express the cluster of differentiation (CD) 8 co-receptor on their surface will be referred to as CTLs throughout this thesis. However, it is important to note that CD4 T cells, which are usually known for cytokine production, can also show cytotoxic activity (Jellison et al., 2005; Pennock et al., 2013). Additionally, NK cells have been reported to develop memory to antigens, a quality usually attributed to the adaptive immune system (Lowry and Zehring, 2017).

CTLs recognise antigens presented in complex with major histocompatibility complex (MHC) class I molecules on the cell surface (de la Roche et al., 2016). MHC class I surface expression can be decreased in virally infected and tumour cells to prevent CTL mediated cytotoxicity. However, cells lacking MHC class I surface expression can be recognised and eliminated by NK cells (Mandal and Viswanathan, 2015; Topham and Hewitt, 2009). Both NK cells and CTLs kill their target cells through the focused secretion of cytotoxic compounds, which are stored in secretory lysosomes, referred to as lytic granules. Thereby cytotoxic cells can kill infected and cancerous cells, protecting the body from disease (de la

Roche et al., 2016; Topham and Hewitt, 2009). Defects in CTL and NK cell cytotoxicity cause immunodeficiency disorders, which are discussed in detail in section 1.4.3. One of the infections that affected patients frequently present with are Epstein-Barr virus infections, indicating that CTL and NK cells are particularly important for effective responses to this pathogen (Janka and Lehmberg, 2014). Additionally, cytotoxic T cells were shown to be effective in the treatment of metastatic melanoma (Rosenberg et al., 2008).

1.2 The role of CTLs in the immune response

Each T cell expresses numerous copies of a unique T cell receptor (TCR) on its surface, which recognises a specific peptide (antigen) presented by an MHC class I molecule. The TCR is a heterodimer and associates with CD3ε, γ, δ and ζ (Wucherpfennig et al., 2010). Selection in the thymus gives rise to T cells that express TCRs that react to non-self peptides displayed by MHC class I molecules (Harty and Badovinac, 2008). TCR variability is mediated by rearrangement of the genes that encode them. It is estimated that up to 10^{18} different $\alpha\beta$ heterodimer TCRs can be produced (Cantrell, 2015). Due to the large repertoire of naive T cells that are generated, T cells that recognise a particular peptide are rare, and therefore need to undergo vast proliferation when they encounter their antigen in order to destroy all diseased cells (Harty and Badovinac, 2008).

Naive CD8 T cells travel between the blood and secondary lymphoid organs, such as the lymph nodes and spleen, where they interact with antigen presenting cells (APCs), such as dendritic cells (Harty and Badovinac, 2008; Zhang and Bevan, 2011). If, for example, an individual is infected by a virus, APCs acquire viral peptides at the site of infection. The APCs then travel from the infected tissue to the secondary lymphoid organs to present the antigens from the infectious agent to CD8 T cells (Harty and Badovinac, 2008). As each naive CD8 T cell expresses a unique TCR, APCs may have to interact with many T cells until they find one that recognises their antigen (Cooper and Herrin, 2010).

Three signals have to be received for naive T cell activation to occur (Mescher et al., 2006). Firstly, the TCR of the naive CD8 T cell has to recognise the specific peptide presented by the MHC class I molecule on the surface of the APCs (signal 1) (Brownlie and Zamoyska, 2013; Harty and Badovinac, 2008). In response to recognition, signalling molecules are recruited to the TCR complex. The molecular effects of signal 1 will be discussed in more detail in section 1.3. The naive T cell also has to receive co-stimulatory signals in order to be activated (Signal 2). Receptors on the APCs interact with co-stimulatory receptors on the

T cells. The best studied interaction is between CD28 on the T cells and B7.1 or B7.2 on APCs (Williams and Bevan, 2007). This interaction stimulates survival, proliferation and production of cytokines, such as interleukin (IL) 2 (Williams and Bevan, 2007). Cytokines, such as IL-12 and type 1 interferons (IFNs) provide the third signal. They contribute to T cell survival and expression of effector molecules, such as granzyme B (Harty and Badovinac, 2008; Mescher et al., 2006; Williams and Bevan, 2007).

Naive CD8 T cells that receive all three signals are triggered to differentiate into effector CTL and proliferate extensively (Harty and Badovinac, 2008; Williams and Bevan, 2007). Numerous transcription factors are activated downstream of TCR signalling. These induce a transcriptional program that results in immense changes, including a doubling in cell size (from 5 μm to 10 μm) (de la Roche et al., 2016), changes in metabolism (MacIver et al., 2013) and proliferation status (Best et al., 2013; Brownlie and Zamoyska, 2013). In total, the differentiation and clonal expansion processes are estimated to take 4-5 days (de la Roche et al., 2016). The differences between naive and effector cells will be explored in more detail in chapter 4.

Mature effector CTL leave the lymph node and enter peripheral tissues to kill diseased cells at the site of infection (Zhang and Bevan, 2011). In the periphery, intracellular peptides are continuously degraded by the proteasome inside the cell and the resulting peptides are loaded into the peptide binding groove of MHC class I proteins in the endoplasmic reticulum (Neefjes et al., 2011). Peptide-MHC class I complexes are then displayed on the cell surface. This process happens in all nucleated cells of the body (Neefjes et al., 2011). The constant monitoring of intracellular antigens by effector CTLs provides a crucial control mechanism to ensure that the cells of the body are healthy. CTLs that recognise a peptide-MHC complex eliminate the infected cell through the secretion of cytotoxic compounds, described in detail in section 1.4, and also release cytokines such as IFNγ and tumour necrosis factor (TNF) (Harty and Badovinac, 2008; Parish and Kaech, 2009; Williams and Bevan, 2007).

The antigen-specific CTLs proliferate and kill target cells, normally resulting in the elimination of the infection. After 5-8 days, CTL numbers decline in a 'contraction' phase, driven by apoptosis (Harty and Badovinac, 2008; Parish and Kaech, 2009). It is estimated that CTL numbers are reduced by 90-95% (Harty and Badovinac, 2008; Williams and Bevan, 2007). This is important, as the immune response has to be terminated to limit damage to the body (Brownlie and Zamoyska, 2013).

However, some cells survive the contraction phase as interaction with antigen also results in the formation of memory T cells (Harty and Badovinac, 2008; Williams and Bevan, 2007). Memory T cells reside in secondary lymphoid organs and peripheral tissues and provide long term protection against the disease. In response to re-stimulation by encountering the antigen for a second time, memory cells can respond rapidly, producing larger amounts of effector cells than during the first immune response (Parish and Kaech, 2009). This ability of the adaptive immune system to form long-lasting memory cells is crucial for the concept of vaccination (Harty and Badovinac, 2008). Memory T cells were found 75 years post vaccination in humans, demonstrating the longevity of this response (Williams and Bevan, 2007).

It is therefore clear that CTLs are crucial to protect us from diseases. This is also demonstrated by disorders that are caused when these lymphocytes are not functioning properly, as discussed in detail in section 1.4.2 and 1.4.3. The following section outlines the intricate mechanism underlying T cell activation.

1.3 TCR signalling

When naive T cells in the secondary lymphoid organs recognise a peptide-MHC complex on APCs, or an effector CTL encounters a target cell in the periphery, binding of the TCR to the peptide MHC complex triggers a complex signalling response (Brownlie and Zamoyska, 2013).

The main signalling events triggered by TCR engagement are outlined in Figure 1.1. The lymphocyte-specific protein tyrosine kinase (Lck) is activated downstream of the TCR and CD3 (Brownlie and Zamoyska, 2013). The TCR depends on Lck, which binds to the cytoplasmic portion of the CD8 co-receptor, to initiate a complex signalling cascade (Brownlie and Zamoyska, 2013). Lck phosphorylates tyrosine residues in immunoreceptor tyrosine-based activation motifs (ITAMS) of the cytoplasmic portions of CD3 γ, δ, ε and ζ chains (Brownlie and Zamoyska, 2013). ζ-chain-associated protein kinase of 70 kDa (Zap70) binds to phosphorylated ITAMs, and Lck also phosphorylates Zap70 (Smith-Garvin et al., 2009). Zap70 is activated by phosphorylation and undergoes conformational change. Subsequently, Zap70 is able to phosphorylate target molecules, such as the linker for activation of T cells (LAT) (Brownlie and Zamoyska, 2013) and Src homology 2 domain-containing leukocyte protein of 76 kDa (SLP76) (Smith-Garvin et al., 2009).

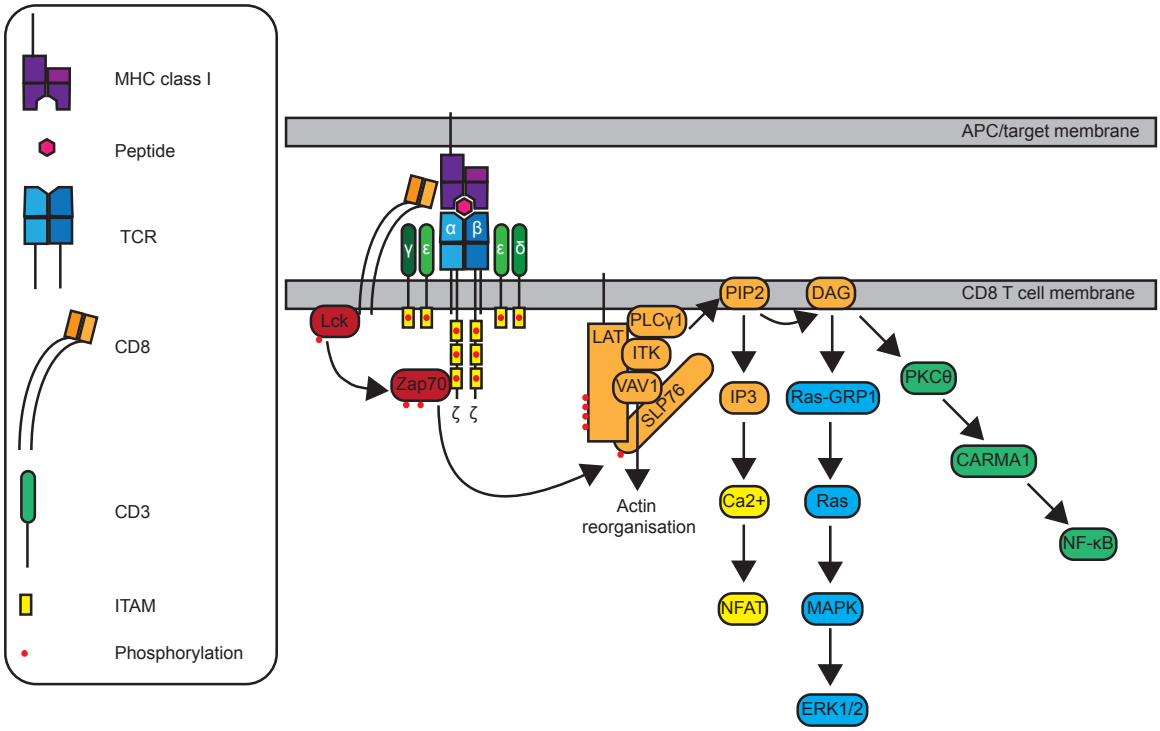

Fig. 1.1 ***TCR signalling.*** *When the TCR recognises a peptide in the context of MHC class I, Lck phosphorylates CD3 chains, as well as Zap70. This triggers the formation of the LAT signalosome, which consists of several molecules, including SLP76, ITK, VAV1 and PLCγ1. The conversion of PI(4,5)P_2 to DAG and IP_3 by PLCγ1 is required for the activation of several signalling molecules and transcription factors, including NFAT, ERK1/2 and NF-κB. This extensive transcription factor activation results in drastic changes in gene expression that are crucial for the differentiation of naive T cells to effector CTL (Brownlie and Zamoyska, 2013; Cantrell, 2015; Navarro and Cantrell, 2014).*

Phosphorylated LAT allows recruitment of further signalling molecules, forming the LAT signalosome, which is crucial for the production of downstream signals (Figure 1.1). ZAP70 phosphorylates SLP76, which subsequently forms a complex with LAT, phospholipase Cγ1 (PLCγ1), interleukin-2-inducible T cell kinase (ITK) and Vav Guanine Nucleotide Exchange Factor 1 (VAV1) (Brownlie and Zamoyska, 2013; Smith-Garvin et al., 2009). This complex is crucial for rearrangement of the actin cytoskeleton. Furthermore, PLCγ1 activation drives conversion of phosphatidylinositol-(4,5)-biphosphate (PI(4,5)P_2) from the plasma membrane to the second messenger molecules inositol-(1,4,5)-triphosphate (IP_3) and diacylglycerol (DAG), which triggers complex downstream events (Brownlie and Zamoyska, 2013; Macian, 2005).

Production of IP_3 results in the release of Ca^{2+} from the endoplasmic reticulum into the cytosol, which in turn leads to the activation of the nuclear factor of activated T cells (NFAT) transcription factor (Hogan et al., 2003; Macian, 2005). Meanwhile, DAG activates Ras and members of the protein kinase D (PKD) and protein kinase C (PKC) families, resulting in the activation of transcription factors (Navarro and Cantrell, 2014).

PKCθ interacts with CARMA1, which leads to activation of the IKK complex, that in turn can induce nuclear factor-κB (NF-κB) transcriptional activity (Matsumoto et al., 2005; Navarro and Cantrell, 2014; Paul and Schaefer, 2013). The NF-κB signalling pathway is outlined in more detail in chapter 5. Additionally, PKCs were found to be important for cell adhesion in effector CTL and centrosome polarisation to the contact site between the CTL and its target (Letschka et al., 2008; Quann et al., 2009). PKD2, which is phosphorylated by PKCs, is needed for transcriptional upregulation of IL-2 and IFNγ (Navarro and Cantrell, 2014). Production of DAG also triggers RAS activation through RAS guanine nucleotide exchange factor RAS guanyl-releasing protein 1 (RAS-GRP1) (Brownlie and Zamoyska, 2013). RAS, in turn, leads to activation of the mitogen-activated protein kinase (MAPK) cascade and subsequent activation of the extracellular signal-regulated kinase (ERK) (Brownlie and Zamoyska, 2013).

In its entirety, this signalling network results in complex intracellular events and changes in gene transcription. In naive T cells this drives differentiation to effectors. In CTL, TCR signalling induces cytoskeletal rearrangements, secretion of lytic granules and cytokine production (Brownlie and Zamoyska, 2013; de la Roche et al., 2016). TCR signalling has furthermore been speculated to be important for re-filling the cytotoxic content of the lytic granules, ensuring that pre-formed granules are available continuously (Isaaz et al., 1995).

1.4 CTL effector function

In response to TCR signalling naive T cells undergo proliferation, metabolic changes and differentiate into effector CTL over several days. In effector CTLs, peptide-MHC complex recognition leads to the rapid polarisation of lytic granules to the contact site between the CTL and the target cell. Within 20 minutes (min) of target cell recognition, the CTL has secreted the cytotoxic proteins contained within lytic granules, resulting in target cell death, and detached from the dying target cell to find its next target (Ritter et al., 2015). CTLs are therefore serial killers that can eliminate one target after another within a short period of time. Some of the intracellular events typically associated with the CTL killing process

are outlined in brief in Figure 1.2. The precise molecular steps underlying this process are covered in detail in the following sections.

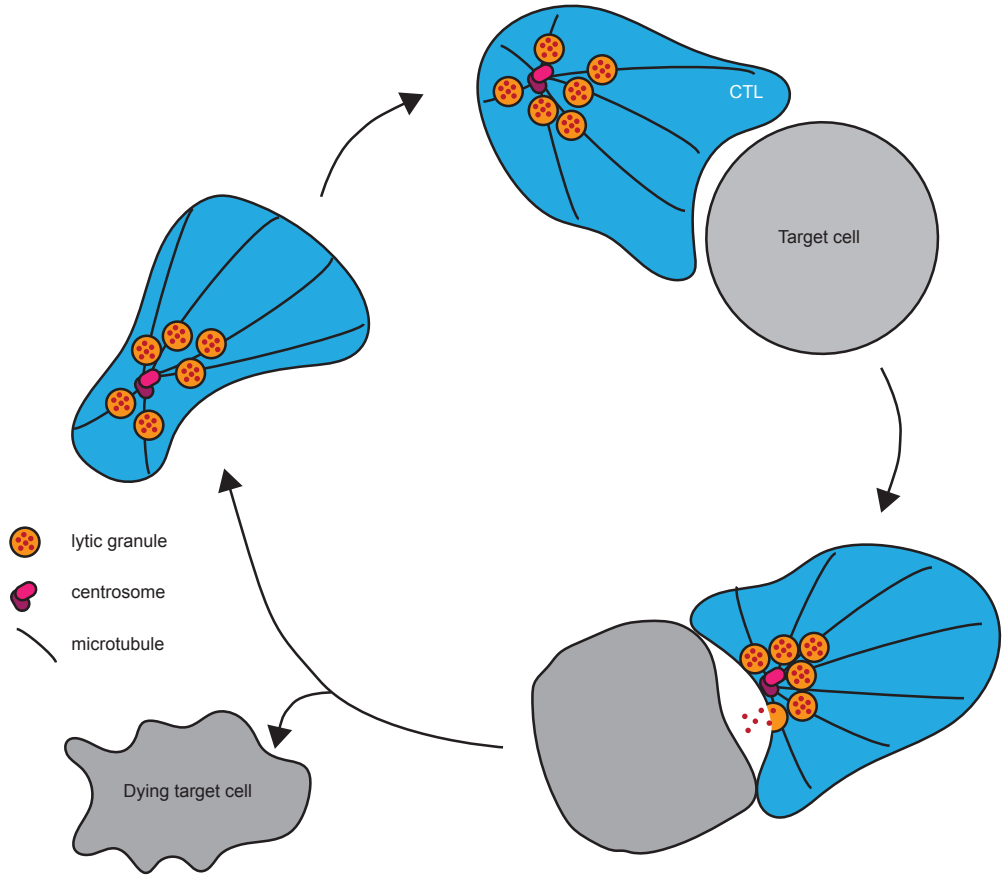

Fig. 1.2 ***CTL killing process.*** *CTL travel around the body, searching for cells that present their specific peptide in complex with MHC class I. As the CTL searches for target cells it adapts a migratory shape with a protruding leading edge and a uropod. Lytic granules and the centrosome are mostly found at the back of the cell. Upon recognition of a target cell, the CTL forms a tight cell-to-cell contact with the target cell. Subsequently, the centrosome polarises towards the contact site, delivering the lytic granules to the immunological synapse. The lytic granule membrane fuses with the plasma membrane, secreting the cytotoxic contents which trigger apoptosis of the target cell. The entire process from target cell recognition to detachment of the CTL takes around 20 min. The CTL can immediately interact with another target, acting as a serial killer (Ritter et al., 2015; Stinchcombe et al., 2001b).*

1.4.1 Formation of the immunological synapse

Both naive T cells and effector CTL form a tight contact with their APCs and target cells, respectively. This contact is known as the immunological synapse (IS) and has a highly organised structure (Figure 1.3). Actin depletes from the centre of the synapse forming an outer ring around the IS, known as the distal supramolecular activation complex (dSMAC) (Carisey et al., 2018; Ritter et al., 2015; Stinchcombe et al., 2001b, 2006). The actin depletion is suggested to be of functional significance as it removes the actin barrier for granule secretion (Ritter et al., 2017). A ring of adhesion molecules, also referred to as the peripheral SMAC (pSMAC), lies within the dSMAC. The pSMAC is reported to contain adhesion molecules such as LFA-1 and talin (Grakoui et al., 1999; Monks et al., 1998; Potter et al., 2001; Stinchcombe et al., 2001b). TCRs and associated signalling molecules, such as Lck and PKCθ can be found at the centre of the IS, also referred to as the central SMAC (cSMAC) (Grakoui et al., 1999; Monks et al., 1998; Stinchcombe et al., 2001b). TCRs are internalised for recycling from the cSMAC (Das et al., 2004). The secretory zone, where the centrosome docks and cytolytic components are released, lies adjacent to the cSMAC (Ritter et al., 2015; Stinchcombe et al., 2006). The polarisation of the centrosome, which is the microtubule organising centre in CTL, is thought to be crucial for the focused delivery of lytic granules to the IS (Stinchcombe and Griffiths, 2007; Stinchcombe et al., 2006). Granule polarisation happens within 6-10 min of target cell recognition (Ritter et al., 2015). The importance of centrosome polarisation during this process was demonstrated by knockdown of Cep83, a distal appendage protein necessary for the centrosome to dock at the plasma membrane (Tanos et al., 2013). Cep83 knockdown decreases lytic granule secretion (Stinchcombe et al., 2015). Additionally, other organelles have been reported to polarise towards the IS, such as the Golgi apparatus (Stinchcombe et al., 2006).

Recently, actin depletion was found to be mediated by changes in the composition of the plasma membrane as the IS forms. As explained in section 1.3, PLCγ1 is recruited to the plasma membrane upon TCR signalling, and hydrolyses PI(4,5)P_2 to DAG and IP_3. It has been observed that loss of PI(4,5)P_2 correlates with actin depletion at the centre of the IS (Gawden-Bone et al., 2018; Ritter et al., 2015, 2017). In the absence of a TCR stimulus, phosphatidylinositol 4-phosphate 5-kinase type I (PIP5K), which controls PI(4,5)P_2 formation, and actin were found at the plasma membrane. Upon TCR engagement, PLCγ1 conversion of PI(4,5)P_2 to DAG leads to a reduction of negative charge in this area of the plasma membrane, resulting in detachment of PIP5K. However, if PIP5K was modified so that it was maintained across the IS membrane, actin depletion did not occur. Furthermore, centrosome docking as well as lytic granule secretion was reduced, and target cell killing

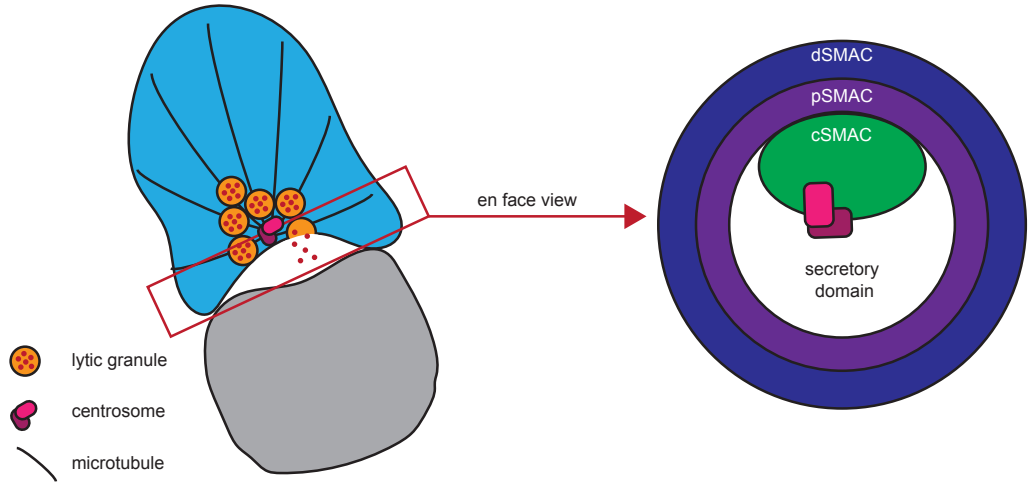

Fig. 1.3 ***Structure of the IS.*** *The en face view of a CTL in contact with its target shows the formation of a 'bulls-eye configuration' at the IS (Stinchcombe and Griffiths, 2007). TCRs and associated signalling molecules form the cSMAC, which lies at the centre of the IS together with the secretory domain, where the centrosome docks and the contents of lytic granules are released (Ritter et al., 2015; Stinchcombe et al., 2006). Centrosome polarisation is thought to be crucial for the delivery of lytic granules precisely to the contact site between CTL and target. A ring of adhesion molecules (pSMAC) surrounds the cSMAC, containing molecules such as LFA-1 and talin. Actin depletes from the centre of the IS and forms the dSMAC (Ritter et al., 2015; Stinchcombe et al., 2006). Once granules are released, actin depletion is reversed, preventing further lytic granule secretion (Ritter et al., 2017).*

was impaired when PIP5K was maintained at the membrane (Gawden-Bone et al., 2018). This demonstrates the importance of membrane composition for actin depletion, although the precise molecular events linking PI(4,5)P_2 to actin still remain to be elucidated.

1.4.2 Lytic granule contents

CTLs kill target cells through the release of lytic granules that contain cytotoxic proteins. Polarisation of the centrosome precisely delivers the lytic granules to the contact site between the CTL and the target cell (Stinchcombe and Griffiths, 2007; Stinchcombe et al., 2006). Lytic granules contain granzymes, granulysin, perforin and Fas ligand (FasL), which are

crucial for inducing apoptosis of target cells (Bossi and Griffiths, 2005). The content of the lytic granules, and how they trigger target cell death, are described in detail below.

Perforin

The lytic granule component perforin multimerises to form pores in the target cell membrane in order to allow cytotoxic proteins to enter target cells (Lopez et al., 2013a,b; Tschopp and Nabholz, 1990). These pores are big enough to allow granzymes to pass into the cytosol of the target cell (Law et al., 2010). Perforin contains a C2 domain that is required for membrane binding via a calcium dependent mechanism (Uellner et al., 1997). While perforin is active at high calcium concentrations and neutral pH in the extracellular environment upon secretion, it was found to be inactive at the low pH within lytic granules (Kuta et al., 1989; Young et al., 1987).

The importance of perforin for cytotoxicity was demonstrated by a study using a knockout (KO) mouse model (Kägi et al., 1994a) and in patients, where perforin deficiency causes an immunodeficiency disorder, familial hemophagocytic lymphohistiocytosis (FHL) type 2 (Kogawa et al., 2002; Stepp et al., 1999). Several other inherited genetic defects can cause FHL, which has 5 subtypes (Janka and Lehmberg, 2014), covered in more detail in section 1.4.3. Patients affected by FHL present with hemophagocytic lymphohistiocytosis (HLH), which is a clinical syndrome characterised by extremely high cytokine levels. This is the result of continuous stimulation of the immune system due to an inability to resolve the infection (Janka and Lehmberg, 2014).

Granzymes

Another component of the lytic granules are granzymes, a family of serine proteases, which were shown to constitute 1-2% of the overall CTL proteome (Hukelmann et al., 2016). Five granzymes have been identified in humans (granzyme A, B, H, K and M) and several additional granzymes have been identified in mice (Bots and Medema, 2006; Masson and Tschopp, 1987). Granzymes are made in an inactive form, and cleavage by cathepsin C in the granules triggers enzymatic activation (Trapani, 2001). As granzymes are inactive at low pH, CTLs likely store these potentially dangerous proteins in granules to avoid autolysis (Masson et al., 1986). To enter the target cell, granzymes rely on perforin to form pores in the plasma membrane (Bots and Medema, 2006; Lopez et al., 2013a,b; Trapani and Sutton, 2003). Interestingly, deficiency in individual granzymes does not cause severe phenotypes in mice, in contrast to the effect observed in response to perforin deficiency, likely due to

redundancy between granzymes (Trapani, 2001).

Granzyme B is the most widely studied granzyme and triggers caspase-dependent apoptosis in target cells (Bots and Medema, 2006). CTLs derived from granzyme B deficient mice showed a defect in their ability to trigger rapid apoptosis in target cells (Heusel et al., 1994). Granzyme B cleaves the protein BID, which together with other proteins permeabilises the outer membrane of mitochondria, triggering the release of pro-apoptotic proteins (Bots and Medema, 2006; Trapani, 2001). Release of cytochrome c activates caspase-9, which cleaves further caspases, triggering a cascade leading to apoptosis (Bots and Medema, 2006). Granzyme B can additionally trigger apoptosis by cleaving members of the anti-apoptotic BCL-2 protein family, as well as cleaving certain caspases, such as caspase 3 and caspase 8 (Bots and Medema, 2006). Granzyme B has been suggested to cleave several other molecular targets, including cytoskeletal proteins and proteins in the nuclear membrane (Bots and Medema, 2006; Trapani and Sutton, 2003). Granzyme A is reported to induce target cell apoptosis by triggering loss of mitochondrial inner membrane potential, which results in release of reactive oxygen species that induce DNA damage and impair DNA repair (Bots and Medema, 2006). Granzyme A does not act via caspases, but is also reported to target histone H1 and nuclear lamins (Bots and Medema, 2006).

Granulysin

Another cytotoxic protein found in lytic granules is granulysin (Peña et al., 1997; Peña and Krensky, 1997). Granulysin triggers membrane damage and mitochondrial damage in target cells, resulting in cytochrome c release and activation of caspases that trigger apoptosis (Krensky and Clayberger, 2009). The acidic pH in the lytic granules is needed for the processing of an inactive 15 kilodalton (kDa) version of granulysin to the lytic 9 kDa version (Hanson et al., 1999; Peña and Krensky, 1997). Additionally, the lower molecular weight (MW) version has reduced cytolytic activity at acidic granule pH (Hanson et al., 1999). This again highlights the importance of lytic granules to store these potentially dangerous proteins so no harm is caused to the CTL (Hanson et al., 1999).

Fas ligand

In addition to the perforin mediated pathway, CTLs can also trigger target cell death through interaction between FasL (also known as CD95L), with Fas (also known as CD95 and APO-1) on the surface of target cells (Krammer, 2000; Strasser et al., 2009). As FasL is also stored in the lytic granules, the expression of FasL on the cell surface is carefully regulated by focused

secretion of lytic granules in response to TCR signals (Bossi and Griffiths, 1999). Upon interaction with FasL, the Fas receptor on target cells induces the formation of a signalling complex containing, among others, caspase 8, which can trigger apoptosis upon activation (Krammer, 2000; Strasser et al., 2009). Fas signalling can additionally trigger cell death through the BCL-2 regulated apoptotic pathway involving release of pro-apoptotic molecules from mitochondria (Krammer, 2000; Strasser et al., 2009). Experiments using CTL deficient in FasL and perforin indicated that these two pathways are the main killing pathways used by CTL (Kägi et al., 1994b).

All lytic granule components discussed here have in common that they need to be released from the lytic granules in order to be exposed to the target cell and trigger apoptosis. Fusion between the lytic granule membrane and the plasma membrane results in localisation of FasL on the CTL plasma membrane and secretion of perforin, granzymes and granulysin. The precise molecular mechanism underlying the fusion of these two membranes will be covered in the next section.

1.4.3 Secretion of lytic granules

The lysosomal membrane fuses with the plasma membrane to release granule content. This process is also referred to as degranulation (Betts et al., 2003). Through precise secretion into the secretory cleft, lytic granules are delivered to the target cell without causing damage to surrounding cells (Stinchcombe and Griffiths, 2003). The machinery required for CTL degranulation was in large part identified through the study of patients suffering from inheritable immunodeficiency conditions, where CTL and NK cells are unable to kill target cells efficiently, such as FHL and Griscelli syndrome (GS) type 2 (de Saint Basile et al., 2010; Janka and Lehmberg, 2014). These immunodeficiency conditions and their genetic causes are summarised in Table 1.1.

FHL is divided into several subtypes according to the underlying genetic defect; mutations in *PRF1*, encoding perforin, cause FHL2 (Stepp et al., 1999), mutations in *MUNC13-4* cause FHL3 (Feldmann et al., 2003), FHL4 is caused by defects in the gene encoding syntaxin-11 (*STX11*) (zur Stadt et al., 2005), FHL5 is caused by mutations in *MUNC18-2* (Côte et al., 2009; zur Stadt et al., 2009) and GS2 was found to be caused by mutations in *RAB27A* (Ménasché et al., 2000). Mutations in these genes were found to result in a degranulation defect in patient-derived CTL and NK cells, with the exception of mutations in *PRF1*, which impairs target cell killing downstream of degranulation (de Saint Basile et al., 2010). Therefore, despite having intact lytic granule content, cytotoxic lymphocytes from FHL3,

FHL4, FHL5 and GS2 patients cannot kill target cells. This indicated that the proteins encoded by the mutated genes are important for the secretion of lytic granule content (de Saint Basile et al., 2010).

Table 1.1 ***List of genes and proteins associated with CTL-related immunodeficiencies.*** *HLH is a hyperinflammatory syndrome that is reported to lead to the following clinical symptoms: fever, cytopenia, hepatosplenomegaly, hypertriglyceridemia and/or hypofibrinogenemia, and hemophagocytosis in bone marrow, lymph nodes or spleen. Additionally, patients can present with further symptoms, such as neurological abnormalities (Henter et al., 2007; Janka and Lehmberg, 2014). HLH = hemophagocytic lymphohistiocytosis, FHL = Familial hemophagocytic lymphohistiocytosis, GS = Griscelli syndrome, CHS = Chediak-Higashi Syndrome and HSP = Hermansky-Pudlak Syndrome.*

Disorder	**Gene/protein affected**	**Symptoms**	**Reference**
FHL1	genetic locus = 9q22, gene/protein not known	HLH	(Ohadi et al., 1999)
FHL2	*PRF1*, PRF1	HLH	(Stepp et al., 1999)
FHL3	*MUNC13-4*, MUNC13-4	HLH	(Feldmann et al., 2003)
FHL4	*STX11*, STX11	HLH	(zur Stadt et al., 2005)
FHL5	*MUNC18-2*, MUNC18-2	HLH	(zur Stadt et al., 2009), (Côte et al., 2009)
GS2	*RAB27A*, RAB27A	HLH, partial albinism	(Griscelli et al., 1978), (Ménasché et al., 2000)
CHS	*LYST*, LYST	HLH, partial albinism, neurological symptoms	(Barbosa et al., 1996), (Perou et al., 1996), (Nagle et al., 1996), (Ward et al., 2000)
HPS2	*AP3B1A*, AP3β3A	HLH, partial albinism, prolonged bleeding time	(Hermansky and Pudlak, 1959), (Dell'Angelica et al., 1999), (Clark et al., 2003)
HPS10	*AP3D1*, AP3δ	HLH, partial albinism, neurological symptoms	(Ammann et al., 2016)

FHL and GS2 tend to have an early onset, usually within the first year of life. Patients present with hyperinflammation caused by a highly activated but unsuccessful immune response. Symptoms include fever, hepatosplenomegaly, cytopenia and these disorders can be fatal in the absence of treatment. Currently, the treatment options are limited to immunosuppressants and the only potential cure is hematopoietic stem cell transplantation (Janka and Lehmberg, 2014). The fact that genetic defects in proteins involved in the lytic granule secretion process, or lytic granule content in the case of perforin, cause immunodeficiency disorders highlights how important the function of cytotoxic cells is to maintain a healthy immune system.

Furthermore, other immunodeficiency disorders, such as Chediak-Higashi Syndrome (CHS) and Hermansky-Pudlak Syndrome (HPS), enabled the identification of proteins important in the maturation of lytic granules and their transport to the IS (de Saint Basile et al., 2010; Janka and Lehmberg, 2014). CHS is caused by defects in LYST, which is reported to cause a lysosome fission defect, resulting in granules that are too big to fuse at the IS (Baetz et al., 1995; Durchfort et al., 2012). HPS type 2 is caused by defects in AP3β (Dell'Angelica et al., 1999) and HPS type 10 is caused by defects in AP3δ (Ammann et al., 2016). Some mutations in AP3 have been shown to result in an inability of lysosomes to move towards the centrosome (Clark and Griffiths, 2003; Clark et al., 2003).

Analysis of the mutations underlying immunodeficiency disorders has therefore been crucial for the identification of the molecular machinery involved in lytic granule movement to the IS, degranulation and target cell killing. Simultaneously, these disorders demonstrate the devastating consequences of defective cytotoxic cells on an organismal level. Below I focus on the key regulators of the final secretion steps at the IS and their point of action in the secretion process is visualised in Figure 1.4.

RAB27A

In RAB27A depleted cells, granules can polarise to the IS but they can not dock at the plasma membrane and fusion between the lytic granule membrane and the plasma membrane is impaired (Stinchcombe et al., 2001a). RAB27A has also been implicated in the secretion of granules from granulocytes (Munafó et al., 2007) and in pigment secretion in melanocytes (Hume et al., 2001; Wu et al., 2001), indicating that RAB27A also regulates fusion between vesicles and the plasma membranes in these biological settings. This explains why GS2 patients often present with albinism as well as immunodeficiency (Stinchcombe et al., 2004).

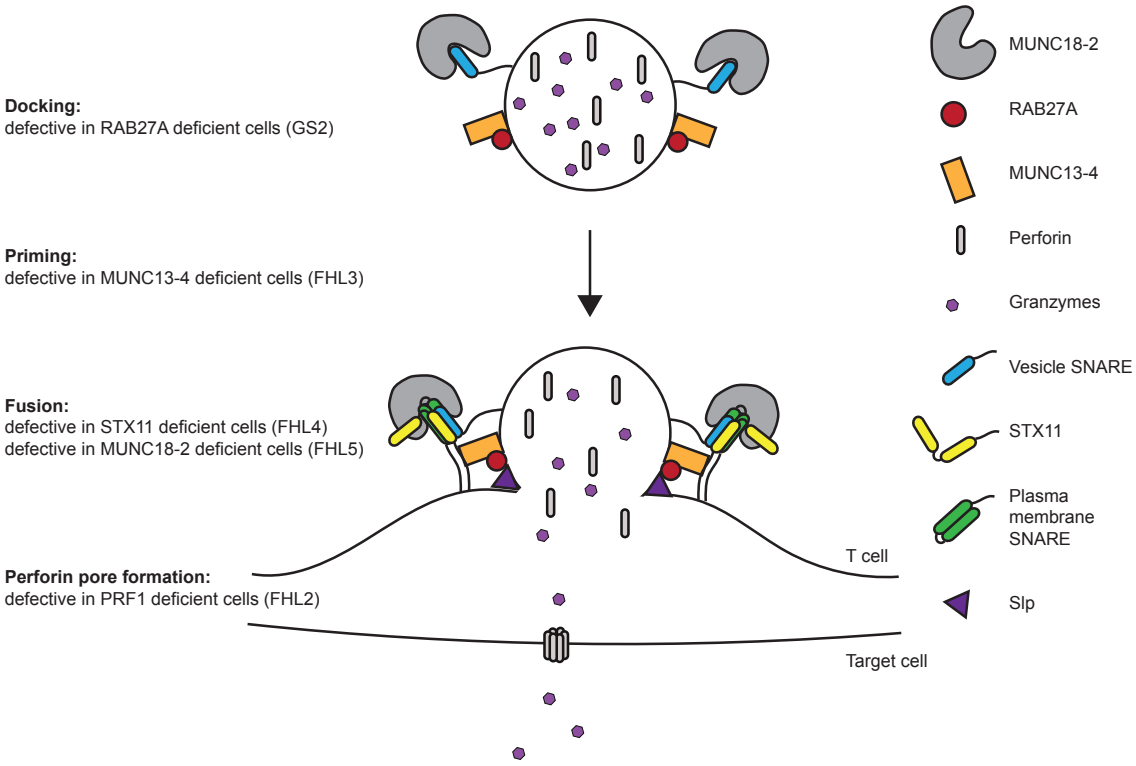

Fig. 1.4 ***Proteins crucial for lytic granule secretion at the IS.*** *Lytic granule secretion is an intricate process that involves fusion between the lytic granule membrane and the plasma membrane. Key regulators of this process are RAB27A, MUNC13-4, MUNC18-2 and several SNARE proteins. Defects in some of the proteins highlighted in this figure cause immunodeficiency diseases, indicated in brackets on the left. RAB27A interacts with MUNC13-4 (Neeft et al., 2005; Shirakawa et al., 2004) and SLPs, which are located on the plasma membrane in CTL (Holt et al., 2008; Kuroda et al., 2002b; Kurowska et al., 2012; Ménasché et al., 2008). MUNC13-4 additionally interacts with STX11 and phospholipids (Boswell et al., 2012; Elstak et al., 2011). MUNC18-2 and STX11 bind to one another (Cetica et al., 2010; Côte et al., 2009; zur Stadt et al., 2009) and STX11 was found to form a SNARE complex with the plasma membrane SNARE SNAP23 and one of the VAMP vesicle SNAREs (Spessott et al., 2017; Ye et al., 2012).*

RAB27A is a member of the Rab protein family, which control numerous cellular processes by acting as molecular switches (Wennerberg et al., 2005). Rab proteins are known to regulate vesicle trafficking, docking and fusion with target membranes by interacting with certain effector molecules. RAB27A switches between its guanosine triphosphate (GTP)-

bound active state and its guanosine diphosphate (GDP)-bound inactive state. The switch is regulated by guanine nucleotide exchange factors (GEFs), which trigger GTP binding, and GTPase-activating proteins (GAPs), which trigger GTP hydrolysis. The structure of the "switch" regions in Rab proteins is altered depending on whether GDP or GTP is bound, thereby affecting binding to effector proteins (Fukuda, 2013). Additionally, membrane attachment, which is mediated by prenylation of Rab cysteine residues, is important for Rab protein function (Pereira-Leal et al., 2001).

RAB27A can bind different effector proteins in different cell types in its active GTP-bound form. Several RAB27A effector molecules have been identified, including Synaptotagmin-like protein lacking C2 domains (SLACs), Synaptotagmin-like proteins (SLPs), and MUNC13-4. SLAC2-a (also known as melanophilin) and SLP1-5 interact with GTP-bound RAB27A via their SLP-homology domain (SHD) (Kuroda et al., 2002a,b). Melanophilin interacts with both RAB27A and MYO5A in melanocytes, thereby mediating melanosome transport and pigment secretion, but melanophilin is not expressed in CTLs and can therefore not mediate lytic granule secretion (Fukuda et al., 2002; Hume et al., 2002; Nagashima et al., 2002; Wu et al., 2002). In contrast, several SLPs were found to be expressed in CTLs, and the expression of a dominant-negative SHD construct, interfering with binding of SHD-domain containing proteins to RAB27A, reduced CTL killing capability (Holt et al., 2008; Ménasché et al., 2008). CTLs derived from *Slp1* and *Slp2-a* KO mice did not show reduced CTL cytolytic activity, indicating that different SLP family members functioned as RAB27A effectors in CTL (Holt et al., 2008). Subsequently, SLP3 was found to be important for lytic granule secretion in CTL (Kurowska et al., 2012). MUNC13-4 has been shown to bind GTP-bound RAB27A in hematopoietic cells, but in contrast to the other RAB27A effector proteins mentioned above, MUNC13-4 does not contain an SHD domain (Neeft et al., 2005; Shirakawa et al., 2004). The role of MUNC13-4 in lytic granule secretion will be covered in more detail in the following subsection.

Missense mutations observed in GS2 patients have led to the identification of functionally important RAB27A residues. For example, the Trp73Gly mutation was found to result in RAB27A protein with reduced GTP hydrolysis and reduced binding to MUNC13-4 and melanophilin, suggesting that residue 73 is important for binding to both of these effector proteins (Menasche et al., 2003; Neeft et al., 2005). A further study investigating the underlying mutations of GS2 patients that presented with immunodeficiency symptoms but not albinism identified that mutations in Arg141, Tyr159 and Ser163 resulted in loss of interaction of RAB27A with MUNC13-4, while interaction with melanophilin was

maintained (Cetica et al., 2015). This demonstrates clearly that RAB27A is able to control secretion in different cell types via interaction with cell-specific effector proteins.

MUNC13-4

In cells carrying mutations in MUNC13-4, granules can dock at the plasma membrane but cannot secrete their contents, suggesting that MUNC13-4 is crucial for lytic granule priming before fusion can occur (Elstak et al., 2011; Feldmann et al., 2003). MUNC13-4 contains two MUNC13-homology domains (MHD1 and MHD2) with a C2 calcium binding domain either side (C2A and C2B) (Feldmann et al., 2003). RAB27A and MUNC13-4 have been shown to interact with one another in platelets, mast cells and CTL (Elstak et al., 2011; Neeft et al., 2005; Shirakawa et al., 2004). MUNC13-4 binds to GTP-bound RAB27A, but not GDP-bound RAB27A, and this binding required the N-terminal region between the C2A and MHD1 domains of MUNC13-4 (Ménager et al., 2007; Neeft et al., 2005). A study using a truncated construct comprised of MUNC13-4 residues 240-290 suggested that this region is sufficient for binding to RAB27A (Elstak et al., 2011), however these findings should be treated with caution as the truncated construct may not be folded correctly.

MUNC13-4 has additionally been shown to interact with soluble NSF attachment protein receptor (SNARE) proteins, such as STX11, as well as syntaxin-1, -2 and -4, which are crucial in membrane fusion (Boswell et al., 2012). While the C2A domain is important for binding to SNAREs in a calcium dependent manner, the C2B domain binds to phosphatidylserine containing membranes (Boswell et al., 2012). MUNC13-4 was furthermore shown to co-immunoprecipitate with MUNC18-2 in platelets (Al Hawas et al., 2012). MUNC13-4 has therefore been linked to both MUNC18-2 and STX11, two components thought to be required for the final fusion between the lytic granule membrane and plasma membrane (Côte et al., 2009; zur Stadt et al., 2009).

MUNC18-2 and STX11

Mutations that cause defects in STX11 and MUNC18-2 cause FHL4 and FHL5, respectively. These two proteins bind to one another and loss of either protein results in a degranulation defect (Bryceson et al., 2007; Cetica et al., 2010; Côte et al., 2009; zur Stadt et al., 2009, 2005).

STX11 belongs to the SNARE protein family but does not contain a C-terminal transmembrane domain, instead it is thought to associate with membranes by palmitoylation of the C-terminus

(Tang et al., 1998; Valdez et al., 1999). Studies in cells derived from FHL4 patients and *Stx11* KO mice showed that STX11 controls CTL and NK cell degranulation (Arneson et al., 2007; Bryceson et al., 2007; D'Orlando et al., 2013; zur Stadt et al., 2005).

MUNC18-2 is part of the Sec1/Munc18-like protein family, members of which function in membrane fusion by interacting with SNAREs (Carr and Rizo, 2010; Südhof and Rothman, 2009). Members of the MUNC18 family of proteins have arch-shaped structures and their cavity binds to syntaxins and SNARE complexes (Misura et al., 2000; Yu et al., 2013). MUNC18-2 binds to the N-terminal peptide of STX11 and MUNC18-2 mutations that cause FHL5 (Arg39Pro, Leu130Ser, Glu132Ala and Pro334Leu) mapped onto the surface of the structure, indicating that these residues may be important for the interaction of MUNC18-2 with SNARE proteins (Hackmann et al., 2013).

In addition to showing that MUNC18-2 and STX11 interact, patient studies have shown that MUNC18-2 deficient cells also show decreased STX11 levels, leading to the conclusion that MUNC18-2 acts as a chaperone, stabilising STX11 (Bin et al., 2013; Cetica et al., 2010; Côte et al., 2009; zur Stadt et al., 2009). Additionally, some mutations in MUNC18-2 (Arg65Gln/Trp) have been identified that do not lead to loss of protein or loss of STX11 binding (Spessott et al., 2015). Instead these mutant proteins seem to stabilise STX11, but interfere with SNARE complex assembly, thereby still blocking secretion and still causing FHL-symptoms in affected individuals (Spessott et al., 2015). In summary, MUNC18-2 is both a chaperone of STX11 and may also be involved in membrane fusion as it can control SNARE complex assembly (Spessott et al., 2017).

STX11 has been described to form a SNARE complex with synaptosome associated protein (SNAP)23 and vesicle-associated membrane protein (VAMP)3 or VAMP8 to regulate fusion between the vesicle membrane and the plasma membrane (Al Hawas et al., 2012; Spessott et al., 2017; Valdez et al., 1999; Ye et al., 2012). Spessott et al. (2017) showed that MUNC18-2 and STX11 interact with VAMP8 and SNAP23 in human CTL, and that knockdown of VAMP8 reduces CTL cytotoxicity. However, different VAMPs may be able to participate in CTL degranulation, and could be important during vesicle maturation, as well as fusion at the IS. In addition to reduced degranulation and cytolytic activity observed in CTL derived from *Vamp8* KO mice, CTL derived from *Vamp2* KO mice showed similar phenotypes (Loo et al., 2009; Matti et al., 2013). Furthermore, VAMP7 knockdown in NK cells decreased degranulation and cytotoxicity (Marcet-Palacios et al., 2008). These results indicate partial redundancy between different VAMPs in the degranulation process.

It is the intricate interaction of the proteins summarised in Figure 1.4, and perhaps further unknown proteins, that leads to the final secretion of cytotoxic granule content into the secretory cleft between the CTL and the target cell, which subsequently leads to target cell death.

1.4.4 Detachment from target and serial killing

Upon degranulation, actin recovers forming a barrier for further lytic granule secretion (Ritter et al., 2015, 2017). Detachment of CTLs from their target cells was shown to depend on the CTL sensing target cell apoptosis (Jenkins et al., 2015). In the absence of perforin, or if the caspase response in the target cell was inhibited, the time that CTLs and targets remained conjugated was extended fivefold, from around 8 min to 40 min (Jenkins et al., 2015). Furthermore, cytokine and chemokine secretion from CTLs was increased in response to this continuing attachment. Sustained secretion of IFNγ caused production of proinflammatory cytokines from other immune cells, such as IL-6 from macrophages (Jenkins et al., 2015). These findings provide a potential molecular mechanism for how the dangerous hyperinflammatory state observed in FHL2 patients is generated. In healthy individuals, the caspase-dependent signal prompts the CTL to detach from its target, so that it can move on to kill the next target cell (Jenkins et al., 2015).

A crucial question that remains largely unanswered is how the secreted proteins damage the membrane of the targets, but not the CTL plasma membrane. The CTL membrane is not generally resistant to perforin, as CTLs could be used as targets and be killed by other CTLs when loaded with appropriate peptide (Lopez et al., 2013a). Degranulation has been suggested to protect from perforin pore formation (Lopez et al., 2013a). Additionally, CTLs were found to strain the surface of their target cell (Basu et al., 2016). Perforin pore formation and target killing were enhanced when target cell tension was increased (Basu et al., 2016). Further studies will be necessary to explain this phenomenon fully.

1.5 Measuring CTL function with the degranulation assay

In addition to the secretion of lytic granule contents, transmembrane proteins of the granules translocate to the cell surface when the lytic granule membrane fuses with the plasma membrane (Betts et al., 2003; Peters et al., 1991). The transmembrane proteins include lysosomal-associated membrane protein 1 (LAMP1, also known as CD107a), as well as

LAMP2 (also known as CD107b) and LAMP3 (also known as CD63) (Peters et al., 1991). These proteins are only found at low levels on the plasma membrane of unstimulated cytotoxic lymphocytes. Upon lytic granule secretion, LAMP levels on the cell surface of CTLs and NK cells are transiently increased and can be used as a marker for degranulation (Alter et al., 2004; Betts et al., 2003). An assay has been developed that measures the increase in cell surface exposure of LAMP1 over time (Betts et al., 2003). The exposure of LAMP1 to the extracellular environment allows binding of fluorescently-conjugated antibodies that recognise LAMP1, which enable the identification of cells that degranulated (Figure 1.5) (Alter et al., 2004). Betts et al. (2003) showed that LAMP1 could be detected on the cell surface within 30 min of T cell stimulation, and that LAMP1 levels peaked after 4-5 hours (h). After degranulation, LAMP1 and the antibody bound to it are internalised from the plasma membrane into an acidic vesicle, as shown by the quenching of some fluorochromes (Figure 1.5) (Betts et al., 2003).

The level of degranulation was found to correlate to cytokine secretion, loss of intracellular perforin and target cell lysis (Alter et al., 2004; Betts et al., 2003). Traditional assays, such as the chromium release assay (Brunner et al., 1968), quantify CTL effector function by measuring the resulting target cell death. In contrast, the degranulation assay does not give a direct readout of CTL killing, but gives a direct readout of effector cell activation. As this was shown to correlate with target cell lysis, it gives an indication of the cytotoxic capability of CTLs (Betts et al., 2003).

The degranulation assay is currently used for the diagnosis of putative FHL patients (Bryceson et al., 2012; Chiang et al., 2013). While it can give an insight into which genes should be sequenced, the assay cannot detect the FHL2 phenotype, as degranulation is not impaired in perforin deficient cells (Bryceson et al., 2012; Janka and Lehmberg, 2014). Furthermore, the LAMP1 degranulation assay has been used to isolate tumour reactive CTLs from patients after vaccination (Rubio et al., 2003). In this thesis, I use the degranulation assay to screen for regulators of CTL function. The concept of the degranulation assay, as well as the different in vitro activation stimuli used in this study, are explained in Figure 1.5.

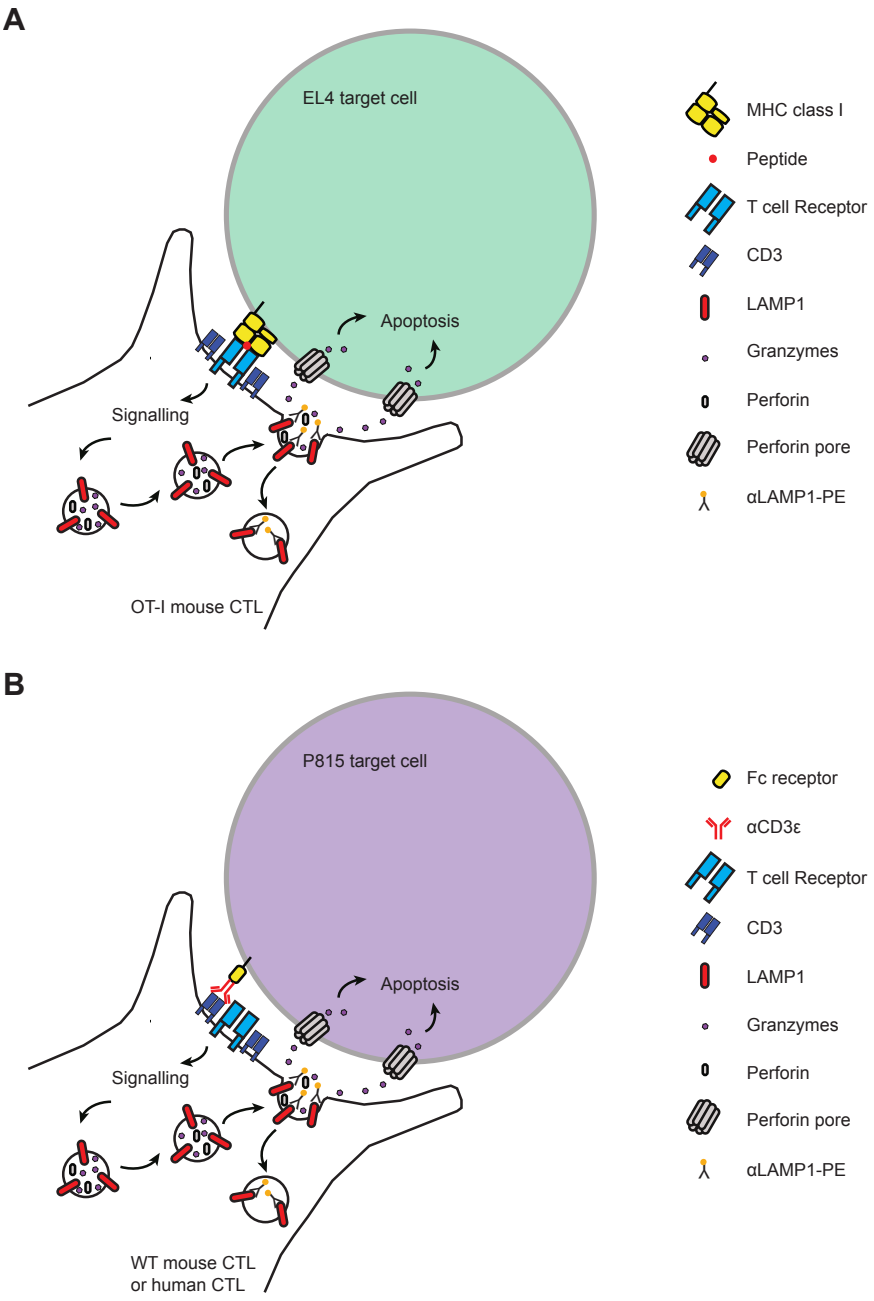

Fig. 1.5 ***Principle of the degranulation assay.***

Fig. 1.5 ***Principle of the degranulation assay.*** *In this thesis I used the degranulation assay to measure functional activation of primary mouse and human CTL. Mouse CTL were either derived from OT-I mice or wild-type (WT) mice.* ***A*** *OT-I CTL express a transgenic TCR that recognises a peptide derived from the ovalbumin (OVA) protein in the context of MHC class I. EL4 lymphoma cells pulsed with OVA peptide were used as target cells for OT-I CTL.* ***B*** *CTL derived from WT mice and human CTL were activated with an antibody recognising mouse or human CD3ε, respectively. The mastocytoma cell line P815 expresses Fc receptors on its surface and can therefore bind to the constant region of antibodies. The variable region of the αCD3ε antibody can then bind to CD3ε on the CTL, triggering TCR signalling. In both experimental set-ups, a fluorescently-conjugated antibody recognising LAMP1 is added to the cell culture supernatant. Upon exposure of LAMP1 to the plasma membrane through lytic granule secretion, the αLAMP1 antibody can bind to LAMP1 and remain bound even upon internalisation of LAMP1. This enables the identification of CTLs that have been activated by the stimulus.*

1.6 Use of CTL for medical purposes

T cells have become of great interest medically due to their successful use for cancer treatment. The treatment options can be broadly separated into cell-based and antibody-based therapies.

1.6.1 Cell-based therapy

Several different cell-based approaches have been used to treat cancer patients. Initially tumour-infiltrating lymphocytes that recognise tumour antigens were isolated from patient samples, expanded in vitro and re-introduced into the patient after lymphodepletion (Rosenberg et al., 2008). This showed promising results in metastatic melanoma. From patients where tumour infiltrating lymphocytes could be isolated, this approach was reported to trigger a response in 50% of the patients. Around 20% of the patients were complete responders, with complete tumour regression over a 3 year follow up period (Rosenberg et al., 2011).

Since tumour infiltrating lymphocytes can be difficult to obtain, two related approaches have been developed that use peripheral T cells of the patients and modify them in vitro to recognise cancer cells. This is achieved through the incorporation of artificial receptors, either genetically-engineered TCRs or chimeric antigen receptors (CARs), which specifically recognise cancer antigens (Sadelain, 2016).

CARs consist of a single-chain variable region of an antibody linked to intracellular signalling components of the TCR to trigger T cell activation. In recent years, CARs have been developed further to also include co-stimulatory domains, such as CD28 (Fesnak et al., 2016; Maher et al., 2002; Sadelain et al., 2013). After genetic modification, the CAR-expressing T cells are transferred back into the patient. Treating patients suffering from acute lymphoblastic leukemia with CARs targeting CD19 expressing cells has shown clinical success, achieving complete remission in 90% of the patients in one study (Maude et al., 2014). Treatment with CTL containing a genetically-modified TCR showed success in melanoma treatment (Morgan et al., 2006).

Both the engineered TCR and the CAR approach have advantages and disadvantages. CARs can recognise any cell surface antigen without the need for it to be presented by an MHC molecule. Additionally, the choice of different TCR signalling components and co-stimulatory domains provides flexibility in CAR design (Sadelain et al., 2013). Genetically-modified TCRs have the advantage of allowing recognition of intracellular peptides and are therefore able to target a broader range of tumour antigens (Corrigan-Curay et al., 2014).

A big challenge that both approaches face is to identify molecular targets for immunotherapy, which should ideally be cancer-specific antigens that are not expressed in healthy tissues (Corrigan-Curay et al., 2014). T cells can identify even very low antigen expression levels in normal tissues, leading to off-target attacks and adverse effects (Coulie et al., 2014; Fesnak et al., 2016). Additionally, successful tumour clearance by cell-based therapies often coincides with other symptoms of hyperactivation of the immune system, such as cytokine release syndrome, and such side effects require additional treatment (Fesnak et al., 2016). However, the effects of the cell-based immunotherapy treatment can be long-lasting, resulting in an improvement of patient survival, likely due to the memory capabilities of the adaptive immune response (Sharma et al., 2017).

1.6.2 Antibody-based therapy

Antibody-based therapies, also known as immune checkpoint blockage, function by counteracting T cell inhibition. Inhibitory molecules, such as cytotoxic T-lymphocyte-associated antigen 4 (CTLA-4) that binds to B7 ligands and therefore competes with the co-stimulatory molecule CD28, can inhibit the T cell response (Krummel and Allison, 1995). Blocking CTLA-4 through the use of antibodies results in enhanced T cell effector function and tumour clearance (Leach et al., 1996). The CTLA-4 checkpoint inhibitor, ipilimumab, has been successfully used for treatment of advanced melanoma in patients, and has been shown to

improve survival (Hodi et al., 2010; Robert et al., 2011). Similarly to cell-based therapies, some toxicity is also observed with antibody-based therapies due to the enhancement of the immune response, requiring systemic steroid treatment (Sharma et al., 2017).

Antibodies against another inhibitory receptor, programmed cell death 1 (PD-1), or its ligand PD-L1, can similarly enhance T cell function, and showed success in clinical trials (Okazaki et al., 2013; Zou et al., 2016). Pembrolizumab and nivolumab, two antibodies that recognise PD-1, and atezolimumab, an antibody recognising PD-L1, have been approved for treatment of a variety of cancer types (Sharma et al., 2017).

Combined treatment with PD-1 and CTLA-4 antibodies has shown even more promise than individual treatments in melanoma patients (Larkin et al., 2015; Postow et al., 2015; Wolchok et al., 2013). Additional immune checkpoints, such as lymphocyte activation gene 3 (LAG-3) and T Cell ITIM Domain (TIGIT), are being explored for checkpoint blockage therapy (Topalian et al., 2015). This highlights the need to identify further immune checkpoints that could be potential therapeutic targets. In contrast to cell-based therapies, the antibody-based approach requires recurrent treatment. Studies that are investigating the effect of combining checkpoint blockade and cell-based therapies are currently ongoing (Fesnak et al., 2016).

Interestingly, there are some patients that do not respond to immunotherapy or relapse after an initial response (Sharma et al., 2017; Sucker et al., 2014). Therefore, a better understanding of how CTL killing is mediated at a genetic and molecular level is desperately needed to inform both cell- and antibody-based therapies.

1.7 Techniques used for functional analysis of genes in primary T cells

Genetic modification of primary cells is a powerful way to study the function of genes and their products. One common approach to assess the function of genes is to investigate the phenotypes caused in response to disruption of gene expression. This method of targeting the gene of interest directly to subsequently investigate the phenotype is generally referred to as reverse genetics. This is in contrast to forward genetic approaches, which screen for interesting phenotypes in response to random mutagenesis and only subsequently try to

identify the particular genetic modification that has been introduced (Doyle et al., 2012).

There are several different ways to disrupt expression of a gene in primary cells. For all approaches, reagents that modify gene expression have to be delivered to cells in culture. The delivery methods can be broadly separated into viral and non-viral methods. Viral delivery, also referred to as transduction, results in stable expression of the delivered material, due to integration into the host genome. Non-viral methods include lipid-based reagents, such as lipofectamine, and electroporation, also referred to as nucleofection (Kim and Eberwine, 2010). Depending on the nature of the transfected material, expression after non-viral transfer can be stable or transient. For example, transposons encoding the gene of interest can result in stable genetic modification by integration into the host genome. Meanwhile nucleofected DNA plasmids, synthetic RNA or protein are generally only expressed transiently (Hackett et al., 2010; Kim and Eberwine, 2010).

With regards to primary T cells, it has been found that both lipid-based reagents and nucleofection can be toxic (Chicaybam et al., 2013; Ebert et al., 1997). Meanwhile, viral transduction may trigger an inflammatory reaction and carries the risk of causing detrimental mutations in the host genome due to random insertion. Additionally, there are restrictions on the size of a construct that a virus can contain while maintaining infectivity (Kim and Eberwine, 2010; Ramezani and Hawley, 2002). It is therefore clear that genetic modification of primary T cells is technically challenging.

One way to circumvent these challenges is by using mouse models, where gene expression can be deleted permanently, or conditionally using the Cre/loxP or FLP/FRT recombination systems. Recombination systems allow for conditional KO of genes in certain cell or tissue types, or at certain time points in the mouse's life (Bouabe and Okkenhaug, 2013). KO mice can be generated by incorporating the desired genetic change into the genome of an embryonic stem cell by homologous recombination. This involves introduction of DNA, e.g. encoding a selection marker, flanked by sequences homologous to the desired insertion site, thereby disrupting the sequence of the gene of interest upon incorporation. Modified embryonic stem cells can be selected for using the selection marker and are subsequently injected into early-stage mouse embryos, resulting in mice that have the gene of interest knocked out in tissues derived from the modified embryonic stem cells (Bouabe and Okkenhaug, 2013). Subsequent breeding generates homozygous KO mice, which can be used for in vivo experiments, or primary cells can be harvested from the mice for in vitro studies.

While mouse models are a powerful tool to study gene function, manipulation of gene expression directly in cells can be advantageous as it can yield results more quickly. Subsequently, I describe two methods that are commonly used to disrupt protein expression in cells, one technique that functions at the messenger RNA (mRNA) level, small interfering RNAs (siRNA), and another that functions at the DNA level, clustered regularly interspaced short palindromic repeats (CRISPR).

siRNAs have been widely used to silence gene expression in mammalian cells, including primary T cells (Stinchcombe et al., 2015). In this approach, siRNAs form a complex with the RNA-induced silencing complex (RISC). Functional RISC particles contain a single stranded siRNA that binds to its complementary mRNA. The RISC complex also contains an RNase which cleaves the mRNA, leading to post transcriptional gene silencing and therefore a reduction in protein expression (Meister and Tuschl, 2004). This mechanism of gene silencing has been used to affect the expression of individual genes as well as gene expression on a genome-wide scale. However, often only partial protein knockdown is achieved, and the knockdown will only be maintained while the siRNA is present (Joung et al., 2017).

In recent years, the discovery of the CRISPR system and its use for gene editing has revolutionised this field by enabling the creation of KOs in mammalian cells where protein expression is permanently lost (Hsu et al., 2014). CRISPR has been used to modify the genome of many species, including human and mouse (Cho et al., 2013; Cong et al., 2013; Doudna and Charpentier, 2014; Jinek et al., 2013; Li et al., 2013; Mali et al., 2013). The system uses CRISPR-associated proteins (Cas), such as Cas9, an endonuclease that cuts DNA and causes double-stranded breaks. Cas9 is guided to a specific region in the genome by RNAs. In bacteria, the system requires two RNAs to function. Firstly, it requires the CRISPR RNA (crRNA) which is the reverse complement of the target site in the genome and binds to the target site by Watson-Crick base pairing. The second RNA that is required is the trans-activating crRNA (tracrRNA), which forms a duplex with the crRNA and is important for complex formation with Cas9 (Doudna and Charpentier, 2014). For genome-editing approaches, the crRNA and tracrRNA duplex has been combined into one molecule to give a single guide RNA (sgRNA) (Jinek et al., 2012). The target sequence in the genome must contain a protospacer adjacent motif (PAM) in order for Cas9 to bind and a cut to occur (Jinek et al., 2012; Sternberg et al., 2014). The PAM sequence therefore limits which sequences can be cut in the genome. However, the PAM sequence that is recognised varies between different Cas nucleases (Cong et al., 2013).

After the Cas9-mediated cut occurred, cell intrinsic DNA repair pathways are triggered and it is the inaccuracy of the DNA repair mechanisms that result in the desired editing of the genome (Hsu et al., 2014). Endonuclease cutting leaves behind a double-stranded break that is repaired by the non-homologous end-joining (NHEJ) or homology-directed repair (HDR) pathways (Hsu et al., 2014). The error-prone NHEJ is induced in the absence of a repair template and can introduce insertions or deletions (indels) during repair (Hsu et al., 2014). Indels may cause frameshift mutations, resulting in gene disruption. Precise genome editing using HDR is also possible, and provides the opportunity to incorporate a specific DNA template containing homology sequences to the cut site. However, HDR occurs less frequently and is therefore more challenging (Hsu et al., 2014; Komor et al., 2017; Ran et al., 2013).

CRISPR allows to KO individual genes, and therefore allows to examine gene function in a clean experimental system. Several different technical approaches to use CRISPR for genome-editing purposes have been developed. Transient expression of CRISPR components is achieved through the transfection of plasmids or ribonucleoprotein complexes (RNPs), which contain recombinant Cas9 protein and synthetic crRNA and tracrRNA (Kim et al., 2014). Stable expression of CRISPR components has been achieved through lentiviral delivery (Hsu et al., 2014; Shalem et al., 2014; Wang et al., 2014a). The CRISPR approach has furthermore been scaled up to a genome-wide level using lentiviral sgRNA libraries, which has given powerful insights into genes that regulate cell viability and resistance to drugs (Shalem et al., 2014; Wang et al., 2014a).

It is clear that using CRISPR in primary CTL has immense clinical potential, and could be used to further enhance the immunotherapy approaches outlined in section 1.6. Clinical trials using CAR T cells in combination with CRISPR-mediated disruption of PD-1 are currently ongoing (Cornu et al., 2017). Related gene-editing technologies, such as zinc finger nucleases (ZFNs) and transcription activator-like effector nucleases (TALENs), have already been used clinically (Fesnak et al., 2016). ZFNs have been used to KO C-C motif chemokine receptor 5 (CCR5), a crucial co-receptor for the human immunodeficiency virus (HIV), in autologous CD4 T cells. Gene-edited CD4 T cells were infused back into patients and this treatment was found to decrease the abundance of HIV RNA in the peripheral blood (Tebas et al., 2014). Allogeneic CAR T cells, where TALENs had been used to KO the endogenous TCR to prevent graft-versus-host disease, were used to treat patients with acute lymphocytic leukemia (Qasim et al., 2017). In addition to TCR KO, TALENs were used to KO CD52 in the

therapeutic CAR T cells. This enabled targeting of the patients' CD52 expressing cancerous cells using an antibody against CD52, without affecting the transferred CAR T cells. This use of genetically-modified T cells resulted in a remarkable clinical outcome (Qasim et al., 2017).

Together, these studies demonstrate the great potential of genome editing in primary human T cells for clinical purposes. Optimisation of the techniques used to deliver the CRISPR components to primary T cells, as well as a more thorough understanding of the fundamental biology underlying CTL function, will contribute to the advancement of this field.

1.8 Aims of this thesis

The work in this thesis aimed to identify regulators of CTL killing through screening approaches. Engineering the genome of CTLs was explored in order to provide a clean experimental system to investigate the involvement of individual genes in the CTL killing process. The currently known regulators of cytotoxic function have largely been identified using cells derived from patients suffering from immunodeficiency disorders or KO mouse strains. The hypothesis is that in addition to the proteins outlined in section 1.4.2 and 1.4.3 there are further proteins important for CTL cytotoxic function, perhaps functioning at the secretion step or further upstream, that remain to be discovered. This thesis aimed to establish the CRISPR Cas9 technique in primary T cells and to discover regulators of CTL function through screening using the CRISPR-Cas9 technique and chemical compounds. Furthermore, the work in this thesis contributes to the goal to perform large-scale screens in primary T cells in order to understand the molecular mechanisms underlying CTL function at large.

- **Aim 1: Develop strategies to use CRISPR-Cas9 in primary mouse CD8 T cells and establish a robust protocol that generates KO at high efficiency and disrupts gene expression reproducibly.**

  In chapter 3, I focus on establishing the CRISPR technology in primary mouse CTL (mCTL) using RNP complexes, which contained recombinant Cas9 protein, synthetic crRNAs and tracrRNA. CRISPR-mediated gene editing had not been performed in primary mouse T cells at the start of this project. I targeted genes whose protein products are known to be important for CTL killing (*Rab27a*, *Prf1* and *Munc13-4*) to confirm that CRISPR generated KOs at an efficiency that allowed detection of a phenotype in functional assays, such as the degranulation assay.

- **Aim 2: Develop an assay to measure cytotoxic capabilities of CTL at scale. Test the newly developed method in combination with a CRISPR screen and a compound library screen to identify regulators of CTL function.**

  Since one of the aims of this project was to identify regulators of CTL function, an assay that measures killing as well as degranulation was desirable. The set up of such an assay is described in chapter 3.

  To inform a targeted CRISPR screen, I compared gene expression between naive and effector CD8 T cells using RNA-sequencing (RNA-seq), described in chapter 4. The underlying hypothesis was that genes that are highly expressed in activated but not naive CD8 T cells are likely to be important for effector CTL functions, including killing capability. I used the readout of this transcriptomic dataset to select a set of genes for a targeted CRISPR screen. Samples were screened using the combined degranulation and killing assay, which was set up in chapter 3, in order to identify if any of these genes regulated CTL function.

  In chapter 5 I investigated whether the combined degranulation and killing assay can also be used in human CTL (hCTL) using samples derived from FHL2 and FHL3 patients. I furthermore tested the scalability of the assay using a compound library that targeted the NF-κB signalling pathway.

- **Aim 3: Establish protocols to use the CRISPR-Cas9 technique in primary human CD8 T cells.**

  An alternative CRISPR screening approach to using RNP complexes would be to stably transduce CTL with a lentivirus encoding Cas9 and sgRNAs. In contrast to the RNP approach, lentiviral transduction would allow for the incorporation of a fluorescent marker or an antibiotic resistance gene, which could be used to select edited cells. As the lifespan of mCTLs is limited to around 10 days in tissue culture, they are not suitable for a long selection procedure. However, this approach could be applied to hCTLs, which can be grown for months in tissue culture. This approach was explored in chapter 6.

Chapter 2

Materials and Methods

2.1 Cell culture

2.1.1 Cell culture conditions and media

The media compositions for all cell types used in this study are listed in Table 2.1. Fetal bovine serum (FBS) (Labtech) was heat inactivated at 56 °C for 30 min before addition to Roswell Park Memorial Institute (RPMI, Gibco, #21875-034 or Sigma, #R8758) or Dulbecco's Modified Eagle Medium (DMEM, Gibco, #41966-029) media. All media contained antibiotics (penicillin (pen) , streptomycin (strep)) (Sigma, #P0781) and was filter sterilised through a 0.22 μm filter. Mouse and human T cell media will subsequently be referred to by their abbreviations: human T cell media (hTCM) , mouse T cell media (mTCM).

All centrifugation steps were performed at 200xg for 5-10 min at room temperature (RT) unless otherwise indicated. Cells were cultured at 37 °C and 10% CO_2 in a humidified atmosphere.

2.1.2 Primary mouse T cell culture

Mice

Mice were bred under specific pathogen-free conditions in accordance with UK home office guidelines. T cells from OT-I mice (Hogquist et al., 1994) (genotype OT-I Rag1^{tm1Bal} on a C57BL/6 background) express a TCR that specifically recognises amino acids 257-264 (peptide sequence: SIINFEKL) of the chicken OVA protein presented in the context of H-2K^{b} MHC class I molecules. This peptide is referred to as 'OVA peptide' or simply 'OVA'

Table 2.1 ***Cell culture media.***

Name	Composition	Source
Human T cell media (hTCM)	RPMI 1640	Gibco, #21875-034, Sigma, #R8758
	2% (v/v) recombinant IL-2 protein	Produced in-house (Ruprecht et al., 2005)
	5% (v/v) human serum	Sigma, #H6914
	2 mM (1% (v/v)) L-glutamine	Sigma, #G7513
	1 mM (1% (v/v)) sodium pyruvate	Gibco, #11360-039
	50 μM β-mercaptoethanol	Gibco, #31350-010
	100 U/ml penicillin, 0.1 mg/ml streptomycin	Sigma, #P0781
Mouse T cell media (mTCM)	RPMI 1640	Gibco, #21875-034, Sigma, #R8758
	20 ng/ml recombinant murine IL-2	Peprotech, #212-12
	10 % (v/v) heat-inactivated FBS	Labtech
	2 mM (1% (v/v)) L-glutamine	Sigma, #G7513
	1 mM (1% (v/v)) sodium pyruvate	Gibco, #11360-039
	50 μM β-mercaptoethanol	Gibco, #31350-010
	100 U/ml penicillin, 0.1 mg/ml streptomycin	Sigma, #P0781
Target cell media	DMEM	Gibco, #41966-029
	10 % (v/v) heat-inactivated FBS	Labtech
	100 U/ml penicillin, 0.1 mg/ml streptomycin	Sigma, #P0781
HEK media	DMEM	Gibco, #41966-029
	10 % (v/v) heat-inactivated FBS	Labtech
YT media	RPMI 1640	Gibco, #21875-034, Sigma, #R8758
	2% (v/v) recombinant IL-2 protein	Produced in-house (Ruprecht et al., 2005)
	10 % (v/v) heat-inactivated FBS	Labtech
	2 mM (1% (v/v)) L-glutamine	Sigma, #G7513
	1 mM (1% (v/v)) sodium pyruvate	Gibco, #11360-039
	50 μM β-mercaptoethanol	Gibco, #31350-010
	100 U/ml penicillin, 0.1 mg/ml streptomycin	Sigma, #P0781
Jurkat media	RPMI 1640	Gibco, #21875-034, Sigma, #R8758
	10 % (v/v) heat-inactivated FBS	Labtech
	100 U/ml penicillin, 0.1 mg/ml streptomycin	Sigma, #P0781

throughout this thesis. Due to breeding on a *Rag1* -/- background, all OT-I T cells express the same TCR from the double positive stage in T cell development and are CD8-positive. This system allows uniform stimulation upon addition of OVA peptide in vitro, resulting in CTL that can kill EL4 target cells loaded with OVA.

C57BL/6N WT mice were obtained through the 3i Consortium (Wellcome Trust Sanger Institute). Spleens from C57BL/6 Cas9 mice, where Cas9 under the control of the human *EF1*α promoter was inserted into the *Rosa26* locus (Tzelepis et al., 2016), were kindly provided by Dr Gabriel Balmus and Dr Kosuke Yusa (Wellcome Trust Sanger Institute). Spleens from *ashen* mice (Wilson et al., 2000) were kindly provided by Dr Melina Schuh (MRC Laboratory for Molecular Biology).

Preparation and stimulation of murine splenocytes

Spleens were manually disrupted using a sterile syringe plunger and resulting splenocytes were filtered through a 70 μm cell strainer before centrifugation at 200xg for 10 min. For OT-I splenocytes, each pellet was resuspended in 100 ml mTCM (Table 2.1) containing 10 nM OVA peptide (Anaspec, #AS-60193-5) and cultured at 37 °C for 3 days. From day 3 onwards, cells were washed daily and resuspended at roughly 1x10^6 cells/ml. OT-I cells were used in functional assays from day 6 - 9 post in vitro stimulation.

To stimulate splenocytes derived from WT, Cas9 or *ashen* mice, 6 well plates were coated with 0.5 µg/ml αCD3ε (clone Bio500A2, eBioscience, #16-0033-86) and 1 µg/ml αCD28 (clone 37.51, eBioscience, #16-0281-86) overnight at 4 °C. 13.6x10^6 splenocytes were seeded per well in 8 ml mTCM on the pre-coated plates. Cells were cultured for 48 h at 37 °C and 10% CO_2. The resulting stimulated T cells were washed, resuspended at 1x10^6 cells/ml in fresh mTCM and transferred to uncoated plates. Subsequently, mCTL were split every 1-2 days and functional assays were performed from day 6 - 9 post in vitro stimulation. CD8 T cells usually grew out to >80% during expansion, but were purified using the mouse CD8a T cell isolation kit (Miltenyi Biotec, #130-104-075) in experiments where a pure CD8 population was required.

2.1.3 Primary human T cell culture

Phytohaemagglutinin (PHA)-blasts from FHL patient samples (Table 2.2) were kindly provided by Professor Stephan Ehl (Medical center, University of Freiburg). T cells derived from healthy donors (HDs) were obtained from buffycoat (NHS Blood and Transplant Centre). Peripheral blood mononuclear cells (PBMCs) were isolated from buffycoats by Ficoll-Paque (GE healthcare, #17-1440-02) gradient centrifugation and washed 5x in RPMI containing 1% FBS.

Human T cells were stimulated with 1 µg/ml PHA (Sigma, #L1668) and allogeneic PBMCs derived from buffycoat residue (NHS Blood and Transplant Centre). Allogeneic PBMCs were isolated as described for HDs, followed by irradiation at 3000 radiation absorbed dose (rad) of gamma rays prior to addition to human T cells. Cells were cultured in hTCM (Table 2.1) at 37 °C and 10% CO_2. Cells were expanded when confluent, roughly

Table 2.2 ***Details of mutations in FHL patients.*** *Cells were derived from patients that presented with FHL2, caused by mutations in PRF1, or FHL3, caused by mutations in MUNC13-4. Patient mutations are described according to published guidelines (Ogino et al., 2007). Mutations are indicated as homozygous (hom) if the same mutation is present on both alleles, heterozygous (het) if only one allele is affected by the mutation and compound het if both alleles are affected, but the mutations differ on each allele. The abbreviation 'c.' stands for coding DNA and is followed by the exact nucleotide mutation at the DNA level (del = deletion). Intronic locations are numbered with reference to exonic sequences (+1 indicates that the mutation affects an intron). The abbreviation 'p.' stands for the protein amino acid sequence and is followed by the change in amino acids (three letter code) caused by the mutation (fs = frameshift, X = early stop codon). The affected exons are given in square brackets.*

Patient	FHL subtype	Mutation
6981	FHL2	hom c.1288G>C; p.Asp430His [Exon 3]
3026	FHL2	compound het c.272C>T; p.Ala91Val [Exon 2] and c.1213C>T; p.Gln405X [Exon 3]
392	FHL2	hom c.1349C>T; p.Thr450Met [Exon 3]
4166	FHL2	c.112G>A; p.Val38Met and c.272C>T; p.Ala91Val [Exon 2 and 3] (het/hom information not provided)
3778	FHL3	hom c.1208C>T; p.Leu403Pro [Exon 14]
1310	FHL3	het c.753(+1) splice site [Exon 9] and c.2346_49del; p.Arg782fsX12 [Exon 24]
4413	FHL3	het c.1389(+1) G>A splice donor site [Exon15] and c.2346_2349del; p.Arg782Ser fsX12 [Exon24]

every 1-3 days until day 14 post in vitro stimulation, at which time the cells usually started to proliferate less. hCTL were used for functional assays from day 12 - 15 post stimulation and were re-stimulated as described above roughly every 21 days. The percentage of CD8 and CD4 positive cells was checked on a regular basis by flow cytometry. If necessary, CD8 T cells were purified using the human CD8 T cell isolation kit (Miltenyi Biotec, #130-045-201). The human CD4 T cell isolation kit (Miltenyi Biotec, #130-045-101) was used to exclude CD4 cells. For blasticidin concentration response and selection experiments human T cells were treated with blasticidin (Sigma, #15205) at the concentrations indicated in figure legends.

2.1.4 Cell line culture

P815 (mouse mastocytoma) cells were used as target cells for human CTL and WT mouse CTL. P815s express Fc receptors on their cell surface that bind to the constant region of antibodies. P815s loaded with αCD3ε can trigger activation of T cells. EL4 (mouse lymphoma) cells were used as target cells for OT-I CTL as they can present the OVA peptide

in the context of H-2K^b MHC class I molecules. Blue fluorescent protein (BFP) P815s and EL4s, stably expressing Farnesyl-5-TagBFP2 through retroviral transduction were established in the Griffiths lab (Ritter et al. (2015) and Alex Ritter's PhD thesis). These target cells are subsequently referred to as blue EL4 or blue P815s for simplicity. I established red P815s and EL4s using lentiviral transduction (see section 2.10). All P815 and EL4 cell lines were cultured in target cell media (Table 2.1) and split 1 in 10 every 2-3 days. For red P815s and EL4s, the target cell media was supplemented with 1 µg/ml puromycin (Thermo Fisher Scientific, #A1113803).

Human embryonic kidney (HEK) 293T cells were maintained in target cell media without antibiotics and split when reaching roughly 80% confluency using trypsin (Sigma, #T3924) for detachment. The human NK cell line YT was maintained in YT media (Table 2.1) and the human Jurkat T cell line was maintained in Jurkat media (Table 2.1). YT cells and Jurkat cells were split 1 in 5 every 2-3 days.

2.2 Nucleofection

2.2.1 Preparation of synthetic RNAs

Synthetic RNAs were obtained as dried pellets from Dharmacon, reconstituted in Tris-EDTA pH 7.4 (Sigma, #93302) to give stock solutions between 1-10 μg/μl and mixed on an orbital shaker at 700 rpm for 30 min at RT. Aliquots were stored at $-20\,^{\circ}$C. Details of all synthetic RNA reagents used are outlined in Table 2.3. siRNA and crRNA sequences were predesigned by Dharmacon/Horizon Discovery. Only crRNAs targeting exons were chosen, with preference given to crRNAs targeting different exons in the same gene in order to increase the possibility of cutting out a large section of the gene.

2.2.2 Nucleofection of primary mouse T cells

mCTLs were nucleofected at day 4-7 post in vitro stimulation. Nucleofections were performed with the Lonza mouse T cell nucleofection kit (Lonza, #VPA-1006) using the 2b nucleofection machine (Lonza) or the P3 primary cell kit (Lonza, #V4XP-3024) using the 4D nucleofector (Lonza). Mouse T cell nucleofection media (Lonza, #VZB-1001) was supplemented with 1% (v/v) medium component A (Lonza, #VZB-1001), 2 mM L-glutamine (Sigma, #G7513) and 5% (v/v) FBS (Labtech). Before use, 1% (v/v) component B (Lonza, #VZB-1001) was added and nucleofection media was pre-warmed at 37 °C for at least 30 min. Subsequently, 5x10^6 cells per condition were centrifuged at 200xg for 5 min. All supernatant

was removed carefully and pellets were resuspended in 100 μl nucleofection solution (Lonza) containing the desired reagents. For siRNA experiments, 5x10^6 T cells were nucleofected with 3 μg scramble or Rab27a siRNA (Table 2.3). For CRISPR experiments, 5x10^6 T cells were nucleofected with 5 μg per crRNA (3 crRNAs per gene means 15 μg crRNAs in total), 15 μg tracrRNA and 10 μg Cas9 protein (Takara, #632640), unless otherwise indicated in figure legends. Nucleofection controls and non-targeting (NT) CRISPR controls were included in every experiment. Cells resuspended in nucleofection solution containing all necessary reagents were transferred to nucleofection cuvettes and nucleofected using program X-001 (2b machine) or program DN-100 (4D machine). Next, each nucleofected sample, containing 5x10^6 mCTL, was transferred to 1 ml prewarmed nucleofection media in 1 well of a 12 well plate. Cells were left to recover in the incubator for 3-4 h before splitting across 3 wells in a 12 well plate and topping up each well with 3 ml mTCM. The following day, cells were pelleted and resuspended in fresh mTCM at roughly 1x10^6 cells/ml.

2.2.3 Nucleofection of primary human T cells

Human T cells were stimulated with 5 μg/ml PHA for 3 days prior to nucleofection. The P3 primary cell kit (Lonza, #V4XP-3024) was used for nucleofection with the 4D nucleofector (Lonza). Prior to nucleofection, hTCM was pre-warmed at 37 °C for at least 30 min. 1-1.5x10^6 cells were pelleted and resuspended in nucleofection solution containing 2 μg lifeact-EGFP plasmid or CRISPR reagents. As only 1-1.5x10^6 cells were nucleofected per condition, the amount of CRISPR reagents used was scaled down accordingly (e.g. as I used 5 μg per crRNA for 5x10^6 mouse T cells, I only used 1 μg per crRNA when nucleofecting 1x10^6 human T cells). Human T cells were nucleofected using program E0-115 on the 4D nucleofector.

For nucleofection with the Neon transfection system (Thermo Fisher Scientific), human T cells were washed once in Dulbecco's Phosphate-Buffered Saline (DPBS) (Gibco, #14190094) and then resuspended in 110 μl buffer T (Neon transfection system kit, Thermo Fisher Scientific, #MPK10025) containing the appropriate CRISPR reagents. The reaction conditions were otherwise identical to the Lonza 4D samples (same number of cells and same amount of reagent). Cells were transfected using the following settings: 1600V, 10 ms, 3 pulses.

Upon nucleofection with neon or 4D nucleofectors, 1-1.5 million human T cells were transferred into 500 μl pre-warmed hTCM in one well of a 24 well plate. Cells were left to recover in the incubator for 2 h before topping up with an additional 500 μl pre-warmed

hTCM. The next day, cells were pelleted at 200xg for 10 min and resuspended in fresh hTCM.

2.2.4 Nucleofection of Jurkat cells

Jurkat cells were nucleofected using the SE Cell line nucleofection kit (Lonza, #V4XC-1012). For nucleofections using cuvettes, 1x10^6 Jurkat cells were pelleted and resuspended in 100 μl nucleofection solution containing CRISPR reagents. For nucleofections using 16-well strips, 0.2x10^6 Jurkat cells were pelleted and resuspended in 20 μl nucleofection solution containing CRISPR reagents. In both experimental conditions, Jurkat cells were nucleofected with 2 μg Cas9 protein, 3 μg tracrRNA, and 1 μg per crRNA (3 crRNAs per gene) targeting *CD2* or the gene encoding β2 microglobulin (*B2M*) using program CK-116 on the 4D nucleofector. Cells were transferred into pre-warmed Jurkat media in 24 well plates (1x10^6 cells samples) or 96 well plates (0.2x10^6 cells samples) and left to recover for 2 h before topping up with pre-warmed Jurkat media.

Table 2.3 ***Overview of synthetic RNAs (siRNAs, crRNAs and tracrRNA) used in this study.*** *All reagents were predesigned and acquired from Dharmacon/Horizon Discovery.*

Reagent	**Catalogue number**
scramble siRNA	D-001810-10-20
Rab27a siRNA	L-060970-01
tracrRNA	U-002005-50
Non-targeting crRNA	U-007501-20
mouse *Thy1* crRNA	CR-041986-01-0005
mouse *Rab27a* crRNA1	CR-060970-01-0005
mouse *Rab27a* crRNA2	CR-060970-04-0005
mouse *Rab27a* crRNA3	CR-060970-05-0005
mouse *Munc13-4* crRNA1	CM-064384-01-0002
mouse *Munc13-4* crRNA2	CM-064384-02-0002
mouse *Munc13-4* crRNA3	CM-064384-03-0002
mouse *Perforin* crRNA1	CM-064701-01-0002
mouse *Perforin* crRNA2	CM-064701-02-0002
mouse *Perforin* crRNA3	CM-064701-03-0002
mouse *Cav2* crRNA1	CM-063000-01-0002
mouse *Cav2* crRNA2	CM-063000-02-0002

Table 2.3 continued from previous page

Reagent	Catalogue number
mouse *Cav2* crRNA3	CM-063000-03-0002
mouse *Anxa1* crRNA1	CM-040923-01-0002
mouse *Anxa1* crRNA2	CM-040923-02-0002
mouse *Anxa1* crRNA3	CM-040923-03-0002
mouse *Anxa2* crRNA3	CM-061993-01-0002
mouse *Anxa2* crRNA3	CM-061993-04-0002
mouse *Anxa2* crRNA3	CM-061993-05-0002
mouse *Anxa3* crRNA1	CM-046409-01-0002
mouse *Anxa3* crRNA2	CM-046409-02-0002
mouse *Anxa3* crRNA3	CM-046409-05-0002
mouse *Anxa4* crRNA1	CM-057375-02-0002
mouse *Anxa4* crRNA2	CM-057375-04-0002
mouse *Anxa4* crRNA3	CM-057375-05-0002
mouse *Nfil3* crRNA1	CM-063246-01-0002
mouse *Nfil3* crRNA2	CM-063246-02-0002
mouse *Nfil3* crRNA3	CM-063246-03-0002
mouse *Slc7a5* crRNA1	CM-041166-01-0002
mouse *Slc7a5* crRNA2	CM-041166-02-0002
mouse *Slc7a5* crRNA3	CM-041166-03-0002
mouse *Hif1α* crRNA1	CM-040638-01-0002
mouse *Hif1α* crRNA2	CM-040638-03-0002
mouse *Hif1α* crRNA3	CM-040638-04-0002
mouse *Dysf* crRNA1	CM-040311-02-0002
mouse *Dysf* crRNA2	CM-040311-03-0002
mouse *Dysf* crRNA3	CM-040311-04-0002
mouse *Cpne5* crRNA1	CM-053834-01-0002
mouse *Cpne5* crRNA2	CM-053834-02-0002
mouse *Cpne5* crRNA3	CM-053834-03-0002
mouse *Ppfia3* crRNA1	CM-066090-01-0002
mouse *Ppfia3* crRNA2	CM-066090-02-0002
mouse *Ppfia3* crRNA3	CM-066090-05-0002
mouse *Tns2* crRNA1	CM-040926-01-0002
mouse *Tns2* crRNA2	CM-040926-02-0002

Table 2.3 continued from previous page

Reagent	Catalogue number
mouse *Tns2* crRNA3	CM-040926-03-0002
human *CD2* crRNA1	CM-017854-01-0002
human *CD2* crRNA2	CM-017854-02-0002
human *CD2* crRNA3	CM-017854-05-0002
human *B2M* crRNA1	CM-004366-01-0002
human *B2M* crRNA2	CM-004366-02-0002
human *B2M* crRNA3	CM-004366-03-0002

2.3 Western blotting

2.3.1 Lysate preparation

Cells were counted and pelleted at 200xg for 5 min, resuspended in 1 ml ice-cold DPBS and pelleted again at 200xg for 5 min at 4 °C. Pellets were dried by removing the supernatant, frozen on dry ice before storage at −80 °C or lysed directly at 2-5x10^7 cells/ml for Western blotting (WB).

Cytoplasmic lysate preparation

Dried pellets were resuspended in lysis buffer [50 mM Tris(hydroxymethyl)aminomethane hydrochloride (Tris-HCl) pH 8, 150 mM sodium chloride (NaCl) , 1 mM magnesium chloride ($MgCl_2$) (all obtained from CIMR media kitchen), 2% Triton X-100 (Sigma, #T8787) in ultrapure H_2O (CIMR media kitchen)]. 1X protease inhibitor cocktail (Roche, #04693132001) was added just before use. Additionally, 1X PhosSTOP (Roche, #4906845001) was included in the lysis buffer for lysates used to blot for phosphorylated proteins. After incubation at 4 °C for 30 min, lysates were centrifuged at 18,800 xg for 25 min at 4 °C. The supernatant was transferred into a fresh tube and sample buffer added as outlined in section 2.3.2.

Nuclear lysate preparation

For the detection of the protein Nuclear factor, interleukin 3 regulated (NFIL3), nuclear proteins were extracted from cell pellets using the NE-PER Nuclear and cytoplasmic extraction reagents (Thermo Fisher Scientific, #78835). This kit uses 3 buffers, cytoplasmic

extraction reagent 1 (CER1), cytoplasmic extraction reagent 2 (CER2) and nuclear extraction reagent (NER). CER1, CER2 and NER were added at a ratio of 200:11:100, as detailed in the manufacturer's instructions, to give a final lysate concentration of $5x10^7$ cells/ml. Protease inhibitors (Roche, #04693132001) were added to CER1 and NER buffers immediately before use. Cell pellets were resuspended in ice-cold CER1, vortexed for 15 seconds (sec) and incubated on ice for 10 min. Next, ice-cold CER2 reagent was added, samples were vortexed for 5 sec and incubated on ice for 1 min prior to centrifugation at 18,800 xg for 5 min at 4 °C. The supernatant, containing cytoplasmic proteins, was transferred to a clean tube. The pellet, containing nuclear proteins, was resuspended in ice-cold NER, vortexed for 15 sec every 10 min for a total of 40 min. Samples were pelleted at 18,800 xg for 5 min at 4 °C and the supernatant, containing nuclear proteins, was transferred to a clean tube and sample buffer added as outlined in section 2.3.2.

Whole cell lysate preparation

The following method was used to enable detection of Hypoxia-inducible factor (HIF)-1α by WB. Four days after nucleofection, control (nuc control and NT CRISPR) mCTL and mCTL nucleofected with *Hif1*α CRISPR reagents were transferred to plates coated with 1 µg/ml αCD3ε (clone Bio500A2, eBioscience, #16-0033-86). $5x10^6$ mCTL were seeded per well and the plate was transferred to a hypoxia chamber (Whitley H35 hypoxystation) kept at 1% O_2 and 37 °C. After 4 h, samples were collected on ice, centrifuged briefly for 1 min at 200xg and 4 °C, washed 1x with ice-cold DPBS containing 1x protease inhibitor (Roche, #04693132001), and pelleted again. After removing the supernantant, pellets were resupsended at $5x10^7$ cells/ml in the following lysis buffer, kindly provided by Natalie Burrows (Patrick Maxwell's lab, Cambridge Institute for Medical Research): H_2O containing 50 mM Tris-HCl pH 7.4, 120 mM NaCl, 5 mM ethylene-Diamine Tetraacetic acid (EDTA), 0.5% nonidet P40 (NP40), 1mM DL-Dithiotheitol (DTT), 1 mM Phenylmethylsulfonyl fluoride (PMSF), 2 mM sodium orthovanadate (NaOV), 2 mM sodium fluoride (NaF), 20 mM β-glycerol phosphate (BGP), 5 mM sodium pyrophosphate (NaPPi) and 1x protease inhibitor cocktail (Roche, #04693132001). Each sample was sonicated twice for 2 sec at an amplitude of 8 using a soniprep 150 plus sonicator (MSE). After 10 min incubation on ice samples were centrifuged at 16,200xg for 10 min at 4 °C. The resulting supernatant was transferred to a clean tube and sample buffer added as outlined in section 2.3.2.

Table 2.4 ***Primary antibodies used for WB.*** *Abbreviations: Rb = Rabbit, Ms = mouse, Rt = rat, Gt = goat.*

Target	Species reactivity	Clonality	Dilution	Source
Ms α-Rab27a	mouse	monoclonal	1 in 100	Abcam, #ab55667
Rb α-Munc13-4	mouse	monoclonal clone 1223B	1 in 200	R&D Systems, #MAB89662
Gt α-Munc13-4	human	polyclonal	1 in 300	Eversest Biotech, #EB06383
Rt α-Perforin	mouse	monoclonal clone CB5.4	1 in 500	Enzo life sciences, #ALX-804-057-C100
Ms α-Perforin	human	monoclonal (supernatant) clone 2D4	1 in 50	(Baetz et al., 1995)
Ms α-Cas9	not applicable	monoclonal clone 7A9	1 in 100	Epigentek, #A9000-100
Rb α-Calnexin	mouse/human	polyclonal	1 in 2000	Sigma, #C4731
Ms α-βactin	mouse/human	monoclonal clone AC-15	1 in 5000	Sigma, #CA5441
Rb α-NFIL3	mouse	monoclonal clone DK580	1 in 500	Cell Signaling Technology, #14312S
Ms α-Hif1α	mouse	monoclonal clone 241809	1 in 500	R&D Systems, #MAB1536
Rb α-Lamin B1	mouse/human	polyclonal	1 in 5000	Abcam, #ab16048
Rb α-p65 (S536)	human	monoclonal clone 93H1	1 in 500	Cell Signaling Technology, #3033S
Ms α-IkBα	human	monoclonal clone L35A5	1 in 500	Cell Signaling Technology, #4814S
Rb α-p105/p50	human	monoclonal clone D4P4D	1 in 100	Cell Signaling Technology, #13586S

2.3.2 Protein electrophoresis and transfer

Nupage LDS sample buffer (Invitrogen, #NP0007) containing 10% NuPAGE Sample reducing reagent (Invitrogen, #NP0009) was added to WB lysates at a final concentration of 1X. Samples were boiled at 95 °C for 5 min prior to loading onto pre-cast NuPAGE 4-12% Bis-Tris gels (Invitrogen, #NP0335) alongside 5 μl of Precision Plus Protein Kaleidoscope MW marker (BioRad, #161-0375). Gels were run at 110-130 V for 1-2 h in MES (life technologies, #NP0002) or MOPS (for high MW proteins, life technologies, #NP0001) sodium dodecyl sulfate (SDS) running buffer diluted to 1X in distilled H_2O. Proteins were transferred to nitrocellulose membranes (GE Healthcare life sciences, #10600003) in NuPAGE transfer buffer (life technologies, #NP0006) diluted to 1X in distilled H_2O and 10% (v/v) methanol at RT for 95-100 min at 100 V. Successful transfer was confirmed by staining with ponceau red (0.1% (w/v) ponceau, 5% (v/v) acetic acid in H_2O) for 5 min at RT while shaking, followed by several washes in H_2O to remove the red stain.

2.3.3 Incubation with antibodies and protein detection

Blocking was performed in 1X Tris buffered saline-Tween (TBS-T) (1XTBS + 0.05% (v/v) Tween-20) containing 5% (w/v) skimmed milk. When blotting for phosphorylated proteins 1X TBS-T (0.05% Tween-20) containing 5% (w/v) BSA was used instead. Blots were incubated with primary antibodies (Table 2.4) diluted into blocking buffer while rotating overnight at 4 °C. The following day, blots were washed four times for a total of 20 min in 1x TBS-T solution before addition of horseradish peroxidase (HRP) conjugated secondary antibodies (Table 2.5) diluted into blocking buffer for 1 h at RT. Following four more

Table 2.5 ***Secondary antibodies used for WB.***

Target	Conjugation	Dilution	Source
Goat α-mouse	Peroxidase	1 in 3000	Thermo Fisher Scientific, #32430
Goat α-rabbit	Peroxidase	1 in 3000	Thermo Fisher Scientific, #32460
Goat α-rat	Peroxidase	1 in 10000	SouthernBiotech, #3030-05
Donkey α-goat	Peroxidase	1 in 10000	Jackson ImmunoResearch, #705-035-147

washes, proteins were detected using ECL prime western blotting reagent (GE Healthcare, #RPN2232) and images were acquired using the ChemiDoc MP imaging system (Bio-Rad). Band intensities were quantified using the ImageLab4.1 software (Bio-Rad) and samples were normalised to loading controls and expressed relative to an appropriate experimental control, as detailed in figure legends.

2.4 Flow cytometry

2.4.1 Cell surface staining

Cells were washed in fluorescence-activated cell sorting (FACS) buffer (DPBS + 1% (v/v) FBS) and stained with live dead markers (Table 2.6) and fluorescently-conjugated antibodies (Table 2.7) diluted into FACS buffer for 10-15 min at RT or at 4 °C for 30 min. Subsequently, cells were washed to remove excess antibody and resuspended in FACS buffer for sample acquisition on LSRFortessa (BD biosciences), Accuri C6 (BD biosciences) or Attune NxT (Thermo Fisher Scientific) flow cytometers. Data was analysed with FlowJo version 10.4.2 (FlowJo, LLC).

Table 2.6 ***Live/dead stains used in flow cytometry experiments.***

Reagent	Dilution	Source
Fixable yellow	1 in 1000	Thermo Fisher Scientific, #L34959
Zombie Red	1 in 500	Biolegend, #423110
DAPI	1 in 5000 (1 μg/ml)	Thermo Fisher Scientific, #D3571

Table 2.7 ***Directly conjugated antibodies used in flow cytometry experiments.*** *Abbreviations: FITC = Fluorescein isothiocyanate, PE = Phycoerythrin, APC = Allophycocyanin, BV421 = Brilliant Violet 421, BV711 = Brilliant Violet 711, AF488 = Alexa Fluor 488.*

Antibody specificity and conjugation	Clone	Isotype	Species specificity	Dilution	Source
B2M-FITC	2M2	mouse IgG1 κ	human	1 in 400	Biolegend, #316304
CD107a(LAMP1)-PE	1D4B	rat IgG2a κ	mouse	1 in 100	eBioscience, #12-1071-83
CD107a(LAMP1)-PE	H4A3	mouse IgG1 κ	human	1 in 200	eBioscience, #12-1079-42
CD2-FITC	RPA-2.10	mouse IgG1 κ	human	1 in 200	Biolegend, #300206
CD2-PE	RPA-2.10	mouse IgG1 κ	human	1 in 200	Biolegend, #300208
CD4-PE	RM4-5	rat IgG2a κ	mouse	1 in 200	Biolegend, #100511
CD4-PE	A161A1	rat IgG2b κ	human	1 in 200	Biolegend, #357404
CD8-APC	53-6.7	rat IgG2a κ	mouse	1 in 200	Biolegend, #100712
CD8-BV421	RPA-T8	mouse IgG1 κ	human	1 in 400	Biolegend, #301036
CD8-BV711	53-6.7	rat IgG2a κ	mouse	1 in 200	Biolegend, #100747
CD8-BV711	RPA-T8	mouse IgG1 κ	human	1 in 200	Biolegend, #301044
Thy1.2-APC	53-2.1	rat IgG2a κ	mouse	1 in 200	BD Biosciences, #561974
Thy1.2-AF488	30-H12	rat IgG2b κ	mouse	1 in 200	Biolegend, #105316
TNF-PE	MAb11	mouse IgG1 κ	human	1 in 100	BD Biosciences, #554513

2.4.2 Intracellular staining for TNFα detection

Flat bottom 96 well plates were coated with 1 μg/ml αCD3ε (clone OKT3, eBioscience, #14-0037-82) overnight at 4 °C. hCTL were treated with drug 19/parthenolide (Medchem express, #HY-N0141) or dimethyl sulfoxide (DMSO) (Sigma, #D2650) vehicle control overnight at 8.3 μM. The following day, coated wells were washed with hTCM before addition of 200,000 hCTL treated with drug 19 or DMSO per well. Golgi stop (BD biosciences, #554715), containing the protein transport inhibitor monensin, was added at 0.67 μl/ml to inhibit protein secretion, including the secretion of TNFα. Cells were incubated with and without the αCD3ε stimulus at 37 °C. After 4 h, cells were washed in ice-cold DPBS and stained with αhuman-CD8-BV711 (Table 2.7) and fixable yellow live dead dye (Table 2.6) for 30 min at 4 °C. After washing with FACS buffer, cells were fixed and permeabilised using 100 μl of fixation/permeabilisation solution (BD biosciences, #554715) per well for 20 min at 4 °C. After 2 washes with 1x permeabilisation/wash buffer (BD biosciences, #554715), samples were incubated with human Fc-block (Miltenyi, #130-059-901) at 4 μl/1x10^6 cells for 15 min at RT. Next, mouse αhuman-TNFα-PE (Table 2.7) or mouse IgG1-PE isotype control (Abcam, #ab81200) were added and incubated for a further 30 min at 4 °C. Following 2 washes in 1x permeabilisation/wash buffer, samples were resuspended in FACS buffer for analysis.

2.4.3 Cell sorting

Samples were washed with sterile FACS buffer containing 100 U/ml pen, 0.1 mg/ml strep, and stained with 4',6-diamidino-2-phenylindole (DAPI) (Table 2.6) to distinguish live cells from dying cells. P815 and EL4 positive for nuclight red or hCTL positive for Cas9-2A-mCh were sorted into appropriate media containing 100 U/ml pen, 0.1 mg/ml strep using an Influx cell sorter (Becton Dickinson). After sorting, cells were pelleted, resuspended in fresh pen/strep-containing media and transferred to the incubator.

2.5 Assays to measure CTL effector function

In this thesis I used degranulation and killing assays to measure CTL effector function. The conditions used to trigger an effector response differed according to whether CTLs were derived from OT-I mice, WT mice or human PBMCs. To measure degranulation and killing capabilities of OT-I CTL, EL4 target cells were used, which present the OVA peptide in the context of their H-2K^b MHC class I molecule. EL4s were pulsed with 1 μM OVA peptide for 1 h at 37 °C. Subsequently, cells were washed three times into mTCM prior to addition to OT-I CTL. Unpulsed EL4 that were incubated and washed in parallel served as a negative control.

To trigger a degranulation and killing response in WT mCTL or hCTL I used P815 target cells, which express Fc receptors on their cell surface that are able to bind to the constant region of antibodies. P815s were loaded with αCD3ε (for hCTL: clone UCHT1, BDPharmingen, #555330; for WT mCTL: clone 145-2C11, eBioscience, #16-0031-86) for 20 min at RT, resulting in a final αCD3ε concentration of 0.5 μg/ml for mCTL and 0.25 μg/ml for hCTL upon addition of target cells to CTL.

The conditions outlined above were used throughout. For simplicity, I will refer to hCTL and mCTL as 'CTL', to P815 and EL4s as 'targets' and to OVA peptide and αCD3ε as 'stimulus' for the remainder of section 2.5. In general, two - four technical replicates were included per condition in every experiment.

2.5.1 Degranulation assay

Both CTL and targets with stimulus were resuspended at 2x10^6 cells/ml and 200,000 cells were seeded per well in a round bottom 96 well plate to give an effector-to-target (E:T) ratio of 1, unless otherwise stated in figure legends. PE-conjugated αCD107a (αLAMP1) antibody (Table 2.7) was added for the duration of the assay in all wells except staining

controls. Unstimulated control wells were included for all conditions, which contained CTL and target cells without stimulus or no target cells at all.

Following incubation at 37 °C for 3 h, or the time periods indicated in figure legends, samples were pelleted at 4 °C and washed in ice-cold DPBS. Next, samples were incubated with fluorescently-conjugated antibodies to stain CD8 and Thy1 cell surface molecules (Table 2.7) and with live/dead markers (Table 2.6) for 30 min on ice. After washing in FACS buffer, samples were resuspended in FACS buffer before acquisition on Accuri C6 (BD biosciences), Attune NxT (Thermo Fisher Scientific) or LSRFortessa (BD biosciences) flow cytometers. Results were analysed with FlowJo version 10.4.2 (FlowJo, LLC). The gating strategy used for analysis with FlowJo is explained in Figure 3.1. A forward scatter (FSC) and side scatter (SSC) gate was used to separate the cell population from debris, a second gate was used to isolate single cells from doublets, a third gate was used to isolate live cells from dead cells, a fourth gate was used to isolate CD8 cells and a final gate was used to isolate LAMP1-PE positive cells. Gates were set according to fluorescence minus one controls and experimental controls (unstimulated CTL).

2.5.2 Combined degranulation and killing assay

For the combined degranulation and killing assay, it was important to use stained target cells in order to be able to clearly distinguish CTL and targets during analysis steps. Initially, CFSE-stained target cells were used in this assay. Later on, targets that were permanently stained blue, as described under section 2.1.4, were used instead. For CFSE staining, target cells were incubated with 0.25 μM CFSE (Thermo Fisher Scientific, #C34570) for 10 min at RT in the dark. Following addition of FBS-containing media to quench the dye for 5 min at RT in the dark cells were washed twice before addition to T cells.

CTL and targets with stimulus were co-cultured at an E:T of 2.5:1 in 96 well round bottom plates, with 125,000 CTL and 50,000 target cells seeded per well. Controls that contained CTL and targets without stimulus, CTL on their own or targets on their own were included in every experiment. After incubation at 37 °C for 3 h, samples were pelleted and washed in ice-cold DPBS. Cells were stained with fluorescently-conjugated αCD8 antibodies (Table 2.7) and a live dead stain (Table 2.6) for 30 min at 4 °C. After washing with FACS buffer, and just before analysis on the Attune NxT flow cytometer (Thermo Fisher Scientific), 10 μl 123count ebeads (Invitrogen, #01-1234-42) were added per well. The contents of each well were mixed thoroughly with a mutlichannel pipette.

The analysis process for the beads killing assay readout is explained in detail in Figure 3.11 . Gates were set around the beads population and the stained target cell population in FlowJo version 10.4.2 (FlowJo, LLC). This enabled to count the number of target cells and beads in each well, and allowed to derive a targets:beads ratio. This ratio was multiplied by the number of beads known to be present in the 10 μl added to each sample (information supplied by the manufacturer) in order to determine the total number of target cells remaining in each well. The number of target cells in wells containing CTL + targets + stimulus, was compared to the number of target cells in wells containing CTL + targets - stimulus. This allowed to calculate the percentage of live and dead target cells in each stimulus-containing well. The degranulation assay readout was analysed as explained in section 2.5.1, with the exception that beads were gated out in the first gate before FSC/SSC and subsequent gating.

2.5.3 Incucyte killing assay

CTLs were co-cultured with targets stably expressing a red nuclear marker (Essen Bioscience, #4625, see section 2.10) in ultralow attachment round-bottomed microplates (VWR, #7007). Cells were mixed at E:T 10:1 or E:T 2.5:1, as indicated in the figure legends. 2000-4000 targets with and without stimulus were plated per well and pelleted at 200xg for 2 min. The appropriate number of CTL, to give the desired E:T, were carefully added on top in order to leave the target cell pellet intact. Plates were briefly centrifuged at 200xg for 1 min, then transferred to an Incucyte S3 live cell analysis system (Essen Bioscience) maintained at 37 °C and 5% CO_2. Samples were imaged once an hour using the 4x objective. Target cell death was detected as loss of red fluorescence and was quantitated using the spheroid quantification tool (Incucyte S3 software). Results were exported and the percentage of target cell lysis over time in each well was calculated relative to the first time point measured.

2.5.4 LDH release killing assay

The CytoTox 96 Non-Radioactive Cytotoxicity Assay (Promega, #G1780) was used to quantitate the enzyme lactate dehydrogenase (LDH), which is released from the cytoplasm of cells upon cell death. The released LDH participates in an enzymatic reaction where a tetrazolium salt is converted into a red formazan product. The amount of cell death is proportional to the amount of red product formed.

The LDH killing assay was performed in a 96 well round bottom plate in killing assay media (RPMI - phenol red + 2%FBS + 100 U/ml pen, 0.1 mg/ml Strep). 100,000 CTLs were seeded per well in one row and serially diluted two fold down the plate. Next, drug

19/parthenolide (Medchem express, #HY-N0141), or equivalent amount of DMSO vehicle control, was added at a final concentration of 8.3 μM. Subsequently, 10,000 targets with stimulus or without stimulus (controls) were added per well, resulting in different E:T ratios ranging from 10:1 to 1.25:1. Samples were mixed by pipetting, centrifuged at 200xg for 1 min, then incubated for 3 h at 37 °C. Lysis buffer (Promega, #G1780) was added to positive control wells to lyse all cells 45 min before the end of the incubation period. After 3 h, samples were pelleted at 200 xg for 2 min and 50 μl supernatant was transferred into a 96 well flat bottom plate and mixed with 50 μl substrate mix (Promega, #G1780). After incubation for 30 min in the dark, absorbance at 490 nm was measured using a spectramax plate reader (Molecular devices) and Softmax software (Molecular devices). The cell death readout was determined by subtracting the absorbance of unstimulated (CTL + target) wells from their stimulated (CTL + targets + stimulus) equivalent, and dividing this number by the absorbance recorded in positive control wells containing lysis buffer. The percentage lysis was calculated by multiplying the resulting number by 100.

2.6 RNA preparation and sequencing

10 spleens were collected from 16 week old WT mice (4 males, 6 females) on two different spleen collection dates. Splenocytes were isolated as described under section 2.1.2. The mouse CD8a T cell isolation kit (Miltenyi Biotec, #130-104-075) was used to purify CD8 cells. 6x10^6 purified CD8 cells were pelleted, washed 2x in ice-cold DPBS and frozen at -80 °C (day 0 samples). An aliquot of each sample was used to determine the CD8 and CD4 expression profile by flow cytometric analysis. The remainder of the cells were transferred onto plates coated with 0.5 µg/ml αCD3ε (clone Bio500A2, eBioscience, #16-0033-86) and 1 µg/ml αCD28 (clone 37.51, eBioscience, #16-0281-86) and cultured as described under section 2.1.2. On day 7, the CD8 purity of each sample was again confirmed by flow cytometry. 6x10^6 cells per sample were pelleted, washed 2x in ice-cold DPBS and frozen at -80 °C (day 7 samples). This resulted in 10 biological replicates for both day 0 and day 7 time points.

RNA was extracted from the cell pellets following the manufacturer's protocol of the RNeasy mini kit (Qiagen, #74104). The concentration and quality of the extracted RNA were determined using a Qubit fluorometer (Thermo Fisher Scientific) and a bioanalyser (Agilent), respectively. A total of 1 μg of RNA per sample was submitted to the Illumina bespoke team at the Wellcome Trust Sanger Institute. The Illumina bespoke team prepared stranded 75

base pairs (bp) paired-end barcoded libraries with oligodT pulldown. For sequencing, all libraries were pooled across 3 different lanes on an llumina Hiseq platform.

2.7 RNA-seq analysis

The following bioinformatic analyses were performed with Martin Del Castillo Velasco-Herrera, following a published workflow (Anders et al., 2013): read alignment, fragment counting, quality control and differential expression analysis of day 7 vs day 0. Reads were aligned to the mouse reference genome (GRCm38) using STAR, a splice-aware mapper (Dobin et al., 2013), guided by the ENSEMBL mouse annotation v84. Htseq count (Anders et al., 2015) was used to count the number of total mapped and uniquely mapped reads. From this, the percent of uniquely mapped reads was determined. The raw counts were normalised by calculating the fragments (read pairs) per kilobase per million (FPKM) reads mapped. Quality control examinations were performed following the DESeq analysis vignette. This included unsupervised hierarchical clustering of samples and principal component analysis (PCA).

The DESeq2 Bioconductor package (Anders and Huber, 2010) was used to identify differentially expressed genes between day 7 and day 0 groups and between males and females within the day 7 group. The spleen collection date was included as a covariate in the analysis. P-values were corrected for multiple testing using the Benjamini-Hochberg method, giving an adjusted p-value (padj). Genes were considered differentially expressed with a padj <0.01 and a log2(fold change) <-2 or >2.

2.8 Toxicity testing and screening of the NF-κB compound library

The NF-κB signalling compound library was obtained from MedChem Express (#HY-L014). Compound toxicity was tested over a range of concentrations in hCTL. First, compounds were added to 96 well plates at 50 μM in duplicates or triplicates and serial threefold dilutions were performed down the plate. The appropriate amount of DMSO (Sigma, #D2650) vehicle control was included on every plate. An equal volume of media containing 125,000 hCTL was added to every well, which halved the concentration of drug. The final concentration range was between 25 μM and 0.1 μM. hCTLs were left to incubate with drugs or DMSO overnight.

The following day the Celltitre96 AQueous One Solution Cell Proliferation Assay (Promega, #G3580) was used to determine drug toxicity after overnight treatment. This kit contains an electron coupling reagent (phenazine ethosulfate, PES) and a tetrazolium compound, which is reduced into a coloured formazan product in metabolically active cells, meaning the quantity of coloured product detected at 490 nm is proportional to the number of live cells. 20 µl reagent were added per well and mixed thoroughly. The plates were incubated for 4 h at 37 °C in the dark, then absorbance at 490 nm was recorded using a spectramax plate reader (Molecular devices) and Softmax software (Molecular devices). hCTL were treated with compounds for 24 h in total. Concentration response curves were plotted using Prism software (Graphpad). For every drug, the highest concentration that did not have toxic effects on hCTLs over a 24 h period was chosen for screening using the combined degranulation and killing assay (section 2.5.2). Assays were performed in hCTL at day 13-15 post in vitro stimulation. Treatments with compounds was performed overnight. In every assay, target cells alone were treated with the compounds in order to test for any effects of the drugs on target cells.

For follow up of drug 19/parthenolide (Medchem express, #HY-N0141), hCTLs were treated with 2.075 - 8.3 µM drug 19/parthenolide for time periods indicated in figure legends followed by analysis using the Incucyte killing assay (section 2.5.3). hCTLs treated with 8.3 µM drug 19/parthenolide were also analysed using the LDH release killing assay (section 2.5.4) and the TNF-expression assay (section 2.4.2).

Additionally, the effect of 8.3 µM drug 19/parthenolide on LAMP1-exposure triggered by treating hCTLs with 4 µM phorbol 12-myristate 13-acetate (PMA) (Sigma, #P8139) and 1 µg/ml Ionomycin (Sigma, #IP657) was tested. PMA and Ionomycin were both prepared in DMSO and controls containing the appropriate amount of DMSO were included in every experiment. After treatment for 3 h in the presence of αhuman-LAMP1-PE (Table 2.7), cells were stained with αhuman-CD8-BV711 (Table 2.7) and the live/dead marker Zombie yellow (Table 2.6) for 30 min on ice. After washing in FACS buffer, samples were resuspended in FACS buffer before acquisition on Attune NxT (Thermo Fisher Scientific) or LSRFortessa (BD biosciences) flow cytometers. Results were analysed with FlowJo version 10.4.2 (FlowJo, LLC).

To investigate the effect of drug 19/parthenolide on p65 protein levels, hCTLs were treated with 8.3 µM drug 19/parthenolide, 4 µM PMA and 1 µg/ml Ionomycin or appropriate DMSO control for 3 h followed by WB lysate preparation (section 2.3.1).

2.9 Molecular cloning

The *Cas9* gene was amplified from the lenti Cas9-Blast vector (Addgene, #52962, see chapter 6 Figure 6.3 for plasmid map) using a forward primer containing upstream homology sequences to pHRSIN-mCherry (pHRSIN-mCh) and a XhoI restriction enzyme (RE) site and one of two different reverse primers. Reverse primer 1 contained a downstream BamHI RE site and homology region to pHRSIN-mCh. Reverse primer 2 contained a downstream P2A sequence, as well as the BamHI RE site and homology region to pHRSIN-mCh. The primer sequences are given in Table 2.8. The PCR mastermix used is given in Table 2.9 and the PCR conditions in Table 2.10.

Table 2.8 ***Overview of primers used in this thesis.*** *Primers were acquired from Sigma and resuspended in nuclease free water to give 100 μM stock solutions.*

Purpose	**Primer**	**Sequence 5' to 3'**
Cloning Cas9 into pHRSIN	Cas9-Fwd	GGGGATCTGGAGCTCTCGAGAAATGGACAAGAAGTACAGCATCGGCCTG
	Cas9-mCh-Rev	ATGGTGGCGACCGGTGGATCCCCCTTATCGTCATCGTCTTTGTAATCTTTCTTCTTCTTAG
	Cas9-2A-mCh-Rev	ATGGTGGCGACCGGTGGATCCCCCGGTCCAGGATTCTCTTCGACATCTCCGGCTTGTTT CAGCAGAGAGAAGTTTGTTGCCTTATCGTCATCGTCTTTGTAATCTTTCTTCTTCTTAG
Sequencing Cas9-Blast	Cas9-Blast Fwd	CCAAAGAGGTGCTGGACG
	Cas9-Blast Rev	GCTCTTTCAATGAGGGTGGA
Sequencing pHRSIN	pHRSIN_SFFV_Fwd	TGCTTCTCGCTTCTGTTCG
	pHRSIN_WPRE_Rev	CCACATAGCGTAAAAGGAGC
Sequence Cas9 fully	Cas9_1_Fwd	CTTCGGCAACATCGTGGA
	Cas9_1_Rev	GGTTCTTCTTGATGCTGTGC
	Cas9_2_Fwd	ACGACCTGGACAACCTGCT
	Cas9_2_Rev	CCGTCTGCTCTTGCTCAGTC
	Cas9_3_Fwd	GAAGATTTTTACCCATTCCTGAAG
	Cas9_3_Rev	TTGCTCTGGTCGAAGAAAATC
	Cas9_4_Fwd	AAATCTCCGGCGTGGAAG
	Cas9_4_Rev	CGCTCGATGAAGCTCTGG
	Cas9_5_Fwd	AGCCCCGCCATTAAGAAG
	Cas9_5_Rev	GCTGCTTCATCACTTTGTCGT
	Cas9_6_Fwd	GAGGTCGTGAAGAAGATGAAGAA
	Cas9_6_Rev	CGGGGTGTTCTTTCAGGAT
	Cas9_7_Fwd	GCAAGGCTACCGCCAAGT
	Cas9_7_Rev	TCAGCTTGTCATTCTCGTCGT
	Cas9_8_Fwd	GGCTACAAAGAAGTGAAAAAGGA
	Cas9_8_Rev	GTCTGCACCTCGGTCTTTTTC
	Cas9_9_Fwd	GTACACCAGCACCAAAGAGGT
	Cas9_9_Rev	AGCTGTTTCTGCTCATTATCCTC
	Cas9_10_Fwd	AAGGCTGGACAGGCTAAGAA
	Cas9_10_Rev	CGACATCTCCGGCTTGTTT

Table 2.9 ***PCR mastermix composition for Cas9 amplification from the Cas9-Blast plasmid.***

Reagents	**μl/reaction**
10X Pfx reaction mix	5 μl
10 μM Fwd primer	1.5 μl
10 μM Rev primer	1.5 μl
10 ng/μl template DNA	1 μl
Accuprime Pfx DNA polymerase	0.4 μl
$MgSO_4$	1 μl
Nuclease free water	39.6 μl

Agarose gels were prepared by adding the desired amount of agarose (Sigma, #A9539) to Tris-acetate-EDTA (TAE) buffer (CIMR media kitchen). This mixture was heated in the microwave to mix and allowed to cool before addition of gel red (Biotium, #41003, final dilution 1:10,000). PCR products were mixed with Orange loading dye (Thermo Fisher Scientific, #SM1173) and run alongside O'gene ruler DNA ladder mix (Thermo Fisher Scientific, #SM1173) on a 0.7% (w/v) agarose gel in 1x TAE buffer (CIMR media kitchen). 5 μg of pHRSIN-mCh plasmid was digested with 1x fast digest green buffer (Thermo Fisher Scientific, #B72), 1 μl alkaline phosphatase (Sigma, #11097075001), 1 μl XhoI (Thermo Fisher Scientific, #FD0694), 1 μl BamHI (Thermo Fisher Scientific, #FD0055) and topped up to 50 μl with nuclease free H_2O. The digest was performed at 37 °C overnight and products were separated on a 0.7% agarose gel. The expected size of the PCR products were 4220 bp for the Cas9 construct and 4278 bp for the Cas9+P2A construct. The expected size of pHRSIN digested with XhoI and BamHI was 9665 bp.

Table 2.10 ***PCR conditions for amplification of Cas9 from the Cas9-Blast plasmid.*** *Cas9 was amplified from the Cas9-Blast plasmid and XhoI and BamHI restriction enzyme sites as well as homology regions to the pHRSIN plasmid were added.*

	Step	Temperature and time
Cycle 5 times	denaturation	95 °C for 15 sec
	annealing	59 °C for 30 sec
	elongation	68 °C for 4 min 20 sec
Cycle 35 times	denaturation	95 °C for 15 sec
	annealing and elongation	68 °C for 4 min 20 sec

Both PCR products and the digested plasmid were extracted from gels using the QIAquick gel extraction kit (Qiagen, #28704). 100 ng recipient vector and 2x excess insert were mixed with the Gibson Assembly mastermix (New England Biolabs, #E2611S) and topped up with nuclease free H_2O to 20 μl per reaction. This mix was kept for 1 h at 50 °C on a heatblock, then transferred to ice for 3 min before addition to NEB 10-beta *E.coli* (New England Biolabs, #C3019H).

2 μl of the gibson product were added to NEB 10-beta *E.coli*, mixed by flicking 5 times and allowed to recover for 30 min on ice. Subsequently, *E.coli* were heatshocked for 30 sec at 42 °C, then placed on ice for 5 min before addition of 950 μl super optimal broth with catabolite repression (SOC) media. After rotating at 250 rpm for 60 min at 37 °C, 100-150 μl of bacteria were streaked out onto Luria-Bertani (LB) agar plates containing 100 µg/ml ampicillin (CIMR media kitchen), and left to grow at 37 °C overnight. 8 individual colonies were picked per plate (plate 1 = XhoI-Cas9-BamHI plasmid, plate 2 = XhoI-Cas9-2A-BamHI plasmid) and expanded while shaking at 230 rpm and 37 °C for two days in 4 ml ampicillin containing media (LB media + 100 µg/ml ampicilin). Plasmids were purified using the QIAprep Spin Miniprep kit (Qiagen, #27106).

A restriction digest was performed with 1x fast digest green buffer (Thermo Fisher Scientific, #B72), 1 μl XhoI (Thermo Fisher Scientific, #FD0694), 1 μl BamHI (Thermo Fisher Scientific, #FD0055) and 5 μl of DNA from the miniprep, topped up to 25 μl with nuclease free H_2O. Resulting products were separated on a 0.7% (w/v) agarose gel for size confirmation. This allowed isolation of colonies that contained intact XhoI and BamHI RE sites and an insert corresponding to the *Cas9* gene in size. Sequencing by Source BioScience confirmed that *Cas9* was correctly inserted. These cultures were expanded to 250 ml, and plasmids were purfied using Qiafilter plasmid maxiprep kit (Qiagen, #12263). DNA concentration and purity was determined using a DS-11 spectrophotometer (DeNovix). Primers were designed roughly every 400 bp along the *Cas9* gene to be able to sequence it fully (Table 2.8) and the correct sequence was confirmed by sanger sequencing carried out by Source BioScience. Plasmid maps of the resulting pHRSIN-Cas9-mCh and pHRSIN-Cas9-2A-mCh were prepared using snapgene (GSL Biotech).

2.10 Nuclight red lentiviral transduction

The nuclight red lentivirus (Essen bioscience, #4625, #lot611110) encodes a nuclear-restricted red fluorescent protein (mKate2) and a puromycin resistance gene. P815 and

blue EL4s were transduced with nuclight red lentivirus at a low multiplicity of infection (MOI) of 0.07 in the presence of 6 µg/ml protamine sulfate. Cells expressing mKate2 were isolated by FACS, as explained in section 2.4.3, and subsequently cells were cultured in the presence of 1 µg/ml puromycin (see section 2.1.4).

2.11 pHRSIN lentiviral production and transduction

The following conditions were used to produce lentivirus with pHRSIN-GFP (for plasmid map see Appendix A, Figure A.1), pHRSIN-mCh (for plasmid map see chapter 6, Figure 6.3), pHRSIN-Cas9-mCh (for plasmid map see chapter 6, Figure 6.4) and pHRSIN-Cas9-2A-mCh (for plasmid map see chapter 6, Figure 6.4) plasmids. The pHRSIN-GFP plasmid was a gift from Adrian Thrasher (Institute of Child Health). The pHRSIN-mCh plasmid (James and Vale, 2012) was a gift from John James (MRC Laboratory for Molecular Biology). pCMVδ8.91 (packaging plasmid, for plasmid map see Appendix A, Figure A.2) and pMD-G (encoding the viral envelope protein VSV-G, for plasmid map see Appendix A, Figure A.3) plasmids were a gift from Paul Lehner's lab (Cambridge Institute for Medical Research).

HEK293Ts were seeded in T75 flasks so they reached 70% confluency overnight. The next day, the following 2 tubes were prepared for each T75: Tube 1 contained 1.5 ml Opti-MEM (Gibco, #31985-047), 30 μl 1M HEPES (Gibco, #15630-080) and 42 μl TransIT 293 reagent (Mirus, #MIR2700). Reagents were mixed and incubated at RT for 5 min. Tube 2 contained 4 μg pCMVδ8.91, 4 μg pMD-G and 6 μg of the desired pHRSIN plasmid. The contents of tube 1 were added dropwise to tube 2 and mixed gently by bubbling air through a pipette boy held under the liquid for 1 min. After incubation for 15 min at RT, 12 ml pre-warmed HEK media were added slowly. This mix was added dropwise to HEK293Ts and cells were transferred to a 37 °C incubator. Viral supernatant was collected after 48 h and 72 h. The supernatant was centrifuged at 500xg for 10 min and filtered through a 0.45 μM pvdf filter to remove cell debris. Next, the viral supernatant was concentrated by incubation with lenti-X (Takara Clontech, #631232) for 1 h at 4 °C at a lenti-X-to-viral supernatant ratio of 1-to-3 . After centrifugation at 1500xg for 45 min at 4 °C, the viral pellet from one T75 was resuspended in 100 μl ice-cold hTCM. This effectively resulted in a 100-120X more concentrated lentivirus. Concentrated lentivirus was aliquoted and stored at -80 °C.

The following conditions were used to transduce cell lines with pHRSIN-Cas9 lentiviruses: For transduction of P815s, 2x10^6 P815s were resuspended in target cell media containing 6 µg/ml protamine sulfate (Sigma, #P4020) and 100 μl concentrated pHRSIN-Cas9-2A-mCh

or pHRSIN-Cas9-mCh lentivirus. For transduction of YTs, 1x10^6 cells were resuspended in YT media containing 6 µg/ml protamine sulfate and 55 μl concentrated pHRSIN-Cas9-2A-mCh lentivirus. For transduction of Jurkats, 1x10^6 cells were resuspended in Jurkat media containing 6 µg/ml protamine sulfate and 45 μl concentrated pHRSIN-Cas9-2A-mCh lentivirus.

For transduction of primary human T cells with pHRSIN-GFP or pHRSIN-mCh lentiviruses, 1x10^6 T cells were resuspended in 300 μl hTCM containing lentivirus and 6 µg/ml protamine sulfate or lentiboost (1 in 100 dilution, meaning 8 µg/ml reagent A and 1 mg/ml reagent B, Sirion Biotech, #SB-P-LV-101-01), as indicated in figure legends. Cells were incubated in this small volume in one well of a 24 well plate for 4 h at 37 °C. After 4 h, wells were topped up to 2 ml with hTCM containing 1x10^6 irradiated allogeneic PBMCs and 1 μg/ml PHA.

Before transduction of primary human T cells with pHRSIN-Cas9-2A-mCh lentivirus the viral titre was determined by transducing Jurkat cells. 0.2x10^6 Jurkats were infected with varying volumes of concentrated lentivirus (between 50 μl and 0.05 μl) in a total volume of 2.5 ml Jurkat media containing 6 µg/ml protamine sulfate. The lentiviral titre was determined as outlined in Figure 6.7. The number of transduced cells was multiplied by the percentage of fluorescent cells and the dilution factor. The resulting number was divided by the transduction volume to give the number of transducing units (TU) per ml. For transductions, primary human T cells were activated on plates coated with 1 µg/ml αCD3ε (clone OKT3, eBioscience, #14-0037-82) and 2 µg/ml αCD28 (clone CD28.2, BD Biosciences, #555726). The next day, T cells were transduced with pHRSIN-Cas9-2A-mCh lentivirus at an MOI of 1.17 in the presence of 6 µg/ml protamine sulfate or lentiboost (1 in 100 dilution, Sirion Biotech, #SB-P-LV-101-01), as an alternative transduction enhancer.

2.12 Cas9-Blast lentiviral production and transduction

The virapower packaging mix (Thermo Fisher Scientific, #K497500) was used for lentiviral production with the lenti Cas9-Blast plasmid (Addgene, #52962), a gift from Professor Feng Zhang (Massachusetts Institute of Technology). HEK293T were seeded in T75 flasks so they reached 70% confluency overnight. The next day, the following 2 tubes were prepared for each T75: Tube 1 contained 1.5 ml Opti-MEM, 9 μg virapower, 3 μg lenti Cas9-Blast and 12 μl plus reagent (Thermo Fisher Scientific, #15338100). Tube 2 contained 1.5 ml Opti-MEM containing 36 μl lipofectamine LTX (Thermo Fisher Scientific, #15338100). Both tubes were incubated at RT for 5 min, then mixed together and incubated for a further 30 min at

RT. HEK293T media was removed and replaced with 5 ml Opti-MEM. Subsequently, the DNA-lipofectamine mix was added to the cells and left overnight. The following day, the cell culture supernatant was removed and replaced with HEK media. Viral supernatant was collected after 48 h and 72 h and concentrated using ultracentrifugation (SW-28 swinging-bucket rotor, Beckmann) at 25,000 rpm for 90 min at 4 °C. The resulting viral pellets were resuspended in 200 μl ice-cold DPBS + 1% FBS per flask, aliquoted and stored at −80 °C.

For transduction of primary T cells, 3x10^6 cells were resuspended in concentrated lentivirus from one T75 containing 6 µg/ml protamine sulfate. Samples were centrifuged at 754xg for 15 min at 32 °C. 1x10^6 cells were aliquoted per well in a 24 well plate and topped up to 2 ml with hTCM containing 1x10^6 irradiated allogeneic PBMC and 1 μg/ml PHA. Selection with 5 µg/ml Blasticidin was started on day 6 post transduction.

2.13 PCR for Cas9-Blast

DNA was extracted from frozen pellets of HEK293T cells transduced with Cas9-Blast lentivirus (10,000 cells) or treated with protamine sulfate alone (0.25x10^6 cells) and from frozen pellets of hCTL transduced with Cas9-Blast lentivirus (0.45x10^6 cells) or treated with protamine sulfate alone (1.3x10^6 cells). Each pellet was resuspended in 200 μl of DNA extraction buffer. 1 ml DNA extraction buffer contained 975 μl 10% (w/v) Chelex 100 chelating resin (Bio-Rad, #1421253) diluted into nuclease-free H_2O, 10 μl 10% (v/v) Tween 20 (Sigma, #P1379) and 15 μl proteinase K (Sigma, #P8044). The resulting samples were incubated at 50 °C for 90 min, followed by heating at 95 °C for 25 min and then cooled to RT.

PCR was used to test for the presence of Cas9-Blast in the extracted DNA. PCR was performed with primers targeting a region between the 3' end of the *Cas9* gene and the blasticidin resistance gene (Table 2.8), producing a product of 274 bp. PCR was performed using the mastermix outlined in Table 2.11 and the conditions outlined in Table 2.12. Negative controls including nuclease-free water instead of DNA were included in the PCR reaction.

Table 2.11 ***PCR mastermix for Cas9-Blast PCR.*** *PCR mastermix for amplifying a stretch of DNA between Cas9 and the Blasticidin resistance gene in the Cas9-Blast plasmid.*

Reagents	**μl/reaction**
10X PCR buffer	2.5 μl
50 nM $MgCl_2$	0.75 μl
10 mM dNTP mix	0.5 μl
Fwd primer	0.5 μl
Rev primer	0.5 μl
Platinum taq DNA polymerase	0.1 μl
Template DNA	1 μl
Nuclease free water	18.75 μl

Table 2.12 ***PCR conditions for Cas9-Blast PCR.*** *PCR conditions to amplify a stretch of DNA between Cas9 and the Blasticidin resistance gene in the Cas9-Blast plasmid.*

	Step	**Temperature and time**
Cycle 35 times	initial denaturation	94 °C for 2 min
	denaturation	94 °C for 30 sec
	annealing	58 °C for 30 sec
	elongation	72 °C for 30 sec

The resulting PCR products were separated on a 1.5% (w/v) agarose gel, prepared as explained in section 2.9. Gel extraction was performed with the QIAquick gel extraction kit (Qiagen, #28704) and DNA concentration was determined using a DS-11 spectrophotometer (DeNovix). Sanger sequencing to confirm the sequence of the PCR product was performed by Source BioSciences.

2.14 Statistical analysis

Graphs were created and statistical analyses were performed using Prism 7 (GraphPad Software). The statistical tests used are stated in every figure legend and where relevant in the text. Statistical analysis was only performed on data obtained from three or more independent experiments. Paired t-tests were applied for statistical analysis of degranulation and killing assay results. Samples were paired according to the days that the experiments

were performed, in order to account for any day-to-day variations. Statistical analysis of WB results was performed using one sample t-tests. For all other comparisons, unpaired t-tests with Welch's correction, which does not assume equal standard deviations (SD), were performed. For all statistical analyses, differences between samples were considered statistically significant if $p<0.05$.

Chapter 3

Establishing the CRISPR-Cas9 technology in primary mouse T cells

3.1 Introduction

Before the advent of CRISPR, gene expression was primarily modulated using siRNAs, which trigger degradation of mRNA (Dorsett and Tuschl, 2004). The effect of siRNAs is transient and often results in only partial protein knockdown. In contrast, CRISPR has the potential to stably and homozygously KO genes, resulting in permanent loss of gene function. While the siRNA technique was previously established in CTLs (Stinchcombe et al., 2015), the CRISPR technology was yet to be tested in primary mouse CTLs at the start of this project.

To test whether gene manipulation technologies are working as expected it is desirable to use target genes where the KO has a known CTL phenotype. Studies of patients suffering from immunodeficiency diseases have identified several suitable genetic targets. For example, mutations in *RAB27A* can cause GS2 in humans (Clark and Griffiths, 2003). This disease is the consequence of RAB27A deficient CTL not being able to kill target cells due to a degranulation defect. A study using CTL derived from *Rab27a* KO mice showed that while lytic granules polarise towards the immunological synapse, they cannot be secreted (Stinchcombe et al., 2001a). This indicated that RAB27A is involved in the final stages of granule secretion. Similarly, mutation of *MUNC13-4* causes FHL3 due to a degranulation defect (Bossi and Griffiths, 2005; Dieckmann et al., 2016; Feldmann et al., 2003). In fact, RAB27A and MUNC13-4 interact with one another in this process (Neeft et al., 2005). Perforin is another protein with a well understood function in CTL cytotoxicity. Perforin defective CTL are unable to kill target cells, causing the immunodeficiency disease FHL2

(Stepp et al., 1999). These immunodeficiency diseases demonstrate the importance of correct CTL function.

3.1.1 Chapter aims

- Test the robustness of the degranulation assay and adapt it for screening.
- Manipulate gene expression in primary mouse CTLs using siRNA.
- Optimise the CRISPR-Cas9 technology in primary mouse CTLs.
- Use the CRISPR-Cas9 technology in primary mouse CTLs to target genes where the KO has a known phenotype in the degranulation assay.

3.2 Results

3.2.1 The effect of *Rab27a* depletion on CTL degranulation

CTLs derived from the *ashen* mouse model, where a mutation in *Rab27a* results in loss of protein expression, cannot kill target cells as they are unable to release their granule content (Stinchcombe et al., 2001a; Wilson et al., 2000). CTLs derived from *ashen* mice were tested in a degranulation assay, which measures lytic granule secretion by the appearance of the granule membrane component LAMP1 on the extracellular surface (Figure 3.1). The exposed extracellular LAMP1 can be bound by a fluorescently-conjugated antibody to allow robust detection and quantification of the amount of degranulation by flow cytometry. Figure 3.1A shows the gating strategy typically used in degranulation experiments. The LAMP1 gate was set so that the signal in the experimental control, which were unstimulated CTLs, was less than 1%. The percentage of degranulated (LAMP1-PE) positive cells was determined after 45 min, 90 min and 180 min. CTLs derived from homozygous (hom, *ash/ash*) *ashen* mice degranulated significantly less than CTLs derived from heterozygous (het, *+/ash*) *ashen* mice or WT (+/+) mice (Figure 3.1B-D) [45 min (n=2), 90 min (n=2) and 180 min (n=3, $p<0.05$, paired t-test)]. RAB27A protein expression in CTLs derived from WT, het and hom *ashen* mice was tested by WB, confirming that hom *ashen* CTL did not express RAB27A protein (Figure 3.1E).

Due to the robust loss of degranulation observed in *ashen* CTL, *Rab27a* provided a suitable target to test whether manipulation of gene expression in CTLs derived from WT

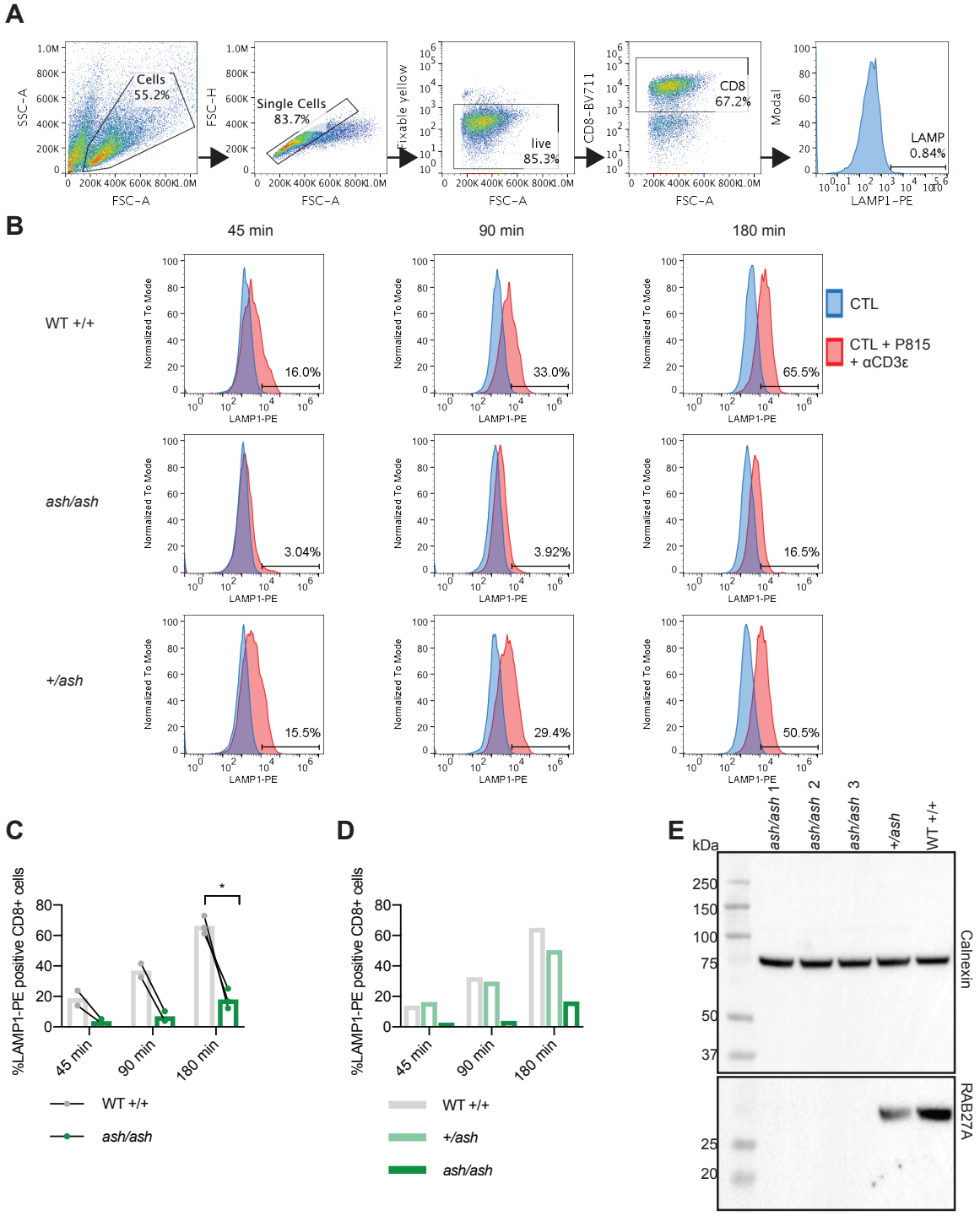

Fig. 3.1 ***Degranulation defect in CTL derived from ashen mice.***

Fig. 3.1 ***Degranulation defect in CTL derived from ashen mice.*** ***A*** *Degranulation assays were analysed using the following gating strategy: initial gate to separate the cell population from debris, second gate to isolate single cells from doublets, third gate to isolate live cells from dead cells, fourth gate to isolate CD8-positive cells and a final gate to isolate LAMP1-PE positive cells.* ***B*** *CTLs were derived from WT (+/+), het (+/ash) or hom (ash/ash) ashen mice. At day 6-7 after in vitro stimulation CTLs were tested for their ability to degranulate in response to exposure to αCD3ε-loaded P815 target cells. Representative histograms for CTLs incubated on their own (blue histograms) or mixed at an E:T ratio of 1:1 with αCD3ε-loaded P815 target cells (red histograms) for 45 min, 90 min or 180 min are shown.* ***C*** *Average degranulation result. During each independent repeat the experiment was performed at least in technical duplicates, n=2/3 independent experiments, * p<0.05 calculated by paired t-test. Samples were paired by day of experiment.* ***D*** *One experiment from C that included CTL from het (+/ash) ashen mice.* ***E*** *Western blot showing RAB27A and calnexin (loading control) protein expression in cells derived from WT (+/+), hom (ash/ash) and het (+/ash) ashen mice. WT = wild-type, het = heterozygous, hom = homozygous.*

mice could decrease degranulation. Initially, this was attempted using a pool of siRNAs targeting Rab27a mRNA, as the siRNA technique was already established in the Griffiths lab (Stinchcombe et al., 2015). CTLs were tested for their ability to degranulate one day after nucleofection with Rab27a siRNA or scramble control siRNA. Rab27a siRNA nucleofection significantly decreased degranulation at all time points tested [45 min (n=8, $p<0.05$, paired t-test), 90 min (n=8, $p<0.001$, paired t-test) and 180 min (n=8, $p<0.01$, paired t-test)] (Figure 3.2A-B). However, the decrease was not as striking as observed with *ashen* CTL (Figure 3.1). WB showed that RAB27A protein levels were never fully depleted, but reproducibly decreased, in response to siRNA treatment (Figure 3.2C-D) (n=7, $p<0.01$, one sample t-test).

As treatment with 3 μg siRNA did not fully deplete RAB27A protein levels after one day, protein levels were tested 2 and 3 days post nucleofection. However, longer treatment time did not reduce RAB27A protein further (Figure 3.3A). Additionally, RAB27A protein levels were not further decreased when the amount of siRNA was doubled (to 6 μg) (Figure 3.3B). In a final attempt to improve the loss of RAB27A protein, CTLs were transfected with 3 μg siRNA and left to recover for two days before a second transfection with 3 μg siRNA (Figure 3.3C). However, this 'double hit' did not deplete RAB27A protein further than treatment with 3 μg siRNA for one day (Figure 3.2D and Figure 3.3A).

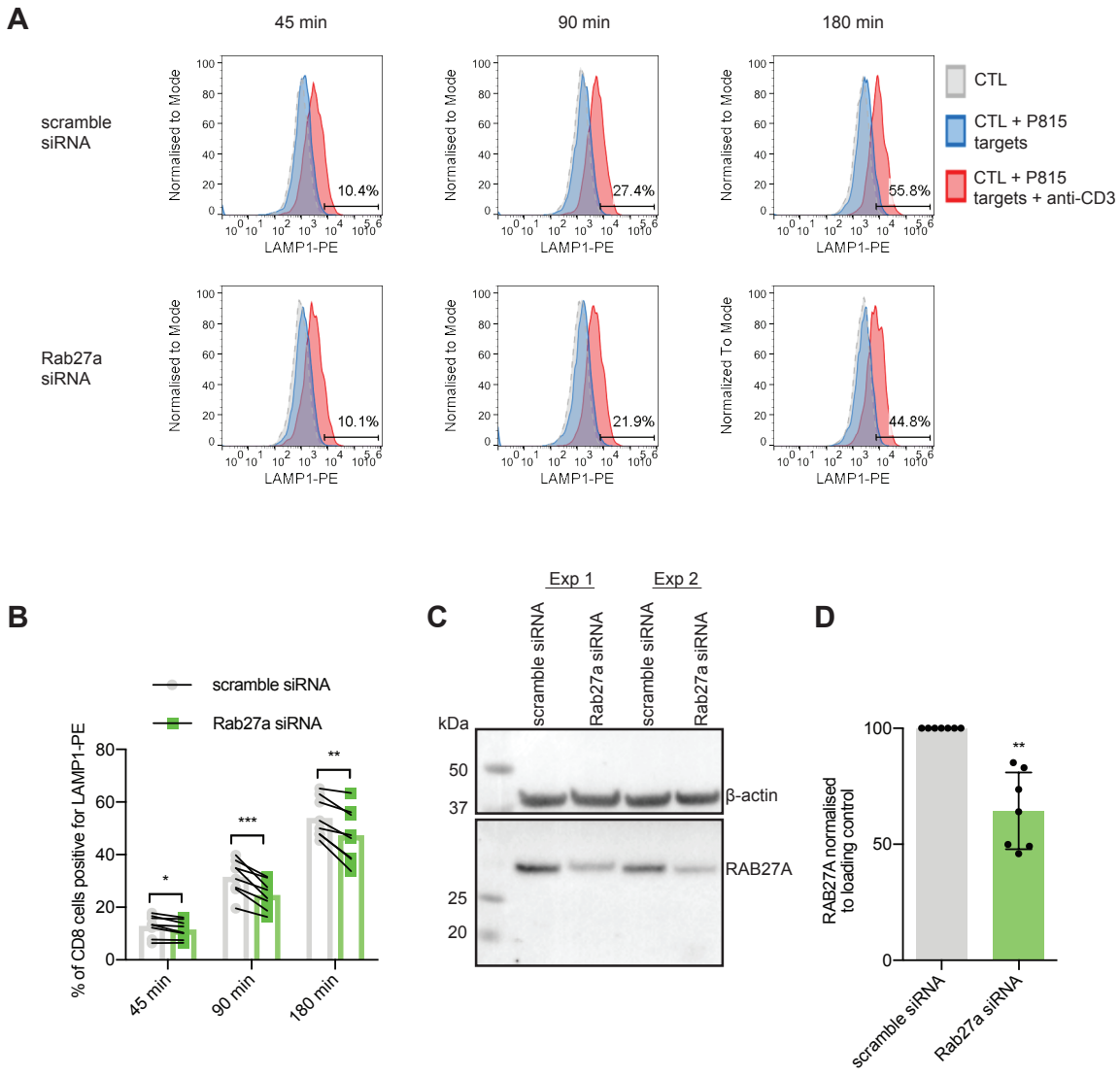

Fig. 3.2 ***RAB27A knockdown in WT mouse CTLs decreased degranulation.***

Fig. 3.2 ***RAB27A knockdown in WT mouse CTLs decreased degranulation.*** ***A*** *CTLs were nucleofected with 3 µg scramble siRNA or 3 µg Rab27a siRNA at day 5-7 after in vitro stimulation. Degranulation assays were performed the following day. Representative histograms for unstimulated CTL (grey), CTL co-cultured with P815 target cells (blue) and CTL co-cultured with αCD3ε-loaded P815 target cells (red) are shown. Degranulation was measured by extracellular exposure of LAMP1 after 45 min, 90 min and 180 min. Degranulation assays were analysed using the following gating strategy: initial gate to separate the cell population from debris, second gate to isolate single cells from doublets, third gate to isolate live cells from dead cells, fourth gate to isolate CD8-positive cells and a final gate to isolate LAMP1-PE positive cells.* ***B*** *Average degranulation result, each independent experiment was performed at least in technical duplicates. n=8 independent experiments, *p<0.05, **p<0.01, ***p<0.001 calculated by paired t-test according to the days the experiments were performed on.* ***C*** *Western blot showing RAB27A and β-actin (loading control) protein expression one day after scramble or Rab27a siRNA nucleofection in two independent experiments.* ***D*** *Average RAB27A protein knockdown achieved. In each repeat the RAB27A protein level was expressed relative to the RAB27A level in the respective scramble siRNA sample and normalised to calnexin or β-actin loading controls. Bar graphs show the mean, error bars show the SD, n=7 independent experiments, **P<0.01 calculated by one sample t-test. exp = experiment.*

3.2.2 Optimising the CRISPR technology in primary mouse CTL

Rab27a was established as a good genetic target to test CRISPR, as a decrease in degranulation could be observed despite only partial protein depletion. However, for the initial set up of the CRISPR technique in CTL it would be desirable to be able to monitor KO efficiency at single cell resolution, rather than using a technique like WB, which measures a bulk population. Therefore, CRISPR was used to target the cell surface protein Thy1.2 (also known as CD90.2), referred to as Thy1 from now on. Thy1 is a glycosylphosphatidylinositol-anchored cell surface protein, which is abundantly expressed in mouse T cells (Haeryfar and Hoskin, 2004; Killeen, 1997). Due to the extracellular expression of Thy1 and the availability of good antibodies it can be easily monitored at single cell resolution using flow cytometry (Doench et al., 2014).

CTLs were derived from homozygous Cas9 mice (Tzelepis et al., 2016) and nucleofected with synthetic crRNAs and tracrRNAs. The concentration of 3 µg used for siRNA experiments was used as a starting point for a concentration response with the CRISPR RNAs. The

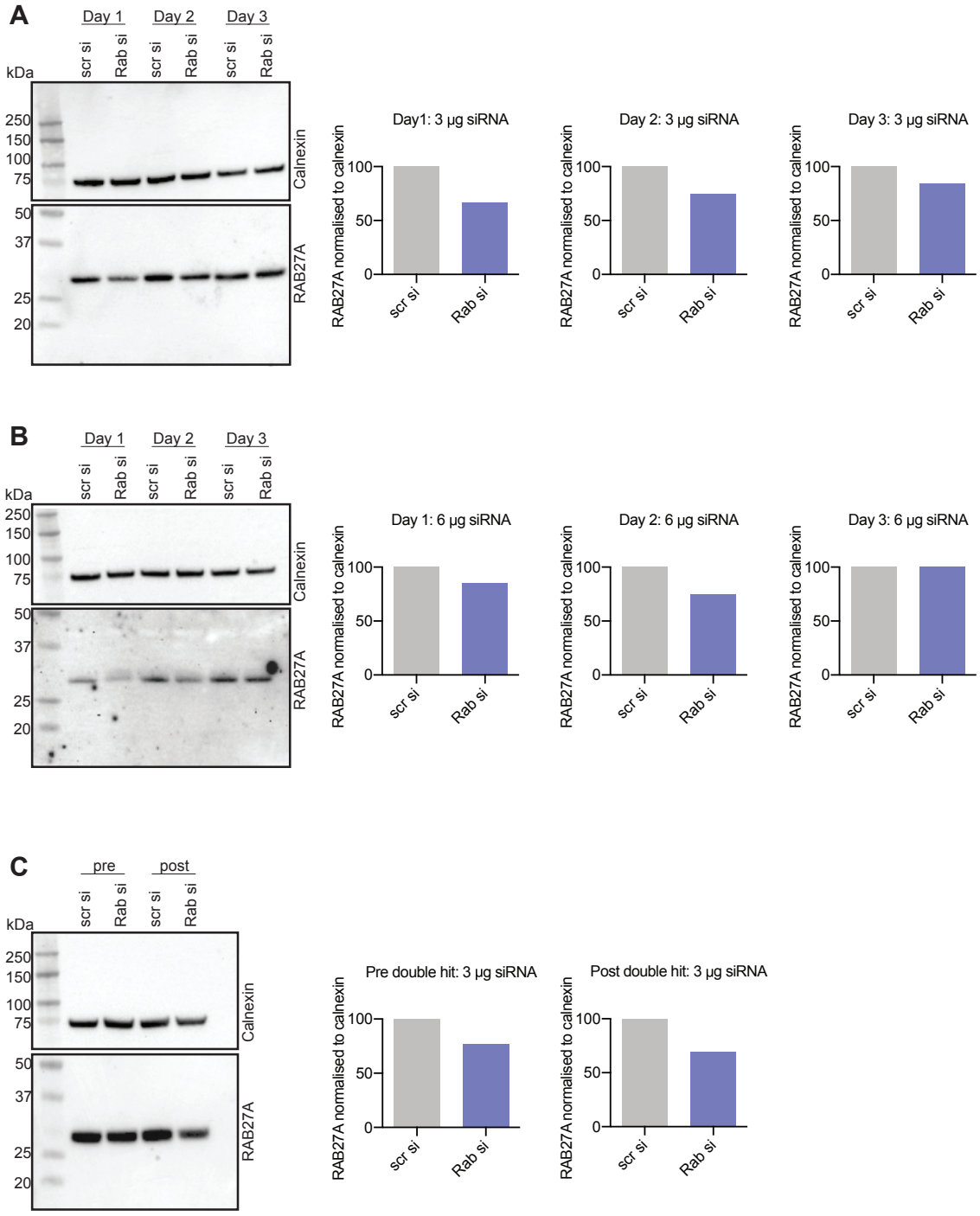

Fig. 3.3 ***Optimisation of RAB27A knockdown in WT mouse CTL.***

Fig. 3.3 ***Optimisation of RAB27A knockdown in WT mouse CTL. A*** *CTLs were nucleofected with 3 µg scramble siRNA or 3 µg Rab27a siRNA and RAB27A protein expression was monitored by WB over 3 days, n=1 for each time point.* ***B*** *CTLs were nucleofected with 6 µg scramble siRNA or 6 µg Rab27a siRNA and RAB27A protein expression was monitored by WB over 3 days, n=1 for each time point.* ***C*** *CTLs were nucleofected with 3 µg scramble siRNA or 3 µg Rab27a siRNA . Two days later, the same cells were nucleofected again with 3 µg scramble siRNA or 3 µg Rab27a siRNA. RAB27A protein expression was monitored by WB before and after the siRNA double hit, n=1 for each time point. In all experiments, RAB27A protein levels were normalised to calnexin (loading control) and expressed relative to the RAB27A level in the respective scramble siRNA sample. scr si = scramble siRNA, Rab si = Rab27a siRNA.*

expression of Thy1 on the cell surface of CD8 T cells was monitored by flow cytometry over 5 consecutive days (Figure 3.4A). Toxicity was sometimes observed in response to nucleofecting 10 μg crRNA reagents, as demonstrated by less events recorded in the 10 μg *Thy1* crRNA sample in Figure 3.4A. While almost all samples were 100% positive for Thy1 at day 1 post nucleofection, by day 2 post nucleofection a decrease in the Thy1-positive population could be observed in the samples nucleofected with *Thy1* CRISPR reagents. The Thy1 levels in samples nucleofected with a non-targeting control crRNA remained unchanged. The decrease became more prominent at day 3 post nucleofection, and was stably maintained up until the final time point measured (day 5 post nucleofection). The greatest decrease in the Thy1 positive population was observed with 10 μg crRNA/tracrRNA (average decrease of 41.6% at day 5 post nucleofection), closely followed by 5 μg crRNA/tracrRNA (average decrease of 33.3% at day 5 post nucleofection) and then 3 μg crRNA/tracrRNA (average decrease of 28.8% at day 5 post nucleofection) (Figure 3.4B). To avoid toxic side effects and overloading the cells with RNA, while also giving the highest chance of generating KOs, 5 μg crRNA/tracrRNA was chosen as the amount to use in future experiments.

While KO of Thy1 using the approach outlined in Figure 3.4 worked reproducibly, it depended on the availability of Cas9 homozygous mice. While these experiments were being conducted, another study was published that used Cas9 protein alongside synthetic crRNA/tracrRNA (forming RNP complexes) in human T cells (Schumann et al., 2015). Co-nucleofection of Cas9 protein alongside crRNA and tracrRNA was tested in cells derived from OT-I mice, which were readily available in the Griffiths lab. OT-I mice express TCRs that recognise the OVA peptide in the context of H-2K^b MHC class I molecules (Hogquist

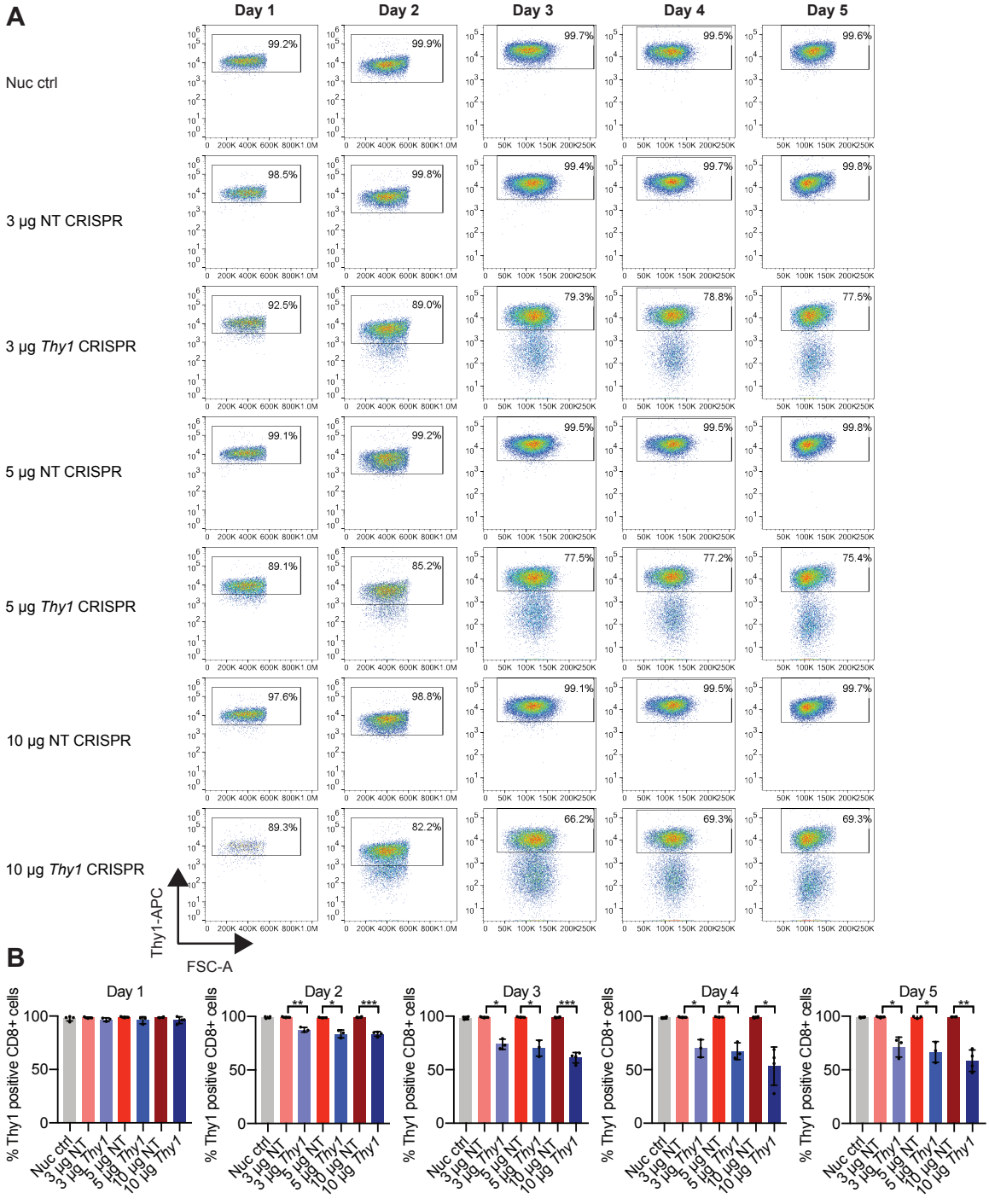

Fig. 3.4 ***CrRNA and tracrRNA concentration response and time course.***

Fig. 3.4 ***CrRNA and tracrRNA concentration response and time course. A*** *Cas9 hom CTLs were nucleofected with the indicated amount of non-targeting or Thy1 crRNA, in addition to the identical amount of tracrRNA at day 5-7 after in vitro stimulation. Additionally, a nucleofection control was included, where CTLs were nucleofected but not exposed to any RNA. Thy1 cell surface protein levels were monitored by flow cytometry over 5 days and analysed using the following gating strategy: initial gate to seperate cell population from debris, second gate to isolate single cells from doublets, third gate to isolate live cells from dead cells, fourth gate to isolate CD8-positive cells and a final gate to determine the percentage of Thy1 positive cells. The Thy1 gate was set according to the appropriate nucleofection control for every time point.* ***B*** *Average of Thy1 cell surface expression in CD8 cells over the course of 5 days, n=4 independent experiments for nuc ctrl, 10 µg NT and 10 µg Thy1 samples, n=3 independent experiments for all other samples. Bar graphs show the mean, error bars the SD, *p<0.05, **p<0.01, ***p<0.001 calculated by unpaired t-test with Welch's correction. Nuc ctrl = Nucleofection control, NT = non-targeting.*

et al., 1994). OT-I were nucleofected with 5 µg *Thy1* crRNA/tracrRNA and varying amounts of Cas9 protein (Figure 3.5A). As in Figure 3.4 the cell surface expression of Thy1 was monitored by flow cytometry over 5 consecutive days. Again, a decrease in the Thy1-positive population could be observed in the samples nucleofected with *Thy1* CRISPR reagents, but not in cells nucleofected with non-targeting control crRNA (Figure 3.5A). This decrease was stably maintained up until the final time point (day 5 post nucleofection). The greatest decrease in the Thy1 positive population was observed with 10 µg Cas9 (average decrease of 64.7% at day 5 post nucleofection), followed by 5 µg Cas9 (average decrease of 44.9% at day 5 post nucleofection) and then 2.5 µg Cas9 (average decrease of 29.5% at day 5 post nucleofection) (Figure 3.5B). Therefore, 10 µg Cas9 protein was chosen as the amount to use in future experiments.

To understand why *Thy1* KO was more efficient using Cas9 protein than using CTLs derived from Cas9 homozygous mice, Cas9 protein levels in samples derived from Cas9 hom mice or conditions outlined in Figure 3.5 were investigated. Cas9 levels were much higher in samples one day after nucleofection with 5 µg or 10 µg of Cas9 protein than in the samples derived from Cas9 homozygous mice (Figure 3.6A-B). Additionally, I tested whether using 20 µg Cas9 protein further increases KO efficiency, but this was not the case (Figure 3.6C). Finally, Cas9 levels were monitored over 3 days post nucleofection of Cas9 protein, demonstrating that the nucleofected Cas9 protein is only present transiently in cells,

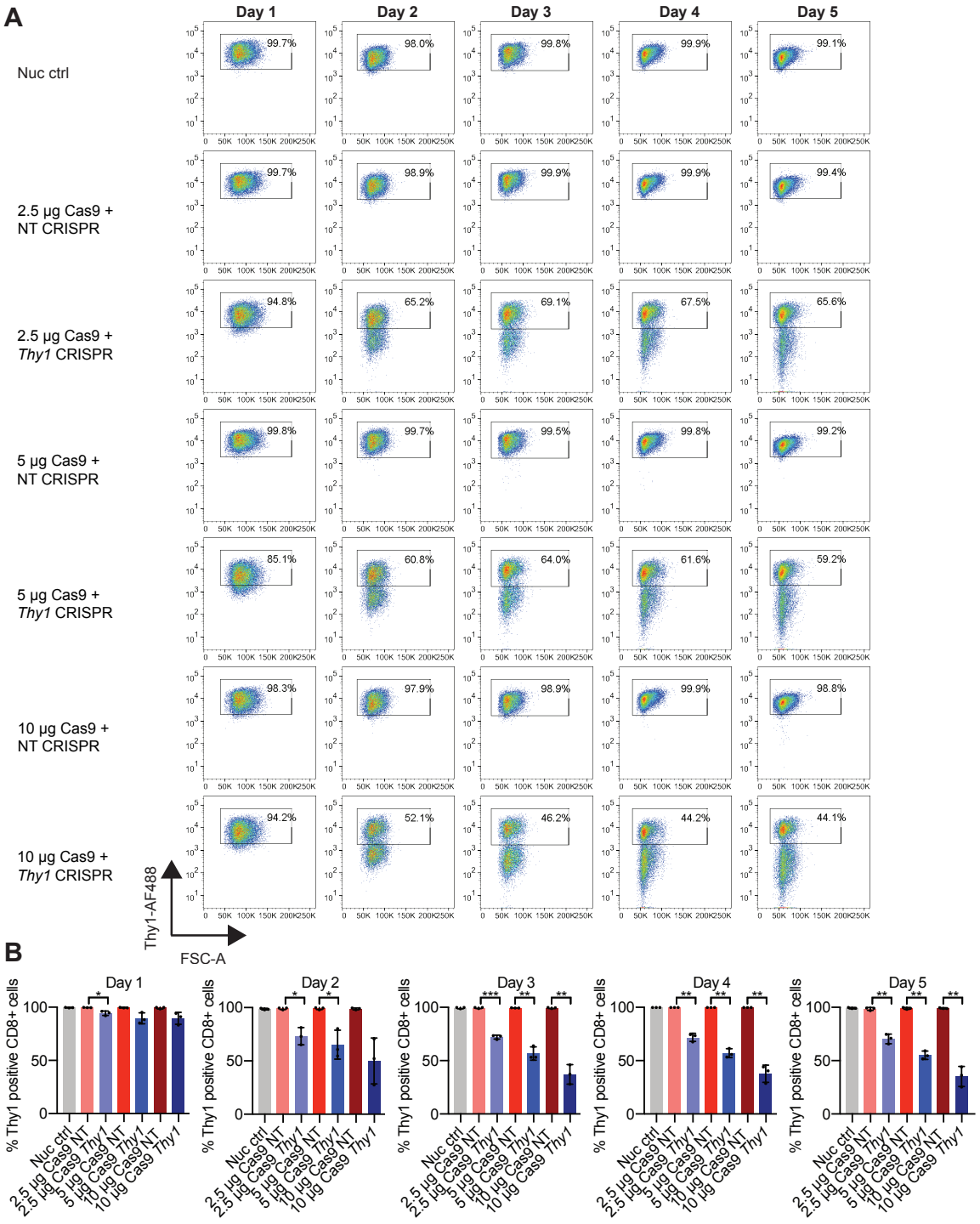

Fig. 3.5 ***Titration of Cas9 protein for use with synthetic crRNA and tracrRNA.***

Fig. 3.5 ***Titration of Cas9 protein for use with synthetic crRNA and tracrRNA.*** ***A*** *OT-I CTLs were nucleofected with the indicated amount of Cas9 protein in addition to 5 µg tracrRNA and 5 µg crRNA targeting Thy1 or a non-targeting control crRNA at day 4 after in vitro stimulation. Additionally, a nucleofection control was included, where CTLs were nucleofected but not exposed to any RNA or protein. Thy1 cell surface protein levels were monitored by flow cytometry over 5 days and analysed using the following gating strategy: initial gate to seperate cell population from debris, second gate to isolate single cells from doublets, third gate to isolate live cells from dead cells, fourth gate to isolate CD8-positive cells and a final gate to determine the percentage of Thy1 positive cells. The Thy1 gate was set according to the appropriate nucleofection control for every time point.* ***B*** *Thy1 cell surface expression in CD8 cells over the course of 5 days, n=3 independent experiments. Bar graphs show the mean, error bars the SD, *p<0.05, **p<0.01, ***p<0.001 calculated by unpaired t-test with Welch's correction. Nuc ctrl = Nucleofection control, NT = non-targeting.*

and all Cas9 protein is lost by day 2 post nucleofection (Figure 3.6D).

3.2.3 Targeting genes that are crucial for CTL killing function by CRISPR

After successfully optimising the CRISPR-Cas9 technology for mouse CTLs by targeting *Thy1*, the optimised method was used to target *Rab27a*, due to the well established effect of RAB27A loss on degranulation (Figure 3.1), as well as *perforin* and *Munc13-4*. To ensure that the technical aspects of the experiments were working, the *Thy1* crRNA was included as an efficiency control in every experiment and co-nucleofected alongside crRNAs against the genes of interest. Therefore, each experiment included the following controls: 1) a nucleofection control, 2) CTLs nucleofected with a non-targeting crRNA, tracrRNA and Cas9 protein, and 3) CTLs nucleofected with *Thy1* targeting CRISPR reagents. Each target gene was targeted with 3 crRNAs, to increase the chances of a cut, and perhaps even a large deletion, occurring. To allow time for the protein pool to be turned over, CTLs were tested in a degranulation and a killing assay four days after nucleofection. Additionally, pellets were frozen to test protein levels by WB at this time point.

Targeting *Rab27a* by CRISPR reproducibly resulted in a decrease in degranulation in comparison to controls (Figure 3.7A-B) (n=5, $p<0.05$, paired t-test). WB for the RAB27A protein confirmed that *Rab27a* CRISPR samples expressed less RAB27A protein than *Thy1* CRISPR or nucleofection controls (Figure 3.7C-D) (n=4, $p<0.05$, one sample t-test). The

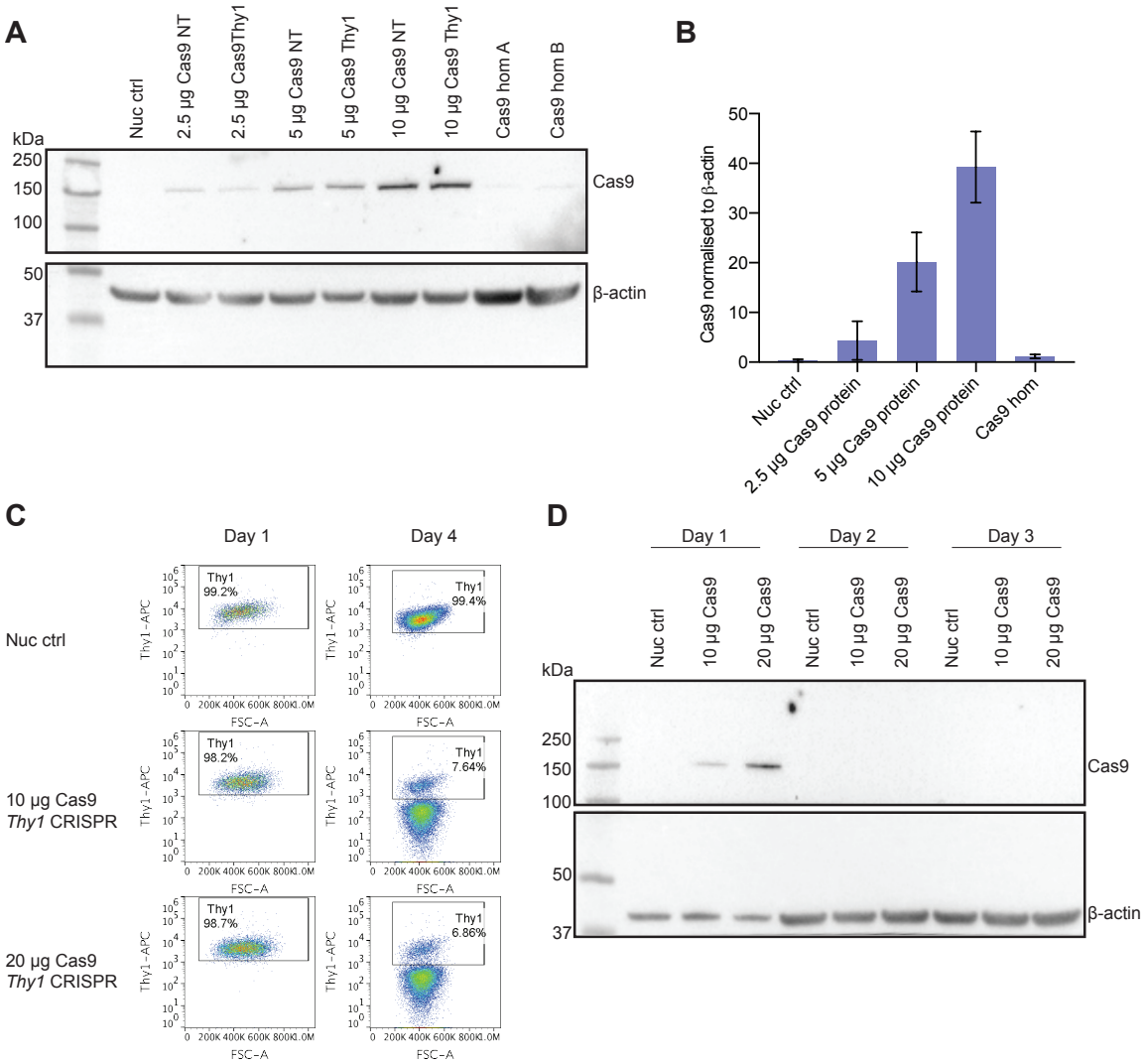

Fig. 3.6 ***Comparison of stable and transient Cas9 expression.*** ***A*** *Representative WB showing Cas9 protein expression levels in T cells derived from homozygous Cas9 mice and T cells nucleofected with indicated amounts of Cas9 protein.* ***B*** *Quantification of WBs showing Cas9 protein expression levels. In each repeat, the Cas9 protein level was normalised to the β-actin loading control and expressed relative to the Cas9 hom samples. Bar graphs show the mean, error bars the SD, n=2 independent experiments.* ***C*** *Thy1 protein cell surface expression one day and four days after CTL nucleofection with the indicated reagents, n=1.* ***D*** *WB for Cas9 and β-actin (loading control) levels 1, 2 and 3 days after nucleofection with indicated amounts of Cas9 protein, n=1. Nuc ctrl = Nucleofection control, NT = non-targeting.*

CTLs ability to kill target cells was determined by an assay that measures death of target cells stably expressing a red nuclear marker by loss of red fluorescence. There were more red target cells remaining in wells containing *Rab27a* CRISPR CTL than in control wells, meaning that less killing occurred in response to targeting *Rab27a* by CRISPR (Figure 3.7E-F).

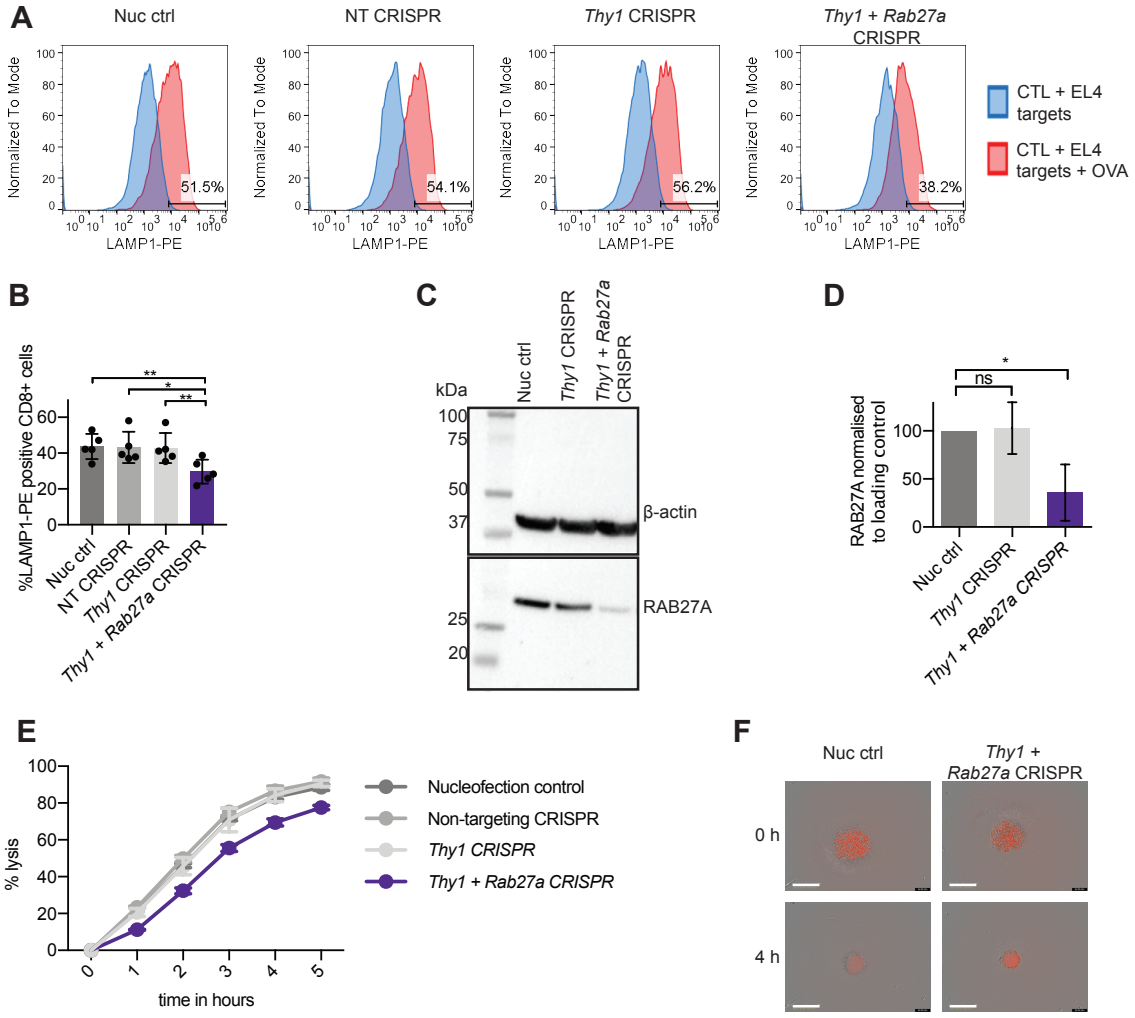

Fig. 3.7 ***Decreased degranulation and killing in response to targeting Rab27a using CRISPR.***

Fig. 3.7 ***Decreased degranulation and killing in response to targeting Rab27a using CRISPR.*** *OT-I CTL were nucleofected at day 4 after in vitro stimulation and tested in functional assays at day 8.* ***A*** *For degranulation assays CTLs were mixed with target cells at an E:T ratio of 2.5:1. Degranulation was measured by extracellular exposure of LAMP1 after 180 min. The following gating strategy was applied: initial gate to separate the cell population from debris, second gate to isolate single cells from doublets, third gate to isolate live cells from dead cells, fourth gate to isolate CD8-positive cells and a final gate to isolate LAMP1-PE positive cells. Representative histograms for unstimulated CTL co-cultured with EL4 target cells (blue) and CTL co-cultured with OVA-loaded EL4 target cells (red) are shown.* ***B*** *Average percentage of LAMP1-PE positive CD8 cells nucleofected with the indicated reagents in response to 180 min of co-culture with OVA-loaded EL4 target cells, n=5 independent experiments, *p<0.05, **p<0.01 calculated by paired t-test. Samples were paired by day of experiment. During each independent repeat the experiment was performed at least in technical duplicates. Bar graphs show the mean, error bars the SD.* ***C*** *Representative WB showing RAB27A and β-actin (loading control) protein expression four days after nucleofection.* ***D*** *Average RAB27A protein levels across 4 independent repeats. In each repeat, the RAB27A protein level was expressed relative to the nucleofection control and normalised to calnexin or β-actin loading controls. Bar graphs show the mean, error bars the SD, *p<0.05 calculated by one sample t-test, ns = not significant.* ***E*** *Incucyte killing assay showing % lysis of red EL4 target cells. One representative plot for 3 independent experiments is shown. E:T = 10:1. Each datapoint is an average of 3-4 technical repeats and the error bars show the SD.* ***F*** *Raw data from Incucyte killing assay showing comparable levels of red EL4 target cells between treatments at 0 h, but increased levels of red target cells in Thy1 + Rab27a CRISPR samples after 5 h. Scale bar = 800 μm.*

Perforin is another gene that is known to be crucial for CTL killing function. Perforin protein deficiency in humans causes an immunodeficiency disease (FHL2), and CTL killing is inhibited in *perforin* KO mice (Dieckmann et al., 2016; Kägi et al., 1994a; Walsh et al., 1994). However, while perforin KO should affect the CTLs ability to kill, it should not decrease their ability to release LAMP1 (Dieckmann et al., 2016). CTLs in which *perforin* was targeted by CRISPR did not result in a decrease in degranulation in comparison to the controls (Figure 3.8A-B). Instead, degranulation was increased in *perforin* CRISPR samples (n=4, $p<0.05$, paired t-test). Meanwhile, the CTLs ability to kill target cells was diminished, as more red target cells remained in wells containing *perforin* CRISPR CTL than in control wells (Figure 3.8E-F). Additionally, WB showed that perforin protein levels were decreased

in *perforin* CRISPR CTL in comparison to *Thy1* CRISPR and nucleofection control samples (n=3, P<0.001, one sample t-test) (Figure 3.8C-D).

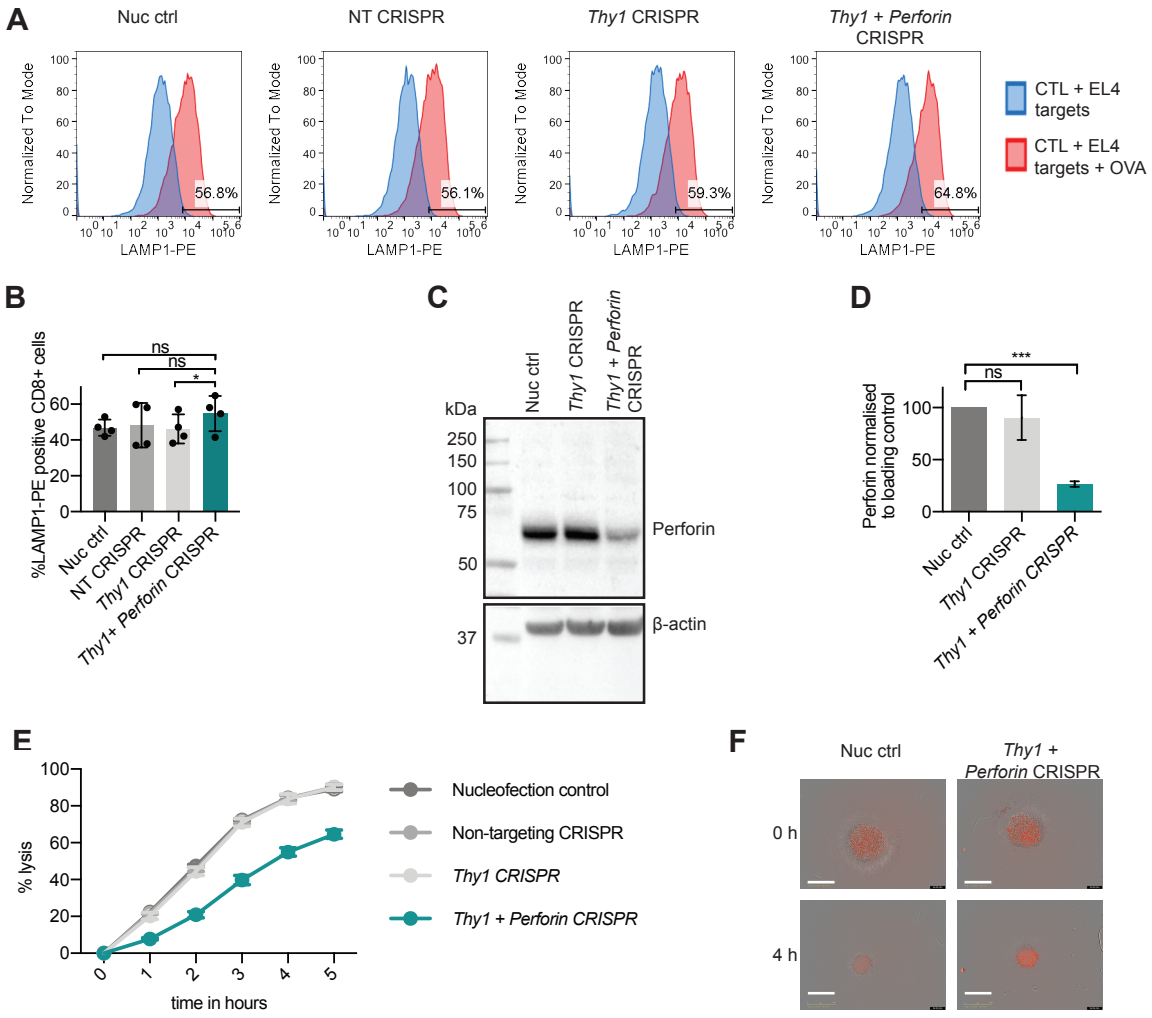

Fig. 3.8 ***Targeting Perforin by CRISPR decreased CTL killing, but not degranulation.***

Fig. 3.8 ***Targeting Perforin by CRISPR decreased CTL killing, but not degranulation.*** *OT-I CTL were nucleofected at day 4 after in vitro stimulation and tested in functional assays at day 8.* ***A*** *For degranulation assays CTLs were mixed with target cells at an E:T ratio of 2.5:1. Degranulation was measured by extracellular exposure of LAMP1 after 180 min. The following gating strategy was applied: initial gate to separate the cell population from debris, second gate to isolate single cells from doublets, third gate to isolate live cells from dead cells, fourth gate to isolate CD8-positive cells and a final gate to isolate LAMP1-PE positive cells. Representative histograms for unstimulated CTL co-cultured with EL4 target cells (blue) and CTL co-cultured with OVA-loaded EL4 target cells (red) are shown.* ***B*** *Average percentage of LAMP1-PE positive CD8 cells nucleofected with the indicated reagents in response to 180 min of co-culture with OVA-loaded EL4 target cells. Bar graphs show the mean, error bars the SD, n=4 independent experiments, *p<0.05 calculated by paired t-test, ns = not significant. Samples were paired by day of experiment. During each independent repeat the experiment was performed at least in technical duplicates.* ***C*** *Representative WB showing Perforin and β-actin (loading control) protein expression four days after nucleofection.* ***D*** *Average perforin protein levels across 3 independent repeats. In each repeat, the perforin protein level was expressed relative to the nucleofection control and normalised to calnexin or β-actin loading controls. Bar graphs show the mean, error bars the SD, ***p<0.001 calculated by one sample t-test.* ***E*** *Incucyte killing assay showing % lysis of red EL4 target cells. One representative plot for 3 independent experiments is shown. E:T = 10:1. Each datapoint is an average of 3-4 technical repeats and the error bars show the SD.* ***F*** *Raw data from Incucyte killing assay showing comparable levels of red EL4 target cells between treatments at 0 h, but increased levels of red target cells in Thy1 + Perforin CRISPR samples after 5 h. Scale bar = 800 μm.*

MUNC13-4 deficiency causes immunodeficiency in humans (FHL3) and similar phenotypes in mice (Crozat et al., 2007). Targeting *Munc13-4* by CRISPR resulted in a decrease in degranulation in comparison to controls (Figure 3.9A-B, n=5, p<0.05, paired t-test). MUNC13-4 protein levels were successfully decreased in response to CRISPR as shown by WB (n=3, P<0.01, one sample t-test) (Figure 3.9C-D). In addition to decreasing degranulation, *Munc13-4* CRISPR also decreased the ability of CTLs to kill target cells (Figure 3.9E-F).

The data generated in the *Rab27a*, *perforin* and *Munc13-4* CRISPR experiments was used to investigate whether Thy1 expression could be used to isolate cells where the CRISPR had worked. As a crRNA against *Thy1* was co-nucleofected in these experiments, I could

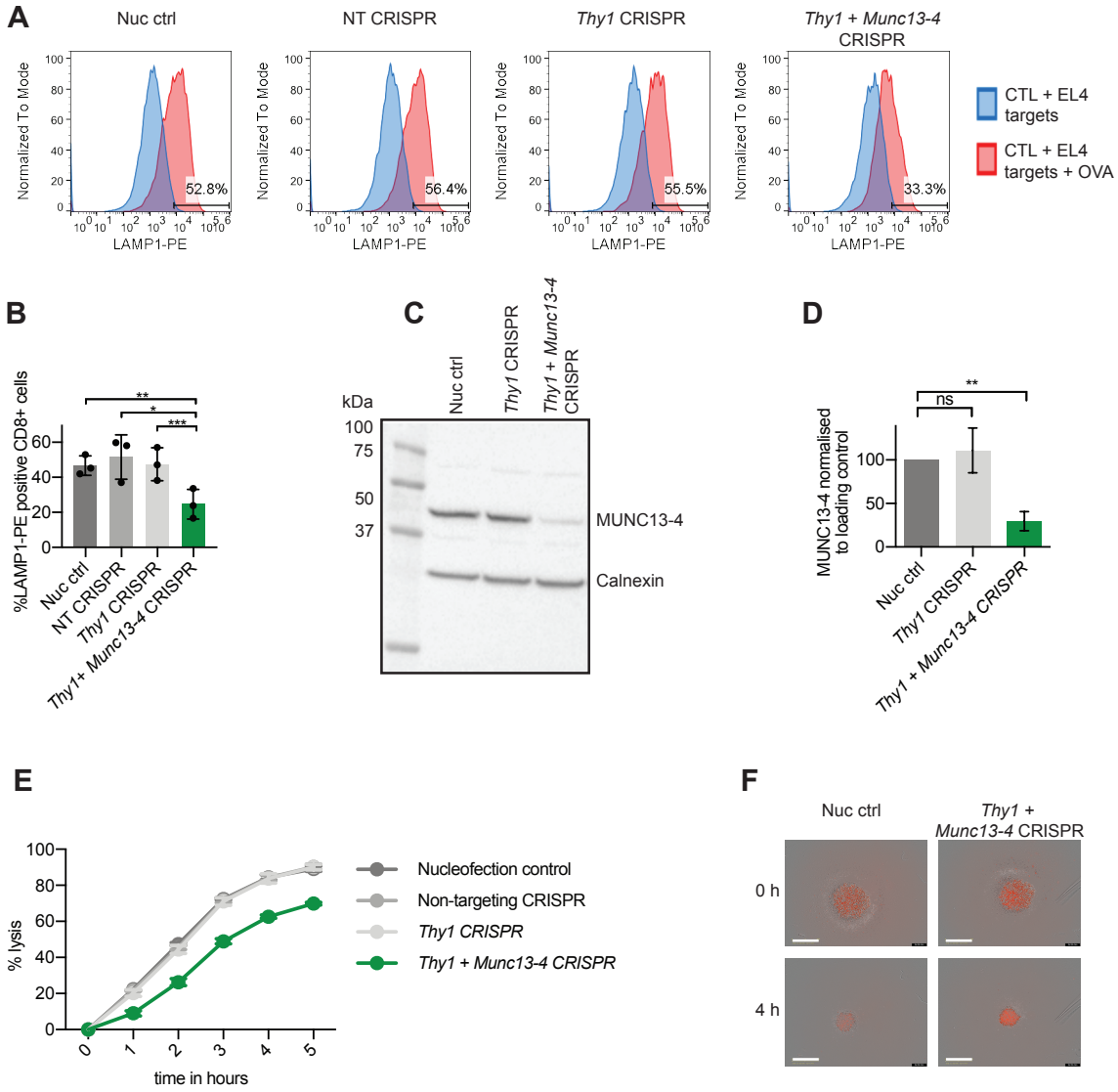

Fig. 3.9 ***Munc13-4*** **CRISPR results in decreased degranulation and killing.**

Fig. 3.9 ***Munc13-4 CRISPR results in decreased degranulation and killing.*** *OT-I CTL were nucleofected at day 4 after in vitro stimulation and tested in functional assays at day 8.* ***A*** *For degranulation assays CTLs were mixed with target cells at an E:T ratio of 2.5:1. Degranulation was measured by extracellular exposure of LAMP1 after 180 min. The following gating strategy was applied: initial gate to separate the cell population from debris, second gate to isolate single cells from doublets, third gate to isolate live cells from dead cells, fourth gate to isolate CD8-positive cells and a final gate to isolate LAMP1-PE positive cells. Representative histograms for unstimulated CTL co-cultured with EL4 target cells (blue) and CTL co-cultured with OVA-loaded EL4 target cells (red) are shown.* ***B*** *Average percentage of LAMP1-PE positive CD8 cells nucleofected with the indicated reagents in response to 180 min of co-culture with OVA-loaded EL4 target cells. Bar graphs show the mean, error bars the SD, n=3 independent experiments. During each independent repeat the experiment was performed at least in technical duplicates.* ***C*** *Representative WB showing MUNC13-4 and calnexin (loading control) protein expression four days after nucleofection.* ***D*** *Average MUNC13-4 protein levels across 3 independent repeats. In each repeat, the MUNC13-4 protein level was expressed relative to the nucleofection control and normalised to calnexin loading controls. Bar graphs show the mean, error bars the SD, ***p<0.01 calculated by one sample t-test, ns = not significant.* ***E*** *Incucyte killing assay showing % lysis of red EL4 target cells. One representative plot for 3 independent experiments is shown. E:T = 10:1. Each datapoint is an average of 3-4 technical repeats and the error bars show the SD.* ***F*** *Raw data from Incucyte killing assay showing comparable levels of red EL4 target cells between treatments at 0 h, but increased levels of red target cells in Thy1 + Munc13-4 CRISPR samples after 5 h. Scale bar = 800 µm.*

gate on Thy1 negative cells during the degranulation assay. This allowed to select cells that 1) have been nucleofected successfully and 2) have taken up Cas9-RNP complexes. Data from these assays was analysed using two different gating strategies, outlined in Figure 3.10A, in order to investigate whether gating on the Thy1-negative population resulted in a more striking degranulation phenotype in CRISPR samples. Gating on Thy1 negative cells showed a trend towards further decreasing the percentage of LAMP1-PE positive cells observed in *Munc13-4* and *Rab27a* CRISPR experiments, in comparison to the results obtained without gating on Thy1 negative cells. This indicated that gating on Thy1 negative cells could be used to isolate edited cells to some extent, however this effect was not statistically significant when tested using a paired t-test (Figure 3.10B).

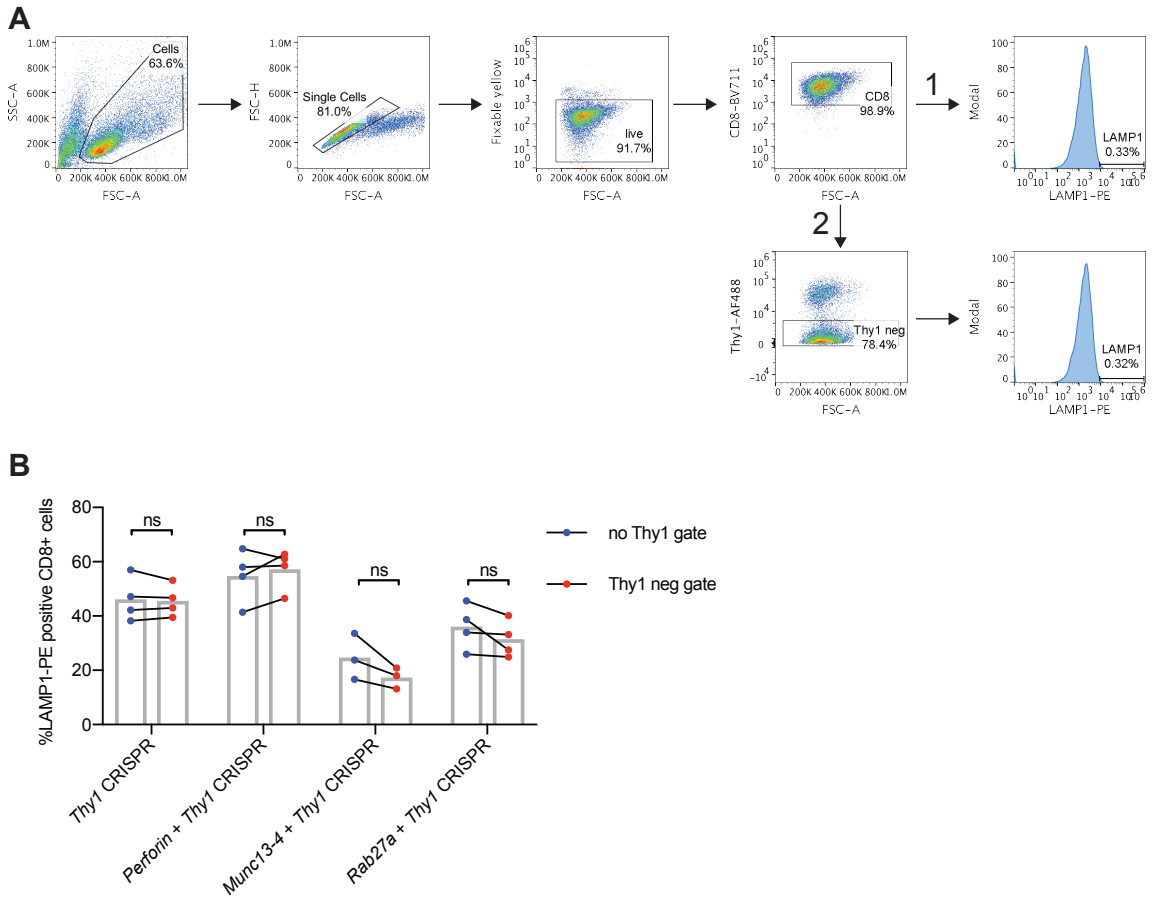

Fig. 3.10 ***The effect of gating on Thy1 negative cells on degranulation.*** ***A*** *Degranulation assays were analysed using two gating strategies: initial gate to separate the cell population from debris, second gate to isolate single cells from doublets, third gate to isolate live cells from dead cells and a fourth gate to isolate CD8-positive cells. This was followed by either 1) a final gate to isolate LAMP1-PE positive cells or 2) a fifth gate to isolate Thy1 negative cells prior to a sixth gate to isolate LAMP1-PE positive cells.* ***B*** *Average percentage of LAMP1-PE positive CD8 cells in response to 180 min of co-culture with OVA-loaded EL4 target cells. Each experiment was analysed with gating strategy 1 (blue) and gating strategy 2 (red). The results from both gating strategies were compared using paired t-tests, with sample pairing by day of experiment, n=3/4 independent experiments. During each independent repeat the experiment was performed at least in technical duplicates. neg = negative, ns = not significant.*

While a degranulation defect often overlaps with a killing phenotype, as observed for *Rab27a* and *Munc13-4* CRISPR samples (Figure 3.7 and 3.9), the *perforin* CRISPR result highlighted that some genes implicated in CTL killing could be missed if the degranulation assay is used as the sole readout in a screen. For example, genes that affect the cytolytic components of the granules, rather than granule release, could not be detected using the traditional degranulation assay. Since the aim of this project is to identify genes involved in CTL killing, an assay that measures killing as well as degranulation would be desirable. To achieve this, the standard degranulation assay was modified. Firstly, target cells stably expressing BFP (see chapter 2, section 2.1.4) were used. Secondly, a known amount of fluorescent cell counting beads was added to each sample just before analysis on the flow cytometer. Gating on these populations allowed me to determine the number of beads and the number of blue target cells that were recorded in each sample. This enabled the ratiometric enumeration of target cells, accounting for any differences in acquisition between samples. As a result, the percentage of live and dead EL4 target cells in each well could be determined at the same time as CTL degranulation was measured (Figure 3.11A,B, please see figure legend for a more detailed description of this calculation).

To test this assay, I used the *Rab27a*, *Munc13-4* and *perforin* CRISPR samples previously shown to result in protein loss and a reduced killing phenotype (Figures 3.7, 3.8, 3.9). For nucleofection control samples, the reduction of EL4 target cells can even be seen by eye when comparing the EL4 population between CTL+EL4-OVA and CTL+EL4+OVA conditions, indicating that target cell killing is occurring (Figure 3.11C). In contrast, such a decrease in the EL4 population cannot be observed for *Thy1 + Rab27a* CRISPR samples, indicating that target cell killing is reduced (Figure 3.11C). The bead method enabled quantification of this difference and allowed me to plot the percentage of target cells killed (Figure 3.11D). A decrease in target cell killing was observed for *Thy1 + Rab27a* CRISPR samples (n=3, $p<0.05$, paired t-test), *Thy1 + Munc13-4* CRISPR samples (n=3, $p<0.05$, paired t-test) and *Thy1 + perforin* CRISPR samples (n=2).

A

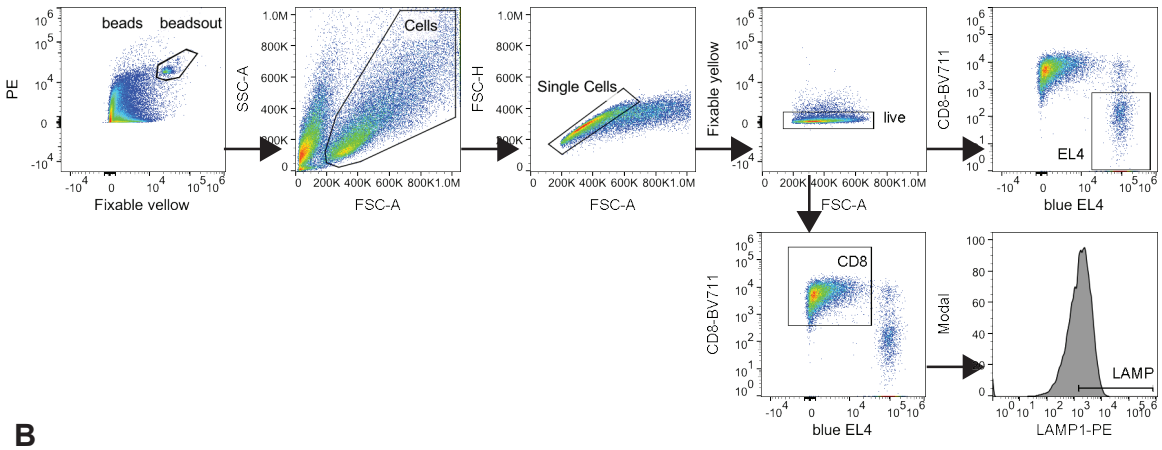

B

Sample	Count in EL4 gate	Count in beads gate	EL4:beads ratio	*10100 = no. of live EL4	% live	% dead
CTL + EL4 - OVA	2132	2540	0.84	8484		
CTL + EL4 + OVA	1276	2744	0.47	4747	55.40	44.60

C

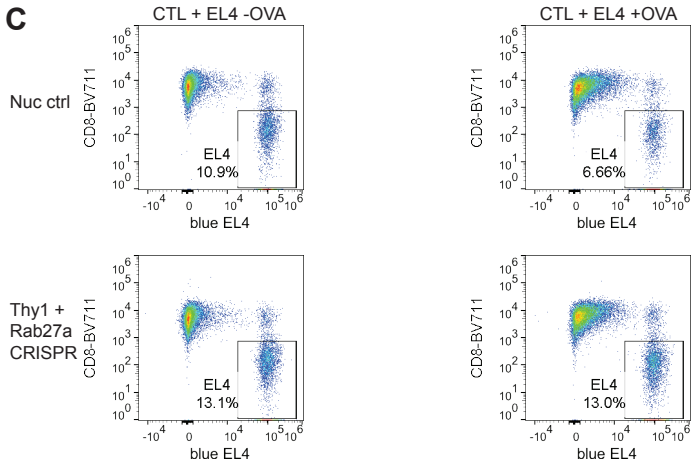

D

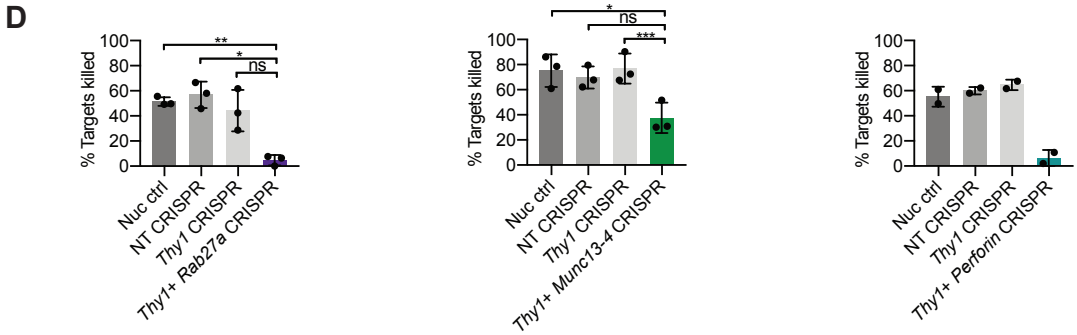

Fig. 3.11 **The combined degranulation and killing assay.**

Fig. 3.11 ***The combined degranulation and killing assay.*** ***A*** *Gating strategy used to analyse the combined degranulation and killing assay. The fluorescent 123count ebeads can be separated from cells by size and using different fluorescence channels. One gate is drawn around the beads ('beads') to determine the number of beads present in the sample. Another identical gate is used to select all events except for the beads ('beadsout'), so that the beads do not interfere with any other fluorescent signal. Within the 'beadsout' gate, a gate to separate the cell population from debris is followed by a gate to isolate single cells from doublets. Next, live cells are isolated from dead cells before gating on CD8 cells to determine the degranulation readout or blue EL4 target cells to determine the target cell count.* ***B*** *Example quantification of the killing response using the beads method. The count in the EL4 gate is divided by the count in the beads gate, giving an EL4:beads ratio. This can be multiplied by the number of beads added per well (in this example 10,100 beads, information supplied by the manufacturer for every batch) to calculate the absolute number of live target cells in the well. Normalising the +OVA sample to its respective -OVA sample allows determination of the percentage of live target cells remaining in the +OVA sample. This, in turn, allowed me to deduce the percentage of dead target cells that have been killed by CTLs.* ***C*** *Representative example of the killing response of CTLs derived from nucleofection control and Thy1 + Rab27a CRISPR samples. In the nucleofection control sample, a decrease in blue EL4 target cells from -OVA to +OVA plots can be seen. No decrease in blue EL4 target cells could be detected between -OVA and + OVA plots from Thy1 + Rab27a CRISPR samples.* ***D*** *Average killing assay readout for Thy1 + Rab27a CRISPR (n=3 independent experiments), Thy1 + Munc13-4 CRISPR (n=3 independent experiments) and Thy1 + Perforin CRISPR (n=2 independent experiments). E:T ratio = 2.5:1, assay duration = 180 min. Bar graphs show the mean, error bars the SD. Statistical analysis was not performed on Thy1 + Perforin CRISPR experiments as data was derived from only two independent experiments (see section 2.14). ns = not significant, *p<0.05, **p<0.01, ***p<0.001 as calculated by paired t-test. Samples were paired by day of experiment to account for day-to-day variations.*

3.3 Discussion

Figure 3.1 shows that RAB27A was expressed in CTLs derived from WT and het *ashen* mice, but not in hom *ashen* mice. CTLs derived from hom *ashen* mice furthermore showed a striking degranulation defect (Figure 3.1). Using siRNA to knockdown RAB27A protein in CTLs derived from WT mice resulted in a consistent decrease in degranulation in comparison to the respective controls. It was not possible to reproduce the striking decrease in degranulation

observed in CTLs derived from hom *ashen* mice with siRNA knockdown (Figure 3.2). The mild siRNA phenotype can be explained by only partial protein knockdown being achieved (Figure 3.2). The biggest decrease in protein level was achieved with 3 μg siRNA one day after nucleofection, but this only reduced protein levels by 36% on average (n=7). Increasing Rab27a siRNA concentration, incubation time or nucleofecting CTLs twice with siRNA did not decrease RAB27A protein levels further (Figure 3.3). This indicated either low nucleofection efficiency, or that the siRNA did not work as effectively as expected. Nonetheless, it is important to note, that even only partial RAB27A protein knockdown still reproducibly resulted in a decrease in degranulation, making *Rab27a* a good target for testing phenotypic effects of CRISPR KO.

The partial protein knockdown observed in response to Rab27a siRNA treatment highlighted the disadvantage of using a technique like WB for the detection of protein loss, as WB shows the bulk cell population. Only a small proportion of the cell population may take up the CRISPR reagents upon nucleofection. Furthermore, even in cells where CRISPR will introduce cuts in the desired gene, there will be a mixed population of heterozygous and homozygous KOs. A technique that gives single cell resolution, such as flow cytometry, allows observation of the effect even if the KO only occurs in a small subset of the entire cell population.

For ease of detection by flow cytometry, the cell surface protein Thy1 was targeted using synthetic CRISPR reagents for the initial set up of the CRISPR technique. The best KO efficiency without toxic side effects was observed with 5 μg crRNA/tracrRNA and 10 μg Cas9 protein (Figure 3.4 and 3.5). This reproducibly achieved loss of Thy1 surface expression in over 60% of the cell population (Figure 3.5B), sometimes achieving over 90% KO (Figure 3.6C). Increasing the amount of Cas9 protein beyond 10 μg did not further improve KO efficiency (Figure 3.6C). Nucleofecting Cas9 protein likely resulted in a higher KO efficiency than using CTLs from Cas9 hom mice due to the higher Cas9 level in the former samples (Figure 3.6A-B).

Time course experiments (Figures 3.4 and 3.5) showed that it took 2-3 days for the CRISPR effect to show, which indicated that this is the amount of time it took for the CRISPR-induced damage to accumulate and for the Thy1 protein pool to be turned over. As protein longevity varies greatly, it would be best to wait as long as possible to allow protein turnover when targeting other genes using CRISPR. However, mouse CTL lifespan in tissue culture is limited, and they are best used for functional assays around day 7-8 post in vitro

stimulation. Therefore, CTLs were nucleofected at day 4 post in vitro stimulation and tested in functional assays at day 8. This optimised CRISPR approach was successfully used to knock out genes that are known to be crucial for CTL killing function. Targeting *Rab27a* and *Munc13-4* decreased the degranulation and killing capabilities of CTLs (Figures 3.7 and 3.9). Targeting *perforin* affected CTL killing without decreasing degranulation (Figure 3.8).

A downside to any approach involving nucleofection of synthetic RNAs is that there is no way to select cells that have taken up the reagents. Therefore, the population studied will always be a mix of WT and genetically modified cells meaning that genes that have subtle effects upon KO may be overlooked. Because of this it is important to optimise the reagent concentration in order to maximise the KO efficiency as done in Figure 3.4 to 3.5.

To isolate cells that have been nucleofected successfully in a degranulation assay, others have co-nucleofected a GFP-plasmid alongside siRNAs (Kabanova et al., 2016). The underlying assumption is that cells which have taken up the GFP plasmid are also more likely to have taken up the co-nucleofected reagents. A more accurate approach would be to use synthetic crRNAs or tracrRNAs fused to a fluorescent marker, as done by Seki and Rutz (2018). However this fusion may affect the function of the RNA and such products were not yet available when the experiments outlined in this chapter were performed.

As an alternative approach, a *Thy1* crRNA was co-nucleofected alongside the crRNAs against the gene of interest. The percentage of Thy1 KO could be measured alongside the percentage of LAMP1-PE positive cells in the degranulation assay. In addition to allowing to monitor the nucleofection efficiency, targeting Thy1 gave an idea of how well the CRISPR worked in each experimental condition. A lack of Thy1 KO would indicate a technical mistake, such as accidentally not adding Cas9 protein. Using the Thy1 readout to select cells where the CRISPR technique worked, by gating on Thy1 negative cells in the degranulation assay, did not significantly improve the readout in *Rab27a*, *Munc13-4* or *perforin* CRISPR experiments (Figure 3.10).

While it was beneficial to co-nucleofect a *Thy1* crRNA in initial experiments to ensure the CRISPR technique was working robustly, it also raised some concerns. Firstly, targeting an additional region in the genome could result in unanticipated side effects. Secondly, it could decrease CRISPR efficiency for the gene of interest by competing for the available Cas9 and tracrRNA reagents. Thirdly, gating on Thy1 negative cells during the degranulation assay means that I cannot meaningfully compare the data to the controls that are closest to the

unmanipulated cells (nucleofection controls and non-targeting CRISPR controls), as these do not contain a Thy1 negative population. Finally, others have suggested that Thy1 can affect T cell activation, which could result in unwanted side effects (Haeryfar and Hoskin, 2004; Killeen, 1997). In summary, I therefore concluded that it would be preferable not to co-nucleofect the *Thy1* crRNA alongside crRNAs against other genes from now on.

3.3.1 Development of an assay to measure both degranulation and killing

The degranulation assay is suitable for high throughput screening as it can be performed in a 96 well format. Picking one time point would maximise the number of samples fitting on one plate. The 90 min and 180 min time points showed the clearest separation between scramble and Rab27a siRNA treated samples (Figure 3.2). As the 180 min time point also showed a clear separation in Incucyte killing assays (Figure 3.7 to 3.9) it was chosen as the most suitable end point for the degranulation assay in an effort to miniaturise the assay.

The beads assay (Figure 3.11) allowed to determine the percentage of target cells killed in the same well as the degranulation readout. This was achieved by making two simple changes to the traditional degranulation assay: 1) the addition of stained target cells and 2) the addition of a known amount of cell counting beads. This assay will enable to test killing phenotypes at the same scale as the degranulation assay. To maximise the number of samples fitting on one plate this assay was limited to one E:T ratio and one time point. Therefore, any promising hits should be followed up further with additional phenotypic assays.

3.3.2 Summary and evaluation of aims

- Degranulation assay set up and adaptation for a screen.
  - The degranulation assay successfully showed a defect in response to RAB27A and MUNC13-4 depletion. As the 180 min time point showed a clear separation between experimental samples and controls it was chosen as the only time point to be used subsequently in order to maximise the number of samples per degranulation assay. Furthermore, an assay that simultaneously measures degranulation and killing was developed.
- Manipulate gene expression in primary mouse CTLs using siRNA.

  - RAB27A protein levels were successfully reduced in response to treatment with Rab27a siRNA, although not to the desired extent. This highlighted the potential of CRISPR which can stably and homozygously KO genes.

- Optimise the CRISPR-Cas9 technology in primary mouse CTLs.

  - The use of synthetic crRNA and tracrRNA reagents as well as Cas9 protein was optimised through concentration response and time course experiments targeting the cell surface protein Thy1. Conditions that resulted in reproducible and efficient KO were successfully established.

- Use the CRISPR-Cas9 technology in primary mouse CTLs to target genes where the KO has a known phenotype in the degranulation assay.

  - *Rab27a*, *perforin* and *Munc13-4* were successfully targeted by CRISPR in mCTL as demonstrated by WB, degranulation and killing assays.

Chapter 4

Transcriptome analysis of CD8 T cells to inform a targeted CRISPR screen

4.1 Introduction

TCR stimulation triggers naive CD8 T cells to differentiate into effector CTL. This causes a small and quiescent naive cell to undergo rapid clonal expansion, substantially increase in size and acquire effector functions (de la Roche et al., 2016). The genome will be identical between a naive CD8 T cell and its corresponding differentiated effector CTL version, but the genes that are actively expressed will likely differ. In this chapter, RNA-seq was used to understand what genes are differentially expressed between naive and effector CD8 T cells. RNA-seq allows measurement of the complete set of transcripts of a cell (Wang et al., 2009) and therefore allowed me to determine which genes are upregulated in response to activation. Some of these upregulated genes will be necessary for CTL effector functions, such as target cell killing. The result of this RNA-seq project formed the basis of a subsequent screen to investigate how CD8 T cells are regulated at the genetic level. Targeting hits from the RNA-seq dataset using the CRISPR technology, as optimised in chapter 3, allowed me to determine whether the upregulated genes affect CTL killing function.

4.1.1 Study design

The experimental approach was to compare the transcriptome of naive CD8 T cells freshly isolated from spleens of WT mice ("day 0" samples) to the transcriptome of effector CD8 T cells that were activated on αCD3ε and αCD28 antibody-coated plates for two days, followed by 5 days of expansion ("day 7" samples) (Figure 4.1A). This experimental design

was identical to the standard procedure used to activate WT mouse T cells in vitro. Day 7 was chosen as the end time point as cells are typically used for functional assays, such as degranulation or killing assays, around this time. At the time that the RNA-seq experiment was performed the plan was to use T cells derived from Cas9 hom mice for the screen. As the Cas9 hom mice were on a C57BL/6 background, WT C57BL/6 mice were used for the RNA-seq study. The study included cells from 10 different mice (4 males and 6 females, all $\sim$16 weeks old). While the main question of interest was what genes are differentially expressed in day 7 vs day 0 samples, the RNA-seq dataset could additionally be used to investigate differentially expressed genes between males and females.

4.1.2 Chapter aims

- Determine the differences in gene expression between naive and activated CD8 T cells. The hypothesis is that there are substantial changes in gene expression between these two states of CD8 T cells.
- Explore the functional association of the differentially expressed genes using bioinformatic tools.
- Test the effect of targeting differentially expressed genes by CRISPR in phenotypic assays (degranulation and killing assays).
- Explore what genes are differentially expressed in CD8 T cells derived from male and female mice.

4.2 Results

4.2.1 RNA sample preparation and quality control

CD8 T cells were purified from spleens derived from WT mice to ensure that the RNA-seq data was predominantly derived from CD8 T cells. In order to have a record of the CD8 purity of each sample, the percentage of CD8 positive cells was determined by flow cytometry on the same day as freezing cell pellets for RNA extraction. CD8 positive cells constituted >94.7% of all samples except for one sample where the percentage of CD8s was slightly lower (Sample 33 day 7: 87.5%) (Figure 4.1B). After RNA extraction with the RNeasy Mini Kit (Qiagen), the quality of RNA was tested using a Bioanalyser (Agilent). High quality RNA is critical to ensure successful library preparation for sequencing. The Bioanalyser determined RNA quality by estimating a RNA integrity number (RIN) (Schroeder

et al., 2006). The Bioanalyser electrophoretically separated RNA fragments and visualised their size and distribution via laser-induced fluorescence (see Figure 4.1C and D for a representative bioanalyser gel and electrophoretic trace). The RIN algorithm takes the entire electrophoretic trace into account before allocating a score between 1 and 10 to the sample, with 10 indicating highest quality RNA (Schroeder et al., 2006). Library preparation and sequencing was performed by the Illumina bespoke team at the Sanger Institute. For library preparation the Illumina bespoke team required the RNA samples to have a RIN value higher than 8. All RNA samples in this study had a RIN score between 8.2 and 9.6 (Figure 4.1E). The Illumina bespoke team performed a stranded library prep with oligodT pulldown. The 20 samples (10 samples for day 0 and 10 samples for day 7) were pooled across 3 paired-end lanes of an Illumina Hi-Seq and 75 bp reads were sequenced.

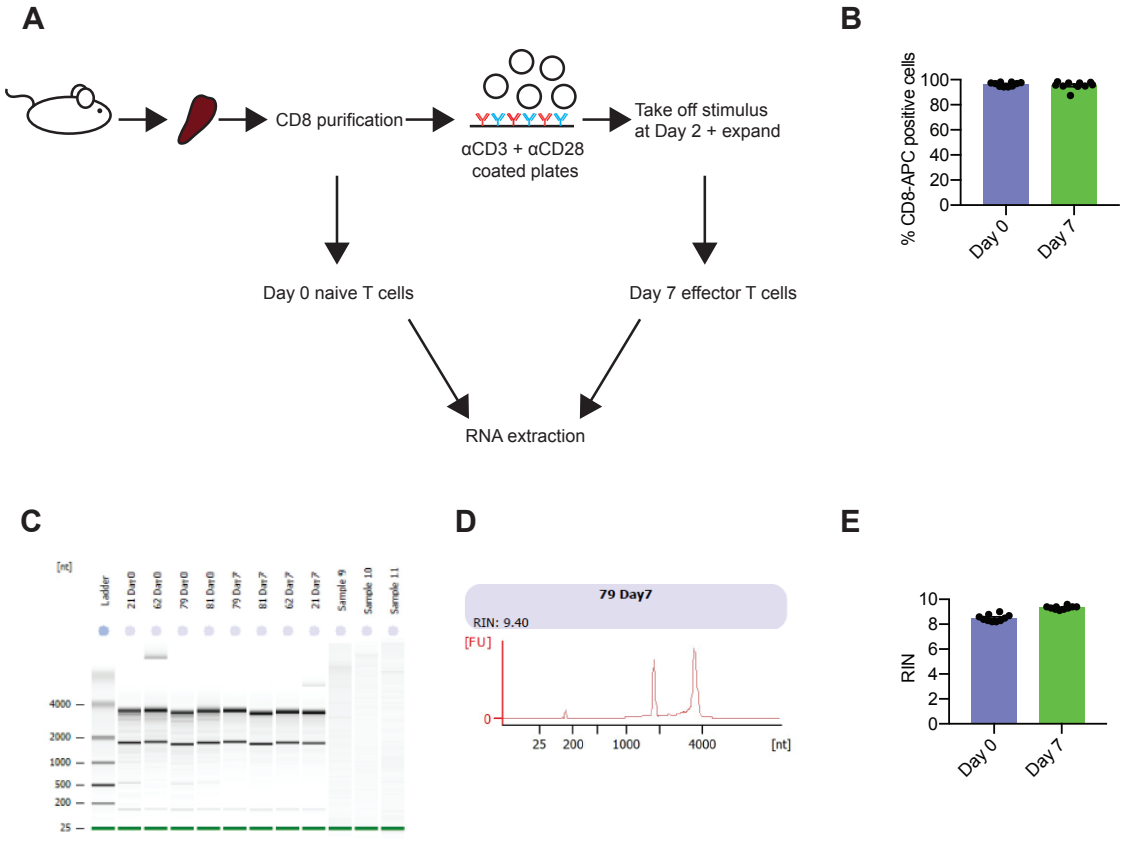

Fig. 4.1 ***RNA-seq study design and sample preparation.***

Fig. 4.1 ***RNA-seq study design and sample preparation.*** ***A*** *CD8 T cells were purified from spleens derived from C57BL/6N WT mice (10 biological replicates, 4 males and 6 females) across two spleen collection dates. After purification, 6 million cells per sample were frozen as "day 0" naive cells. The remaining cells were stimulated for two days on* 0.5 µg*/ml* α*CD3*ε *and* 1 µg*/ml* α*CD28 coated plates. On day 3 cells were removed from the stimulus, washed and expanded for a further 5 days. At day 7 post in vitro stimulation 6 million cells per sample were frozen as "day 7" activated cells. RNA from matched day 0 and day 7 samples was extracted on the same days.* ***B*** *The percentage of CD8 positive cells was determined by flow cytometry on the same day as cell pellets were frozen for RNA extraction.* ***C*** *A representative bioanlayser gel showing the typical banding pattern for a high quality RNA sample. The two prominent bands correspond to the 28S and 18S ribosomal RNA.* ***D*** *The bioanalyser electrophoretic trace corresponding to sample 79 day 7 shown in C. The trace is used to derive the RIN number.* ***E*** *RIN numbers for all samples included in the RNA-seq experiment as determined by the bioanalyser.*

4.2.2 Read mapping, fragment count and quality control

The subsequent bioinformatic analysis steps were performed with Martin Del Castillo Velasco-Herrera (PhD student in David Adams' team) following a previously published workflow (Anders et al., 2013). Reads were aligned to the reference genome (version GRCm38) using the splice-aware mapper tool STAR (Dobin et al., 2013) guided by version 84 of the Ensembl mouse annotation. Next, the number of read pairs (fragments) that uniquely aligned to a particular region in the genome were counted using Htseq-count (Anders et al., 2015). Between 21,786,497 and 49,939,333 reads were mapped per sample, 85.84 - 88.71% of which mapped uniquely to the reference genome. In order to estimate transcript expression levels, read counts were normalised by calculating the FPKM (see chapter 2, section 2.7) (Garber et al., 2011). Pairwise comparisons were performed with the log2-transformed FPKM values by calculating the pearson correlation coefficient of all possible comparisons. Hierarchical clustering showed that the samples clustered together according to which group (i.e. day 0 or day 7) they belonged to (Figure 4.2A), indicating that the gene expression differs between these two states of cells.

To further identify sources of variance in my dataset a PCA was performed (see chapter 2, section 2.7). In PCA, data points are projected onto a 2D plane. The x-axis represents the first principal component (PC1), which explains the greatest variance in the dataset. The y-axis represents the second principal component (PC2), which is independent from PC1 (Figure

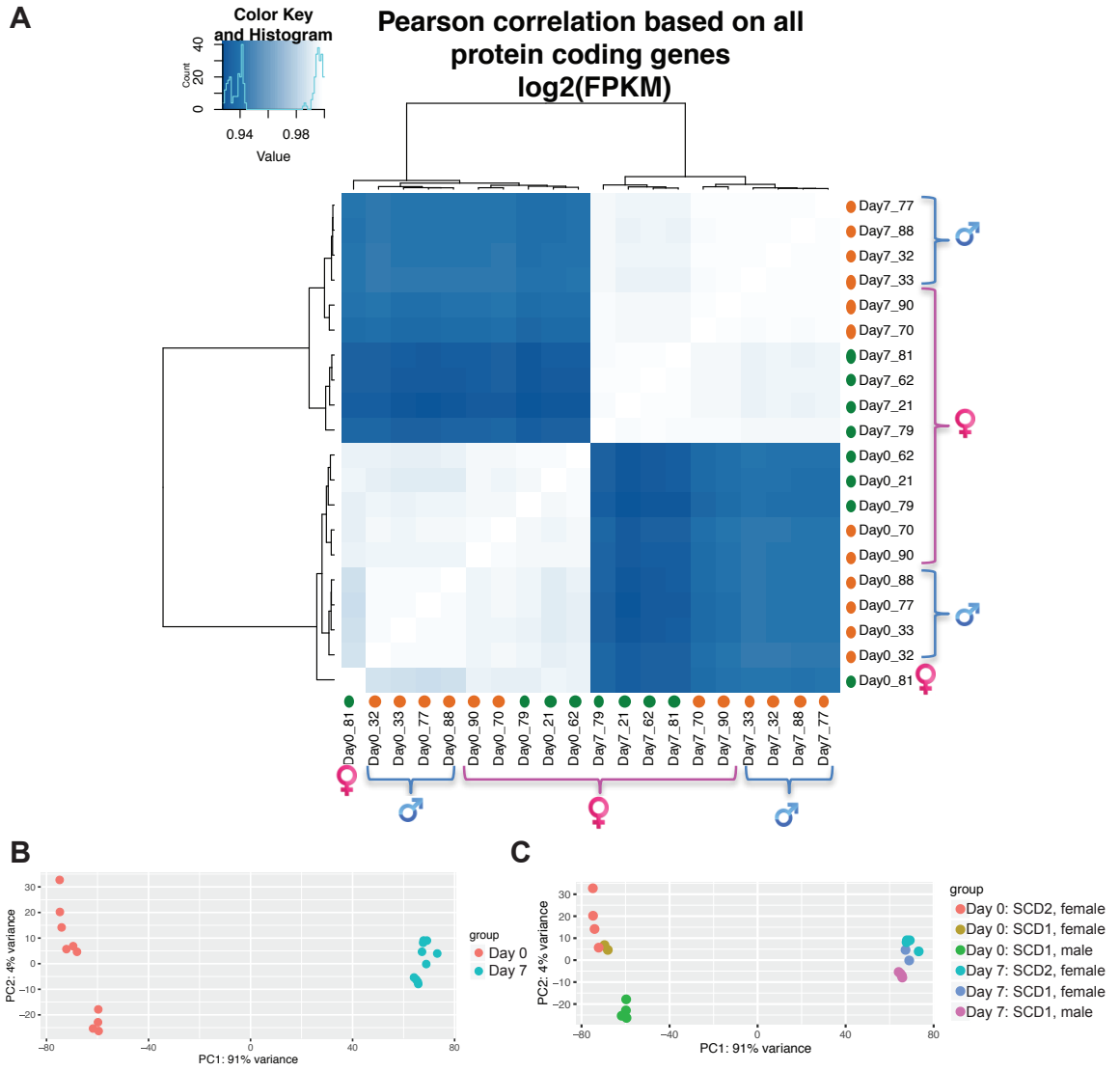

Fig. 4.2 ***RNA-seq quality control.***

Fig. 4.2 ***RNA-seq quality control.*** *RNA-seq was performed on RNA from CD8 T cells derived from 10 WT mice (4 males, 6 females) before stimulation and 7 days after stimulation.* ***A*** *Heatmap comparing samples pairwise in terms of the log2(FPKM) of all protein coding genes. White indicates a higher pearson correlation coefficient (samples on x and y axis are similar to one another), blue indicates a lower pearson correlation coefficient (samples on x and y axis are comparatively different from one another). The hierarchical clustering of the samples, as shown by the dendrogram, separates the samples by whether they belong to the day 0 group or the day 7 group. Samples were derived from ∼16 week old male or female mice and collected on two different spleen collection dates (SCD, orange = SCD 1, green = SCD 2) as indicated.* ***B*** *PCA was performed using the top 2000 most variable transcripts with regularised log transformed expression values for each sample. The percent of the total variance associated with each principal component is printed on the axis label. Samples are colour coded according to which group they belong to.* ***C*** *PCA plot where samples are colour coded according to which group they belong to, as well as which date the spleen was collected on and whether the spleen was derived from a female or male mouse. The plots in this figure were prepared with the help of Martin Del Castillo Velasco-Herrera. PC = principal component. SCD = spleen collection date.*

4.2B,C). In agreement with the data in Figure 4.2A, colour coding the samples showed that the group (i.e. whether a sample belongs to the group day 0 or day 7) is the biggest source of variance in my dataset. Expanding the colour code to include details such as spleen collection date and whether the samples were derived from males or females showed that samples also clustered together due to these factors. This demonstrated that all these factors affected gene expression, meaning that the spleen collection date should be accounted for in subsequent analyses.

4.2.3 Comparing gene expression in activated and naive CD8 T cells

The DESeq2 package (Love et al., 2014) was used to identify differentially expressed genes. DESeq2 tests for differential expression using a negative binomial distribution model (Anders and Huber, 2010). The spleen collection date was included as a covariate to accommodate this as a potential confounding factor. P-values were corrected for multiple testing using the Benjamini-Hochberg correction, giving an adjusted p-value (padj) (see chapter 2, section 2.7). In order to focus on genes with big changes in expression, genes were only considered

Table 4.1 ***Top 10 activated differentially expressed genes when comparing day 7 T cells to day 0 T cells.***

Gene	Log2(FoldChange)	p-value	B-H adjusted p-value
Spp1	11.793	0.00E+00	0.00E+00
Lif	10.579	0.00E+00	0.00E+00
Lrrc32	9.477	0.00E+00	0.00E+00
Gzmb	9.103	0.00E+00	0.00E+00
Cdkn1a	9.072	0.00E+00	0.00E+00
Tubb6	8.654	0.00E+00	0.00E+00
Il2ra	7.490	0.00E+00	0.00E+00
Galnt3	7.407	0.00E+00	0.00E+00
Slc16a3	7.397	0.00E+00	0.00E+00
Adam8	7.214	0.00E+00	0.00E+00

to be differentially expressed when the padj was smaller than 0.01 and the log2(fold change) was larger than 2 (upregulated genes) or smaller than -2 (downregulated genes).

The volcano plot in Figure 4.3A gives an overview of the number of differentially expressed genes. The fact that there were many significantly up and down regulated genes upon activation demonstrated how large the effect of activation is on the transcriptome of CD8 T cells. Genes that are highlighted in blue were detected as differentially expressed at 1% false discovery rate (FDR) and passed the log2(fold change) cut off. In total, there were 1803 activated and 2584 repressed significantly differentially expressed genes when comparing day 7 to day 0. From here on I will focus on the upregulated differentially expressed genes when comparing day 7 to day 0 samples, as this dataset should include the genes required for CTL effector functions. The top 10 upregulated genes, as ordered by the log2(fold change), are shown in Table 4.1. These included *Gzmb* and *Il2ra*, which encode granzyme B and the α-subunit of the high affinity IL2 receptor, respectively. These two proteins are known to be important for effector CTL function (de la Roche et al., 2016; Zhang and Bevan, 2011). The complete list of the 1803 upregulated differentially expressed genes is included digitally on a CD alongside this thesis (Appendix B).

To gain a better overall understanding of what biological pathways are enriched in the upregulated gene list, I used the Functional Interpretation of Differential Expression Analysis (FIDEA) server (D'Andrea et al., 2013). FIDEA mapped the genes in my dataset to functional categories in publicly available databases, such as Gene ontology (GO) (Gene Ontology Consortium et al., 2012) categories and Kyoto Encyclopaedia of Genes and Genomes (KEGG)

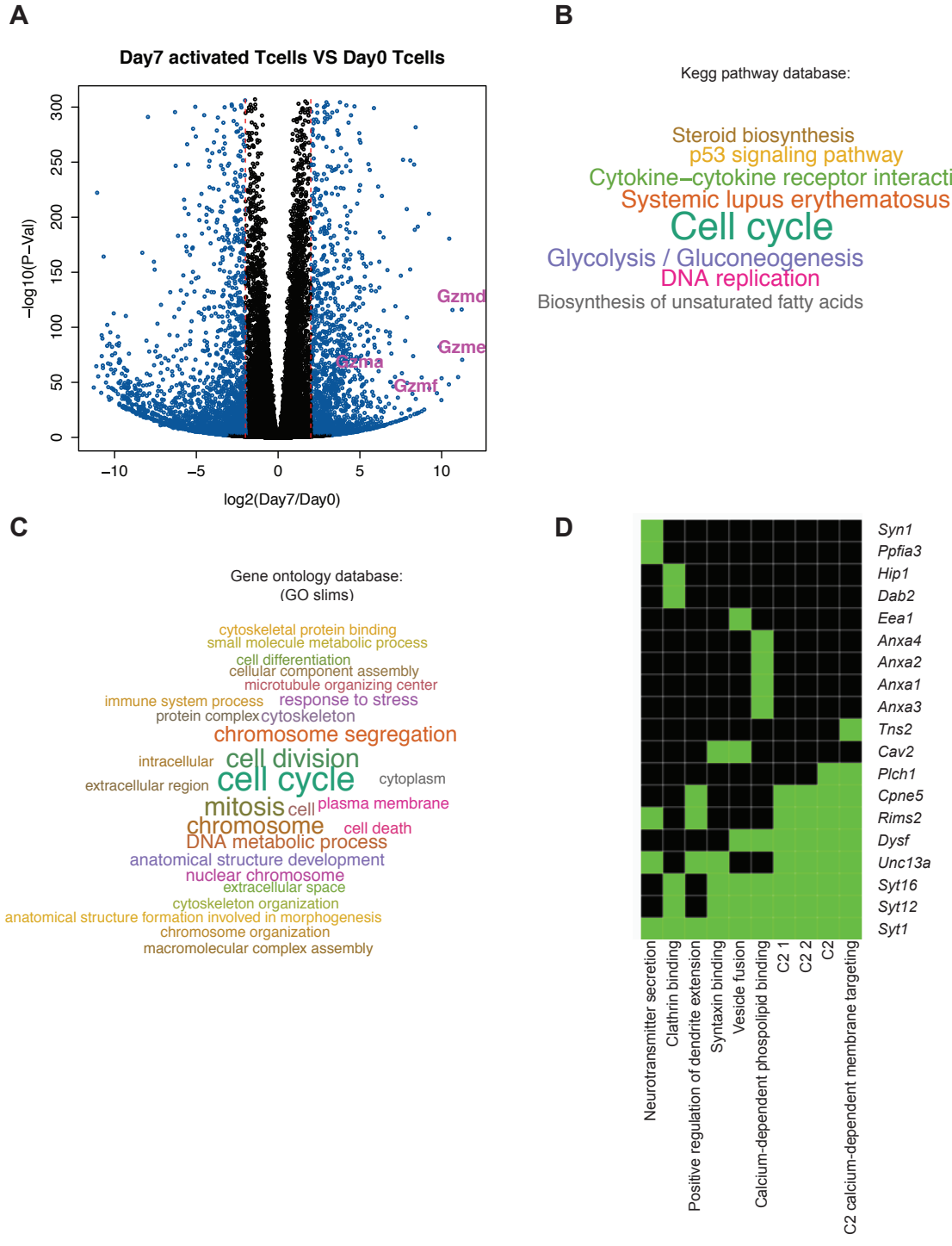

Fig. 4.3 ***Differential expression analysis between activated and naive CD8 T cells.***

Fig. 4.3 ***Differential expression analysis between activated and naive CD8 T cells.*** ***A*** *Volcano plot showing the -log10 of the p-value (y-axis) vs the log2 of the fold change of expression (x-axis) for each gene. Dotted lines indicate the log2(fold change) cut off at -2 and + 2. The blue colour is used to highlight genes that passed the log2(fold change) cut off and were detected as differentially expressed at 1% FDR when using the Benjamini-Hochberg multiple testing adjustment. Some genes encoding members of the granzyme protein family (Gzmd, Gzme, Gzmf and Gzma) are highlighted on the plot.* ***B*** *Word cloud derived from FIDEA mapping the significantly upregulated gene set to the KEGG pathway database. Words are sized according to enrichment using the FIDEA calculated p-value corrected for multiple testing.* ***C*** *Word cloud derived from FIDEA mapping the significantly upregulated gene set to the GO database. Words are sized according to enrichment using the FIDEA calculated p-value corrected for multiple testing.* ***D*** *Annotation cluster derived from the DAVID functional annotation tool that includes terms related to vesicle fusion, which could be relevant to CTL function. The heatmap shows the overlap between genes in my upregulated dataset (y-axis) and genes in the annotation cluster terms (x-axis). Green colour indicates that a gene is contained within the term, black colour indicates that a gene is not found in the term. FIDEA = Functional Interpretation of Differential Expression Analysis, DAVID = Database for Annotation, Visualization and Integrated Discovery, KEGG = Kyoto Encyclopaedia of Genes and Genomes, GO = Gene ontology.*

pathways (Kanehisa et al., 2012). These provide curated gene sets classified according to participation in common biological processes and can therefore be used to identify enriched biological themes in large gene lists. The gene sets are largely manually curated based on available experimental evidence and are therefore limited to published scientific knowledge (Gene Ontology Consortium et al., 2012). As each database has its own methods for assigning genes to categories it can be useful to compare the results obtained from separate curations. The results of the FIDEA analysis using KEGG and GO Slim databases are represented in word clouds (Figure 4.3B,C). The GO Slim database contains a smaller subset of the GO terms and is useful for broadly classifying which biological processes a set of genes is associated with (Gene Ontology Consortium, 2012). The size of the writing for each functional category in the word clouds corresponds to how enriched the particular category is in my dataset (D'Andrea et al., 2013). The word clouds particularly showed an enrichment of genes belonging to the "cell cycle" term of GO Slim and KEGG databases (Figure 4.3B,C). Other enriched pathways were pathways that are needed to replicate and make bigger cells, such as DNA replication and metabolism-related pathways (Figure 4.3B,C).

Using a different functional annotation tool, the Database for Annotation, Visualization and Integrated Discovery (DAVID) version 6.8 (Huang et al., 2009a,b) for functional enrichment analysis revealed 192 annotation clusters, representing biological processes, as enriched in the protein coding genes in my dataset. Annotation clusters group functionally similar terms together, with each term containing a list of genes associated with the term. DAVID determined whether these clusters were statistically overrepresented (enriched) in my dataset of upregulated genes. As for FIDEA, the sources of the functional annotation are databases such as KEGG and GO. One of the enriched clusters included terms related to vesicle fusion, which is a key event for CTL killing via the degranulation pathway (Dieckmann et al., 2016). The heatmap in Figure 4.3D visualises the overlap between upregulated genes in my dataset and the gene lists in the vesicle fusion annotation cluster. Ten genes were chosen from this list to target using CRISPR. These genes were *Ppfia3*, *Anxa1*, *Anxa2*, *Anxa3*, *Anxa4*, *Tns2*, *Cav2*, *Cpne5*, *Dysf* and *Unc13a*. Additionally, three other genes, *Slc7a5*, *Hif1*α and *Nfil3*, that were significantly upregulated in my activated gene list were added as further CRISPR targets. These three genes were previously found to have interesting phenotypes in CD8 T cells. Lack of SLC7A5 protein was shown to result in failure of CD8 T cells to differentiate into CTL (Sinclair et al., 2013) and HIF-1α and NFIL3, also known as E4BP4, depleted CD8 T cells were shown to lack perforin (Rollings et al., 2018). As these studies used mouse models, it would be interesting to test if these genes are also crucial for effector functions when only knocked out at day 4 post in vitro stimulation, as in my experimental set up. An overview of how differentially expressed the genes chosen for the targeted screen were can be seen in Table 4.2.

4.2.4 Targeted CRISPR screen

The genes of interest were targeted by CRISPR as explained in detail in chapter 3. In short, at day 4 post in vitro activation CTLs derived from OT-I mice were nucleofected with 3 crRNAs against the genes of interest, in addition to the tracrRNA reagent and Cas9 protein. Subsequently, CTLs were expanded for four days before measuring their degranulation and killing ability. As can be seen in Figure 4.4A, no degranulation defect was observed in response to targeting the genes of interest using CRISPR. Instead, some targets, most notably *Nfil3*, showed a trend towards increasing degranulation upon CRISPR treatment (Figure 4.4A). Two genetic targets, *Nfil3* and *Hif1*α, seemed to decrease CTL killing reproducibly after being targeted by CRISPR (Figure 4.4B).

Table 4.2 ***Differentially expressed genes chosen for the targeted CRISPR screen.***

Gene	Log2(FoldChange)	p-value	B-H adjusted p-value
Nfil3	5.450	0.00E+00	0.00E+00
Anxa2	4.143	0.00E+00	0.00E+00
Slc7a5	3.591	0.00E+00	0.00E+00
Hif1α	2.446	0.00E+00	0.00E+00
Unc13a	4.223	4.01E-202	1.19E-200
Anxa4	3.115	6.03E-191	1.60E-189
Anxa3	5.661	1.12E-138	1.82E-137
Anxa1	4.261	6.69E-117	8.39E-116
Cav2	5.133	5.14E-40	2.39E-39
Tns2	2.940	2.61E-27	9.64E-27
Cpne5	2.878	1.29E-20	4.16E-20
Ppfia3	2.963	4.34E-14	1.19E-13
Dysf	2.162	0.000626692	0.001118686

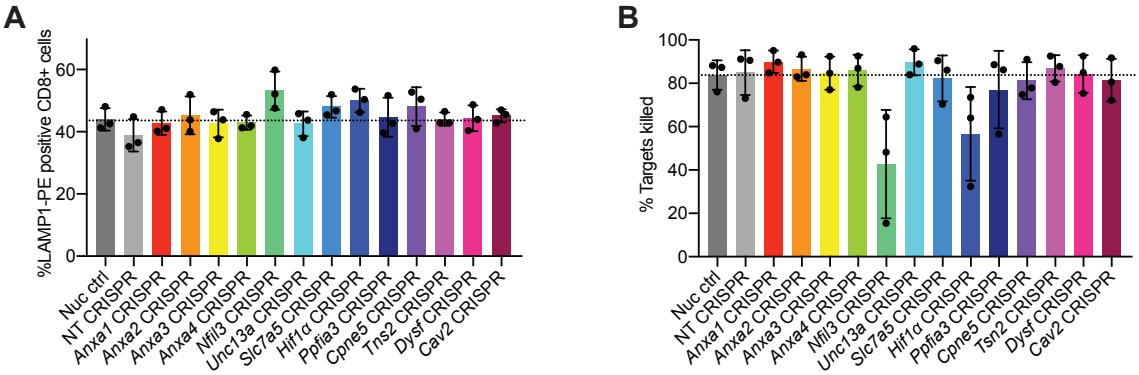

Fig. 4.4 ***Screening RNA-seq target genes using CRISPR.*** *CTLs were tested for their ability to degranulate and kill in response to exposure to EL4 target cells loaded with OVA-peptide.* ***A*** *The degranulation and* ***B*** *the killing readout of the combined degranulation and killing assays were analysed following the gating strategy and calculations described in chapter 2, section 2.5.1 and 2.5.2. E:T ratio = 2.5:1, assay duration = 180 min. The bar graphs show the average of 3 independent experiments, error bars show the SD. During each independent repeat the experiment was performed in technical duplicates.*

Based on the screening results, the effect of *Nfil3* and *Hif1α* CRISPR was investigated further. This confirmed that *Nfil3* CRISPR significantly increased degranulation (n=5, $p<0.05$, paired t-test) and decreased killing (n=5, $p<0.01$, paired t-test) as shown using two different killing assays (Figure 4.5A-C).

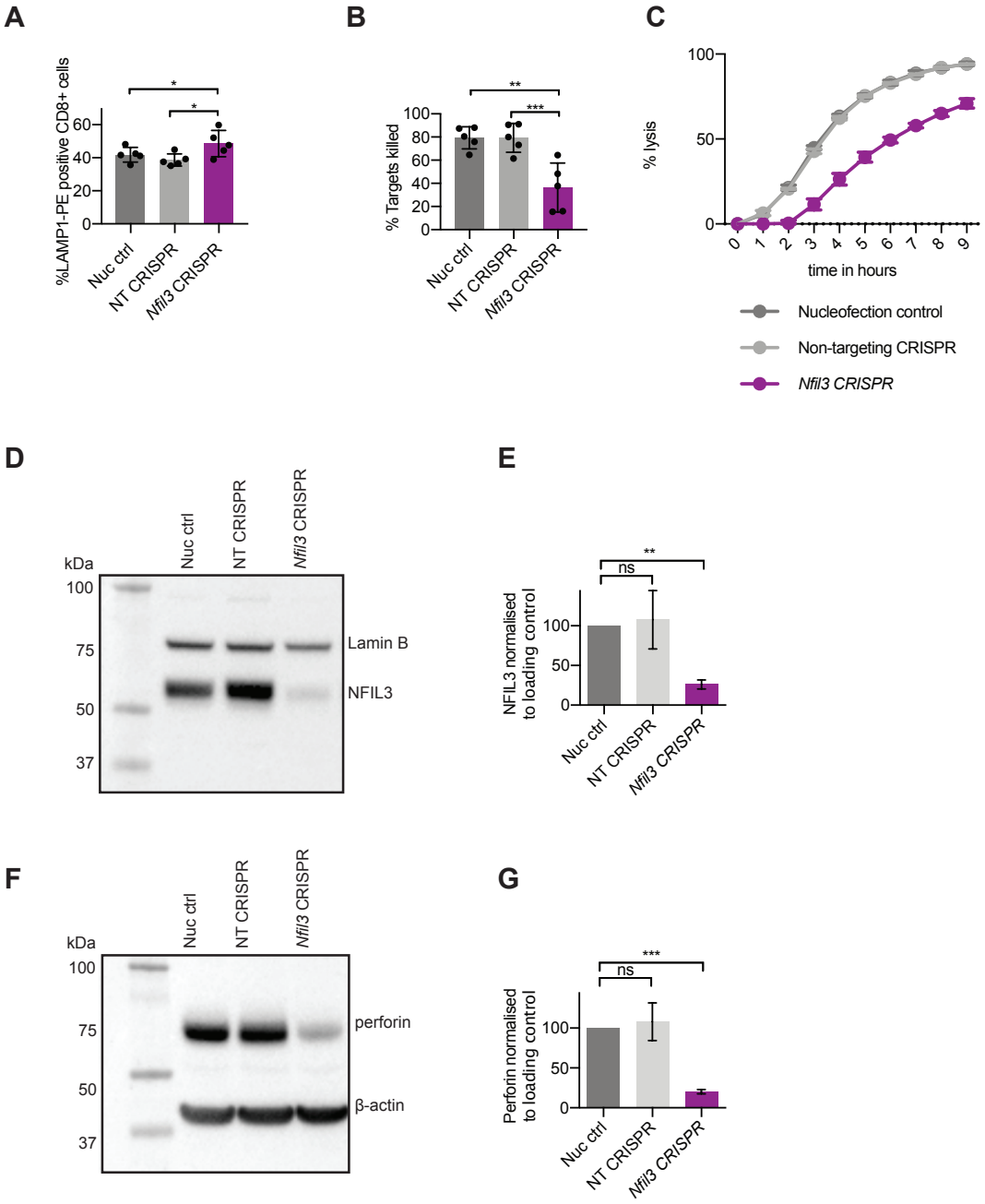

Fig. 4.5 ***Targeting Nfil3 by CRISPR resulted in a CTL killing defect.***

Fig. 4.5 ***Targeting Nfil3 by CRISPR resulted in a CTL killing defect.*** *OT-I CTL were nucleofected at day 4 after in vitro stimulation and tested in functional assays at day 8. CTLs were tested for their ability to degranulate and kill in response to exposure to EL4 target cells loaded with OVA-peptide.* ***A*** *The degranulation and* ***B*** *the killing readout of the combined degranulation and killing assays were analysed following the gating strategy and calculations described in chapter 2, section 2.5.1 and 2.5.2. E:T ratio = 2.5:1, assay duration = 180 min. The bar graphs show the average of 5 independent experiments, error bars show the SD. During each independent repeat the experiment was performed in technical duplicates, *p<0.05, **p<0.01, ***P<0.001 as calculated by paired t-test. Samples were paired by day of experiment to account for day-to-day fluctuations.* ***C*** *Incucyte killing assay readout showing % lysis of red EL4 target cells. One representative plot for 3 independent experiments is shown. E:T ratio = 10:1 Each datapoint corresponds to the mean ± SD of 3-4 technical repeats.* ***D*** *Representative WB showing NFIL3 and Lamin B1 (loading control) protein expression four days after nucleofection.* ***E*** *Quantification of the NFIL3 protein level. In each repeat the NFIL3 protein level was expressed relative to the nucleofection control and normalised to the loading control, n=3 independent experiments, **p<0.01 calculated by one-sample t-test.* ***F*** *Representative WB showing perforin and β-actin (loading control) protein expression four days after nucleofection.* ***G*** *Quantification of the perforin protein level. In each repeat the perforin protein level was expressed relative to the nucleofection control and normalised to the loading control, n=3 independent experiments, ns = not significant, ***p<0.001 calculated by one sample t-test. All bar graphs show the mean ± SD.*

Hif1α CRISPR also significantly decreased the ability of CTLs to kill (n=5, p<0.01, paired t-test), but only showed a trend towards increasing degranulation (Figure 4.6A-C). To validate CRISPR efficiency I tested for target protein expression by WB. Decreased NFIL3 protein levels were observed in *Nfil3* CRISPR samples (n=3, p<0.01, one sample t-test) (Figure 4.5D,E). HIF-1α protein could initially not be detected by WB, most likely because the samples were unstimulated and kept under normoxic conditions (Nakamura et al., 2005). When stimulated with αCD3ε for 4 h in hypoxic conditions (1% O_2) HIF-1α could be detected by WB, and HIF-1α levels were found to be reduced in *Hif1α* CRISPR samples (n=1) (Figure 4.6D). Additionally, *Hif1α* CRISPR samples were shown to have decreased NFIL3 protein levels (n=2) (Figure 4.6E,F), which was in agreement with a study where *Hif1α* was deleted in all Vav-expressing cells using the Cre-lox system in mice (Rollings et al., 2018).

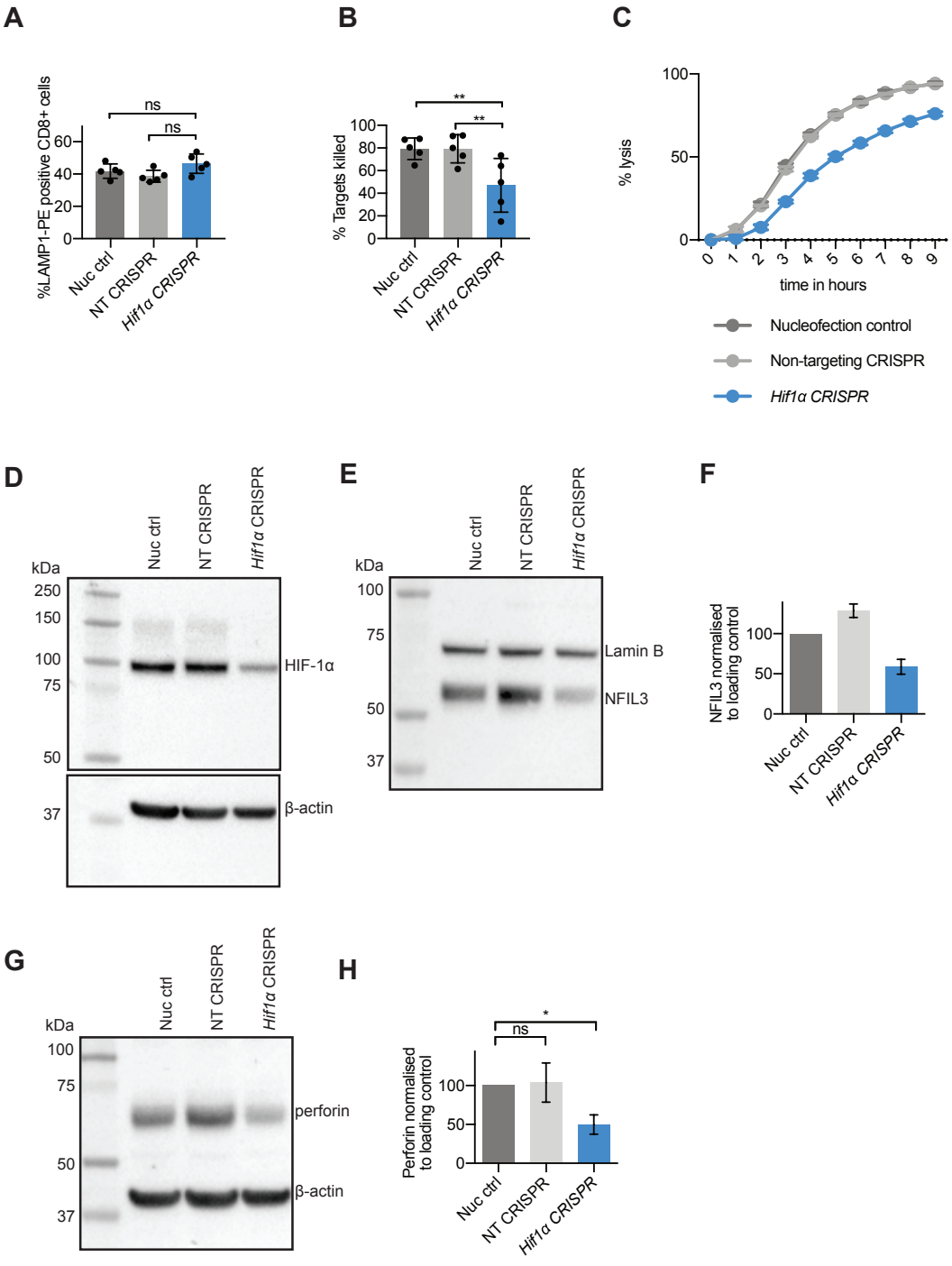

Fig. 4.6 ***Decreased killing in response to targeting Hif1α by CRISPR.***

Fig. 4.6 ***Decreased killing in response to targeting Hif1α by CRISPR.*** *OT-I CTL were nucleofected at day 4 after in vitro stimulation and tested in functional assays at day 8. CTLs were tested for their ability to degranulate and kill in response to exposure to EL4 target cells loaded with OVA-peptide.* ***A*** *The degranulation and* ***B*** *the killing readout of the combined degranulation and killing assays were analysed following the gating strategy and calculations described in chapter 2, section 2.5.1 and 2.5.2. E:T ratio = 2.5:1, assay duration = 180 min. The bar graphs show the average of 5 independent experiments, error bars show the SD. During each independent repeat the experiment was performed in technical duplicates, **p<0.01 as calculated by paired t-test. Samples were paired by day of experiment to account for day-to-day fluctuations.* ***C*** *Incucyte killing assay readout showing % lysis of red EL4 target cells. One representative plot for 3 independent experiments is shown. E:T ratio = 10:1 Each datapoint corresponds to the mean ± SD of 3-4 technical repeats.* ***D*** *WB showing HIF-1α and β-actin (loading control) protein expression four days after nucleofection of CRISPR reagents and 4 h after αCD3ε stimulation under hypoxic conditions, n=1.* ***E*** *Representative WB showing NFIL3 and Lamin B1 (loading control) protein expression four days after nucleofection.* ***F*** *Quantification of the NFIL3 protein level. In each repeat the NFIL3 protein level was expressed relative to the nucleofection control and normalised to the loading control, n=2 independent experiments.* ***G*** *Representative WB showing perforin and β-actin (loading control) protein expression four days after nucleofection.* ***H*** *Quantification of the perforin protein level. In each repeat the perforin protein level was expressed relative to the nucleofection control and normalised to the loading control, n=3 independent experiments, ns = not significant, *p<0.05 calculated by one sample t-test. All bar graphs show the mean ± SD.*

The phenotype of increased degranulation and decreased killing was reminiscent of the phenotype observed upon *perforin* CRISPR (Figure 3.8). Other studies showed that deleting components of the HIF-1 complex or NFIL3 in mice resulted in decreased perforin expression (Finlay et al., 2012; Rollings et al., 2018). I therefore investigated the effect of *Hif1α* and *Nfil3* CRISPR on perforin protein levels by WB, which confirmed that perforin was decreased in *Hif1α* (n=3, p<0.05, one sample t-test) and *Nfil3* CRISPR samples (n=3, p<0.001, one sample t-test) (Figure 4.5F,G and Figure 4.6G,H).

4.2.5 Comparing gene expression in activated CD8 T cells derived from males and females

As the PCA plot in Figure 4.2 indicated that some of the variance in my dataset was due to differences between sexes, I investigated which genes were differentially expressed between CD8 T cells derived from males and females. For this, I compared male and female samples derived from the day 7 group and applied the same significance thresholds as before to identify differentially expressed genes (padj<0.01, log2(fold change) >2 or <-2). Differentially expressed genes that passed these stringent selection criteria were limited to *Ddx3y*, *Kdm5d*, *Eif2s3y* and *Uty*, all of which are located on the Y chromosome according to the NCBI website (Table 4.3). Not taking into account the stringent log2(fold change) cut-off revealed 79 significantly up- or down regulated genes (all with padj<0.01). Interestingly, this gene list included *Nfil3*, as well as genes that encode several different granzymes (Table 4.3).

Table 4.3 ***Differentially expressed genes when comparing activated T cells derived from males to activated T cells derived from females.***

Gene	Log2(FoldChange)	p-value	B-H adjusted p-value
Ddx3y	4.231	0.00E+00	0.00E+00
Kdm5d	3.348	0.00E+00	0.00E+00
Eif2s3y	3.081	0.00E+00	0.00E+00
Uty	2.478	1.18E-206	4.07E-203
Eif2s3x	-0.649	7.24E-29	2.00E-25
Kdm5c	-0.481	2.10E-23	4.81E-20
Kdm6a	-0.627	1.85E-22	3.64E-19
Il10	-0.651	1.93E-17	3.32E-14
Pbdc1	-0.477	6.07E-14	9.29E-11
Gm29650	0.333	3.93E-13	5.41E-10
Fosb	-0.519	3.29E-11	4.12E-08
Gldc	0.379	8.06E-11	9.25E-08
Esm1	-0.414	5.19E-10	5.49E-07
Eng	-0.488	1.24E-09	1.22E-06
Gm5861	-0.471	1.37E-09	1.26E-06
Cdh17	-0.456	1.10E-08	9.46E-06
Gzma	-0.377	1.47E-08	1.16E-05
Tcrg-C2	-0.447	1.51E-08	1.16E-05
Maf	0.425	3.14E-08	2.17E-05

Table 4.3 continued from previous page

Gene	Log2(FoldChange)	p-value	B-H adjusted p-value
Gzmf	-0.39	3.13E-08	2.17E-05
5530601H04Rik	-0.424	3.69E-08	2.31E-05
Epas1	-0.426	3.59E-08	2.31E-05
Xist	-0.211	8.06E-08	4.82E-05
Pkhd1l1	-0.388	1.41E-07	8.11E-05
Gzmc	-0.384	2.63E-07	0.000145102
Cyp11a1	-0.248	3.82E-07	0.000202287
Pparg	-0.297	4.70E-07	0.000239877
Epsti1	0.282	6.22E-07	0.000295237
Gm8897	-0.373	6.17E-07	0.000295237
Ms4a4c	0.37	8.01E-07	0.000367891
Csgalnact1	-0.304	9.44E-07	0.000406428
Slc16a10	-0.395	9.19E-07	0.000406428
She	0.334	9.76E-07	0.000407425
Batf3	-0.332	1.01E-06	0.000407867
Cxcr6	0.381	1.08E-06	0.000411676
Btla	0.378	1.08E-06	0.000411676
Spry2	-0.385	1.70E-06	0.000632598
Il24	-0.293	2.09E-06	0.000757181
Speer1	-0.337	2.29E-06	0.000809682
Nfil3	-0.299	3.90E-06	0.001343211
Procr	-0.266	4.08E-06	0.001369305
Scin	-0.307	6.21E-06	0.002035039
Fcgrt	0.271	7.35E-06	0.002355526
Avil	-0.353	7.72E-06	0.002416567
Trp53inp1	0.335	8.60E-06	0.002576152
Prss12	0.317	8.56E-06	0.002576152
Map1a	0.324	8.92E-06	0.002613249
Arhgap4	0.212	9.15E-06	0.002625824
Mxd4	0.343	9.63E-06	0.002678748
Mcpt8	-0.27	9.72E-06	0.002678748
Spire1	-0.292	1.21E-05	0.003170046
Gm8890	-0.3	1.22E-05	0.003170046

Table 4.3 continued from previous page

Gene	Log2(FoldChange)	p-value	B-H adjusted p-value
Atf3	-0.349	1.20E-05	0.003170046
Jdp2	-0.327	1.39E-05	0.0035429
Gm19705	0.341	1.57E-05	0.003862068
Gm8879	-0.299	1.57E-05	0.003862068
Il6ra	0.28	1.72E-05	0.00402067
Loxl2	-0.244	1.71E-05	0.00402067
Gzmg	-0.265	1.67E-05	0.00402067
Cd7	0.285	1.90E-05	0.004372669
Trgv2	-0.341	1.95E-05	0.004401909
Il2ra	-0.222	2.21E-05	0.004918823
Cxcr3	0.326	2.35E-05	0.005068284
Pisd-ps1	-0.291	2.35E-05	0.005068284
Fkbp11	-0.285	2.43E-05	0.005098991
Lag3	-0.339	2.44E-05	0.005098991
Epdr1	-0.238	2.61E-05	0.005361774
Fcer1g	-0.331	2.76E-05	0.005581624
Vipr1	0.297	3.16E-05	0.006255572
Tcrg-C4	-0.327	3.18E-05	0.006255572
Dgka	0.264	3.31E-05	0.006429906
Myo1e	-0.314	3.68E-05	0.007031746
Nt5e	0.331	3.84E-05	0.007150566
Plcg2	-0.267	3.81E-05	0.007150566
Nod1	0.292	4.79E-05	0.008801724
Tmem37	0.319	4.98E-05	0.00902281
Slc22a21	-0.247	5.06E-05	0.00905477
Chd3	0.263	5.66E-05	0.009986283
Slc4a7	-0.3	5.73E-05	0.009986283

4.3 Discussion

The RNA-seq study set up was designed to show differences between the transcriptome of naive CD8 T cells and effector CD8 T cells that were stimulated and kept in culture for 7 days (Figure 4.1A). The heatmap and PCA plots in Figure 4.2 demonstrated that samples

were mainly separated according to whether the RNA was derived from naive cells (day 0) or effector cells (day 7), indicating that the gene expression differs between these two states of cells. The PCA plots further revealed that some variance in the dataset was due to the spleen collection date and whether samples were derived from males or females (Figure 4.2C). The former was accounted for during subsequent analysis steps.

Differential expression analysis using the DESeq2 package revealed 1803 differentially expressed genes where gene expression is upregulated, and 2584 differentially expressed genes where gene expression is downregulated. Subsequently, I focussed on the 1803 activated differentially expressed genes, as this dataset should include genes that are required for CTL killing. However, this dataset will additionally also include genes that are required for other processes in T cell differentiation to cytolytic effectors, such as cell proliferation and switching glucose metabolism from oxidative phosphorylation to glycolysis to fuel cell growth (Fox et al., 2005). Using the functional annotation tool FIDEA confirmed that most of the genes in my activated dataset associated with pathways related to proliferation (e.g. cell cycle) (Figure 4.3B,C). This was reproducible using two different curations, KEGG and GO, for the analysis (Figure 4.3B,C).

While I could have taken the approach to target the top upregulated genes in my dataset (Table 4.1), a more targeted approach to isolate genes that may affect CTL killing was chosen instead due to the concerns mentioned above. The DAVID functional annotation tool was used in order to identify annotation clusters of genes related to what is known to be important for CTL killing function. An annotation cluster was identified that was enriched in my dataset and contained gene lists associated with vesicle fusion (Figure 4.3D). Vesicle fusion is known to be important during the degranulation mechanism of CTL killing. 10 genes were chosen from this list with a focus on genes that had not been studied extensively in CTL. Additionally, 3 other genes were included that were identified as interesting targets from the literature (Finlay et al., 2012; Rollings et al., 2018; Sinclair et al., 2013).

The screen was performed in primary mouse CTL derived from OT-I mice as these had been used successfully with the CRISPR technology (chapter 3) and were readily available in the Griffiths lab. The results of the RNA-seq study should be applicable to the OT-I system, as these mice are bred on a C57BL/6 background. T cells derived from OT-I mice express the OT-I TCR, which specifically recognises the OVA peptide presented by the H-2K^b MHC class I molecule (Hogquist et al., 1994). Out of the 13 genes that were targeted by CRISPR (Table 4.2), only *Hif1*α and *Nfil3* showed a reproducible phenotype across three independent

repeats (Figure 4.4). Due to time constraints, the other 11 genes were not followed up further. However, I can not conclude that these genes have no effect on CTL degranulation or killing without validating that the genes were successfully targeted by CRISPR. Since not all of these genes have commercially available antibodies against their protein, the effect of CRISPR could instead be confirmed by sequencing the DNA or by looking at the mRNA levels using qRT-PCR. While these techniques would show if a cut occurred at the DNA level, or if there is a decrease in mRNA, respectively, neither approach would be guaranteed to reflect the expression of functional protein.

The killing defect observed in response to *Nfil3* and *Hif1α* CRISPR was confirmed using two different in vitro killing assays (Figure 4.5B,C and Figure 4.6B,C). Western blotting confirmed that NFIL3 protein levels were decreased upon *Nfil3* CRISPR (Figure 4.5D,E). HIF-1α protein levels were only detectable by WB after samples were stimulated with αCD3ε under hypoxic conditions (Figure 4.6D). Other studies have shown that while HIF-1α cannot be detected by WB when effector CTL are kept under normoxic conditions, HIF-1α levels are increased after switching cells to hypoxic conditions and in response to TCR stimulation (Doedens et al., 2013; Nakamura et al., 2005; Palazon et al., 2017; Rollings et al., 2018). In agreement with the literature, NFIL3 levels were reduced in *Hif1α* CRISPR samples, providing further evidence that the *Hif1α* gene was successfully targeted by CRISPR (Figure 4.6E,F). Furthermore, perforin protein levels were decreased in both *Nfil3* and *Hif1α* CRISPR samples (Figure 4.5F,G and Figure 4.6G,H). This has previously been observed in a study using the Cre-lox system, with Cre expression under the control of the *vav*-promoter, to delete *Nfil3* and *Hif1α* in hematopoietic cells (Rollings et al., 2018). However, HIF-1 regulation of perforin was found to be indirect, as the perforin promoter did not contain HIF-1 complex binding sites (Finlay et al., 2012). In future experiments, it would be interesting to investigate whether the *Nfil3* promoter contains HIF-1α binding sites, to determine whether *Nfil3* is directly regulated by HIF-1α. Additionally, it would be interesting to overexpress NFIL3 in *Hif1α* KO cells. If this rescues the killing phenotype it could suggest that the killing defect in *Hif1α* KO CTLs is mediated via NFIL3.

Although the exact mechanism by which *Hif1α* and *Nfil3* KO lead to a decrease in perforin is not understood, this explained at least in part why targeting these genes by CRISPR resulted in a CTL killing defect at the molecular level. In agreement with my findings, other studies showed that deletion of the HIF-1 complex in CTL resulted in decreased production of other effector molecules (IFNγ, TNFα and granzyme B) as well as reduced tumour cell killing in vivo (Finlay et al., 2012; Palazon et al., 2017). Meanwhile, increased *Hif1α* expression,

achieved through the loss of one of the main negative regulators of the HIF transcription factors (the von Hippel-Lindau complex), resulted in increased effector function of CTL, as measured by an increase in the expression of effector molecules, such as granzyme B and perforin, and in an in vivo cytotoxicity assay (Doedens et al., 2013). Additionally, *Nfil3* KO mice were found to have severely reduced levels of peripheral NK cells and impaired NK cell cytotoxicity (Gascoyne et al., 2009).

In addition to comparing the transcriptome of effector and naive CD8 T cells, my RNA-seq dataset also allowed me to compare effector CD8 T cells derived from male and female mice. Only Y-linked genes passed the log2(fold change)>2 or <-2 and padj<0.01 cut offs (Table 4.3). This was expected, as females do not have Y chromosomes. Looking at the genes that were significantly differentially expressed (padj<0.01), but had a smaller effect size (log2(fold change)>-2 and <2), interestingly identified that CD8 T cells derived from males had less mRNA encoding several members of the granzyme family, IL2RA and NFIL3 (Table 4.3). It would therefore be interesting to compare expression of NFIL3 protein between males and females, to see if this transcriptional effect is also present at the protein level. Furthermore, it could be investigated whether this also translates to a better killing capability in cells derived from female mice.

In summary, my data, together with published studies, convincingly showed that HIF-1α and NFIL3 are crucial for CTL killing function. The data in this chapter demonstrated that loss of NFIL3 and HIF-1α showed an effect even when these genes are only knocked out in effector CTL. This indicated that the phenotype is not dependent on HIF-1α and NFIL3 being absent during T cell development or effector CTL differentiation. Furthermore, the RNA-seq dataset revealed interesting differences in expression of mRNAs encoding NFIL3 and several cytotoxic effector molecules between CTLs derived from male and female mice.

4.3.1 Summary and evaluation of aims

- Determine the differences in gene expression between naive and activated CD8 T cells. The hypothesis is that there are substantial changes in gene expression between these two states of CD8 T cells.
  - Significant differences in gene expression were observed: 1803 significantly activated differentially expressed genes with padj<0.01 and log2(fold change)>2 were identified using DESeq2.

- Explore the functional association of the differentially expressed genes using bioinformatic tools.
  - Using FIDEA and DAVID bioinformatic tools identified that upregulated genes in my dataset predominantly associated with pathways related to cell proliferation, which was not unexpected as CD8 T cells undergo rapid clonal expansion upon stimulation.
- Test the effect of targeting differentially expressed genes by CRISPR in phenotypic assays (degranulation and killing assays).
  - *Hif1α* and *Nfil3* were identified as interesting genetic targets that decreased killing but not the degranulation capability of CTL. *Hif1α* and *Nfil3* have previously been identified as affecting CD8 T cell cytotoxicity in KO mouse models (Doedens et al., 2013; Finlay et al., 2012; Rollings et al., 2018). Here I show that loss of these genes also had an effect on cytotoxicity when expression of these genes is only lost in differentiated effector CTL in vitro, as opposed to in naive T cells or during T cell development in vivo. This suggested a more immediate importance of these genes in CTL killing.
- Explore what genes are differentially expressed in CD8 T cells derived from male and female mice.
  - Highly differentially expressed genes (log2(fold change)>2) were limited to Y-linked genes when comparing males to females. Interestingly, genes that were significantly differentially expressed, but that did not pass the stringent log2(fold change) cut-off, included genes known to be important for CTL function (such as *Gzma* and *Il2ra*), as well as *Nfil3*.

Chapter 3 and chapter 4 make up the portion of the thesis that focuses on primary mouse T cells. One of the main conclusions from this aspect of the PhD project is that gene expression in primary mouse CTLs can be efficiently disrupted using the CRISPR Cas9-RNP approach as optimised in the last two chapters. Importantly, this approach can be used in cells derived from any mouse line, regardless of the genetic background. This provides an effective and versatile tool to study the function of genes in primary mouse T cells.

Additionally, the newly established assay that simultaneously measures degranulation and killing can be used to identify phenotypes of interest, as demonstrated using an arrayed CRISPR screen. The readout of the assay was reliable, as comparable results were obtained

using a separate phenotypic assay, the Incucyte killing assay. In combination with the optimised CRISPR technology, the assay enables to identify genes important for CTL killing and/or degranulation.

In hindsight, the experimental design of the RNA-seq study could have been more targeted to the overall aim of the thesis, which was to identify regulators of CTL killing. Instead, the RNA-seq study more broadly identified genes that are implicated in CD8 T cell activation. While some of the genes upregulated in response to activation are necessary for CTL killing, they are overshadowed by genes important for other biological functions, such as the proliferation response. A possible alternative approach would have been to incorporate purified CD4 T cells in the study design. Comparing the transcriptome of activated CD4 and CD8 T cells would have allowed to filter out genes associated with proliferation in response to activation, and would have revealed genes relevant for CD8 T cell specific functions. Nonetheless, the RNA-seq dataset presented in this chapter is a useful resource, as it presents a comprehensive readout of all genes that are expressed in primary mouse naive and activated CD8 T cells.

Chapter 5

Screening a compound library that targets the NF-κB pathway in human T cells

5.1 Introduction

The assay developed to measure degranulation and killing simultaneously was successfully used for a small screen in mCTL in chapter 4. The work in this chapter aimed to 1) test whether this assay also works in hCTL, as a more medically relevant cell type, and 2) to test the extent to which the combined degranulation and killing assay can be scaled.

In chapter 3, CRISPR was used to target *Munc13-4*, *Rab27a* and the gene encoding perforin (*Prf1*) in mCTL and the resulting samples were used to validate the newly developed combined degranulation and killing assay. Since I had not yet set up the CRISPR technology in hCTL, I instead used cells derived from FHL2 and FHL3 patients to address point 1. FHL2 is caused by mutations in *PRF1*, and FHL3 is associated with mutations in *MUNC13-4*. Both of these genes are crucial for CTL function as demonstrated by data shown in chapter 3 and the literature (Crozat et al., 2007; Feldmann et al., 2003; Kägi et al., 1994a; Stepp et al., 1999).

To test the scalability of the assay, I used a chemical compound library targeting the NF-κB signalling pathway obtained from Medchem express. The combined degranulation and killing assay, performed in a 96 well format, was reasoned to be easily adaptable for screening dozens of compounds. The NF-κB compound library consisted of 64 drugs, and allowed me to test the scalability of the combined degranulation and killing assay while

simultaneously asking whether NF-κB has a direct role in CTL killing.

The canonical NF-κB signalling pathway is known to be activated in response to TCR recognition of its cognate antigen in the context of MHC class I. TCR signalling and CD28 co-stimulatory signals trigger activation of PKCθ and its recruitment to the IS (Oh and Ghosh, 2013; Paul and Schaefer, 2013). PKCθ has been shown to phosphorylate CARMA1, and phosphorylated CARMA1 can bind to BCL10 and MALT1 (Schulze-Luehrmann and Ghosh, 2006; Vallabhapurapu and Karin, 2009). MALT1 and BLC10 are thought to be polyubiquitinated by TRAF6 (Paul and Schaefer, 2013), resulting in recruitment of the IκB kinase (IKK) complex, consisting of IKKα, IKKβ and IKKγ, via the polyubiquitination binding motif of IKKγ (Paul and Schaefer, 2013). Subsequently, IKKγ and IKKβ are activated by polyubiquitination and phosphorylation, respectively. Activated IKKβ phosphorylates the inhibitor of κB (IκB), which triggers ubiquitination and degradation of IκB via the 26S proteasome (Paul and Schaefer, 2013; Vallabhapurapu and Karin, 2009).

The NF-κB family of transcription factors consists of p105/p50 (NFkB1), p100/p52 (NFkB2), p65 (RelA), RelB and c-Rel (Paul and Schaefer, 2013; Vallabhapurapu and Karin, 2009). They share a Rel homology domain that is important for DNA binding and dimerisation (Oh and Ghosh, 2013; Vallabhapurapu and Karin, 2009). Under basal conditions, NF-κB is retained in the cytoplasm as inactive heterodimers or homodimers bound by the inhibitor of κB. TCR-mediated degradation of IκB, as outlined above, allows NF-κB dimers to translocate into the nucleus and regulate transcription of their target genes (Vallabhapurapu and Karin, 2009).

In the nucleus, NF-κB transcription factors bind to promoters that contain κB binding sites. One crucial NF-κB target gene is the gene encoding IκBα, thereby ensuring a negative feedback mechanism to terminate NF-κB signalling (Vallabhapurapu and Karin, 2009). NF-κB is reported to activate expression of over 150 target genes, including cytokines, chemokines and adhesion molecules (Pahl, 1999). NF-κB target genes are important for T cell activation, proliferation, differentiation and survival (Schulze-Luehrmann and Ghosh, 2006; Vallabhapurapu and Karin, 2009). It is clear that the NF-κB signalling pathway is crucial for T cell function, but less is known about its importance for CTL killing specifically. The NF-κB drug library was used to investigate the role of NF-κB in degranulation of CTLs and their killing.

5.1.1 Chapter aims

- Test the combined degranulation and killing assay in hCTL using FHL2 and FHL3 patient samples.
- Investigate the scalability of the assay using a NF-κB compound library.
- Follow up promising hits to elucidate their mechanism of action.

5.2 Results

5.2.1 Testing the combined degranulation and killing assay using patient-derived CTL

The combined degranulation and killing assay was tested in hCTL using cells derived from FHL3 patients (carrying mutations in *MUNC13-4*) and FHL2 patients (carrying mutations in *PRF1*). The exact mutations of all patients are outlined in chapter 2, Table 2.2. hCTL derived from FHL3 patients significantly degranulated less (n=3, $p<0.0001$, unpaired t-test with Welch's correction) and killed target cells less efficiently (n=3, $p<0.01$, unpaired t-test with Welch's correction) than hCTL derived from HDs (Figure 5.1A,B). The killing phenotype was confirmed for every patient using the Incucyte killing assay (Figure 5.1C-E). In agreement with the phenotype observed, WB showed that less MUNC13-4 protein was expressed in patient-derived cells than in cells derived from HDs (Figure 5.1F).

Cells derived from FHL2 patients did not show a defect in degranulation (Figure 5.2A), but showed a significant decrease in the ability to kill target cells (n=4, $p<0.0001$, unpaired t-test with Welch's correction) (Figure 5.2B). Again, the killing phenotype was confirmed using the Incucyte killing assay (Figure 5.2C-F). WB for perforin showed that less protein was expressed in patient-derived cells than in cells derived from HDs (Figure 5.2G). Interestingly, the perforin antibody recognised two bands in lysates derived from patient 6981 and patient 3026 (Figure 5.2G). These bands were of a higher molecular weight than the banding pattern produced in samples derived from 5 different HDs. This suggested that while the mutations in patients 6981 and 3026 did not cause a complete loss of perforin, they still resulted in impaired protein function. In summary, the patient results demonstrated that the combined degranulation and killing assay can be used to reliably identify hCTLs with a defect in killing, degranulation, or both.

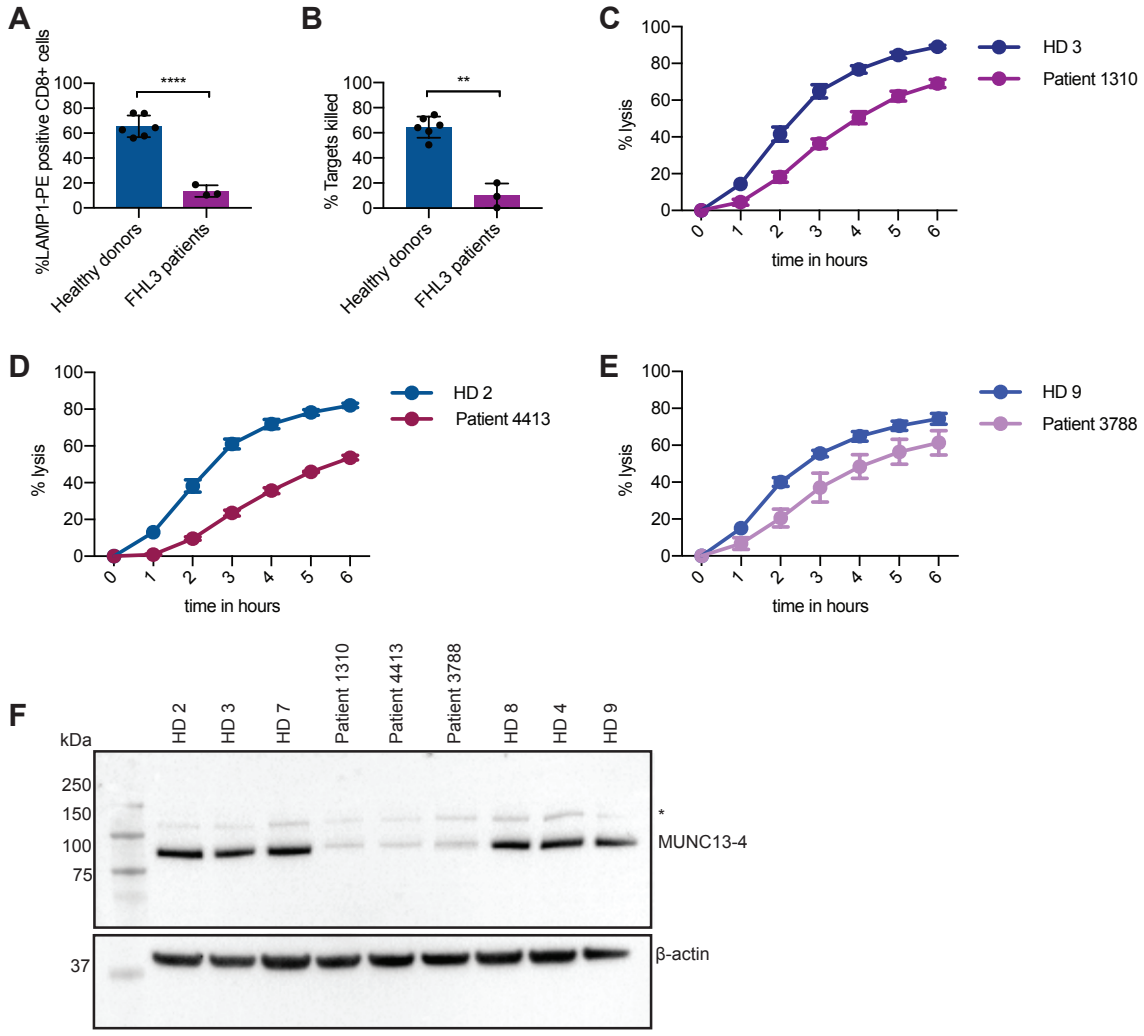

Fig. 5.1 ***Decreased degranulation and killing in cells derived from FHL3 patients.*** ***A*** *The degranulation and* ***B*** *killing readout of the combined degranulation and killing assays were analysed following the gating strategy and calculations described in chapter 2, section 2.5.2. CTLs were derived from three independent FHL3 patients and compared to CTLs derived from 6 independent HDs. All samples were purified to isolate CD8 cells. E:T ratio = 2.5:1, assay duration = 180 min. Each data point is the average of 2-4 technical repeats. **p<0.01, ****p<0.0001 as calculated by unpaired t-test with Welch's correction. Bar graphs show the mean ± SD.* ***C*** *Incucyte killing assay showing % lysis of red P815 target cells in the presence of αCD3 and HD 3 or patient 1310,* ***D*** *HD 2 or patient 4413 and* ***E*** *HD 9 or patient 3788. E:T = 2.5:1. Each datapoint is an average of 3-4 technical repeats and the error bars show the SD.* ***F*** *WB showing MUNC13-4 and β-actin (loading control) protein expression in CTL derived from the indicated HDs and patients. HD = healthy donor, SD = standard deviation, us = unspecific, FHL = familial hemophagocytic lymphohistiocytosis. * = potentially non-specific band.*

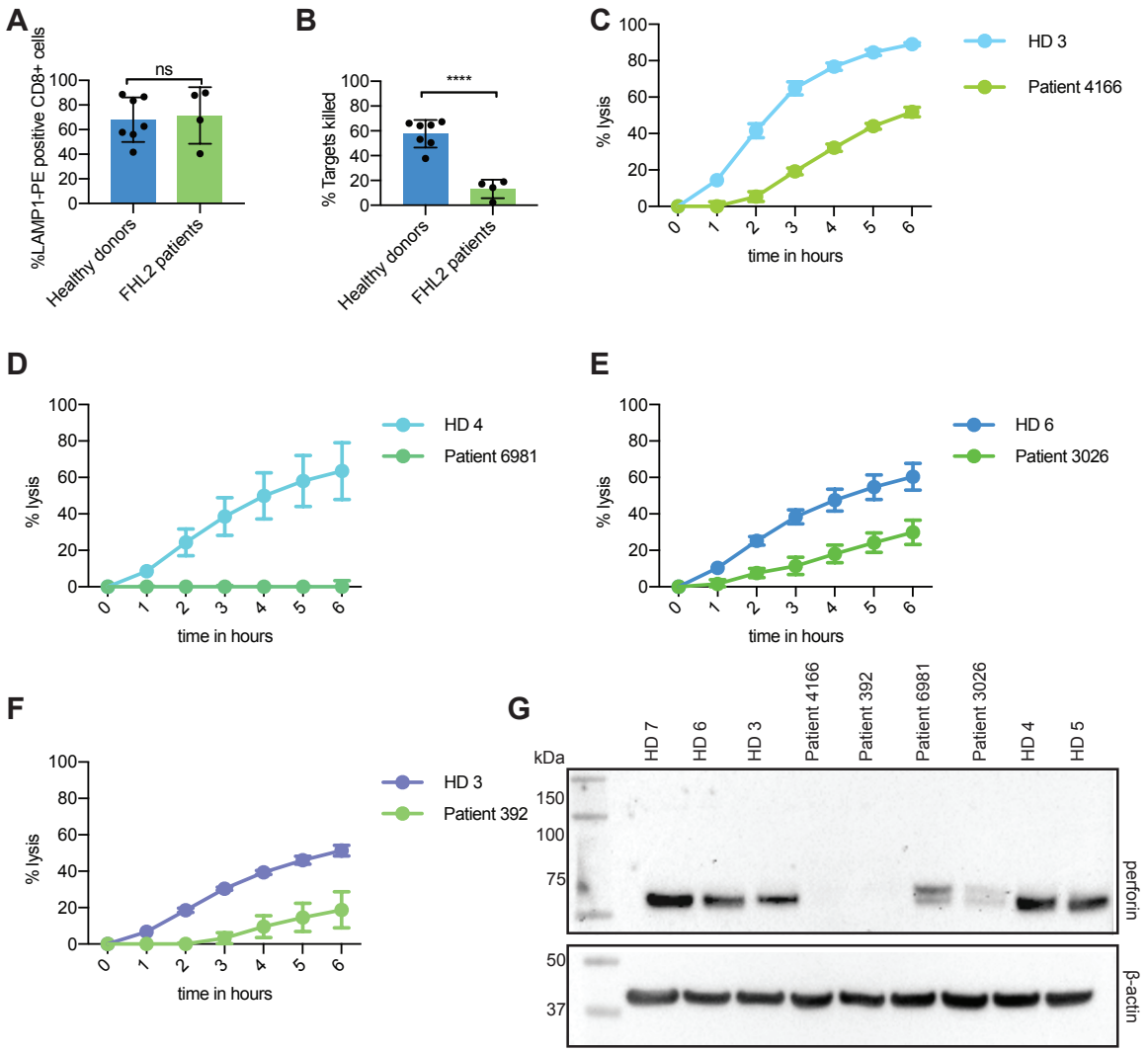

Fig. 5.2 ***CTLs derived from FHL2 patients showed a killing defect.*** ***A*** *The degranulation and* ***B*** *killing readout of the combined degranulation and killing assays were analysed following the gating strategy and calculations described in chapter 2, section 2.5.2. CTLs were derived from four independent FHL2 patients and compared to CTLs derived from 7 independent HDs. All samples were purified to isolate CD8 cells. E:T ratio = 2.5:1, assay duration = 180 min. Each data point is the average of 2-4 technical repeats. ****p<0.0001 as calculated by unpaired t-test with Welch's correction. Bar graphs show the mean ± SD.* ***C*** *Incucyte killing assay showing % lysis of red P815 target cells in the presence of αCD3 and HD 3 or patient 4166,* ***D*** *HD 4 or patient 6981,* ***E*** *HD 6 or patient 3026 and* ***F*** *HD 3 or patient 392. E:T = 2.5:1. Each datapoint is an average of 3-4 technical repeats and the error bars show the SD.* ***G*** *WB showing perforin and β-actin (loading control) protein expression in CTL derived from the indicated HDs and patients. HD = healthy donor, SD = standard deviation, FHL = familial hemophagocytic lymphohistiocytosis.*

5.2.2 Compound library toxicity testing

So far, the combined degranulation and killing assay had been used to screen just over a dozen genetic targets (chapter 4). To test the scalability of this assay, I used a drug library of 64 compounds reported to target the NF-κB signalling pathway. Figure 5.3 shows the composition of this library in terms of molecular targets. Some molecular targets, such as MALT1, IKK and NF-κB, are direct components of the NF-κB signalling cascade downstream of the TCR, as outlined in section 5.1. The RIP kinase is also implicated in activation of the NF-κB signalling pathway (He and Wang, 2018), therefore inhibitors of RIP kinase should inhibit NF-κB function. In contrast members of the PPAR family have been shown to inhibit NF-κB (reviewed by Ricote and Glass (2007)). NRF2, regulated by the protein KEAP1, was shown to inhibit NF-κB, and NF-κB activity is enhanced when NRF2 levels are decreased (reviewed in Wardyn et al. (2015)).

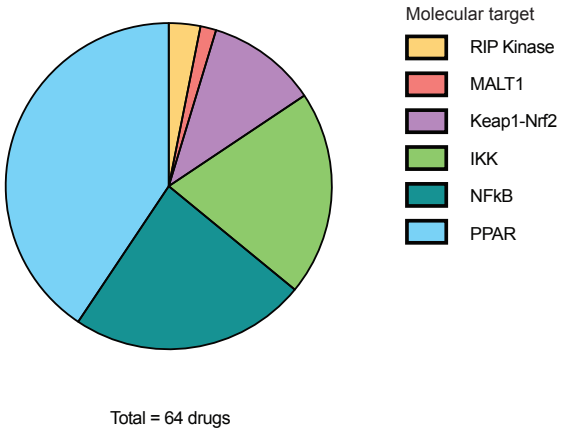

Fig. 5.3 ***Overview of molecular targets of the NF-κB signalling compound library.*** *Piechart showing the molecular targets of the 64 compounds contained in the library obtained from Medchem express. The library contained activators as well as inhibitors. 2 drugs are reported to target RIP kinase, 1 drug is reported to target MALT1, 7 drugs target Keap1-Nrf2, 13 drugs target IKK, 15 drugs target NF-κB and 26 drugs target PPAR. This information was provided by Medchem express.*

For simplicity, the drugs were labelled 1-64 according to the order in which they were supplied. The Celltitre assay (see chapter 2, section 2.8) was used as a toxicity test to determine whether the drugs were toxic to hCTL after overnight treatment with a range of concentrations (Figure 5.4). Initially, I tested the sensitivity of the Celltitre assay, in which absorbance at 490 nm should correspond to the amount of metabolically active cells. I seeded

a range of hCTL per well and measured the absorbance after 4 h incubation with the Celltitre reagents. This clearly showed that absorbance decreased as the number of cells decreased (Figure 5.4A), indicating that this assay could be used to test for toxicity in response to drug treatment.

The highest concentration to be tested was set to 25 μM. This upper threshold was in part based on the EC50/IC50 information provided by the supplier of the compound library, although this information was not available for all 64 compounds. Additionally, using drugs at a maximum of 25 μM meant that the percentage of DMSO to be added to the vehicle control could be kept at, or below, 0.25%. The Celltitre assay was used to show that treating cells with 0.25% DMSO for 24 h did not show toxic effects (Figure 5.4B).

Next, drugs were tested for toxic effects at concentrations between 0.1 μM and 25 μM, achieved by performing serial three-fold dilutions. Corresponding DMSO controls were included on every plate. The change in absorbance in response to treatment with drugs at various concentrations was plotted as a curve (example plots shown in Figure 5.4C-F). This was used to visually determine the highest concentrations that were not toxic to hCTLs over a 24 h time period. To give an example, drug 4 only showed toxic effects above a concentration of 0.9 μM (Figure 5.4C). Therefore 0.9 μM was chosen as the highest non-toxic concentration for drug 4. For drugs that did not show a toxic effect, such as drug 22, the highest concentration tested, 25 μM, was chosen as the concentration to use in the functional assay (Figure 5.4F). The Table C.1 (Appendix C) outlines the highest non-toxic concentration for all drugs in the library, determined as described above, as well as their official names and their reported molecular target. The highest non-toxic concentration was the concentration used for each drug in all further assays.

5.2.3 Compound screen using the combined degranulation and killing assay

hCTL were treated with the highest non-toxic concentration overnight before functional testing using the combined degranulation and killing assay. The screen was performed across seven 96-well plates using cells from the same HD used for toxicity testing at day 13-15 post in vitro stimulation. Up to 12 samples fit per plate when testing each condition in duplicate. In addition to the stimulated experimental samples (containing hCTL + P815s + αCD3), I also included unstimulated controls (hCTL + P815s) as well as hCTL and P815s on their

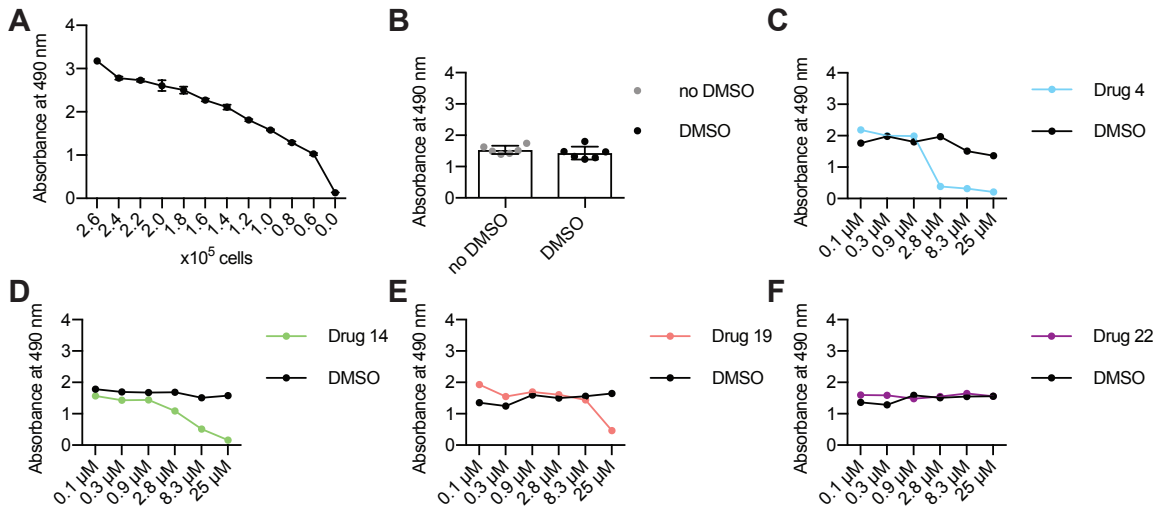

Fig. 5.4 ***Testing the toxic effect of compounds on hCTL. A*** *The indicated number of cells were seeded in each well of a 96 well plate and incubated with Celltitre reagent for 4 h. Absorbance at 490 nm was measured.* ***B*** *Cells were treated with the amount of DMSO equivalent to treatment with 25 µM drugs. Cell viability after 24 h treatment was compared to control cells that were not treated with DMSO. The Celltitre reagent was added 4 h before the end of the 24 h incubation period. Absorbance at 490 nm was measured, n=6 independent experiments. Bar graphs show the mean ± SD.* ***C-F*** *125,000 hCTL were seeded per well in a 96 well plate and treated with drugs at the indicated concentrations for approximately 24 h. Examples for drug 4, 14, 19 and 22 are shown. The assay readout was used to determine the highest non-toxic concentration for every drug in the library.*

own treated with drugs, in order to be able to detect any effects the drugs might have on these cell types. The degranulation readout from the screen is shown in Figure 5.5 and the killing readout is shown in Figure 5.6. Drug 37 had to be excluded in the killing assay analysis, as it appeared to be toxic to P815 target cells over the course of the 3 h assay, therefore affecting the killing assay result for this sample.

While there were many drugs that seemed to decrease degranulation or killing, there were no drugs that substantially increased degranulation or killing. Only drugs that reduced degranulation or killing by more than 50% in comparison to the appropriate DMSO control were chosen for follow up analysis. Drug 26 was therefore classified as a potential hit according to the degranulation aspect of the screen (Figure 5.5), and drugs 4, 13, 19, 24, 30 were classified as potential hits according to the killing aspect of the screen (Figure 5.6). Drug 14 was not classified as a potential hit due to large variability between technical repeats.

It is likely that some drugs that do have an effect on degranulation or killing did not pass these stringent cut-off criteria. For example, drug 30 (46% decrease in degranulation) and drug 4 (48% decrease in degranulation) were close to passing the degranulation threshold, but encouragingly they were also picked up as potential hits in the killing aspect of the screen. The aim of this screen was not to identify and characterise every single promising drug, but to investigate the possibility to use the combined degranulation and killing assay for a mid-size screen, while focusing on the most promising hits that could be useful to further investigate the importance of NF-κB in the CTL killing process.

5.2.4 Testing the reproducibility of potential hits

To test whether the effects of drug 4, 13, 19, 24, 26 and 30 in the combined degranulation and killing assay were reproducible, hCTLs derived from independent HDs were treated with drugs at the same concentrations previously used (Figure 5.7). Each drug treatment is connected to its corresponding DMSO control treatment, which was performed simultaneously on the same cells (Figure 5.7). Not all hits were reproducible, indicating that some hits were false positives. Additionally, as the screen was performed on cells derived from one HD, some donor-to-donor variability was expected upon further follow up.

Upon further investigation, drug 24 (n=3) and 13 (n=5) did not significantly affect degranulation or killing (Figure 5.7B, D). Drug 26 (n=5, $p<0.01$, paired t-test, mean of differences = -13.25) and 30 (n=5, $p<0.05$, paired t-test, mean of differences = -11.35) significantly decreased degranulation to a small extent, but they did not have a significant effect on CTL killing (Figure 5.7E,F). The striking killing defect of drug 4 observed in the screen was not reproducible, however, CTL killing was decreased, at least to a small extent, in every experiment (n=7, Figure 5.7A). This possibly did not reach statistical significance due to the variability of the differences between DMSO and drug 4 treatment between repeats. Drug 19 was the only drug that reproducibly and significantly decreased degranulation (n=7, $p<0.01$, paired t-test, mean of differences = -40.41) and killing (n=7, $p<0.001$, paired t-test, mean of differences = -42.54) (Figure 5.7C).

The drug with the biggest effect size, drug 19, was investigated further. So far, drug 19 had only been tested with overnight treatment. I used the Incucyte killing assay, which measures the killing response over time, to test how quickly treatment with drug 19 resulted in a killing defect. In these assays hCTLs were not pre-treated with drug 19, instead the compound was only added at the start of the assay. This showed that drug 19 exerted its effect

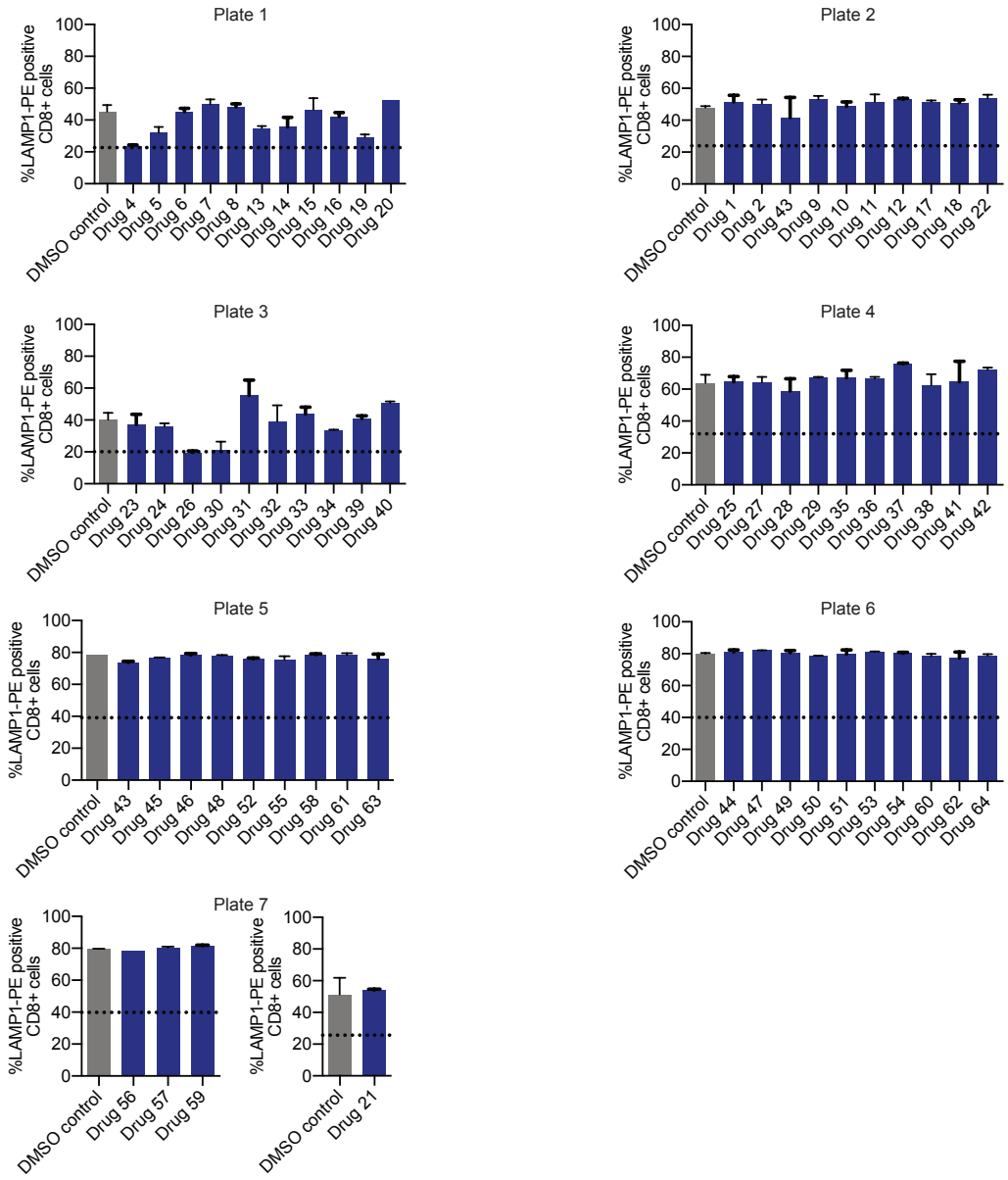

Fig. 5.5 ***Screening identified one drug that reduced degranulation by more than 50%.*** *Drugs were roughly grouped into plates according to their highest non-toxic concentration. A control containing the equivalent amount of DMSO to the highest concentration tested was included on every plate. CD8 cells from one HD were treated with compounds overnight. The following day, target cells with and without αCD3 were added. E:T ratio = 2.5:1, assay duration = 180 min. Technical duplicates were prepared for every condition, error bars represent the SD of technical repeats. Screening was performed in 7 plates across 3 days (2-3 plates per day). Degranulation assays were analysed following the gating strategy described in chapter 2, section 2.5.1 and 2.5.2. Drugs were classified as potential hits when the treatment decreased degranulation by more than 50% in comparison to the appropriate DMSO control. The dotted line indicates the 50% cut-off on each graph.*

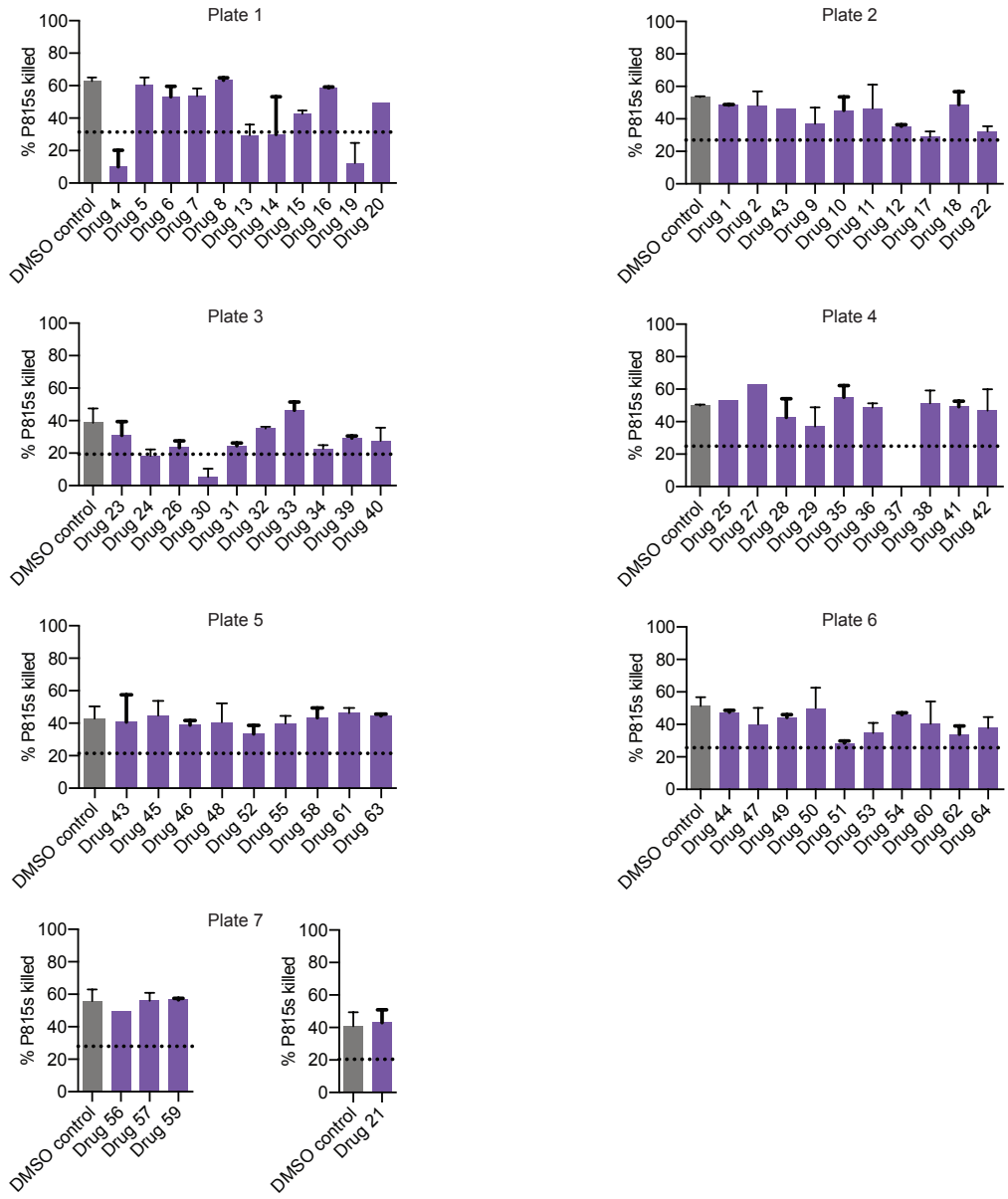

Fig. 5.6 ***Screening identified five drugs that reduced killing by more than 50%.*** *Drugs were roughly grouped into plates according to their highest non-toxic concentration. A control containing the equivalent amount of DMSO to the highest concentration tested was included on every plate. CD8 cells from one HD were treated with compounds overnight. The following day, target cells with and without αCD3 were added. E:T ratio = 2.5:1, assay duration = 180 min. Technical duplicates were prepared for every condition, error bars represent the SD of technical repeats. Screening was performed in 7 plates across 3 days (2-3 plates per day). Killing assays were analysed following the gating strategy and calculations described in chapter 2, section 2.5.2. Drugs were classified as potential hits when the treatment decreased killing by more than 50% in comparison to the appropriate DMSO control. The dotted line indicates the 50% cut-off on each graph. Drug 37 was excluded due to toxic effects on P815 target cells. SD = standard deviation.*

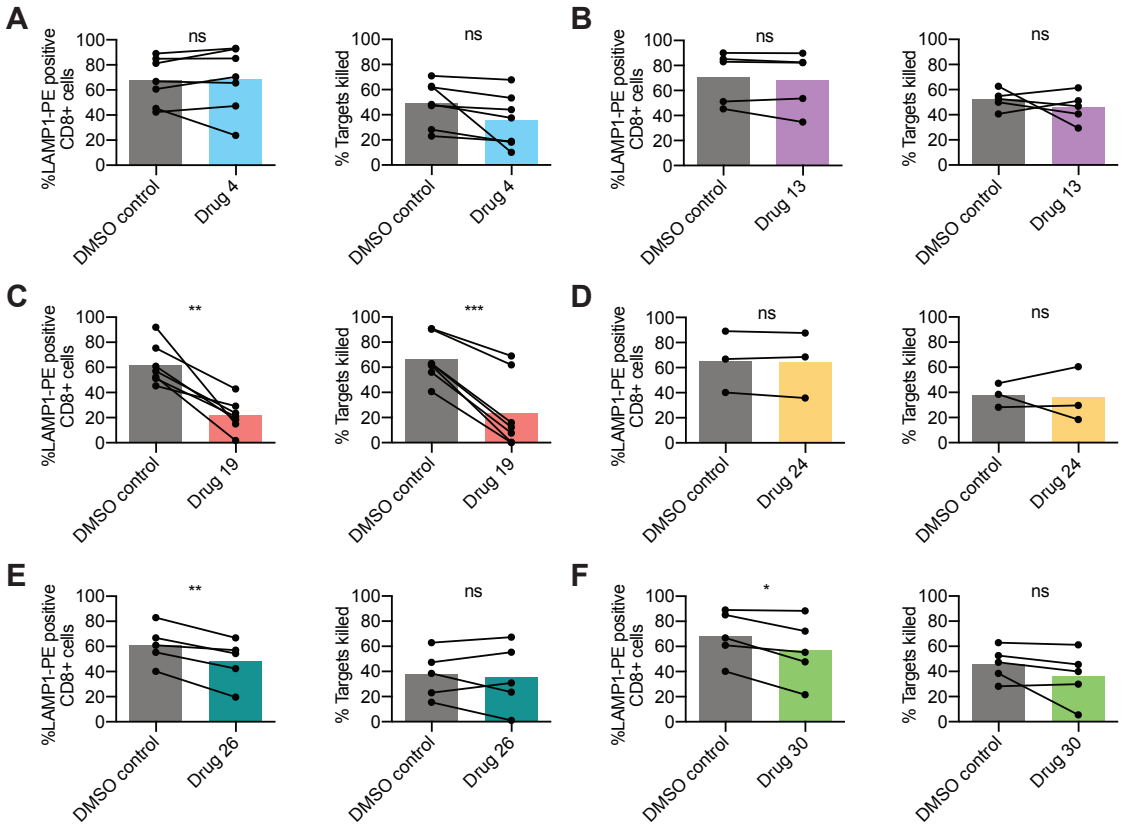

Fig. 5.7 ***Follow up of the effect of promising compounds on degranulation and killing.*** *Cells derived from independent HDs were treated overnight with drugs identified as potential hits in the screen. Each treatment is connected to its corresponding DMSO control. Each pair of data points represents an independent experiment. The combined degranulation and killing assay was analysed following the gating strategy and calculations described in chapter 2, section 2.5.2. E:T ratio = 2.5:1, assay duration = 180 min, each data point represents the average of technical duplicates. The following drugs were tested* ***A*** *drug 4 at 0.9 µM (n=7 independent experiments),* ***B*** *drug 13 at 8.3 µM (n=5 independent experiments),* ***C*** *drug 19 at 8.3 µM (n=7 independent experiments),* ***D*** *drug 24 at 0.9 µM (n=3 independent experiments),* ***E*** *drug 26 at 0.1 µM (n=5 independent experiments) and* ***F*** *drug 30 at 0.9 µM (n=5 independent experiments). *p<0.05, **p<0.01, ***P<0.001, calculated by paired t-test.*

on killing within the first hour (Figure 5.8A). Encouragingly, the killing defect observed with drug 19 treatment was also titratable in response to a two-fold (Figure 5.8B) and four-fold (Figure 5.8C) decrease in concentration.

A third kind of killing assay, the LDH release assay, was used to test the effect of drug 19 treatment when using a variety of E:T ratios (Figure 5.8D). Increasing the amount of effectors while keeping the amount of target cells constant resulted in an increase in the percentage of target cells killed over 3 h. The killing observed was significantly reduced in the presence of drug 19 across three different E:T ratios (n=4, p<0.001 for E:T 10:1, n=4, p<0.001 for E:T 5:1 and n=4, p<0.01 for E:T 2.5:1, paired t-test), further confirming the inhibitory effect of drug 19 on CTL killing.

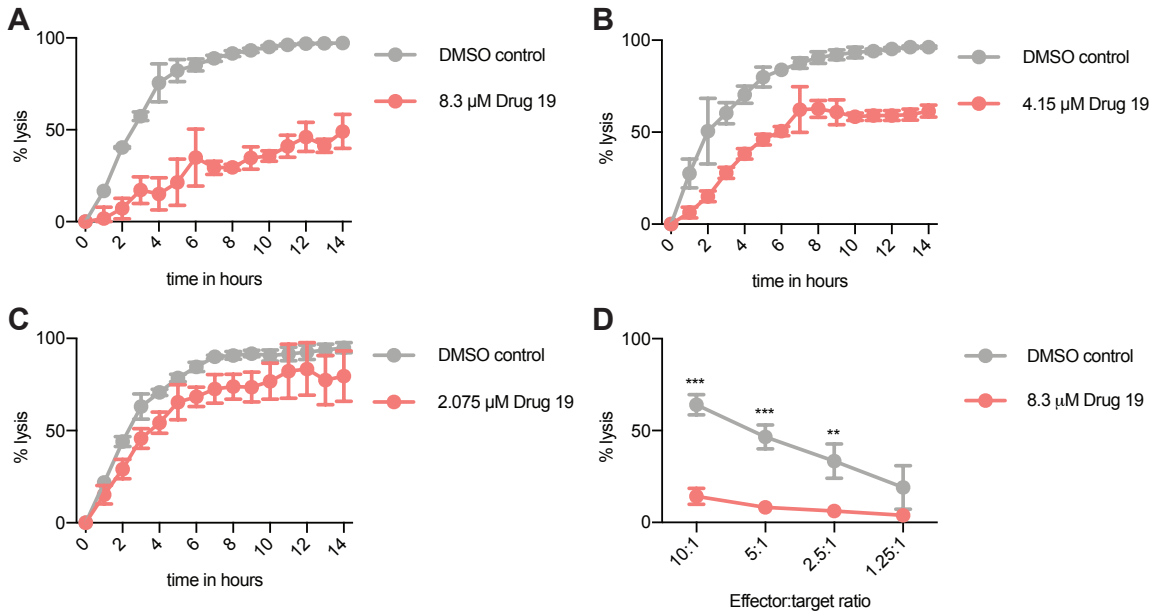

Fig. 5.8 ***Drug19 has an immediate effect on CTL killing.*** *Incucyte killing assays showing the percentage lysis of red P815 target cells over the course of 14 hours in the presence of αCD3, hCTL and drug 19 or equivalent DMSO vehicle control. One representative plot for 3 independent experiments is shown for using drug 19 at a concentration of* ***A*** *8.3 µM,* ***B*** *4.15 µM and* ***C*** *2.075 µM. E:T = 10:1. Each datapoint is an average of 3 technical repeats and the error bars show the SD.* ***D*** *LDH release killing assay showing the % lysis of P815 target cells at varying E:T ratios and in the presence of 8.3 µM drug 19 or equivalent DMSO vehicle control for 3 h, n=4 independent experiments for all E:T except E:T 1.25:1, where n=2 independent experiments. **p<0.01, ***P<0.001, calculated by paired t-test.*

5.2.5 The effect of drug 19 on NF-κB

Next, I tried to investigate at which point in the NF-κB activation cascade drug 19 intervenes in NF-κB signalling. Initially I used PMA and ionomycin stimulation in combination with drug 19 treatment. Studies have shown that PMA and ionomycin can be used to activate NF-κB in the absence of TCR, αCD3 or αCD28 stimulation (Liu et al., 2016). This treatment essentially bypasses TCR signalling and triggers degranulation. PMA activates PKCs, while ionomycin induces calcium release from the endoplasmic reticulum (Liu et al., 2016). I used PMA and ionomycin stimulation and measured surface exposure of LAMP1 in the presence and absence of drug 19 treatment. The fact that drug 19 treatment still reduced degranulation in response to PMA (n=5, $p<0.05$, paired t-test), ionomycin (n=5, $p<0.001$, paired t-test) and combined PMA and ionomycin (n=5, $p<0.01$, paired t-test) treatment suggested that the molecular target of drug 19 was not proximal to the TCR, but downstream of the molecular targets of PMA and ionomycin (Figure 5.9A).

To investigate whether drug 19 affected NF-κB transcription I measured the expression of the NF-κB target gene TNFα in the presence and absence of αCD3ε stimulation (Figure 5.9B). NF-κB p65/p50 heterodimers were shown to be involved in transcriptional activation of TNFα expression in response to LPS activation in macrophages (Liu et al., 2000). TNFα can therefore be used as a readout of p65/p50 transcriptional activity. TNFα was not produced in the absence of αCD3ε stimulation, independent of addition of DMSO or drug 19 (Figure 5.9B). Production of TNFα was upregulated in DMSO samples in response to αCD3ε stimulation for 4 h. This upregulation was significantly lowered in the presence of drug 19 (Figure 5.9B, n=3, $p<0.01$, paired t-test).

Using PMA and ionomycin treatment I investigated whether drug 19 affected phosphorylation of p65 at Ser536. Levels of phosphorylated p65 were increased in response to PMA and ionomycin treatment in the DMSO control (Figure 5.9C-D). This upregulation was decreased with drug 19 treatment (Figure 5.9C-D). Interestingly even basal levels of p65 phosphorylated at Ser536 seemed slightly lower in response to drug 19 treatment (Figure 5.9C-D). Taken together, these results suggest that drug 19 acts between PKC (Figure 5.9A) and p65 (Figure 5.9C-D) to potently inhibit p65-mediated transcription (Figure 5.9B).

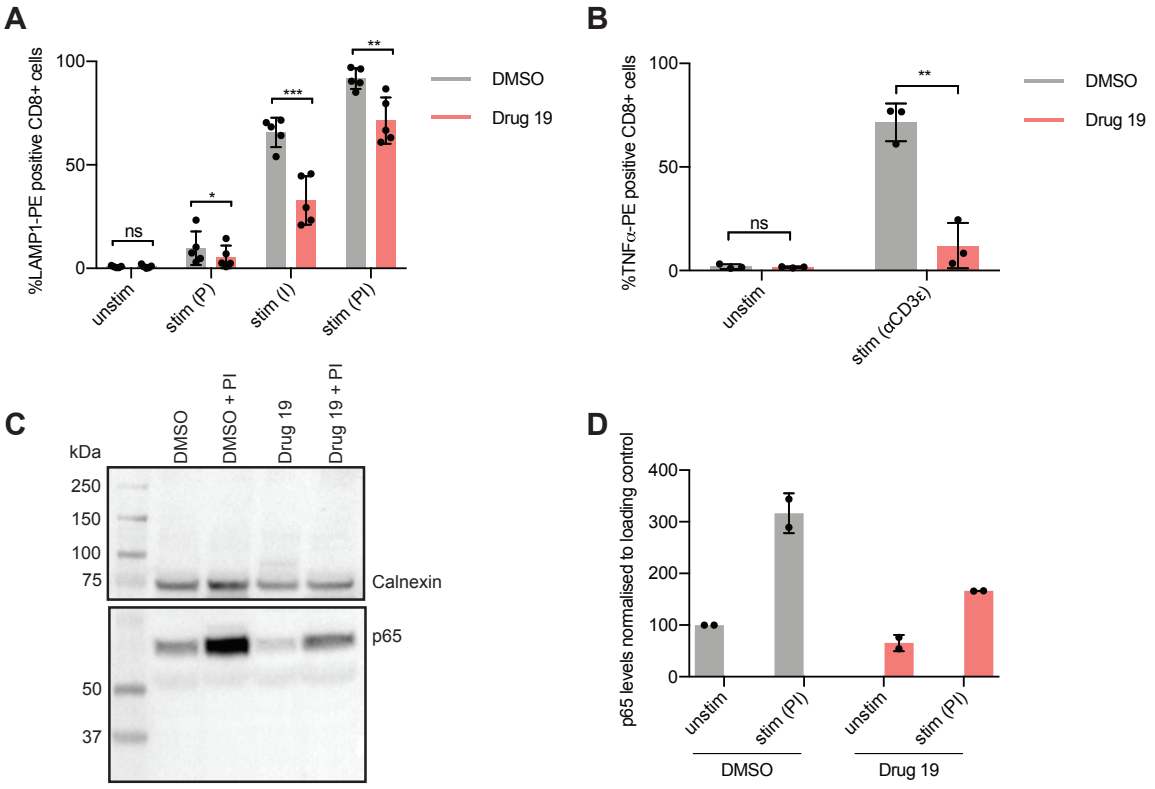

Fig. 5.9 ***Determination of the molecular effect of drug19 on NF-κB.*** ***A*** *Surface LAMP1 levels in response to treatment of hCTL with PMA (P), ionomycin (I), or both in the presence or absence of drug 19 for 3 h. The bar graphs show the average of 5 independent experiments, error bars show the SD, *p<0.05, **p<0.01, ***p<0.001 calculated by paired t-test.* ***B*** *TNFα expression in hCTL treated overnight with 8.3 µM drug 19 or DMSO followed by 4 h stimulation on αCD3-coated plates (stim) or uncoated plates (unstim control) was measured by intracellular FACS. The bar graphs show the average of 3 independent experiments, error bars show the SD, **p<0.01 calculated by paired t-test.* ***C*** *Representative WB showing p65 phosphorylated at Ser536 and calnexin (loading control) protein levels 4 h after treatment with PMA and ionomycin or appropriate DMSO vehicle control in addition to treatment with 8.3 µM drug 19 or DMSO vehicle control.* ***D*** *Average levels of p65 protein phosphorylated at Ser536 upon PMA and ionomycin treatment in the presence or absence of drug19 in 2 independent repeats. In each repeat p65 protein levels were expressed relative to the unstimulated control and normalised to calnexin. Bar graphs show the mean ± SD, n=2 independent experiments. P = PMA, I = ionomycin, unstim = unstimulated, stim = stimulated, ns = not significant, SD = standard deviation.*

5.3 Discussion

The combined degranulation and killing assay successfully detected phenotypes in hCTL derived from FHL2 and FHL3 patients (Figure 5.1A-B). The relatively mild killing phenotype observed with *MUNC13-4* patients in the Incucyte killing assay (Figure 5.1C-E) could be explained by only partial protein loss in these patients (Figure 5.1F). In patients with mutations in *PRF1* either no perforin protein was detected (patient 4166 and 392) or the perforin antibody recognised two bands of a higher MW (patient 6981 and 3026) than in the HDs (Figure 5.2G). Functional assays indicated that the higher MW versions of perforin were not functional (Figure 5.2A-F). Perforin undergoes various processing steps during its formation. First a ∼65 kDa version gets modified by glycans to give a 70 kDa version. Cleavage of the C-terminus yields the final functional 60 kDa version of perforin (Uellner et al., 1997). The final processing step did not seem to occur in patients 6981 and 3026, indicating that the domains affected by their mutations may be important for the C-terminal cleavage step. Uellner et al. (1997) reported that a mutant version of perforin, where the C-terminus is truncated, is located in the endoplasmic reticulum, rather than in lytic granules when expressed in RBL cells. It would therefore be interesting to test the localisation of perforin in CTL derived from patient 6981 and patient 3026 by immunofluorescence. In summary, the patient results confirmed that the combined degranulation and killing assay can be used in hCTL, and shows potential as a diagnostic test for patients suspected to have a CTL defect.

Next, the combined degranulation and killing assay was used to screen 64 compounds. To further improve the scalability of the assay, sample fixation to stably maintain the endpoint could be explored. Additionally it would be interesting to test the assay in a 384-well format, in order to be able to screen even more samples per plate while reducing the amount of cells and reagents needed per sample.

The drug screen identified 6 compounds that reduced degranulation or killing by more than 50% (Figures 5.5 and 5.6). There may be additional compounds in the library that affect degranulation or killing that were not identified due to using a suboptimal concentration, as I did not test concentrations above 25 μM. Additionally, the stringent 50% cut-off applied to the degranulation and killing readouts likely excluded some hits. For example, drug 19 was not picked up as an inhibitor of degranulation in the initial screen, as it did not decrease degranulation by more than 50% (Figure 5.5). However, drug 19 turned out to significantly decrease degranulation upon repetition (Figure 5.7). To avoid such false negatives, it would be preferable to perform screens in triplicates, as done for the genetic screen in chapter 4.

This would allow the identification of hits with greater certainty, however, the vast amount of time required to set up these assays limits the scale of such screens without a robot.

The most promising hit, drug 19, significantly reduced degranulation and killing after overnight treatment (Figure 5.7). A different kind of killing assay, the Incucyte assay, demonstrated that drug 19 already affected target cell killing within 1 h of treatment (Figure 5.8). Encouragingly, the effect of drug 19 was titratable when reducing the concentration by two-fold and four-fold, indicating that the effect on killing is mediated by the drug (Figure 5.8). I analysed distinct steps in the NF-κB activation cascade to determine where drug 19 mediated its effect. If the degranulation defect with drug 19 had been rescued with PMA and ionomycin treatment this would have suggested that drug 19 inhibits signalling proximal to the TCR. As this was not the case, drug 19 must act downstream of the molecular targets of PMA and ionomycin (Figure 5.9). TNFα transcription is known to be regulated by p65/p50 heterodimers (Liu et al., 2000). As TNFα production in response to αCD3ε stimulation was decreased in the presence of drug 19 (Figure 5.9), the effect of drug 19 on p65 was investigated. I found that drug 19 decreased the levels of p65 phosphorylated at Ser536 both in response to PMA and ionomycin treatment as well as at basal levels (Figure 5.9).

In the literature, parthenolide, the official name for drug 19, has been shown to directly bind to two components of the NF-κB cascade. It inhibits the ability of p65 to bind to DNA by alkylating cysteine-38 of p65 (Garcia-Pineres et al., 2001) and it inhibits IKKβ by alkylation of cysteine-179, leading to stabilisation of IκBα and IκBβ (Hehner et al., 1999; Kwok et al., 2001). In addition, other studies have shown that parthenolide also induced HDAC1 depletion (Gopal et al., 2007) and inhibits DNA methyltranferase 1 (Liu et al., 2009). With the data available in this chapter, I can therefore not be certain that the effect of parthenolide on CTL killing is due to its inhibition of NF-κB. This highlights a general disadvantage to using chemical compounds for screening, as they may affect multiple molecular targets, in contrast to a targeted genetic approach. The striking effect of parthenolide on CTL killing is nonetheless interesting, but how exactly the effect is mediated remains to be determined. Specifically targeting p65 by CRISPR or siRNA would help to clarify whether p65 is directly involved in CTL degranulation and killing. Furthermore, it would be interesting to investigate which steps in the killing pathway are affected by drug 19 treatment. The degranulation readout demonstrated that the lytic granule content is not secreted in response to drug 19 treatment. This could be due to a defect in fusion between the granule membrane and plasma membrane, or due to a block at an earlier step in the CTL killing process. Immunofluorescent microscopy could be used to determine whether treated CTLs can still form contacts with

target cells and whether the centrosome and lytic granules still polarise towards the contact site.

Several other studies have suggested parthenolide as a potential cancer treating drug (reviewed by Ghantous et al. (2013)). A recent study noted anti-proliferative and pro-apoptotic effects of parthenolide in glioma cells, and showed that parthenolide inhibits tumour growth in mice (Yu et al., 2018). For such medical purposes, it is crucial to be aware of the suppressive effect that parthenolide has on CTL killing.

In its current format, the combined degranulation and killing assay can be used to screen many dozens of compounds over the course of several days. It is therefore a useful tool to screen compounds as well as genetic targets. Furthermore, the experiments with patient-derived CTL demonstrated the potential of the assay as a diagnostic test. Using patient derived NK cells and CTLs in a simple degranulation assay has already been proposed as a tool for diagnostic evaluation of patients presenting with FHL symptoms (Bryceson et al., 2012; Chiang et al., 2013). However, it has been noted that this approach requires additional monitoring of perforin expression in all clinical samples, as the defect resulting from mutations in *PRF1* cannot be detected using the degranulation assay (Bryceson et al., 2012). The combined degranulation and killing assay presented in this thesis therefore provides an advantage over the current gold standard. By cutting out the requirement of analysing perforin separately the assay reduces time, effort and the amount of patient material required for diagnosis.

5.3.1 Summary and evaluation of aims

- Test the combined degranulation and killing assay in hCTL using FHL2 and FHL3 patient samples.
  - The assay was successfully validated using patient-derived samples. The defects caused by *PRF1* mutations would not have been picked up by the simple degranulation assay, which is currently being used for diagnostic purposes. The combined assay that is able to detect both degranulation and killing simultaneously could therefore have great diagnostic potential.
- Investigate the scalability of the assay using the NF-κB compound library.
  - 64 compounds were screened in technical duplicates across 3 days using CD8 T cells derived from one HD. Out of the drugs tested, 1 drug decreased degranulation

and 5 drugs decreased killing by more than 50 % in the screen. These promising hits were followed up using CTL derived from independent HDs. The most promising compound, drug 19 (parthenolide), reproducibly decreased CTL degranulation (n=7, $p<0.01$, paired t-test) and killing (n=7, $p<0.001$, paired t-test).

- Follow up promising hits to elucidate their mechanism of action.
  - Measuring CTL killing over time revealed that parthenolide reduced CTL killing within the first hour of treatment. The effect of parthenolide on NF-κB in primary human T cells was tested at various steps along the NF-κB activation cascade. Parthenolide treatment was shown to suppress phosphorylation of p65 at Ser536 and decreased TNFα gene expression in response to αCD3ε stimulation, indicating potent inhibition of gene transcription that is regulated by p65.

Chapter 6

Establishing the CRISPR-Cas9 technology in primary human T cells

6.1 Introduction

As an unbiased approach pooled genome-wide CRISPR screens have lead to many novel discoveries (Doench, 2017; Shalem et al., 2014; Wang et al., 2014a). In such genome-wide screens, cell lines are usually transduced with a lentivirus to introduce Cas9 stably into the cells and a genome-wide sgRNA lentiviral library. Cells containing Cas9 and sgRNAs are then selected using antibiotics prior to phenotypic screening (Doench, 2017). Cells with the phenotype of interest are isolated and the sgRNAs that cause the phenotype are determined by sequencing (Doench, 2017). Performing such a screen in primary T cells would be of immense interest in order to improve understanding of how the response of T cells to target antigen is regulated at the genetic level. For example, this could lead to progress in using T cells to target cancers by immunotherapy.

Several researchers have taken the approach of performing genome-wide screens in cancer cell lines in order to identify cancer genes that affect T cell killing (Pan et al., 2018; Patel et al., 2017). These type of screens have identified new immunotherapy targets, or mechanisms of cancer resistance to immunotherapy. However the findings may be specific to the cell lines used and may not always reflect complex cancer biology in vivo. Performing screens in primary T cells could increase the possibility of finding a broadly applicable strategy for improving T cell mediated killing of tumours.

While pooled genome-wide screens can be performed in immortalised cancer cell lines,

this approach is more challenging in primary T cells for several reasons. Firstly, pooled screens usually require large cell numbers (10s of millions) (Doench, 2017). Secondly, a selection procedure for cells that have incorporated Cas9 and sgRNAs after lentiviral transduction is required. This can be in the form of antibiotic selection or sorting by FACS. The selection procedure can take several weeks, and therefore cannot be used on cells with a limited life span in vitro (Doench, 2017), such as mouse T cells. However, primary human T cells in theory fit the required criteria. They are able to survive for many months in tissue culture by regular re-stimulation using PHA and irradiated buffycoat from allogeneic donors. Through re-stimulation, they can also be expanded to give the desired amount of cells. Furthermore, any findings in primary human T cells could have immense medical potential.

An early study trying to use CRISPR in primary human T cells revealed transfection difficulties when nucleofecting plasmids encoding Cas9 and sgRNAs, leading to low CRISPR efficiency (Mandal et al., 2014). Nucleofecting human T cells with Cas9-RNPs has been more successful (Schumann et al., 2015), but this approach only allowed targeting a select set of genes, rather than unbiased, genome-wide screening.

One option to enable a genome-wide screen would be to produce human T cells that stably express Cas9. This could be achieved by transducing human T cells with a lentiviral vector encoding Cas9, however lentiviral vectors containing large inserts (the *Cas9* gene is $\sim$4000 bp in size) often result in low viral titre (Doench, 2017; Ramezani and Hawley, 2002; Sanjana et al., 2014). This chapter describes my efforts to test CRISPR in human T cells and to produce primary human T cells that stably express Cas9 using lentiviral transduction. Such cells would provide the possibility to generate stable KOs in primary human T cells. Perhaps such cells could even be used for a genome-wide screen in primary human T cells using the same approach of a pooled genome-wide lentiviral sgRNA library commonly used in cell lines.

6.1.1 Chapter aims

- Transduce hCTL with a lentivirus encoding Cas9 as well as antibiotic resistance or a fluorescent marker to be able to select successfully transduced cells.
- Test nucleofection of hCTL and the transient Cas9-RNP CRISPR approach (optimised in chapter 3) in primary hCTL.

- Compare the stable (Cas9 lentivirus) and transient (Cas9-RNP) approaches in terms of CRISPR efficiency.

6.2 Results

6.2.1 Transduction of hCTL with Cas9-Blast lentivirus

Initially hCTL were transduced with the Cas9-Blast lentivirus (Sanjana et al., 2014), encoding Cas9 separated by a 2A sequence derived from porcine teschovirus (P2A) from a gene encoding resistance to the antibiotic blasticidin. Therefore, any cells that express Cas9 upon transduction could be selected by treatment with blasticidin. In order to be able to select transduced cells, it was first necessary to establish what concentration of blasticidin killed all untransduced cells, which can vary greatly between cell types (Doench, 2017). Therefore, I tested the blasticidin sensitivity of hCTL by exposing them to a variety of blasticidin concentrations over a time period of 15 days. Blasticidin was renewed every two days and viability measured by flow cytometry. Changes in cell morphology as detected by forward scatter/side scatter analysis and staining with DAPI were used as an indicator of whether cells were alive or dead. 5 μg/ml was determined as the lowest blasticidin concentration that I tested that killed all hCTL within 15 days of treatment, as live cells were still remaining after 15 days treatment with 1 μg/ml blasticidin (Figure 6.1). Therefore, 5 μg/ml Blasticidin was used to select hCTL transduced with the Cas9-Blast lentivirus.

As a control for transduction, hCTL were transduced with a lentivirus encoding just the fluorescent protein GFP in parallel to transduction with the Cas9-Blast lentivirus. 44.5% of the cells were successfully transduced with the GFP lentivirus, as visualised by flow cytometry (Figure 6.2A), confirming that there was no technical problem during the transduction process. No band corresponding to Cas9 was detected by WB using lysates derived from hCTL transduced with Cas9-Blast lentivirus, in contrast to lysates from Cas9 hom mice which served as a positive control for the Cas9 protein (Figure 6.2B). However, Cas9 could be detected by WB after transduction of HEK293T cells with the Cas9-Blast lentivirus (Figure 6.2C). This indicated low transduction efficiency with this lentivirus in hCTL, but not in HEK293Ts. PCR was used as a more sensitive technique to show that the Cas9 lentivirus had successfully integrated in some hCTL (Figure 6.2D). DNA isolated from transduced HEK293T (positive control) was run alongside DNA from hCTLs on the agarose gel. It is noteworthy that while DNA was isolated from 450,000 hCTLs for the PCR reaction, the signal is lower than the signal generated by DNA derived from only 10,000 transduced HEK

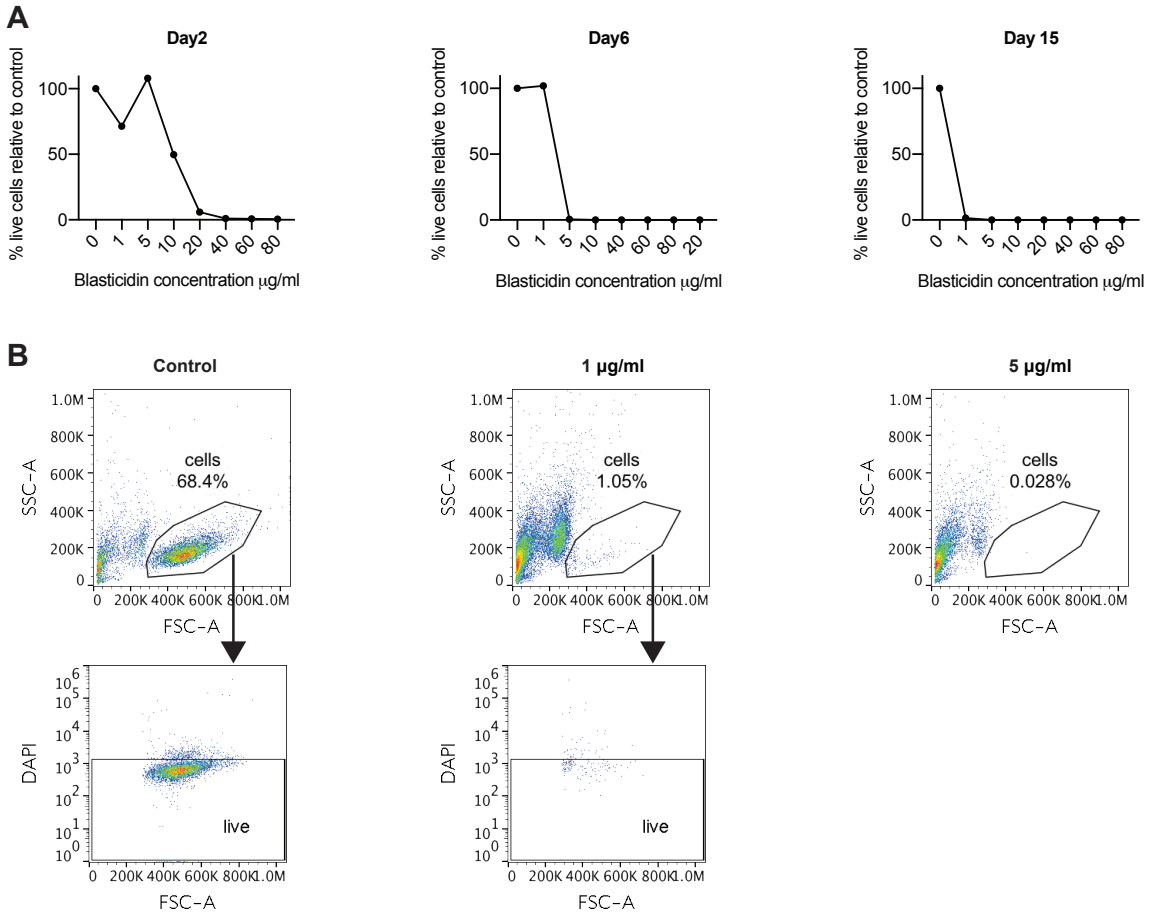

Fig. 6.1 ***Blasticidin concentration response. A*** *Human T cells were treated with blasticidin at the indicated concentrations for 15 days. Blasticidin-containing media was renewed every 2-3 days. Viability was measured by gating on forward scatter (FSC) and side scatter (SSC) parameters by flow cytometry. The percentage of cells in the FSC/SSC gate was normalised to the treatment control (no blasticidin treatment) at each time point.* ***B*** *Representative flow cytometry plots after 15 days of blasticidin treatment showing the change in the FSC/SSC profile and the DAPI signal within the FSC/SSC gate.*

cells. This confirmed that transduction of hCTLs with the Cas9-Blast lentivirus was much less efficient than transduction of HEK293T with the same lentivirus. Selecting the hCTLs in blasticidin almost killed transduced and untransduced cells to a comparable level after 6 days of blasticidin treatment (Figure 6.2E). Only a few live cells remained in the transduced samples, providing further evidence that the transduction efficiency was very low (Figure 6.2E). These live cells were sorted by FACS and single cell dilutions were performed in the hope to expand Cas9 expressing clones, but the cells did not grow subsequently.

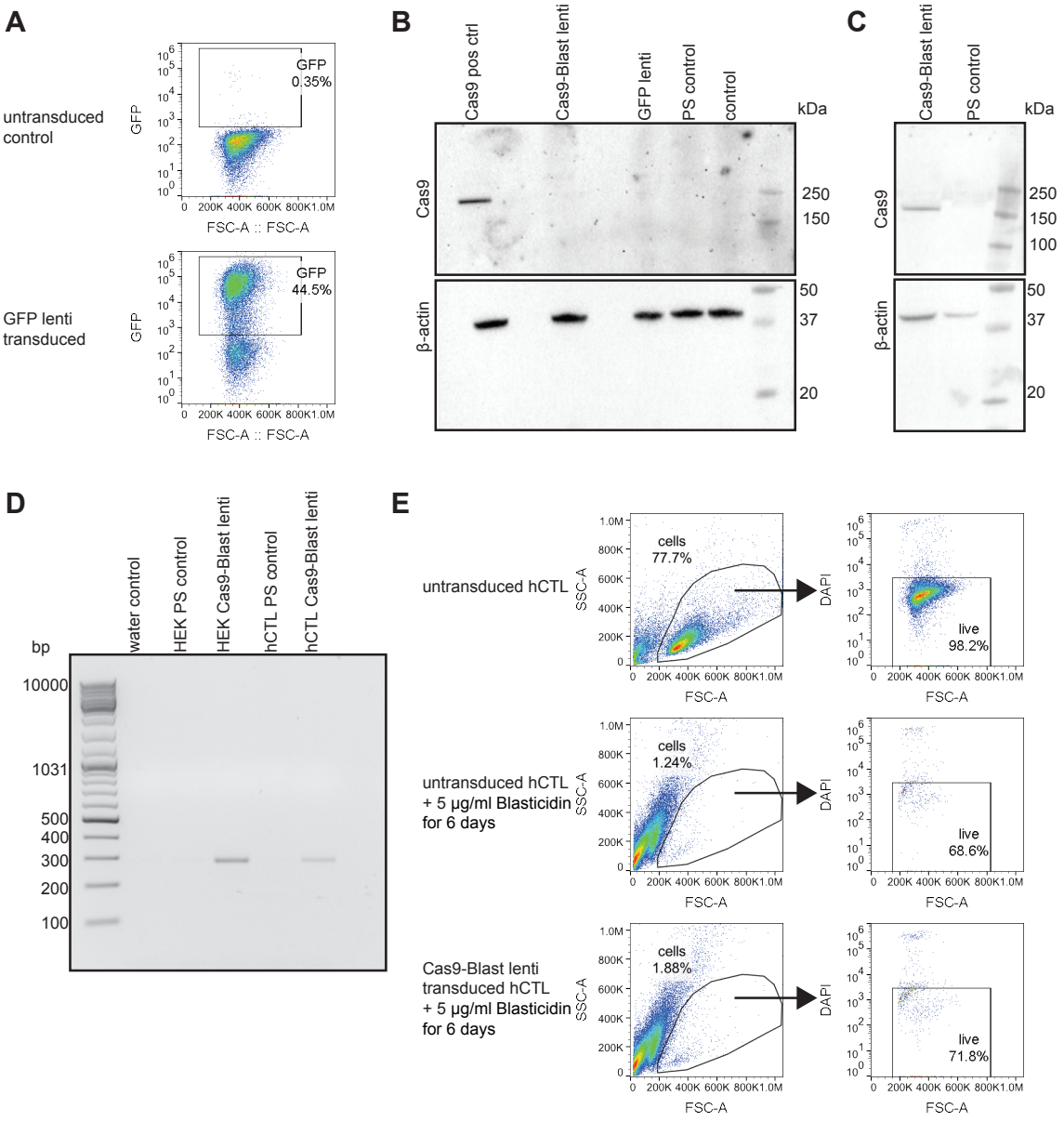

Fig. 6.2 ***Transduction of hCTL with Cas9-Blast lentivirus.*** ***A*** *GFP expression profile of untransduced hCTL and hCTL transduced with pHRSIN-GFP lentivirus.* ***B*** *WB showing Cas9 protein expression in lysates derived from Cas9 hom mice (positive control), but not in samples transduced with Cas9-Blast lentivirus or any of the negative controls (samples transduced with a pHRSIN-GFP lentivirus, protamine sulfate (PS) treatment control samples, or untransduced control samples).* ***C*** *WB showing Cas9 protein expression in lysates derived from HEKs transduced with Cas9-Blast lentivirus, but not in PS treatment control samples.* ***D*** *Agarose gel of products from a PCR with primers spanning a 274 bp region between the 3' end of the Cas9 gene and the blasticidin resistance gene.* ***E*** *Viability of untransduced hCTL and hCTL transduced with Cas9-Blast lentivirus after 6 days treatment with 5 µg/ml blasticidin. PS = protamine sulfate, HEK = HEK293T.*

6.2.2 Generation of a lentivirus encoding Cas9 and a fluorescent tag

As an alternative approach to antibiotic selection, Cas9 can be co-expressed with a fluorescent marker, which allows to detect successfully transduced cells by flow cytometry (Doench, 2017). As hCTL were successfully transduced with the GFP lentivirus (pHRSIN-GFP) used in Figure 6.2A, the *Cas9* gene was cloned into a mCherry fluorescent protein encoding version of the pHRSIN plasmid (pHRSIN-mCh).

The approach taken to insert *Cas9* into the pHRSIN-mCh vector is outlined in Figure 6.3A. I generated two plasmids, in the first plasmid mCherry was immediately downstream of the *Cas9* gene, in the second plasmid the *Cas9* gene was linked to mCherry via a sequence encoding the self-cleaving P2A peptide, shown to have high cleavage efficiency in human cells (Kim et al., 2011). For simplicity, the P2A sequence is referred to as 2A for the remainder of this results section.

Primers were designed that amplify the *Cas9* gene from the Cas9-Blast lentiviral plasmid by PCR. The primers included sequences that overlap with the pHRSIN-mCh plasmid, as well as a XhoI RE site upstream of *Cas9* and a BamHI RE site downstream of *Cas9*. The resulting PCR products were run on a gel (Figure 6.3B) and purified. The recipient plasmid (pHRSIN-mCh) was cut with XhoI and BamHI RE, run on a gel and also purified. The resulting insert and recipient vector fragments were joined by Gibson assembly. After bacterial transformation and selection on ampicillin plates, 8 colonies were picked per plate and expanded. After DNA purification, the DNA from the various different colonies was subjected to a restriction digest with XhoI and BamHI. Running the products of the restriction digest on a gel allowed for the isolation of colonies that appeared to have the correct insert as indicated by the excision of a band corresponding to the *Cas9* gene in size ($\sim$4000 bp) (Figure 6.3C,D). Sanger sequencing carried out by Source Bioscience confirmed the correct sequence of DNA derived from colonies 1c and 2e, while DNA from colonies 1e and 2h contained point mutations. The entire *Cas9* gene and its flanking regions to the pHRSIN-mCh vector were sequenced. Figure 6.4 shows plasmid maps for the final pHRSIN-Cas9-mCh and pHRSIN Cas9-2A-mCh plasmids that were subsequently used for lentivirus production.

As a control to test these lentiviral plasmids, I transduced P815 cells, as this mastocytoma cell line is more easily transduced than primary human T cells. The mCherry signal was measured by flow cytometry, and Cas9 protein expression was confirmed by WB (Figure 6.5). While only one band corresponding to Cas9 was observed in the Cas9-mCh lentivirus transduced samples, two bands were observed in the Cas9-2A-mCh lentivirus transduced

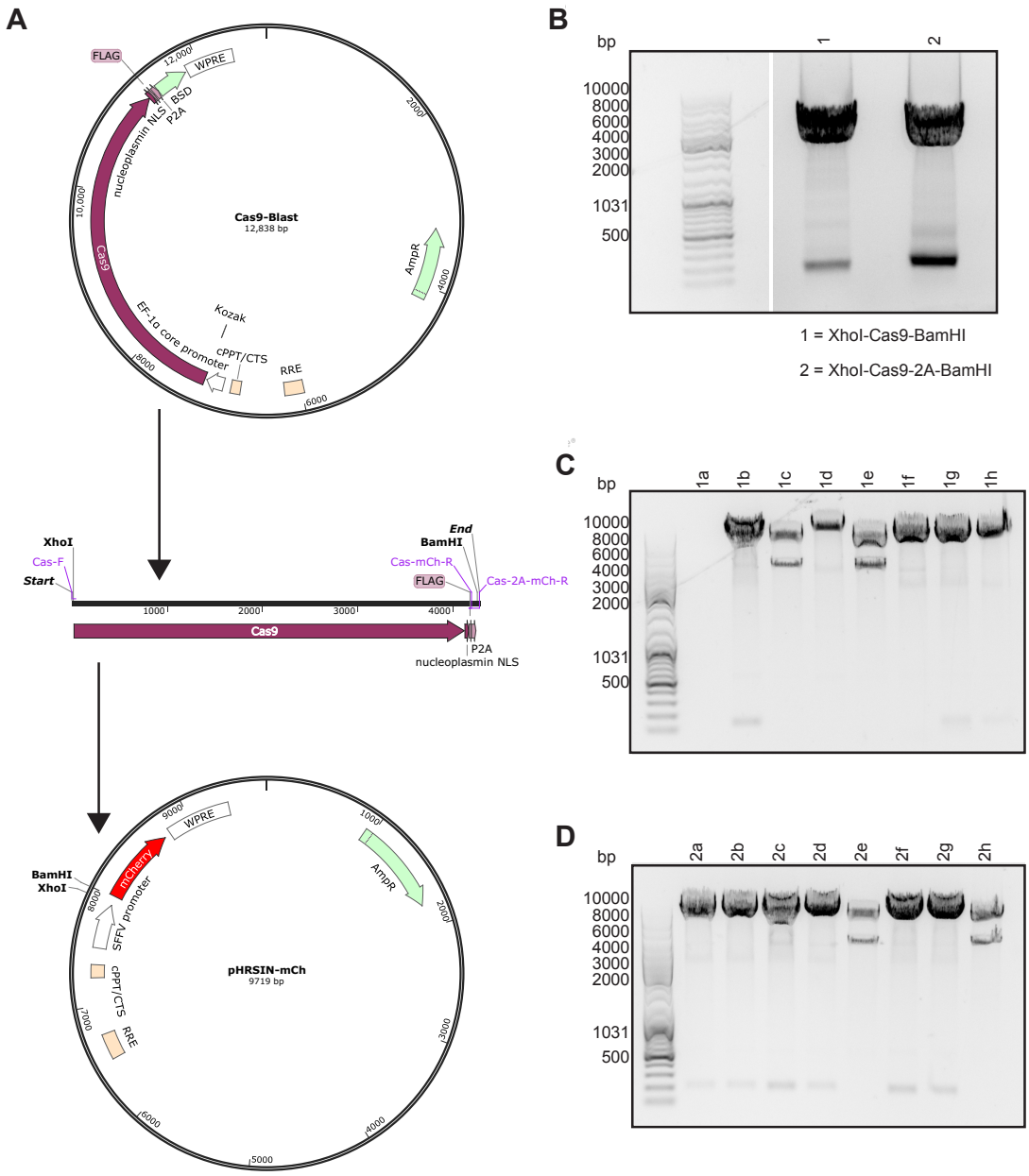

Fig. 6.3 ***Cloning Cas9 into the pHRSIN-mCh vector.***

Fig. 6.3 ***Cloning Cas9 into the pHRSIN-mCh vector.*** ***A*** *Schematic showing the plasmid map for the Cas9-Blast lentivirus (top) that acted as the source to amplify the Cas9 gene (middle) in order to insert it into the recipient plasmid pHRSIN-mCh (bottom). Location of the forward primer (Cas9-F) and reverse primers (Cas9-mCh-R and Cas9-2A-mCh-R) are indicated on the Cas9 gene (middle). Plasmid maps were created with snapgene.* ***B*** *Agarose gel showing Cas9 amplified from the Cas9-Blast plasmid using primers that add on a 5' XhoI restriction enzyme site and a 3' BamHI restriction enzyme site with (2) or without (1) the 3' 2A sequence. These PCR products were cloned into the pHRSIN-mCh vector digested with XhoI and BamHI restriction enzymes using Gibson assembly.* ***C and D*** *Agarose gels showing the banding pattern after using XhoI and BamHI restriction enzymes to digest the DNA derived from ampicillin-resistant clones (a-h) of NEB10beta bacteria that were transformed with the Gibson assembly products. DNA that showed the expected banding pattern, cutting out a ∼4000 bp fragment corresponding to Cas9, were sequenced. RRE = rev response element, cPPT = central polypurine tract, SFFV = spleen focus forming virus promoter, EF1alpha = elongation factor 1alpha promoter, Cas9 = CRISPR-associated protein 9, NLS = nuclear localisation sequence, Flag = flag octapeptide tag, P2A = P2A self-cleaving peptide, BSD = blasticidin selection marker, WPRE = woodchuck hepatitis virus post-transcriptional regulatory element, AmpR = ampicillin resistance gene.*

samples (Figure 6.5A). These two bands should correspond to two versions of Cas9, one where the 2A sequence successfully cleaved Cas9 from mCherry, and another where cleavage was not successful. Therefore, the higher MW band likely corresponded to Cas9 fused to mCherry, and the lower molecular weight band corresponded to Cas9 where the mCherry tag was cleaved. While this indicated that the 2A peptide was functional, I would have expected the 2A cleavage ability to be more efficient. However, to avoid any potential functional effects of tagging mCherry directly to Cas9, which may block Cas9 activity, the Cas9-2A-mCh lentivirus was used from now on.

Next, the Cas9-2A-mCh lentivirus was tested on two cell lines that are more closely related to hCTL than P815s: 1) Jurkat cells, a human T cell line, and 2) YT, a human NK cell line. Both cell lines were successfully transduced with the lentivirus as shown by the detection of mCherry signal by flow cytometry and detection of Cas9 by WB (Figure 6.6). Strikingly, the Cas9 expression was much stronger in the lentivirally transduced samples than in samples derived from Cas9 hom mice (described in chapter 3) (Figure 6.6B). While only faint bands corresponding to Cas9 can be seen in the Cas9 hom samples, it was reassuring

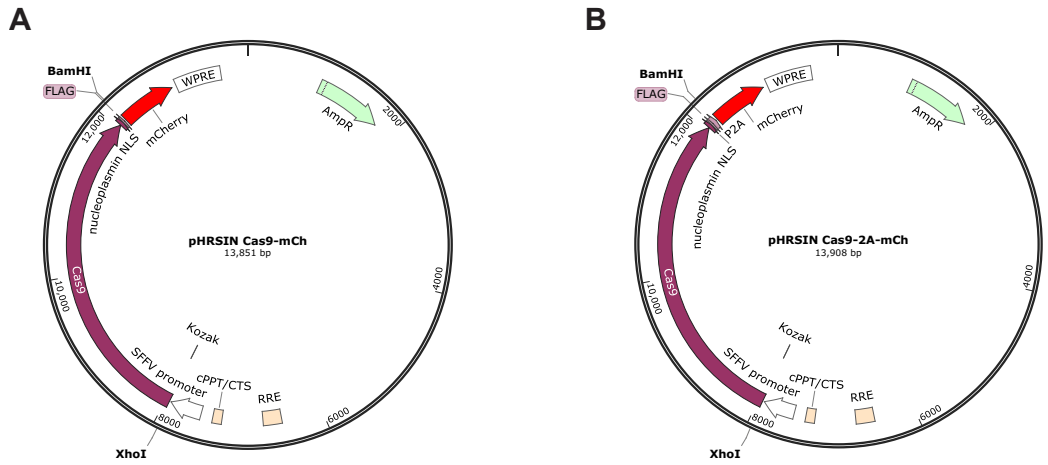

Fig. 6.4 ***Final Cas9-mCh and Cas9-2A-mCh pHRSIN plasmids maps.*** *Two Cas9-containing pHRSIN-mCh plasmids were produced:* ***A*** *One plasmid with Cas9 directly fused to mCherry.* ***B*** *A second plasmid where Cas9 and mCherry are separated by a P2A sequence. Plasmid maps were created with snapgene. RRE = rev response element, cPPT = central polypurine tract, SFFV = spleen focus forming virus promoter, Cas9 = CRISPR-associated protein 9, NLS = nuclear localisation sequence, Flag = flag octapeptide tag, P2A = P2A self-cleaving peptide, WPRE = woodchuck hepatitis virus post-transcriptional regulatory element, AmpR = ampicillin resistance gene.*

that these correspond to the same molecular weight as the lower band in the Cas9-2A-mCh lentivirus transduced samples (the version of Cas9 where mCherry was cleaved from Cas9). However, using lentivirus from the same stock did not result in mCherry positive hCTL (data not shown), again indicating difficulty in transducing this cell type.

6.2.3 Transduction of human T cells with Cas9-2A-mCh lentivirus

Since the Cas9-2A-mCh lentivirus worked on various cell lines, but not on primary hCTL, I set out to determine the titre of the lentivirus produced. I determined the lentivirus viral titre on Jurkat cells (Figure 6.7A), as an easy-to-transduce cell type, that will therefore provide an accurate representation of the viral titre, but is also related to primary human T cells. This showed that my standard lentiviral production protocol produced Cas9-2A-mCh lentivirus at a high titre ($1.8x10^7$ TU/ml).

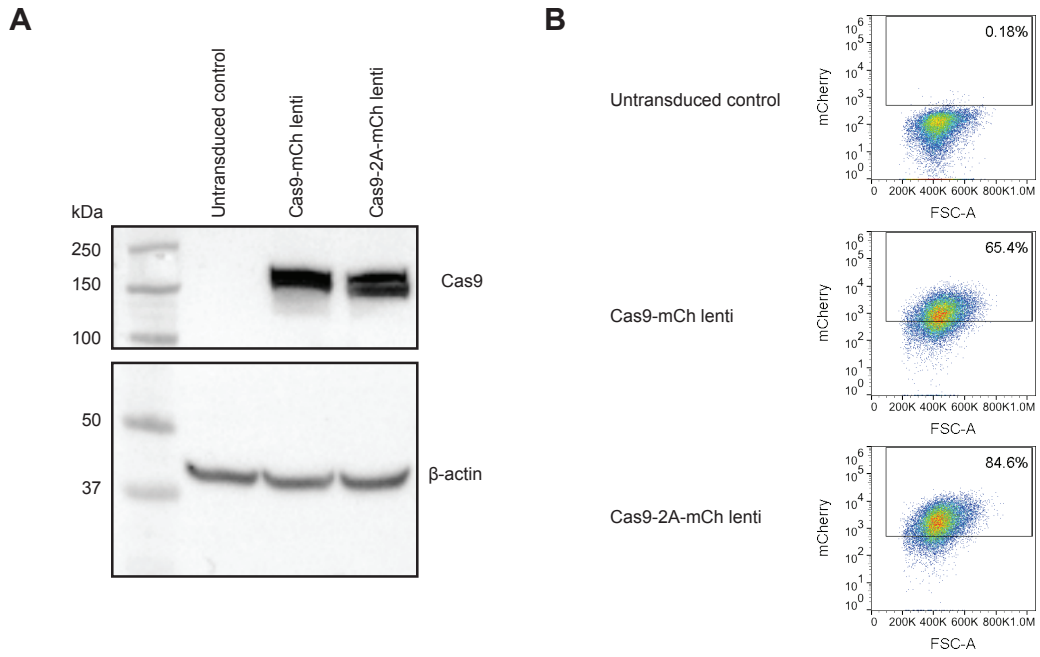

Fig. 6.5 ***Transduction of P815 cells with Cas9-mCh and Cas9-2A-mCh lentivirus.*** ***A*** *WB showing Cas9 expression after transduction of P815 cells with the Cas9-mCh or Cas9-2A-mCh lentivirus.* ***B*** *Flow cytometry plots showing the expression of mCherry-positive P815s after transduction with Cas9-mCh or the Cas9-2A-mCh lentivirus.*

Next, I tried to optimise transduction efficiency in primary human CTL. I normally included protamine sulfate in transduction experiments. Protamine sulfate is a polycationic polymer that neutralises the charge repulsion between the viral membrane and the plasma membrane of the cell and has been shown to enhance transduction efficiencies in human T cells (Cornetta and Anderson, 1989). Another commercially available reagent, the poloxamer synperonic F108, also known as lentiboost, is known to enhance transduction efficiency via a different mechanism. Lentiboost interacts with membranes and increases their permeability (Höfig et al., 2012). A study comparing transduction efficiencies in mouse CD4 and CD8 T cells showed lentiboost performs better than protamine sulfate (Delville et al., 2018). Encouragingly, comparing transduction efficiencies between samples transduced with the 'empty' pHRSIN-mCh lentivirus showed that transduction efficiency was higher in the presence of lentiboost in comparison to protamine sulfate (Figure 6.7B). All of the Cas9-2A-mCh lentivirus remaining from the viral titration was aliquoted between cells derived from three different HDs, meaning that these cells were only transduced at a low MOI of 1.17. As observed with the 'empty' pHRSIN-mCh lentivirus, transduction with the pHRSIN Cas9-2A-mCh lentivirus in the presence of lentiboost resulted in a higher transduction efficiency

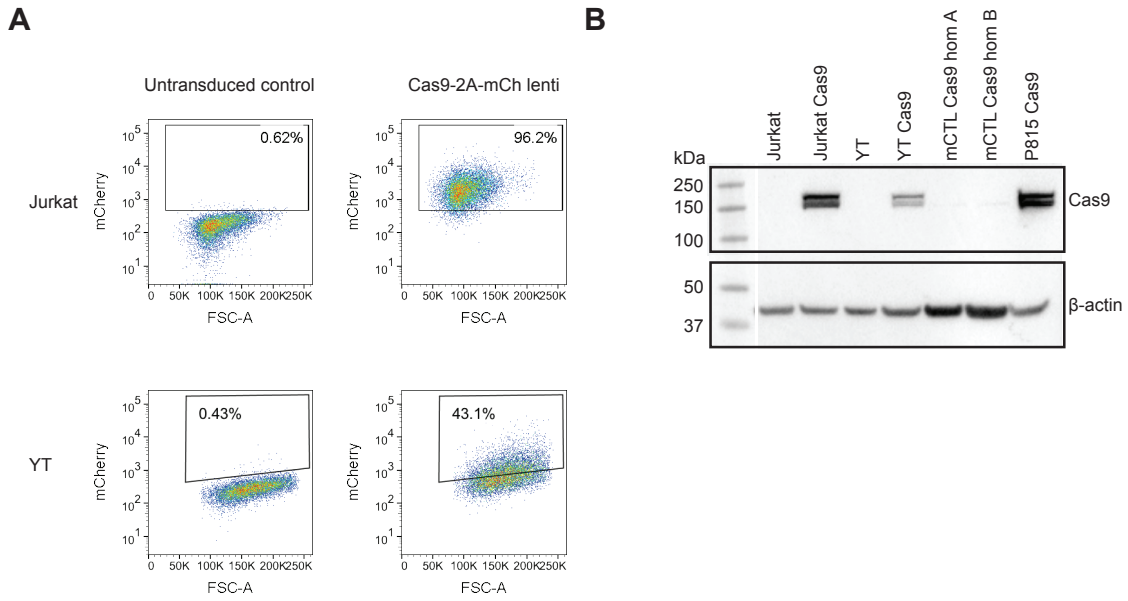

Fig. 6.6 ***Transduction of Jurkat and YT cell lines with Cas9-2A-mCh lentivirus.*** ***A*** *Flow cytometry plots showing the expression of mCherry in YTs and Jurkat cells after transduction with the Cas9-2A-mCh lentivirus.* ***B*** *WB comparing Cas9 expression in lysates derived from Cas9 hom mCTL to lysates derived from YTs, Jurkat cells and P815s transduced with the Cas9-2A-mCh lentivirus.*

in comparison to transduction with protamine sulfate (Figure 6.7B,C). While transduction efficiency was variable in cells from different HDs, up to 17% mCherry-positive cells were achieved after transduction with Cas-2A-mCh lentivirus in the presence of lentiboost (Figure 6.7D). FACS was used to isolate the mCherry-positive population, however, the cells did not expand further after sorting. This indicated that in addition to the challenge of low transduction efficiency with the large Cas9-2A-mCh lentivirus, sorting primary human T cells provided another hurdle to using the lentiviral CRISPR approach in primary human T cells.

6.2.4 Nucleofection of primary human T cells

As an alternative approach that does not require sorting, I tested the CRISPR approach using RNPs, as described in chapter 3, in hCTLs. This approach has been successfully used by others, mostly in human CD4 T cells (Hultquist et al., 2016; Roth et al., 2018; Rupp et al., 2017; Schumann et al., 2015). As hCTL had not previously been successfully nucleofected in our lab, I initially compared the nucleofection efficiency achieved with two different machines (the neon from ThermoFisher Scientific and the 4D from Lonza). When

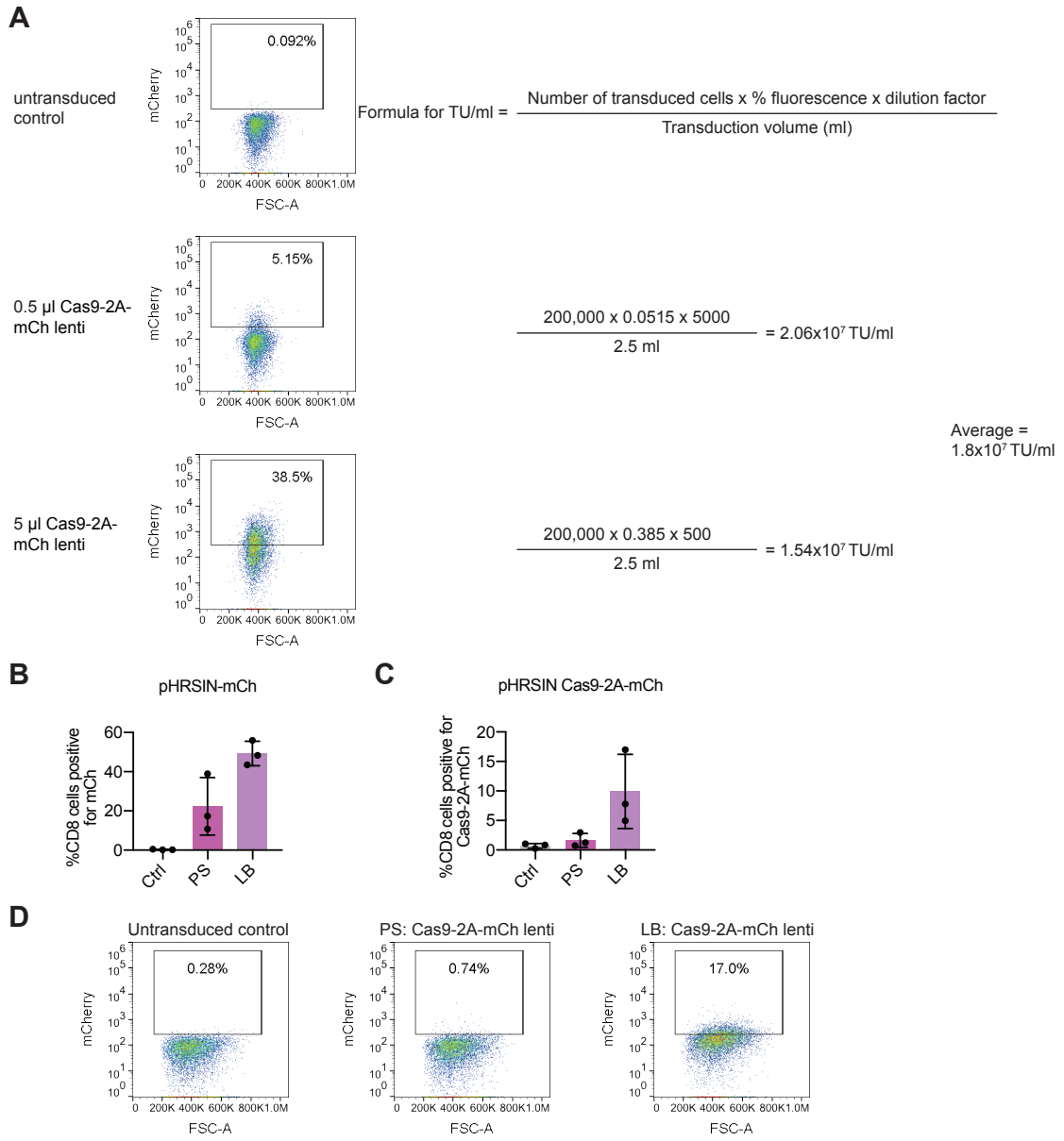

Fig. 6.7 ***Transduction of human T cells with Cas9-2A-mCh lentivirus.*** ***A*** *Determination of viral titre of the Cas9-2A-mCh lentivirus by transducing Jurkat cells.* ***B*** *mCherry expression in primary hCTL transduced with pHRSIN-mCh lentivirus using protamine sulfate (PS) or lentiboost (LB) as transduction enhancers. Bar graphs show the mean ± SD.* ***C*** *mCherry expression in primary hCTL transduced with pHRSIN-Cas9-2A-mCh lentivirus at MOI of 1.17 using PS or LB as transduction enhancers. The bar graphs show the average of 3 independent experiments, error bars show the SD.* ***D*** *Flow cytometry plots showing mCherry expression in response to transduction of hCTL derived from the same HD at MOI of 1.17 in the presence of PS or LB reagents. LB = lentiboost. PS = protamine sulfate.*

nucleofecting a plasmid encoding lifeact-EGFP the nucleofection efficiency achieved with the two machines was similar, showing an average nucleofection efficiency of 51.38% (neon) and 56.52% (4D) after one day (Figure 6.8). The fluorescent signal was maintained until day 4 and decreased by day 7 after nucleofection (Figure 6.8).

To test the RNP CRISPR system I used synthetic crRNA reagents targeting the human *CD2* gene, co-nucleofected alongside tracrRNA and Cas9 protein as established for mCTL in chapter 3. *CD2* was targeted as it encodes a cell surface protein that is easily monitored by flow cytometry. I only used 1-1.5 million cells per nucleofection and scaled down the CRISPR reagents accordingly (e.g. in chapter 3 I used 5 μg per crRNA when nucleofecting 5 million cells, therefore I used 1 μg per crRNA for 1 million cells). A decrease in CD2 levels could be observed 4 days after nucleofection (Figure 6.9). Strikingly, the percentage of cells that lost surface expression of CD2 was higher in samples that were nucleofected with the neon nucleofection system (n=6, $p<0.001$ at day 4, unpaired t-test with Welch's correction). Importantly, the KO was stably maintained until the last time point measured (one month after nucleofection). This confirmed the great potential of using hCTL over mCTL to produce stable KOs that are long-lived in tissue culture.

6.2.5 Comparing CRISPR KO efficiency with stable and transient Cas9 expression

Finally, I asked how the stable expression of Cas9 achieved through using the Cas9-2A-mCh lentivirus compared to the transient nucleofecion of Cas9-RNP complexes in terms of CRISPR efficiency. Jurkat cells were used that were either untransduced or between 90-100% positive for Cas9-2A-mCh after transduction. While Jurkat cells were nucleofected with Cas9 protein, tracrRNA and crRNAs targeting *CD2*, Cas9-2A-mCh-transduced Jurkat cells were only nucleofected with tracrRNA and crRNAs targeting *CD2*. The percentage of CD2 expression at the cell surface was measured at day 5 and day 14 after nucleofection. Initially, I used the same number of cells and same concentration of reagents previously used for *CD2* CRISPR in human T cells. However, a convincing decrease in CD2 levels was not observed at day 5 or day 14 post nucleofection (Figure 6.10A). Following the manufacturer's protocol, I scaled down the number of cells nucleofected from 1 million (using cuvettes for nucleofection) to 0.2 million (using 16-well strips for nucleofection) while keeping the amount of CRISPR reagent the same, thereby increasing the reagent-to-cell ratio. This showed successful CRISPR-mediated loss of CD2 protein cell surface expression in transient

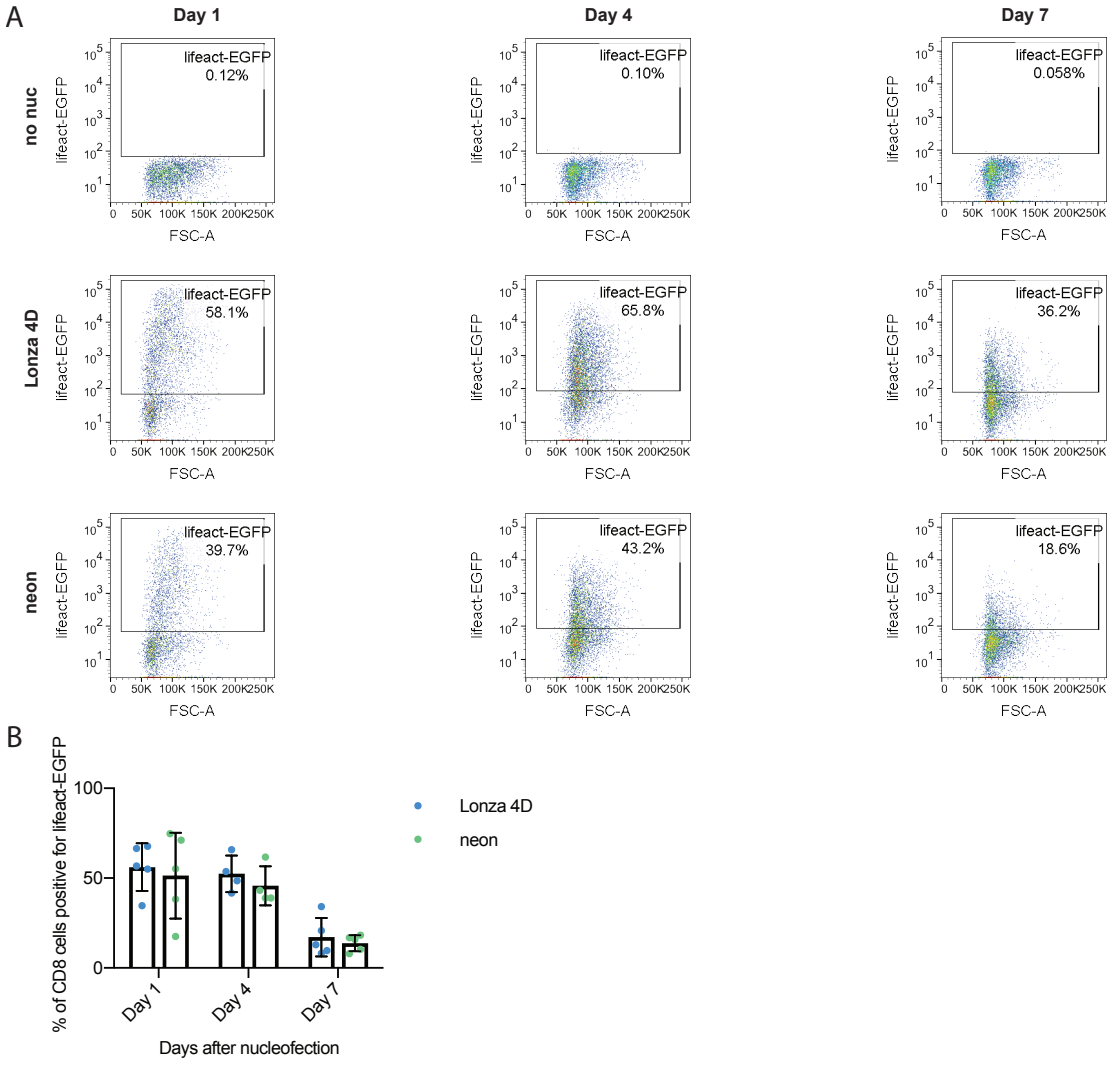

Fig. 6.8 ***Nucleofection of human T cells with lifeact-EGFP.*** *PBMCs were isolated from buffycoat and activated with 5 µg/ml PHA. At day 3 post activation, 1.5 million cells were nucleofected with 2 µg lifeact-EGFP plasmid using the Lonza 4D or neon nucleofection machines. The percentage of cells positive for lifeact-EGFP was determined by flow cytometry at day 1, 4 and 7 post nucleofection.* ***A*** *Representative flow cytometry plots.* ***B*** *Average lifeact-EGFP expression measured by flow cytometry at day 1, 4 and 7 post nucleofection. The bar graphs show the average of 5 independent experiments, error bars show the SD. no nuc = no nucleofection control.*

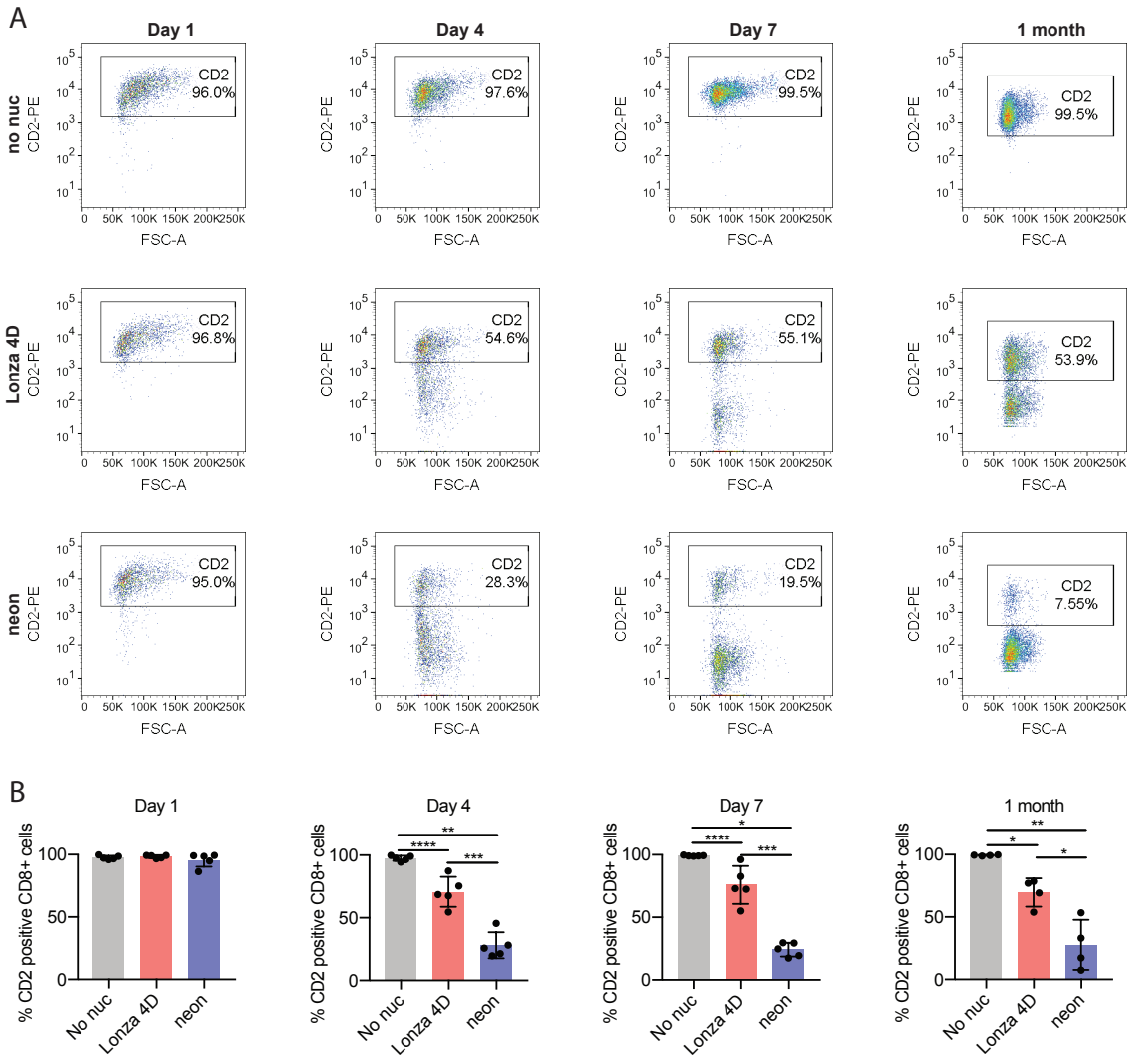

Fig. 6.9 ***Targeting CD2 by CRISPR using Cas9-RNP in human T cells.*** *PBMCs were isolated from buffycoat and stimulated with 5 µg/ml PHA for three days prior to nucleofection. 1-1.5 million cells per condition were nucleofected with Cas9-RNPs targeting CD2. The Lonza 4D and neon nucleofection machines were tested in parallel.* ***A*** *Representative flow cytometry plots showing the percentage of cells positive for cell surface CD2 at day 1, 4 and 7 or one month after nucleofection.* ***B*** *Average CD2 cell surface expression measured by flow cytometry at day 1, 4 and 7 (n=5 independent experiments) and one month post nucleofection (n=4 independent experiments), *p<0.05, **p<0.01, ***p<0.001, ****p<0.0001, unpaired t-test with Welch's correction. Bar graphs show the mean ± SD, no nuc = no nucleofection control.*

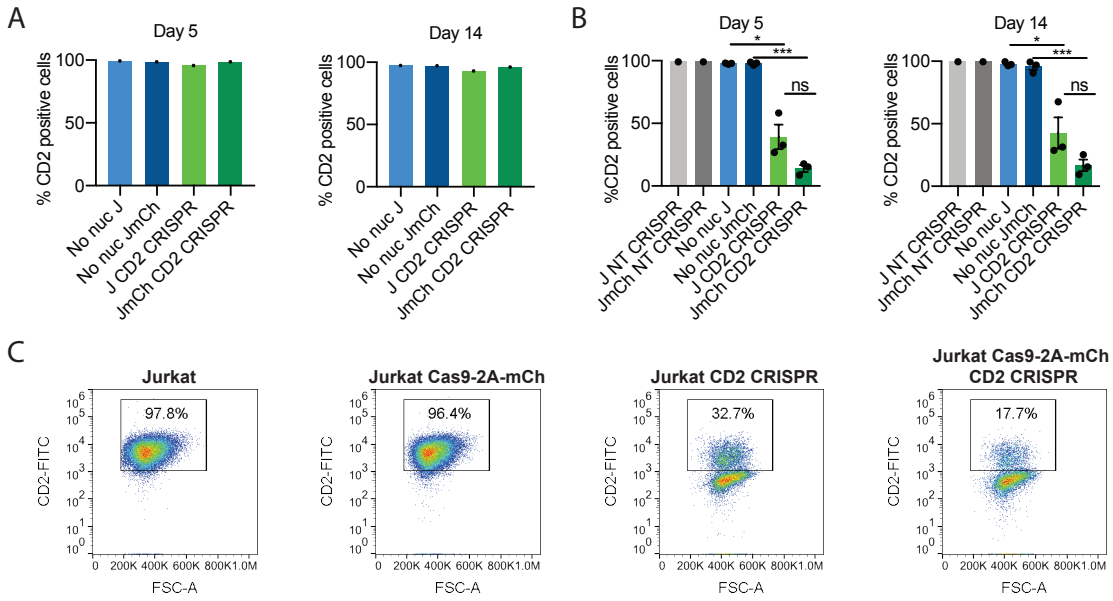

Fig. 6.10 ***CRISPR KO efficiency with transient and stable Cas9 expression targeting CD2 in Jurkat cells.*** ***A*** *1 million Jurkat cells were nucleofected with 1 µg per CD2 crRNA (3 crRNAs in total), 3 µg tracrRNA and 2 µg Cas9 protein using the Lonza 4D nucleofection machine. CD2 cell surface expression was measured by flow cytometry at day 5 and day 14 post nucleofection, n=1.* ***B*** *0.2 million Jurkat cells were nucleofected with 1 µg per CD2 crRNA (3 crRNAs in total), 3 µg tracrRNA and 2 µg Cas9 protein using the Lonza 4D nucleofection machine. CD2 cell surface expression was measured by flow cytometry at day 5 and day 14 post nucleofection. NT samples: n=1, No nuc and CD2 CRISPR samples: n=3 independent experiments, *p<0.05, ***p<0.001, unpaired t-test with Welch's correction. Bar graphs show the mean ± SD.* ***C*** *Representative flow cytometry plots showing CD2 cell surface expression at day 5 post nucleofection. J=Jurkat, JmCh = Jurkat Cas9-2A-mCh, NT = non-targeting, no nuc = no nucleofection control, ns = not significant.*

(n=3, p<0.05 at day 5, unpaired t-test with Welch's correction) and stable (n=3, p<0.001 at day 5, unpaired t-test with Welch's correction) Cas9 samples (Figure 6.10B,C). Similar results were achieved when targeting the gene encoding the cell surface protein B2M (Figure 6.11A,B) (n=3, p<0.01 for transient Cas9, p<0.001 for stable Cas9, unpaired t-test with Welch's correction). This confirmed that the Cas9-2A-mCh construct encoded functional Cas9 protein. For both genetic targets, the sample with stable lentiviral transduction of Cas9 showed a trend towards better CRISPR KO efficiency in comparison to the respective Cas9 protein nucleofected sample, however, this trend was not statistically significant (Figures 6.10 and 6.11).

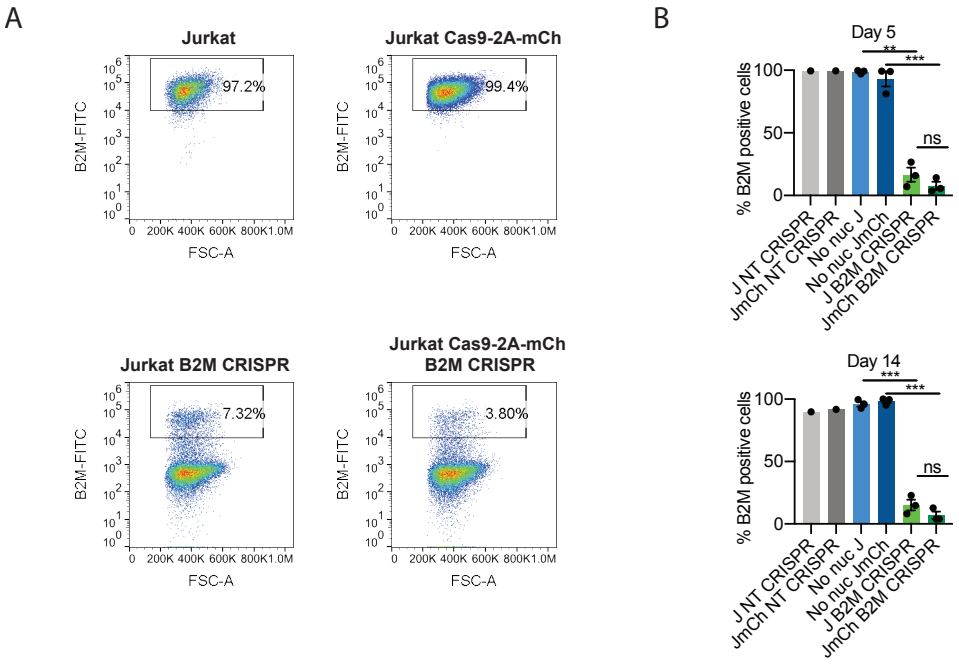

Fig. 6.11 ***CRISPR KO efficiency with transient and stable Cas9 expression targeting B2M in Jurkat cells.*** *0.2 million Jurkat cells were nucleofected with 1 µg per B2M crRNA (3 crRNAs in total), 3 µg tracrRNA and 2 µg Cas9 protein using the Lonza 4D nucleofection machine. B2M cell surface expression was measured by flow cytometry at day 5 and day 14 post nucleofection.* ***A*** *Representative flow cytometry plots showing B2M cell surface expression at day 5 post nucleofection.* ***B*** *Bar graphs showing the average B2M cell surface expression at day 5 and day 14 post nucleofection, NT samples: n=1, No nuc and B2M CRISPR samples: n=3 independent experiments, **p<0.01, ***p<0.001, unpaired t-test with Welch's correction. Bar graphs show the mean ± SD. J=Jurkat, JmCh = Jurkat Cas9-2A-mCh, NT = non-targeting, no nuc = no nucleofection control, ns = not significant.*

6.3 Discussion

The blasticidin selection time and concentration required to select for a transduced population can vary greatly between cell types. Too much antibiotic kills cells including transduced cells, not enough drug will result in untransduced cells being left in the population (Doench, 2017). 5 µg/ml blasticidin was the lowest concentration that seemed to kill all untransduced cells, although even 1 µg/ml blasticidin had a stark effect on the FSC/SSC profile of hCTLs after 15 days of treatment (Figure 6.1). While transduction of hCTL with the Cas9-Blast lentivirus appeared to be successful by PCR, only few cells survived the treatment with 5 µg/ml blasticidin (Figure 6.2), indicating that this blasticidin concentration may have been

too high, killing everything including transduced cells. On top of this, low transduction efficiency, as indicated by the WB and PCR results (Figure 6.2), likely also contributed to the unsuccessful selection of Cas9-expressing cells. In agreement with my results, a published study using a lentivirus encoding a puromycin resistance gene alongside Cas9 observed immense cell death (>90%) upon antibiotic selection (Legut et al., 2018).

In order to be able to visualise transduction efficiency more clearly than by blasticidin selection, I cloned the *Cas9* gene into a lentiviral vector expressing the fluorescent protein mCherry (Figures 6.3 and 6.4). Two versions of the vector were produced, one where Cas9 was directly fused to mCherry and another where Cas9 and mCherry were separated by a self-cleaving 2A peptide (Figure 6.4). Using the resulting vector to produce lentivirus resulted in successful transduction of P815, YT and Jurkat cell lines (Figures 6.5 and 6.6). Due to concerns that directly fusing Cas9 to mCherry might affect its function the Cas9-2A-mCh lentivirus was used subsequently.

2A peptides are used to co-express two genes in one mRNA transcript, which are then cleaved co-translationally (Kim et al., 2011). While 2A peptides have been identified from several different viruses, a study showed that the P2A peptide, derived from porcine teschovirus, has the highest cleavage efficiency in human cell lines in comparison to 2A peptides derived from three other viruses (Kim et al., 2011). However, in this chapter there was only partial cleavage between Cas9 and mCherry in all cells tested, as shown by two bands being detected when blotting for Cas9 (Figures 6.5 and 6.6). The lower molecular weight band likely corresponded to Cas9 cleaved from mCherry and the higher molecular weight band to Cas9 still fused to mCherry. I would have expected higher cleavage efficiency of the P2A peptide based on the published data (Kim et al., 2011). This means that the Cas9 pool in the Cas9-2A-mCh transduced samples is a heterogenous population of Cas9 cleaved from mCherry and Cas9 fused to mCherry. Therefore it was crucial to confirm that this mixed population of Cas9 is functional as fusion to mCherry could affect its activity. The results obtained with Cas9-2A-mCh Jurkat cells showed high KO efficiency when targeting *B2M* and *CD2* using CRISPR (Figures 6.10 and 6.11), indicating that the Cas9-2A-mCh cleaved and uncleaved products are both functional.

It is known that as vector length increases, viral titre decreased (Ramezani and Hawley, 2002), meaning that viruses containing a large insert, such as Cas9, are likely to have a relatively low titre (Doench, 2017). Here I managed to produce the Cas9-2A-mCh lentivirus at a high viral titre (Figure 6.7), however, transduction of human T cells with Cas9-2A-mCh

lentivirus was still challenging, and much less efficient than transduction of Jurkat, YT or P815 cell lines. Lentiboost proved to be a better transduction enhancer than protamine sulfate, yielding 17% transduction efficiency with the Cas9-2A-mCh lentivirus in cells derived from one HD (Figure 6.7). However, the fluorescence level in the population positive for Cas-2A-mCh was low, which could indicate a low level of Cas9 expression (Figure 6.7).

A recently published study also reported low transduction efficiency when transducing T cells with lentivirus encoding Cas9-2A-GFP, obtaining 5% GFP-positive cells (Seki and Rutz, 2018). They noted a low level of GFP fluorescence as well, and concluded that the lentiviral approach is inefficient (Seki and Rutz, 2018). Notably, I achieved up to 17% transduction efficiency when using the Cas9-2A-mCh lentivirus at a low MOI of 1.17. It would therefore be worthwile to try to transduce human T cells at a higher MOI to see if the percentage of transduced cells could be increased further.

Meanwhile, I successfully used the Cas9-RNP nucleofection approach to target *CD2* in human T cells (Figure 6.9). Throughout my PhD project, several studies have been published using this approach, some have used the 4D nucleofector (Hultquist et al., 2016; Roth et al., 2018; Rupp et al., 2017) and others the neon nucleofection machine (Gundry et al., 2016; Schumann et al., 2015). While the two machines seemed similarly efficient when nucleofecting a DNA plasmid encoding lifeact-EGFP (Figure 6.8), nucleofection with the neon resulted in higher *CD2* KO efficiency (Figure 6.9). This may be due to differences between the nucleofection solutions or nucleofection pulses used, which can affect cell permeability and perhaps even Cas9-RNP complex stability. On average, I achieved a 71.88% decrease in CD2 expression when using the neon nucleofection machine, but only a 29.28% decrease in CD2 with the 4D nucleofector at day 4 post nucleofection ($n=5$, $p<0.001$, unpaired t-test with Welch's correction, Figure 6.9).

Finally, I asked if CRISPR efficiency differed when using transient Cas9 expression (Cas9-RNP nucleofection approach) or stable Cas9 expression (transduction with Cas9 lentivirus) in Jurkat cells. Surprisingly, the initial attempt to nucleofect Jurkat cells with *CD2* CRISPR components was unsuccessful (Figure 6.10). Successful CRISPR-mediated KO of *CD2* and *B2M* was achieved when scaling down the number of cells used (Figures 6.10 and 6.11), indicating that a higher reagent-to-cell concentration was needed for CRISPR in Jurkat cells than in hCTL. Jurkat cells may have an abnormal karyotype, and therefore potentially more than two copies of the *CD2* gene, which could explain the requirement for more CRISPR reagents to cut all alleles. In agreement with this, some published studies indicated

that Jurkat cells may have a hypotetraploid genome (Cheng and Haas, 1990; Snow and Judd, 1987). Targeting *CD2* and *B2M* in Cas9-2A-mCh-transduced and untransduced Jurkat cells indicated that the CRISPR efficiency achieved with stable and transient Cas9 expression was comparable. A non-significant trend towards better KO efficiency was observed with stable Cas9 expression. However, this may just be due to Cas9 protein being limited by nucleofection efficiency, while 90-100% of the Cas9-2A-mCh-transduced Jurkat cells were expressing Cas9 according to mCherry expression measured by flow cytometry.

The Cas9-RNP approach is very useful to target specific genes or perform arrayed screens (see chapter 4). However, if complete KOs are desired, it might be worth transducing hCTL with Cas9 lentivirus at a higher MOI and further optimising hCTL survival after sorting in order to generate hCTL that stably express Cas9. Subsequent transduction with a sgRNA-containing lentivirus would likely be more efficient due to the smaller insert size, allowing antibiotic selection and the generation of complete KOs. Stably expressing Cas9-hCTL would also open the possibility of a genome-wide screen in primary human T cells. Until recently, genome-wide screens had only been performed in cell lines related to primary T cells, such as Jurkat and CCRF-CEM cells (Park et al., 2017; Shang et al., 2018). Recently, a group took an alternative approach where they transduced primary human T cells with a lentiviral sgRNA library followed by nucleofection of Cas9 protein (Shifrut et al., 2018). The methods and reagents optimised in this chapter could be used to produce human T cells stably expressing Cas9. If a Cas9-pure population could be isolated, transduction with a genome-wide sgRNA lentiviral library would perhaps allow the unbiased pooled genome-wide screening approach in primary human T cells.

6.3.1 Summary and evaluation of aims

- Transduce hCTL with a lentivirus encoding Cas9 as well as antibiotic resistance or a fluorescent marker to be able to select successfully transduced cells.
  - Initially, hCTL were transduced with a lentivirus encoding Cas9 and antibiotic resistance to blasticidin. However, blasticidin selection was challenging due to low transduction efficiency. To obtain a direct readout of the transduction efficiency, Cas9 was cloned into a lentiviral vector that encodes a fluorescent marker (pHRSIN-mCh). This lentiviral vector has previously been used to transduce primary human hematopoietic cells (Demaison et al., 2002). I successfully used the resulting lentivirus to transduce Jurkat cells, YTs and P815s. Human T cell transduction proved more challenging due to low transduction efficiency with

such a large construct. Using an alternative transduction enhancer to protamine sulfate, lentiboost, improved transduction efficiency.

- Test nucleofection of hCTL and the transient Cas9-RNP CRISPR approach (optimised in chapter 3) in primary hCTL.
  - I tested two machines commonly used to nucleofect human T cells. At day 4 post nucleofection, *CD2* was knocked out in an average of 71.88% of cells using the neon machine and 29.28% of cells using the Lonza 4D nucleofection machine.
- Compare the stable (Cas9 lentivirus) and transient (Cas9-RNP) approaches in terms of CRISPR efficiency.
  - Using Jurkat cells I showed that the CRISPR efficiency was comparable when using stable or transient Cas9. Cells transduced with the Cas9 lentivirus showed a slight trend towards better KO efficiency when targeting *CD2* (averages from day 5: Jurkat: 60.77% KO, Jurkat Cas9-2A-mCh: 86.06% KO) and *B2M* (averages from day 5: Jurkat: 83.26% KO, Jurkat Cas9-2A-mCh: 92.05% KO).

Chapter 7

Conclusions and future perspectives

7.1 Summary of findings

Cytotoxic T cells are a crucial component of the adaptive immune system. They are of great interest for medical therapies as they can kill infected and cancerous cells. They do so via direct contact to target cells and the focused secretion of lytic granules, also known as degranulation, which ensures that target cells are killed while leaving surrounding cells intact. The importance of cytotoxic T cells to maintain a healthy immune system is demonstrated by the CTL defects observed in patients with life-threatening immunodeficiency diseases (Clark and Griffiths, 2003; Feldmann et al., 2003; Stepp et al., 1999).

This study aimed to use the CRISPR-Cas9 gene editing technology in a screening setting to test for genes that regulate CTL killing. In chapter 3, I established the amount of CRISPR-Cas9-RNP reagents needed to efficiently edit primary mCTL by targeting the abundant cell surface protein Thy1. Conditions resulting in reproducible and efficient CRISPR-mediated KO in mCTL were successfully established, in some cases reducing protein expression by over 90% (Figure 3.6). Targeting *Rab27a*, a known mediator of cytotoxic T cell function, using CRISPR-Cas9-RNPs significantly reduced RAB27A protein levels and resulted in a degranulation and killing phenotype (Figure 3.7). CRISPR-mediated KO of other known regulators of CTL cytotoxicity, the lytic granule component perforin and MUNC13-4, a part of the lytic granule fusion machinery, was further used to set up an assay that measures degranulation and killing simultaneously (Figure 3.11). This flow cytometry-based assay allowed detection of regulators of T cell killing, while the degranulation readout gave immediate insight into the underlying molecular mechanism by which the killing is mediated.

The combined degranulation and killing assay was suitable for screening as it could be performed in a 96 well format. To identify targets for a screen I performed an RNA-seq study that compared the transcriptome of naive and effector CD8 T cells (chapter 4). Genes highly expressed in activated but not naive CD8 T cells are likely to be important for CTL effector functions, including killing. This gave a large set (1803 genes) of upregulated differentially expressed genes (Appendix B), which were predominantly associated with the cell cycle (Figure 4.3). 13 genes, chosen based on functional annotation analysis and literature research, were targeted by CRISPR and tested in the combined degranulation and killing assay. *Hif1*α and *Nfil3* were identified as interesting genetic targets where CRISPR-mediated KO decreased the killing but not the degranulation capability of effector CTL (Figures 4.5 and 4.6), a phenotype reminiscent of perforin CRISPR samples (Figure 3.8). This was in line with published studies, which identified that perforin protein expression was affected by the absence of members of the HIF complex and NFIL3 (Finlay et al., 2012; Rollings et al., 2018). However, the precise mechanism by which HIF-1α and NFIL3 affect perforin protein levels remains to be elucidated. Other studies have shown that these genes are important when lost in naive T cells or during T cell development in vivo (Doedens et al., 2013; Finlay et al., 2012; Rollings et al., 2018). The data generated in this thesis demonstrated a direct importance of NFIL3 and HIF-1α in effector CTL to enable killing. This is likely mediated through their effect on perforin. Furthermore, the RNA-seq dataset was used to identify genes that are differentially expressed between males and females. Interestingly this included some genes that are implicated in CTL killing function (such as *Gzma*, *Il2ra* and *Nfil3*) (Table 4.3). It might therefore be interesting to explore whether there are differences between the killing capabilities of males and females.

The screen performed in chapter 4 confirmed that the combined degranulation and killing assay could be used to identify regulators of CTL killing in mCTL. In chapter 5, I successfully tested this assay in hCTL using cells derived from FHL2 and FHL3 patients. The traditional degranulation assay is currently used for diagnostic purposes, but cannot detect defects resulting from perforin mutations (Bryceson et al., 2012). Diagnosis of FHL therefore requires an additional investigation of perforin protein expression (Bryceson et al., 2012). The combined degranulation and killing assay would therefore reduce the number of experiments that need to be performed, making the diagnostic process more efficient. This highlights the potential of the combined degranulation and killing assay as a diagnostic test.

The scalability of the screen was tested in hCTL using a library containing 64 compounds that targeted the NF-κB signalling pathway. In this screen for chemical mediators of CTL

killing, I identified that parthenolide (drug 19) affected CTL killing within 1 h of treatment (Figure 5.8). Parthenolide was found to affect NF-κB activity via the phosphorylation status of p65 at Ser536 (Figure 5.9). However, parthenolide has also been reported to affect HDAC1 and DNA methyltransferase 1 (Gopal et al., 2007; Liu et al., 2009), meaning that I could not conclude that the degranulation and killing defect observed upon CTL treatment with parthenolide was due to its inhibition of p65. KO of p65 using CRISPR could help to clarify the role of NF-κB in CTL killing. The drug screen therefore highlighted two important points. Firstly, that the combined degranulation and killing assay could be used to screen many dozens of compounds. Secondly, it emphasised the advantage of a CRISPR-based screen over a drug screen, as the genetic approach provides a cleaner system that is, at least in theory, not complicated by unanticipated off-target effects.

Finally, I successfully used the CRISPR gene editing technology using the RNP approach in hCTL (Figure 6.9). I also explored stable Cas9 expression through lentiviral transduction as an alternative approach to CRISPR in primary human T cells and related cell lines. This approach could provide an even cleaner system as stable incorporation of antibiotic resistance cassettes or fluorescent markers would allow selection of cells that contain all necessary CRISPR reagents. Additionally, this approach has the potential to allow much larger CRISPR-based screens, as discussed in section 7.4. The difficulties I experienced with lentiviral transduction of human T cells with Cas9 are in line with observations from other labs (Legut et al., 2018; Shifrut et al., 2018; Wang et al., 2014b). However, through careful optimisation of transduction methods I achieved a transduction efficiency of up to 17% (Figure 6.7). Transposon-based stable integration of Cas9 could be explored in parallel to single cell cloning of the Cas9-2A-mCherry transduced cells in future experiments, in order to achieve the aim of creating primary human T cells that stably express Cas9.

7.2 Comparison of findings to published studies using CRISPR in primary T cells

7.2.1 CRISPR in mouse T cells

As this PhD project was ongoing, several papers have been published that use the CRISPR-Cas9 technique in primary mouse T cells. These can broadly be divided into studies using primary cells derived from Cas9 expressing mice and studies that use Cas9-RNPs, two options that were also explored in this thesis. Meanwhile, several studies noted that all-in-one viral vectors encoding both Cas9 and sgRNAs resulted in low transduction efficiencies, likely

due to the large size of Cas9, and are not as efficient at generating KOs (Huang et al., 2019; Seki and Rutz, 2018).

Several Cas9 expressing mice have been generated (Chu et al., 2016b; Platt et al., 2014; Tzelepis et al., 2016). Chu et al. (2016a) used primary T cells derived from transgenic Cas9 mice and achieved KO of CD44 in around 50% of the cells four days after transduction with retroviral vectors encoding sgRNAs. Interestingly they showed that their Cas9 mice expressed more Cas9 in lymphocytes and generate KOs at higher efficiencies than the Cas9 mice generated by Platt et al. (2014).

A paper published after this thesis was submitted used the same transgenic Cas9 mice (generated by Tzelepis et al. (2016)) that I used for the experiments in Figure 3.4 for genome-wide CRISPR screens in primary CD4 T cells (Henriksson et al., 2019). They transduced the Cas9 expressing T cells with a genome-wide retroviral sgRNA library, where each virus encoded a single sgRNA together with BFP and puromycin resistance. This enabled selection of cells that stably expressed sgRNAs. In contrast, I transiently nucleofected synthetic crRNAs and tracrRNAs into primary T cells derived from the transgenic Cas9 mice, a process which does not allow stable expression or selection of cells that have taken up the reagents. Using this approach, I achieved an average protein loss of 41.6% in nucleofected cells when using 10 μg crRNA/tracrRNA (Figure 3.4). In the experimental setup of Henriksson et al. (2019) all cells should have been expressing a sgRNA and Cas9 after selection procedures. Therefore, their approach, in contrast to mine, was not limited by nucleofection efficiency or the stability of synthetic RNAs. Unfortunately, a direct comparison of CRISPR efficiency between my study and Henriksson et al. (2019) is not possible, because they do not show the percentage loss of protein expression they achieved in response to CRISPR. In their methods they state that they used a viral vector encoding BFP, GFP and a sgRNA against GFP to test Cas9 function. With this approach, Cas9 cutting efficiency can be validated and quantified by loss of GFP expression in the presence of the GFP-targeting sgRNA. As the results are not shown it is unclear how efficiently they lose protein expression in their experimental setup. However, it seems that their CRISPR KO worked to some extent as they observed signs of altered CD4 T cell differentiation in response to some sgRNAs (Henriksson et al., 2019).

I was able to improve on the CRISPR KO efficiency I achieved with cells derived from Cas9-expressing mice by using Cas9-RNPs in cells derived from WT mice (64.7% Thy1 KO achieved with Cas9-RNP (Figure 3.5) in contrast to 33.3% Thy1 KO achieved using the same concentration of synthetic crRNA/tracrRNA in cells from Cas9-expressing mice (Figure 3.4)).

Cas9-RNPs have the advantage of allowing gene-editing in primary cells regardless of their genetic background. Due to its higher efficiency, the Cas9-RNP approach was subsequently used throughout this thesis.

While Cas9-RNPs have been widely used in primary human T cells, as outlined in the next section, the first study that used this approach in primary mouse T cells was only published in 2018 (Seki and Rutz, 2018). Using one guide to target Thy1, Seki and Rutz (2018) reported 60% loss of Thy1 expression in primary mouse T cells using the Cas9-RNP approach, which corresponds well to the 64.7% loss of Thy1 expression I achieved with one guide (Figure 3.5). To further improve CRISPR efficiencies, Seki and Rutz (2018) carefully optimised a myriad of further experimental parameters. They tested a range of nucleofection conditions (optimising buffers and pulses), showed that using two or three sgRNAs per gene rather than one sgRNA per gene resulted in improved KO efficiency and even found that some commercially available Cas9 proteins lead to higher KO efficiencies than others (Seki and Rutz, 2018). Using their optimised conditions, Seki and Rutz (2018) achieved 85%-98% KO across a variety of targets in activated and nonactivated primary human and mouse CD4 and CD8 T cells. Similarly to Seki and Rutz (2018), I routinely used three guides per gene, resulting in comparable KO efficiencies across many target genes (*Rab27a* (Figure 3.7), *Perforin* (Figure 3.8), *Munc13-4* (Figure 3.9), *Nfil3* (Figure 4.5), *Hif1a* (Figure 4.6)). The study by Seki and Rutz (2018) indicates that there may be potential to improve the KO efficiency I achieved even further. This could be explore in future experiments, for example by testing a variety of commercially available Cas9 proteins.

7.2.2 CRISPR in human T cells

Several technical approaches have been pursued to achieve CRISPR-Cas9 mediated gene editing in primary human T cells. These include nucleofection of DNA plasmids, viral delivery of CRISPR components and nucleofection of crRNAs and tracrRNAs in combination with Cas9 protein or Cas9 mRNA.

The first published study that used CRISPR in primary human T cells nucleofected plasmids encoding Cas9 and sgRNAs (Mandal et al., 2014). Interestingly, they found that a sgRNA that led to loss of B2M expression in 48% of HEK293T cells only resulted in loss of B2M expression in less than 5% of primary T cells. Even after targeting the gene with two guides, they only achieved 18% loss of B2M expression (Mandal et al., 2014), indicating that their approach to gene-editing in primary T cells was inefficient.

Further technical difficulties were highlighted by several studies that attempted to use viral delivery of CRISPR components to primary human T cells. Wang et al. (2014b) tried to deliver Cas9 and sgRNAs using lentiviral vectors to primary human T cells, but while they were able to KO CCR5 in a human CD4 T cell line, they stated that attempts to disrupt CCR5 gene expression in primary human T cells using the same experimental approach were unsuccessful, although the data is not shown. Similarly, Griffin et al. (2015) tried to deliver Cas9 and sgRNAs using viral vectors and observed that editing efficiency was lower in primary CD4 T cells than in related cell lines. More recently, Legut et al. (2018) managed to transduce primary human T cells with a viral vector encoding Cas9, sgRNA and puromycin resistance. However, 90% of cells died following selection, indicating that only 10% of the cells were successfully transduced (Legut et al., 2018). These results correlate well with my findings in chapter 6, and demonstrate that low transduction efficiency is a key challenge to stable expression of Cas9 in primary T cells.

The most widely published approach to CRISPR-Cas9 gene editing in primary human T cells is the Cas9-RNP method. Schumann et al. (2015) achieved ∼40% loss of cell surface expression of CXCR4 in primary human T cells in response to nucleofection of in vitro transcribed crRNA and tracrRNA alongside Cas9 protein. Nucleofection of CRISPR reagents as RNAs and proteins was found to be less toxic and more efficient at generating KOs than nucleofection of plasmids (Hendel et al., 2015). Another study using Cas9-RNPs in primary human T cells achieved 86% loss of CD45 in response to nucleofecting CRISPR reagents using the neon transfection system (Gundry et al., 2016). These results are comparable to the efficiencies I obtained when targeting *CD2* by CRISPR in primary human T cells, where I achieved 75.8% KO on average at day 7 post nucleofection when using the neon transfection system (Figure 6.9). Further studies have successfully used the Cas9-RNP approach to create more potent CAR T cells, for example by disrupting PD-1 to enhance CAR T cell mediated killing (Rupp et al., 2017) and by disrupting CD7 to avoid fratricide of CD7 specific CAR T cells (Gomes-Silva et al., 2017). While not the focus of this thesis, it is also noteworthy that knock-ins have been achieved using the Cas9-RNP approach (Roth et al., 2018; Schumann et al., 2015).

Similarly to my approach in chapter 4, where I performed an arrayed screen using Cas9-RNPs in primary mouse T cells, the Cas9-RNP approach has also been used for an arrayed screen in primary human T cells. While I targeted 13 genes, Hultquist et al. (2016) targeted 45 genes in order to identify genes that control HIV infection of primary human T cells. Hultquist et al. (2016) were able to perform an arrayed screen at a larger scale because they

had access to a 96-well electroporation device. Together, both my study and the paper by Hultquist et al. (2016) demonstrate the value of the Cas9-RNP technology for the purpose of small to medium sized arrayed CRISPR screens.

Further to the technical approaches outlined above, nucleofection of Cas9 mRNA, rather than Cas9 protein, alongside in vitro transcribed RNA has also been used for successful gene editing in primary human T cells (Ren et al., 2017a). Additionally, the lentiviral delivery of sgRNAs followed by nucleofection of Cas9 mRNA was shown to result in loss of CD3 expression in 90% of cells, in comparison to 82% KOs achieved with synthetic sgRNA and Cas9 protein co-nucleofection and 76% KOs achieved with co-nucleofection of synthetic sgRNAs and Cas9 mRNA (Ren et al., 2017b). Similarly, Shifrut et al. (2018) achieved loss of CD8 expression in over 80% of cells when using lentiviral delivery of sgRNAs followed by nucleofection of Cas9 protein. While the KO efficiencies achieved are convincing across several different technical approaches, the viral delivery of sgRNAs has the additional benefit of enabling delivery of genome-wide sgRNA libraries, allowing large-scale unbiased screens, as recently performed by Shifrut et al. (2018).

In summary, the toolbox for disrupting gene expression using CRISPR-Cas9 in primary human and mouse T cells has been expanding rapidly over the last 5 years as this PhD project was ongoing. The findings in this thesis correlate well with published findings, and contribute to knowledge of how to efficiently and robustly disrupt gene expression in primary T cells. KO efficiencies over 80% have been achieved across many genetic targets, both in this thesis and in the published literature. Cas9-RNPs or viral expression of sgRNAs in combination with Cas9 protein/mRNA nucleofection or cells derived from Cas9-expressing mice have emerged as the most convincing approaches to generate KOs in primary T cells at high efficiencies.

7.3 Evaluation of the Cas9-RNP approach to CRISPR gene editing

The results obtained in this thesis indicate that Cas9-RNPs can generate true genetic KOs in a substantial subset of target cells as measured by WB and flow cytometry (Figures 3.4 - 3.9). Cas9-RNPs generated permanent genetic modifications, which were shown to be stably maintained, at least until 1 month after nucleofection (Figure 6.9). While some cells treated with Cas9-RNP appeared to have lost protein expression completely, other cells had only

partially lost protein expression or not lost it at all. This heterogeneity can be seen clearly in flow cytometry plots where *Thy1* was targeted in mCTL (Figure 3.5) and *CD2* or *B2M* were targeted in Jurkat cells or hCTL (Figures 6.9, 6.10 and 6.11). The variability of the fluorescent signal likely correlated to homozygous KOs, heterozygous KOs and unedited cells. This heterogeneous mix of cells is likely the result of limited transfection efficiency and variability in DNA repair outcomes. This heterogeneity may create noise in a phenotypic readout that can conceal the phenotype of genes where KO only has a moderate effect. One way to limit this noise is to derive clones from the mixed population in order to be able to identify homozygously edited clones and the precise genetic alteration that occurred.

The benefit of analysing clones was also emphasised by a recently published study, that showed that CRISPR can result in complex gene rearrangements, such as deletions of many kilobases, around the cut site (Kosicki et al., 2018). The authors highlighted the need for a comprehensive analysis of CRISPR edited cells before drawing functional conclusion, let alone administering the edited cells to patients. Such comprehensive analysis would best be achieved by cloning cells, followed by performing long-range PCR or sequencing to identify all genetic changes caused by gene editing (Kosicki et al., 2018).

7.4 The potential to perform large scale screens in primary human T cells

Secretion of lytic granules is a crucial part of the CTL killing response. Degranulation is measured by the exposure of LAMP1 on the extracellular surface of CTL. While degranulation was found to correlate with killing (Betts et al., 2003), it only gives an indirect killing readout. The combined degranulation and killing assay presented in this thesis measures target cell death directly, while still including the LAMP1 readout. This allowed me to directly correlate the target cell lysis and degranulation readouts and gave immediate limited mechanistic insight. The new assay is therefore an improvement over the traditional degranulation assay.

I showed that this assay can be used to detect genetic defects and compounds that reduce degranulation and killing. For example, CRISPR-mediated KO of *Rab27a* (Figure 3.7), *Munc13-4* (Figure 3.9) and parthenolide treatment (Figure 5.7) decreased degranulation and killing. I also showed that the assay can detect genetic defects that cause an increase in degranulation while decreasing CTL killing, such as CRISPR-mediated KO of *Prf1* (Figure 3.8) and *Nfil3* (Figure 4.5). This demonstrated that CTL degranulation does not always

correlate to cytolytic activity. No genetic targets or chemical compounds tested in this thesis increased CTL killing, however, the assay should in theory also be able to detect this phenotype, as long as the percentage of target cells killed throughout the assay duration is kept below 100% in the control samples.

It would be interesting to scale this assay up to a 384 well format, where less cells and reagents would be needed per sample. Fixation could be explored in order to stably maintain the end point of the assay across the plate. Furthermore, the assay could be expanded to include a cytokine readout, enabling comprehensive analysis of CTL function at scale. Such an assay would be useful for large-scale arrayed screening approaches of compounds and genetic targets.

While arrayed screens are potentially powerful, they are limited by the quality of available datasets and the literature to inform the choice of genetic targets. In order to scale up the screen even further it would have to be switched from an arrayed to a pooled format. The pooled format is of particular interest as it would allow a genome-wide screen using a lentiviral sgRNA library. This would provide an unbiased approach and maximise the potential of identifying novel regulators of CTL function.

There are three main challenges that I anticipate for a genome-wide screen in primary hCTL. The first challenge would be to produce primary CTL stably expressing Cas9. As demonstrated in chapter 6, and acknowledged in the literature, stable expression of Cas9 in primary human T cells through lentiviral transduction is inefficient (Seki and Rutz, 2018; Shifrut et al., 2018). A recent study transduced primary human T cells with a genome-wide sgRNA library and subsequently introduced Cas9 protein through nucleofection (Shifrut et al., 2018). This approach, however, is limited by nucleofection efficiency, which may not equal the level of Cas9 expression that would be achieved after stable transduction and selection procedures. Given that I was able to produce up to 17% Cas9-2A-mCherry positive hCTL through transduction (Figure 6.7), I would be keen to repeat these experiments and attempt to clone out individual Cas9-expressing cells.

The second potential hurdle after Cas9 expression will be to select for cells that have incorporated an sgRNA after transduction with the lentiviral library. This is usually achieved through antibiotic selection if the sgRNA library contains an antibiotic resistance cassette. While I had difficulty to select Cas9-expressing cells with blasticidin after transduction with the Cas9-Blast lentivirus in chapter 6, I would expect that the transduction efficiency with

the lentiviral sgRNA library would be higher, as the sgRNA construct is smaller than the Cas9 construct. Higher transduction efficiency would result in better survival upon antibiotic selection.

Thirdly, pooled screens are dependent on an appropriate flow cytometry based assay to sort cells with the phenotype of interest. After sorting, samples are sequenced to identify which sgRNAs were present in the cells with the desired phenotype (Joung et al., 2017). LAMP1 expression in the degranulation assay could be used as the sorting phenotype. Similarly to Shang et al. (2018), who sorted Jurkat cells according to increased or decreased expression of CD69, I could sort cells with low or high LAMP1 signal in response to stimulation. However, in the degranulation assay I often observed a proportion of cells that, despite being stimulated, overlapped with the non-degranulating control in terms of the LAMP1 signal (e.g. see Figure 3.7). These cells likely did not degranulate as they did not encounter a target cell throughout the assay. This indicated that further optimisation of the E:T ratio and assay duration would be necessary to minimise the background noise in the degranulation assay.

Additional technical difficulties can be anticipated. Genome-wide screens require sorting of tens of millions of cells, which takes many hours (Doench, 2017). The effect of this sorting time on cell viability and αLAMP1-PE antibody signal needs to be taken into account. How will cell viability be affected if they are kept at room temperature for a prolonged period of time during sorting? Would the αLAMP1-PE antibody still be bound, and how would its brightness be affected over time? These factors have the potential to create further noise in the degranulation assay. Splitting the assay over several days, as done in chapter 5 for the drug screen, would address some of these concerns.

In addition to the technical difficulties identified, the biological caveat that a killing phenotype does not always overlap with a degranulation phenotype, as outlined in section 7.1, needs to be taken into account. In summary, the degranulation assay would be an immensely interesting readout for a genome-wide screen, but requires careful planning and further optimisation.

7.5 Conclusions

In conclusion, the techniques established and optimised in this thesis will be of value to research into the fundamental biology underlying the CTL killing mechanism. Detailed

analysis of individual gene targets as well as larger screens are possible. Additionally, the combined degranulation and killing assay could potentially be valuable as a diagnostic tool to identify immunodeficiency disorders. Efficient CRISPR-Cas9 gene editing in primary human CTL is furthermore of great interest for medical purposes, including cell-based immunotherapies. While better techniques are required to modify T cells, we also need to improve the understanding of fundamental T cell biology to inform future therapies. The methods developed here can be used to discover, study the mechanism of and validate genetic targets for T cell therapies.

References

Al Hawas, R., Ren, Q., Ye, S., Karim, Z. A., Filipovich, A. H., and Whiteheart, S. W. (2012). Munc18b/STXBP2 is required for platelet secretion. *Blood*, 120(12):2493–500.

Alter, G., Malenfant, J. M., and Altfeld, M. (2004). CD107a as a functional marker for the identification of natural killer cell activity. *Journal of Immunological Methods*, 294(1-2):15–22.

Ammann, S., Schulz, A., Krageloh-Mann, I., Dieckmann, N. M. G., Niethammer, K., Fuchs, S., Eckl, K. M., Plank, R., Werner, R., Altmuller, J., Thiele, H., Nurnberg, P., Bank, J., Strauss, A., von Bernuth, H., zur Stadt, U., Grieve, S., Griffiths, G. M., Lehmberg, K., Hennies, H. C., and Ehl, S. (2016). Mutations in AP3D1 associated with immunodeficiency and seizures define a new type of Hermansky-Pudlak syndrome. *Blood*, 127(8):997–1006.

Anders, S. and Huber, W. (2010). Differential expression analysis for sequence count data. *Genome Biology*, 11(10):R106.

Anders, S., McCarthy, D. J., Chen, Y., Okoniewski, M., Smyth, G. K., Huber, W., and Robinson, M. D. (2013). Count-based differential expression analysis of RNA sequencing data using R and Bioconductor. *Nature Protocols*, 8(9):1765–1786.

Anders, S., Pyl, P. T., and Huber, W. (2015). HTSeq–a Python framework to work with high-throughput sequencing data. *Bioinformatics*, 31(2):166–169.

Arneson, L. N., Brickshawana, A., Segovis, C. M., Schoon, R. A., Dick, C. J., and Leibson, P. J. (2007). Cutting edge: syntaxin 11 regulates lymphocyte-mediated secretion and cytotoxicity. *Journal of immunology (Baltimore, Md. : 1950)*, 179(6):3397–401.

Baetz, K., Isaaz, S., and Griffiths, G. M. (1995). Loss of cytotoxic T lymphocyte function in Chediak-Higashi syndrome arises from a secretory defect that prevents lytic granule exocytosis. *Journal of immunology (Baltimore, Md. : 1950)*, 154(11):6122–31.

Barbosa, M. D. F. S., Nguyen, Q. A., Tchernev, V. T., Ashley, J. A., Detter, J. C., Blaydes, S. M., Brandt, S. J., Chotai, D., Hodgman, C., Solari, R. C. E., Lovett, M., and Kingsmore, S. F. (1996). Identification of the homologous beige and Chediak–Higashi syndrome genes. *Nature*, 382(6588):262.

Basu, R., Whitlock, B. M., Husson, J., Le Floc'h, A., Jin, W., Oyler-Yaniv, A., Dotiwala, F., Giannone, G., Hivroz, C., Biais, N., Lieberman, J., Kam, L. C., and Huse, M. (2016). Cytotoxic T Cells Use Mechanical Force to Potentiate Target Cell Killing. *Cell*, 165(1):100–110.

Best, J. A., Blair, D. A., Knell, J., Yang, E., Mayya, V., Doedens, A., Dustin, M. L., Goldrath, A. W., and Immunological Genome Project Consortium (2013). Transcriptional insights into the CD8+ T cell response to infection and memory T cell formation. *Nature Immunology*, 14(4):404–412.

Betts, M. R., Brenchley, J. M., Price, D. A., De Rosa, S. C., Douek, D. C., Roederer, M., and Koup, R. A. (2003). Sensitive and viable identification of antigen-specific CD8+ T cells by a flow cytometric assay for degranulation. *Journal of immunological methods*, 281(1-2):65–78.

Bin, N.-R., Jung, C. H., Piggott, C., and Sugita, S. (2013). Crucial role of the hydrophobic pocket region of Munc18 protein in mast cell degranulation. *Proceedings of the National Academy of Sciences*, 110(12):4610–4615.

Bossi, G. and Griffiths, G. (1999). Degranulation plays an essential part in regulating cell surface expression of Fas ligand in T cells and natural killer cells. *Nature Medicine*, 5(1):90–96.

Bossi, G. and Griffiths, G. M. (2005). CTL secretory lysosomes: biogenesis and secretion of a harmful organelle. *Seminars in Immunology*, 17(1):87–94.

Boswell, K. L., James, D. J., Esquibel, J. M., Bruinsma, S., Shirakawa, R., Horiuchi, H., and Martin, T. F. J. (2012). Munc13-4 reconstitutes calcium-dependent SNARE-mediated membrane fusion. *The Journal of cell biology*, 197(2):301–12.

Bots, M. and Medema, J. P. (2006). Granzymes at a glance. *Journal of Cell Science*, 119(24):5011–5014.

Bouabe, H. and Okkenhaug, K. (2013). Gene Targeting in Mice: A Review. In *Methods in molecular biology (Clifton, N.J.)*, volume 1064, pages 315–336.

Brownlie, R. J. and Zamoyska, R. (2013). T cell receptor signalling networks: branched, diversified and bounded. *Nature Reviews Immunology*, 13(4):257–269.

Brunner, K. T., Mauel, J., Cerottini, J. C., and Chapuis, B. (1968). Quantitative assay of the lytic action of immune lymphoid cells on 51-Cr-labelled allogeneic target cells in vitro; inhibition by isoantibody and by drugs. *Immunology*, 14(2):181–96.

Bryceson, Y. T., Pende, D., Maul-Pavicic, A., Gilmour, K. C., Ufheil, H., Vraetz, T., Chiang, S. C., Marcenaro, S., Meazza, R., Bondzio, I., Walshe, D., Janka, G., Lehmberg, K., Beutel, K., zur Stadt, U., Binder, N., Arico, M., Moretta, L., Henter, J.-I., and Ehl, S. (2012). A prospective evaluation of degranulation assays in the rapid diagnosis of familial hemophagocytic syndromes. *Blood*, 119(12):2754–2763.

Bryceson, Y. T., Rudd, E., Zheng, C., Edner, J., Ma, D., Wood, S. M., Bechensteen, A. G., Boelens, J. J., Celkan, T., Farah, R. A., Hultenby, K., Winiarski, J., Roche, P. A., Nordenskjold, M., Henter, J.-I., Long, E. O., and Ljunggren, H.-G. (2007). Defective cytotoxic lymphocyte degranulation in syntaxin-11-deficient familial hemophagocytic lymphohistiocytosis 4 (FHL4) patients. *Blood*, 110(6):1906–1915.

Cantrell, D. (2015). Signaling in Lymphocyte Activation. *Cold Spring Harbor Perspectives in Biology*, 7(6):a018788.

Carisey, A. F., Mace, E. M., Saeed, M. B., Davis, D. M., and Orange, J. S. (2018). Nanoscale Dynamism of Actin Enables Secretory Function in Cytolytic Cells. *Current Biology*, 28(4):489–502.e9.

Carr, C. M. and Rizo, J. (2010). At the junction of SNARE and SM protein function. *Current Opinion in Cell Biology*, 22(4):488–495.

Cetica, V., Hackmann, Y., Grieve, S., Sieni, E., Ciambotti, B., Coniglio, M. L., Pende, D., Gilmour, K., Romagnoli, P., Griffiths, G. M., and Aricò, M. (2015). Patients with Griscelli syndrome and normal pigmentation identify RAB27A mutations that selectively disrupt MUNC13-4 binding. *The Journal of allergy and clinical immunology*, 135(5):1310–8.e1.

Cetica, V., Santoro, A., Gilmour, K. C., Sieni, E., Beutel, K., Pende, D., Marcenaro, S., Koch, F., Grieve, S., Wheeler, R., Zhao, F., zur Stadt, U., Griffiths, G. M., and Arico, M. (2010). STXBP2 mutations in children with familial haemophagocytic lymphohistiocytosis type 5. *Journal of Medical Genetics*, 47(9):595–600.

Cheng, J. and Haas, M. (1990). Frequent mutations in the p53 tumor suppressor gene in human leukemia T-cell lines. *Molecular and cellular biology*, 10(10):5502–9.

Chiang, S. C. C., Theorell, J., Entesarian, M., Meeths, M., Mastafa, M., Al-Herz, W., Frisk, P., Gilmour, K. C., Ifversen, M., Langenskiold, C., Machaczka, M., Naqvi, A., Payne, J., Perez-Martinez, A., Sabel, M., Unal, E., Unal, S., Winiarski, J., Nordenskjold, M., Ljunggren, H.-G., Henter, J.-I., and Bryceson, Y. T. (2013). Comparison of primary human cytotoxic T-cell and natural killer cell responses reveal similar molecular requirements for lytic granule exocytosis but differences in cytokine production. *Blood*, 121(8):1345–1356.

Chicaybam, L., Sodre, A. L., Curzio, B. A., and Bonamino, M. H. (2013). An Efficient Low Cost Method for Gene Transfer to T Lymphocytes. *PLoS ONE*, 8(3):e60298.

Cho, S. W., Kim, S., Kim, J. M., and Kim, J.-S. (2013). Targeted genome engineering in human cells with the Cas9 RNA-guided endonuclease. *Nature Biotechnology*, 31(3):230–232.

Chu, V. T., Graf, R., Wirtz, T., Weber, T., Favret, J., Li, X., Petsch, K., Tran, N. T., Sieweke, M. H., Berek, C., Kühn, R., and Rajewsky, K. (2016a). Efficient CRISPR-mediated mutagenesis in primary immune cells using CrispRGold and a C57BL/6 Cas9 transgenic mouse line. *Proceedings of the National Academy of Sciences*, 113(44):12514–12519.

Chu, V. T., Weber, T., Graf, R., Sommermann, T., Petsch, K., Sack, U., Volchkov, P., Rajewsky, K., and Kühn, R. (2016b). Efficient generation of Rosa26 knock-in mice using CRISPR/Cas9 in C57BL/6 zygotes. *BMC Biotechnology*, 16(1):4.

Clark, R. and Griffiths, G. M. (2003). Lytic granules, secretory lysosomes and disease. *Current Opinion in Immunology*, 15(5):516–521.

Clark, R. H., Stinchcombe, J. C., Day, A., Blott, E., Booth, S., Bossi, G., Hamblin, T., Davies, E. G., and Griffiths, G. M. (2003). Adaptor protein 3–dependent microtubule-mediated movement of lytic granules to the immunological synapse. *Nature Immunology*, 4(11):1111–1120.

Cong, L., Ran, F. A., Cox, D., Lin, S., Barretto, R., Habib, N., Hsu, P. D., Wu, X., Jiang, W., Marraffini, L. A., and Zhang, F. (2013). Multiplex Genome Engineering Using CRISPR/Cas Systems. *Science*, 339(6121):819–823.

Cooper, M. D. and Herrin, B. R. (2010). How did our complex immune system evolve? *Nature Reviews Immunology*, 10(1):2–3.

Cornetta, K. and Anderson, W. F. (1989). Protamine sulfate as an effective alternative to polybrene in retroviral-mediated gene-transfer: implications for human gene therapy. *Journal of virological methods*, 23(2):187–94.

Cornu, T. I., Mussolino, C., and Cathomen, T. (2017). Refining strategies to translate genome editing to the clinic. *Nature Medicine*, 23(4):415–423.

Corrigan-Curay, J., Kiem, H.-P., Baltimore, D., O'Reilly, M., Brentjens, R. J., Cooper, L., Forman, S., Gottschalk, S., Greenberg, P., Junghans, R., Heslop, H., Jensen, M., Mackall, C., June, C., Press, O., Powell, D., Ribas, A., Rosenberg, S., Sadelain, M., Till, B., Patterson, A. P., Jambou, R. C., Rosenthal, E., Gargiulo, L., Montgomery, M., and Kohn, D. B. (2014). T-Cell Immunotherapy: Looking Forward. *Molecular Therapy*, 22(9):1564–1574.

Côte, M., Ménager, M. M., Burgess, A., Mahlaoui, N., Picard, C., Schaffner, C., Al-Manjomi, F., Al-Harbi, M., Alangari, A., Le Deist, F., Gennery, A. R., Prince, N., Cariou, A., Nitschke, P., Blank, U., El-Ghazali, G., Ménasché, G., Latour, S., Fischer, A., and de Saint Basile, G. (2009). Munc18-2 deficiency causes familial hemophagocytic lymphohistiocytosis type 5 and impairs cytotoxic granule exocytosis in patient NK cells. *Journal of Clinical Investigation*, 119(12):3765–3773.

Coulie, P. G., Van den Eynde, B. J., van der Bruggen, P., and Boon, T. (2014). Tumour antigens recognized by T lymphocytes: at the core of cancer immunotherapy. *Nature Reviews Cancer*, 14(2):135–146.

Crozat, K., Hoebe, K., Ugolini, S., Hong, N. A., Janssen, E., Rutschmann, S., Mudd, S., Sovath, S., Vivier, E., and Beutler, B. (2007). Jinx, an MCMV susceptibility phenotype caused by disruption of Unc13d: a mouse model of type 3 familial hemophagocytic lymphohistiocytosis. *The Journal of experimental medicine*, 204(4):853–63.

D'Andrea, D., Grassi, L., Mazzapioda, M., and Tramontano, A. (2013). FIDEA: a server for the functional interpretation of differential expression analysis. *Nucleic acids research*, 41(Web Server issue):W84–8.

Das, V., Nal, B., Dujeancourt, A., Thoulouze, M.-I., Galli, T., Roux, P., Dautry-Varsat, A., and Alcover, A. (2004). Activation-induced polarized recycling targets T cell antigen receptors to the immunological synapse; involvement of SNARE complexes. *Immunity*, 20(5):577–88.

de la Roche, M., Asano, Y., and Griffiths, G. M. (2016). Origins of the cytolytic synapse. *Nature Reviews Immunology*, 16(7):421–432.

de Saint Basile, G., Ménasché, G., and Fischer, A. (2010). Molecular mechanisms of biogenesis and exocytosis of cytotoxic granules. *Nature Reviews Immunology*, 10(8):568–579.

Dell'Angelica, E. C., Shotelersuk, V., Aguilar, R. C., Gahl, W. A., and Bonifacino, J. S. (1999). Altered trafficking of lysosomal proteins in Hermansky-Pudlak syndrome due to mutations in the beta 3A subunit of the AP-3 adaptor. *Molecular cell*, 3(1):11–21.

Delville, M., Soheili, T., Bellier, F., Durand, A., Denis, A., Lagresle-Peyrou, C., Cavazzana, M., Andre-Schmutz, I., and Six, E. (2018). A Nontoxic Transduction Enhancer Enables Highly Efficient Lentiviral Transduction of Primary Murine T Cells and Hematopoietic Stem Cells. *Molecular therapy. Methods & clinical development*, 10:341–347.

Demaison, C., Parsley, K., Brouns, G., Scherr, M., Battmer, K., Kinnon, C., Grez, M., and Thrasher, A. J. (2002). High-Level Transduction and Gene Expression in Hematopoietic Repopulating Cells Using a Human Imunodeficiency Virus Type 1-Based Lentiviral Vector Containing an Internal Spleen Focus Forming Virus Promoter. *Human Gene Therapy*, 13(7):803–813.

Dieckmann, N. M. G., Frazer, G. L., Asano, Y., Stinchcombe, J. C., and Griffiths, G. M. (2016). The cytotoxic T lymphocyte immune synapse at a glance. *Journal of Cell Science*, 129(15):2881–2886.

Dobin, A., Davis, C. A., Schlesinger, F., Drenkow, J., Zaleski, C., Jha, S., Batut, P., Chaisson, M., and Gingeras, T. R. (2013). STAR: ultrafast universal RNA-seq aligner. *Bioinformatics*, 29(1):15–21.

Doedens, A. L., Phan, A. T., Stradner, M. H., Fujimoto, J. K., Nguyen, J. V., Yang, E., Johnson, R. S., and Goldrath, A. W. (2013). Hypoxia-inducible factors enhance the effector responses of CD8+ T cells to persistent antigen. *Nature Immunology*, 14(11):1173–1182.

Doench, J. G. (2017). Am I ready for CRISPR? A user's guide to genetic screens. *Nature Reviews Genetics*, 19(2):67–80.

Doench, J. G., Hartenian, E., Graham, D. B., Tothova, Z., Hegde, M., Smith, I., Sullender, M., Ebert, B. L., Xavier, R. J., and Root, D. E. (2014). Rational design of highly active sgRNAs for CRISPR-Cas9–mediated gene inactivation. *Nature Biotechnology*, 32(12):1262–1267.

D'Orlando, O., Zhao, F., Kasper, B., Orinska, Z., Müller, J., Hermans-Borgmeyer, I., Griffiths, G. M., Zur Stadt, U., and Bulfone-Paus, S. (2013). Syntaxin 11 is required for NK and CD8+ T-cell cytotoxicity and neutrophil degranulation. *European Journal of Immunology*, 43(1):194–208.

Dorsett, Y. and Tuschl, T. (2004). siRNAs: applications in functional genomics and potential as therapeutics. *Nature Reviews Drug Discovery*, 3(4):318–329.

Doudna, J. A. and Charpentier, E. (2014). The new frontier of genome engineering with CRISPR-Cas9. *Science*, 346(6213):1258096–1258096.

Doyle, A., McGarry, M. P., Lee, N. A., and Lee, J. J. (2012). The construction of transgenic and gene knockout/knockin mouse models of human disease. *Transgenic research*, 21(2):327–49.

Durchfort, N., Verhoef, S., Vaughn, M. B., Shrestha, R., Adam, D., Kaplan, J., and Ward, D. M. (2012). The Enlarged Lysosomes in beigej Cells Result From Decreased Lysosome Fission and Not Increased Lysosome Fusion. *Traffic*, 13(1):108–119.

Ebert, O., Finke, S., Salahi, A., Herrmann, M., Trojaneck, B., Lefterova, P., Wagner, E., Kircheis, R., Huhn, D., Schriever, F., and Schmidt-Wolf, I. (1997). Lymphocyte apoptosis: induction by gene transfer techniques. *Gene Therapy*, 4(4):296–302.

Elstak, E. D., Neeft, M., Nehme, N. T., Voortman, J., Cheung, M., Goodarzifard, M., Gerritsen, H. C., van Bergen en Henegouwen, P. M. P., Callebaut, I., de Saint Basile, G., and van der Sluijs, P. (2011). The munc13-4-rab27 complex is specifically required for tethering secretory lysosomes at the plasma membrane. *Blood*, 118(6):1570–1578.

Feldmann, J., Callebaut, I., Raposo, G., Certain, S., Bacq, D., Dumont, C., Lambert, N., Ouachée-Chardin, M., Chedeville, G., Tamary, H., Minard-Colin, V., Vilmer, E., Blanche, S., Le Deist, F., Fischer, A., and de Saint Basile, G. (2003). Munc13-4 is essential for cytolytic granules fusion and is mutated in a form of familial hemophagocytic lymphohistiocytosis (FHL3). *Cell*, 115(4):461–73.

Fesnak, A. D., June, C. H., and Levine, B. L. (2016). Engineered T cells: the promise and challenges of cancer immunotherapy. *Nature Reviews Cancer*, 16(9):566–581.

Finlay, D. K., Rosenzweig, E., Sinclair, L. V., Feijoo-Carnero, C., Hukelmann, J. L., Rolf, J., Panteleyev, A. A., Okkenhaug, K., and Cantrell, D. A. (2012). PDK1 regulation of mTOR and hypoxia-inducible factor 1 integrate metabolism and migration of CD8+ T cells. *The Journal of experimental medicine*, 209(13):2441–53.

Fox, C. J., Hammerman, P. S., and Thompson, C. B. (2005). Fuel feeds function: energy metabolism and the T-cell response. *Nature Reviews Immunology*, 5(11):844–852.

Fukuda, M. (2013). Rab27 Effectors, Pleiotropic Regulators in Secretory Pathways. *Traffic*, 14(9):949–963.

Fukuda, M., Kuroda, T. S., and Mikoshiba, K. (2002). Slac2-a/Melanophilin, the Missing Link between Rab27 and Myosin Va. *Journal of Biological Chemistry*, 277(14):12432–12436.

Garber, M., Grabherr, M. G., Guttman, M., and Trapnell, C. (2011). Computational methods for transcriptome annotation and quantification using RNA-seq. *Nature Methods*, 8(6):469–477.

Garcia-Pineres, A. J., Castro, V., Mora, G., Schmidt, T. J., Strunck, E., Pahl, H. L., and Merfort, I. (2001). Cysteine 38 in p65/NF-κB Plays a Crucial Role in DNA Binding Inhibition by Sesquiterpene Lactones. *Journal of Biological Chemistry*, 276(43):39713–39720.

Gascoyne, D. M., Long, E., Veiga-Fernandes, H., de Boer, J., Williams, O., Seddon, B., Coles, M., Kioussis, D., and Brady, H. J. M. (2009). The basic leucine zipper transcription factor E4BP4 is essential for natural killer cell development. *Nature Immunology*, 10(10):1118–1124.

Gawden-Bone, C. M., Frazer, G. L., Richard, A. C., Ma, C. Y., Strege, K., and Griffiths, G. M. (2018). PIP5 Kinases Regulate Membrane Phosphoinositide and Actin Composition for Targeted Granule Secretion by Cytotoxic Lymphocytes. *Immunity*, 49(3):427–437.e4.

Gene Ontology Consortium, Blake, J. A., Dolan, M., Drabkin, H., Hill, D. P., Li, N., Sitnikov, D., Bridges, S., Burgess, S., Buza, T., McCarthy, F., Peddinti, D., Pillai, L., Carbon, S., Dietze, H., Ireland, A., Lewis, S. E., Mungall, C. J., Gaudet, P., Chrisholm, R. L., Fey, P., Kibbe, W. A., Basu, S., Siegele, D. A., McIntosh, B. K., Renfro, D. P., Zweifel, A. E., Hu, J. C., Brown, N. H., Tweedie, S., Alam-Faruque, Y., Apweiler, R., Auchinchloss, A., Axelsen, K., Bely, B., Blatter, M. C., Bonilla, C., Bouguerleret, L., Boutet, E., Breuza, L., Bridge, A., Chan, W. M., Chavali, G., Coudert, E., Dimmer, E., Estreicher, A., Famiglietti, L., Feuermann, M., Gos, A., Gruaz-Gumowski, N., Hieta, R., Hinz, C., Hulo, C., Huntley, R., James, J., Jungo, F., Keller, G., Laiho, K., Legge, D., Lemercier, P., Lieberherr, D., Magrane, M., Martin, M. J., Masson, P., Mutowo-Muellenet, P., O'Donovan, C., Pedruzzi, I., Pichler, K., Poggioli, D., Porras Millán, P., Poux, S., Rivoire, C., Roechert, B., Sawford, T., Schneider, M., Stutz, A., Sundaram, S., Tognolli, M., Xenarios, I., Foulgar, R., Lomax, J., Roncaglia, P., Khodiyar, V. K., Lovering, R. C., Talmud, P. J., Chibucos, M., Giglio, M. G., Chang, H. Y., Hunter, S., McAnulla, C., Mitchell, A., Sangrador, A., Stephan, R., Harris, M. A., Oliver, S. G., Rutherford, K., Wood, V., Bahler, J., Lock, A., Kersey, P. J., McDowall, D. M., Staines, D. M., Dwinell, M., Shimoyama, M., Lauledkind, S., Hayman, T., Wang, S. J., Petri, V., Lowry, T., D'Eustachio, P., Matthews, L., Balakrishnan, R., Binkley, G., Cherry, J. M., Costanzo, M. C., Dwight, S. S., Engel, S. R., Fisk, D. G., Hitz, B. C., Hong, E. L., Karra, K., Miyasato, S. R., Nash, R. S., Park, J., Skrzypek, M. S., Weng, S., Wong, E. D., Berardini, T. Z., Huala, E., Mi, H., Thomas, P. D., Chan, J., Kishore, R., Sternberg, P., Van Auken, K., Howe, D., and Westerfield, M. (2012). Gene Ontology Annotations and Resources. *Nucleic Acids Research*, 41(D1):D530–D535.

Gene Ontology Consortium, T. G. O. (2012). The Gene Ontology: enhancements for 2011. *Nucleic acids research*, 40(Database issue):D559–64.

Ghantous, A., Sinjab, A., Herceg, Z., and Darwiche, N. (2013). Parthenolide: from plant shoots to cancer roots. *Drug Discovery Today*, 18(17-18):894–905.

Gomes-Silva, D., Srinivasan, M., Sharma, S., Lee, C. M., Wagner, D. L., Davis, T. H., Rouce, R. H., Bao, G., Brenner, M. K., and Mamonkin, M. (2017). CD7-edited T cells expressing a CD7-specific CAR for the therapy of T-cell malignancies. *Blood*, 130(3):285–296.

Gopal, Y. V., Arora, T. S., and Van Dyke, M. W. (2007). Parthenolide Specifically Depletes Histone Deacetylase 1 Protein and Induces Cell Death through Ataxia Telangiectasia Mutated. *Chemistry & Biology*, 14(7):813–823.

Grakoui, A., Bromley, S. K., Sumen, C., Davis, M. M., Shaw, A. S., Allen, P. M., and Dustin, M. L. (1999). The immunological synapse: a molecular machine controlling T cell activation. *Science (New York, N.Y.)*, 285(5425):221–7.

Griffin, G. E., Liu, Y., Li, C., Jin, W., Shattock, R. J., Wang, P., Wu, B., Guan, X., Hu, B., Du, T., and Hu, Q. (2015). Inhibition of HIV-1 infection of primary CD4+ T-cells by gene editing of CCR5 using adenovirus-delivered CRISPR/Cas9. *Journal of General Virology*, 96(8):2381–2393.

Griscelli, C., Durandy, A., Guy-Grand, D., Daguillard, F., Herzog, C., and Prunieras, M. (1978). A syndrome associating partial albinism and immunodeficiency. *The American journal of medicine*, 65(4):691–702.

Gundry, M., Brunetti, L., Lin, A., Mayle, A., Kitano, A., Wagner, D., Hsu, J., Hoegenauer, K., Rooney, C., Goodell, M., and Nakada, D. (2016). Highly Efficient Genome Editing of Murine and Human Hematopoietic Progenitor Cells by CRISPR/Cas9. *Cell Reports*, 17(5):1453–1461.

Hackett, P. B., Largaespada, D. A., and Cooper, L. J. N. (2010). A transposon and transposase system for human application. *Molecular therapy : the journal of the American Society of Gene Therapy*, 18(4):674–83.

Hackmann, Y., Graham, S. C., Ehl, S., Honing, S., Lehmberg, K., Arico, M., Owen, D. J., and Griffiths, G. M. (2013). Syntaxin binding mechanism and disease-causing mutations in Munc18-2. *Proceedings of the National Academy of Sciences*, 110(47):E4482–E4491.

Haeryfar, S. M. M. and Hoskin, D. W. (2004). Thy-1: more than a mouse pan-T cell marker. *Journal of immunology (Baltimore, Md. : 1950)*, 173(6):3581–8.

Hanson, D. A., Kaspar, A. A., Poulain, F. R., and Krensky, A. M. (1999). Biosynthesis of granulysin, a novel cytolytic molecule. *Molecular immunology*, 36(7):413–22.

Harty, J. T. and Badovinac, V. P. (2008). Shaping and reshaping CD8+ T-cell memory. *Nature Reviews Immunology*, 8(2):107–119.

He, S. and Wang, X. (2018). RIP kinases as modulators of inflammation and immunity. *Nature Immunology*, 19(9):912–922.

Hehner, S. P., Hofmann, T. G., Dröge, W., and Schmitz, M. L. (1999). The antiinflammatory sesquiterpene lactone parthenolide inhibits NF-kappa B by targeting the I kappa B kinase complex. *Journal of immunology (Baltimore, Md. : 1950)*, 163(10):5617–23.

Hendel, A., Bak, R. O., Clark, J. T., Kennedy, A. B., Ryan, D. E., Roy, S., Steinfeld, I., Lunstad, B. D., Kaiser, R. J., Wilkens, A. B., Bacchetta, R., Tsalenko, A., Dellinger, D., Bruhn, L., and Porteus, M. H. (2015). Chemically modified guide RNAs enhance CRISPR-Cas genome editing in human primary cells. *Nature Biotechnology*, 33(9):985–989.

Henriksson, J., Chen, X., Gomes, T., Ullah, U., Meyer, K. B., Miragaia, R., Duddy, G., Pramanik, J., Yusa, K., Lahesmaa, R., and Teichmann, S. A. (2019). Genome-wide CRISPR Screens in T Helper Cells Reveal Pervasive Crosstalk between Activation and Differentiation. *Cell*, 176(4):882–896.e18.

Henter, J.-I., Horne, A., Aricó, M., Egeler, R. M., Filipovich, A. H., Imashuku, S., Ladisch, S., McClain, K., Webb, D., Winiarski, J., and Janka, G. (2007). HLH-2004: Diagnostic and therapeutic guidelines for hemophagocytic lymphohistiocytosis. *Pediatric Blood & Cancer*, 48(2):124–131.

Hermansky, F. and Pudlak, P. (1959). Albinism associated with hemorrhagic diathesis and unusual pigmented reticular cells in the bone marrow: report of two cases with histochemical studies. *Blood*, 14(2):162–9.

Heusel, J. W., Wesselschmidt, R. L., Shresta, S., Russell, J. H., and Ley, T. J. (1994). Cytotoxic lymphocytes require granzyme B for the rapid induction of DNA fragmentation and apoptosis in allogeneic target cells. *Cell*, 76(6):977–987.

Hodi, F. S., O'Day, S. J., McDermott, D. F., Weber, R. W., Sosman, J. A., Haanen, J. B., Gonzalez, R., Robert, C., Schadendorf, D., Hassel, J. C., Akerley, W., van den Eertwegh, A. J., Lutzky, J., Lorigan, P., Vaubel, J. M., Linette, G. P., Hogg, D., Ottensmeier, C. H., Lebbé, C., Peschel, C., Quirt, I., Clark, J. I., Wolchok, J. D., Weber, J. S., Tian, J., Yellin, M. J., Nichol, G. M., Hoos, A., and Urba, W. J. (2010). Improved Survival with Ipilimumab in Patients with Metastatic Melanoma. *New England Journal of Medicine*, 363(8):711–723.

Höfig, I., Atkinson, M. J., Mall, S., Krackhardt, A. M., Thirion, C., and Anastasov, N. (2012). Poloxamer synperonic F108 improves cellular transduction with lentiviral vectors. *The Journal of Gene Medicine*, 14(8):549–560.

Hogan, P. G., Chen, L., Nardone, J., and Rao, A. (2003). Transcriptional regulation by calcium, calcineurin, and NFAT. *Genes & Development*, 17(18):2205–2232.

Hogquist, K. A., Jameson, S. C., Heath, W. R., Howard, J. L., Bevan, M. J., and Carbone, F. R. (1994). T cell receptor antagonist peptides induce positive selection. *Cell*, 76(1):17–27.

Holt, O., Kanno, E., Bossi, G., Booth, S., Daniele, T., Santoro, A., Arico, M., Saegusa, C., Fukuda, M., and Griffiths, G. M. (2008). Slp1 and Slp2-a Localize to the Plasma Membrane of CTL and Contribute to Secretion from the Immunological Synapse. *Traffic*, 9(4):446–457.

Hsu, P., Lander, E., and Zhang, F. (2014). Development and Applications of CRISPR-Cas9 for Genome Engineering. *Cell*, 157(6):1262–1278.

Huang, B., Johansen, K. H., and Schwartzberg, P. L. (2019). Efficient CRISPR/Cas9-Mediated Mutagenesis in Primary Murine T Lymphocytes. *Current Protocols in Immunology*, 124(1):e62.

Huang, D. W., Sherman, B. T., and Lempicki, R. A. (2009a). Bioinformatics enrichment tools: paths toward the comprehensive functional analysis of large gene lists. *Nucleic Acids Research*, 37(1):1–13.

Huang, D. W., Sherman, B. T., and Lempicki, R. A. (2009b). Systematic and integrative analysis of large gene lists using DAVID bioinformatics resources. *Nature Protocols*, 4(1):44–57.

Hukelmann, J. L., Anderson, K. E., Sinclair, L. V., Grzes, K. M., Murillo, A. B., Hawkins, P. T., Stephens, L. R., Lamond, A. I., and Cantrell, D. A. (2016). The cytotoxic T cell proteome and its shaping by the kinase mTOR. *Nature Immunology*, 17(1):104–112.

Hultquist, J., Schumann, K., Woo, J., Manganaro, L., McGregor, M., Doudna, J., Simon, V., Krogan, N., and Marson, A. (2016). A Cas9 Ribonucleoprotein Platform for Functional Genetic Studies of HIV-Host Interactions in Primary Human T Cells. *Cell Reports*, 17(5):1438–1452.

Hume, A. N., Collinson, L. M., Hopkins, C. R., Strom, M., Barral, D. C., Bossi, G., Griffiths, G. M., and Seabra, M. C. (2002). The leaden gene product is required with Rab27a to recruit myosin Va to melanosomes in melanocytes. *Traffic (Copenhagen, Denmark)*, 3(3):193–202.

Hume, A. N., Collinson, L. M., Rapak, A., Gomes, A. Q., Hopkins, C. R., and Seabra, M. C. (2001). Rab27a regulates the peripheral distribution of melanosomes in melanocytes. *The Journal of cell biology*, 152(4):795–808.

Isaaz, S., Baetz, K., Olsen, K., Podack, E., and Griffiths, G. M. (1995). Serial killing by cytotoxic T lymphocytes: T cell receptor triggers degranulation, re-filling of the lytic granules and secretion of lytic proteins via a non-granule pathway. *European Journal of Immunology*, 25(4):1071–1079.

James, J. R. and Vale, R. D. (2012). Biophysical mechanism of T-cell receptor triggering in a reconstituted system. *Nature*, 487(7405):64–69.

Janka, G. E. and Lehmberg, K. (2014). Hemophagocytic syndromes — An update. *Blood Reviews*, 28(4):135–142.

Jellison, E. R., Kim, S.-K., and Welsh, R. M. (2005). Cutting edge: MHC class II-restricted killing in vivo during viral infection. *Journal of immunology (Baltimore, Md. : 1950)*, 174(2):614–8.

Jenkins, M. R., Rudd-Schmidt, J. A., Lopez, J. A., Ramsbottom, K. M., Mannering, S. I., Andrews, D. M., Voskoboinik, I., and Trapani, J. A. (2015). Failed CTL/NK cell killing and cytokine hypersecretion are directly linked through prolonged synapse time. *The Journal of experimental medicine*, 212(3):307–17.

Jinek, M., Chylinski, K., Fonfara, I., Hauer, M., Doudna, J. A., and Charpentier, E. (2012). A Programmable Dual-RNA-Guided DNA Endonuclease in Adaptive Bacterial Immunity. *Science*, 337(6096):816–821.

Jinek, M., East, A., Cheng, A., Lin, S., Ma, E., and Doudna, J. (2013). RNA-programmed genome editing in human cells. *eLife*, 2:e00471.

Joung, J., Konermann, S., Gootenberg, J. S., Abudayyeh, O. O., Platt, R. J., Brigham, M. D., Sanjana, N. E., and Zhang, F. (2017). Genome-scale CRISPR-Cas9 knockout and transcriptional activation screening. *Nature Protocols*, 12(4):828–863.

Kabanova, A., Sanseviero, F., Candi, V., Gamberucci, A., Gozzetti, A., Campoccia, G., Bocchia, M., and Baldari, C. (2016). Human Cytotoxic T Lymphocytes Form Dysfunctional Immune Synapses with B Cells Characterized by Non-Polarized Lytic Granule Release. *Cell Reports*, 15(10):2313.

Kägi, D., Ledermann, B., Bürki, K., Seiler, P., Odermatt, B., Olsen, K. J., Podack, E. R., Zinkernagel, R. M., and Hengartner, H. (1994a). Cytotoxicity mediated by T cells and natural killer cells is greatly impaired in perforin-deficient mice. *Nature*, 369(6475):31–37.

Kägi, D., Vignaux, F., Ledermann, B., Bürki, K., Depraetere, V., Nagata, S., Hengartner, H., and Golstein, P. (1994b). Fas and perforin pathways as major mechanisms of T cell-mediated cytotoxicity. *Science (New York, N.Y.)*, 265(5171):528–30.

Kanehisa, M., Goto, S., Sato, Y., Furumichi, M., and Tanabe, M. (2012). KEGG for integration and interpretation of large-scale molecular data sets. *Nucleic Acids Research*, 40(D1):D109–D114.

Killeen, N. (1997). T-cell regulation: Thy-1 - hiding in full view. *Current biology : CB*, 7(12):R774–7.

Kim, J. H., Lee, S.-R., Li, L.-H., Park, H.-J., Park, J.-H., Lee, K. Y., Kim, M.-K., Shin, B. A., and Choi, S.-Y. (2011). High Cleavage Efficiency of a 2A Peptide Derived from Porcine Teschovirus-1 in Human Cell Lines, Zebrafish and Mice. *PLoS ONE*, 6(4):e18556.

Kim, S., Kim, D., Cho, S. W., Kim, J., and Kim, J.-S. (2014). Highly efficient RNA-guided genome editing in human cells via delivery of purified Cas9 ribonucleoproteins. *Genome research*, 24(6):1012–9.

Kim, T. K. and Eberwine, J. H. (2010). Mammalian cell transfection: the present and the future. *Analytical and bioanalytical chemistry*, 397(8):3173–8.

Kogawa, K., Lee, S. M., Villanueva, J., Marmer, D., Sumegi, J., and Filipovich, A. H. (2002). Perforin expression in cytotoxic lymphocytes from patients with hemophagocytic lymphohistiocytosis and their family members. *Blood*, 99(1):61–6.

Komor, A. C., Badran, A. H., and Liu, D. R. (2017). CRISPR-Based Technologies for the Manipulation of Eukaryotic Genomes. *Cell*, 168(1-2):20–36.

Kosicki, M., Tomberg, K., and Bradley, A. (2018). Repair of double-strand breaks induced by CRISPR–Cas9 leads to large deletions and complex rearrangements. *Nature Biotechnology*, 36(8):765.

Krammer, P. H. (2000). CD95's deadly mission in the immune system. *Nature*, 407(6805):789–795.

Krensky, A. M. and Clayberger, C. (2009). Biology and clinical relevance of granulysin. *Tissue antigens*, 73(3):193–8.

Krummel, M. F. and Allison, J. P. (1995). CD28 and CTLA-4 have opposing effects on the response of T cells to stimulation. *The Journal of experimental medicine*, 182(2):459–65.

Kuroda, T. S., Fukuda, M., Ariga, H., and Mikoshiba, K. (2002a). Synaptotagmin-like protein 5: a novel Rab27A effector with C-terminal tandem C2 domains. *Biochemical and Biophysical Research Communications*, 293(3):899–906.

Kuroda, T. S., Fukuda, M., Ariga, H., and Mikoshiba, K. (2002b). The Slp Homology Domain of Synaptotagmin-like Proteins 1–4 and Slac2 Functions as a Novel Rab27A Binding Domain. *Journal of Biological Chemistry*, 277(11):9212–9218.

Kurowska, M., Goudin, N., Nehme, N. T., Court, M., Garin, J., Fischer, A., de Saint Basile, G., and Menasche, G. (2012). Terminal transport of lytic granules to the immune synapse is mediated by the kinesin-1/Slp3/Rab27a complex. *Blood*, 119(17):3879–3889.

Kuta, A. E., Reynolds, C. R., and Henkart, P. A. (1989). Mechanism of lysis by large granular lymphocyte granule cytolysin: generation of a stable cytolysin-RBC intermediate. *Journal of immunology (Baltimore, Md. : 1950)*, 142(12):4378–84.

Kwok, B. H., Koh, B., Ndubuisi, M. I., Elofsson, M., and Crews, C. M. (2001). The anti-inflammatory natural product parthenolide from the medicinal herb Feverfew directly binds to and inhibits IkappaB kinase. *Chemistry & biology*, 8(8):759–66.

Larkin, J., Chiarion-Sileni, V., Gonzalez, R., Grob, J. J., Cowey, C. L., Lao, C. D., Schadendorf, D., Dummer, R., Smylie, M., Rutkowski, P., Ferrucci, P. F., Hill, A., Wagstaff, J., Carlino, M. S., Haanen, J. B., Maio, M., Marquez-Rodas, I., McArthur, G. A., Ascierto, P. A., Long, G. V., Callahan, M. K., Postow, M. A., Grossmann, K., Sznol, M., Dreno, B., Bastholt, L., Yang, A., Rollin, L. M., Horak, C., Hodi, F. S., and Wolchok, J. D. (2015). Combined Nivolumab and Ipilimumab or Monotherapy in Untreated Melanoma. *New England Journal of Medicine*, 373(1):23–34.

Law, R. H. P., Lukoyanova, N., Voskoboinik, I., Caradoc-Davies, T. T., Baran, K., Dunstone, M. A., D'Angelo, M. E., Orlova, E. V., Coulibaly, F., Verschoor, S., Browne, K. A., Ciccone, A., Kuiper, M. J., Bird, P. I., Trapani, J. A., Saibil, H. R., and Whisstock, J. C. (2010). The structural basis for membrane binding and pore formation by lymphocyte perforin. *Nature*, 468(7322):447–451.

Leach, D. R., Krummel, M. F., and Allison, J. P. (1996). Enhancement of antitumor immunity by CTLA-4 blockade. *Science (New York, N.Y.)*, 271(5256):1734–6.

Legut, M., Dolton, G., Mian, A. A., Ottmann, O. G., and Sewell, A. K. (2018). CRISPR-mediated TCR replacement generates superior anticancer transgenic T cells. *Blood*, 131(3):311–322.

Letschka, T., Kollmann, V., Pfeifhofer-Obermair, C., Lutz-Nicoladoni, C., Obermair, G. J., Fresser, F., Leitges, M., Hermann-Kleiter, N., Kaminski, S., and Baier, G. (2008). PKC-selectively controls the adhesion-stimulating molecule Rap1. *Blood*, 112(12):4617–4627.

Li, D., Qiu, Z., Shao, Y., Chen, Y., Guan, Y., Liu, M., Li, Y., Gao, N., Wang, L., Lu, X., Zhao, Y., and Liu, M. (2013). Heritable gene targeting in the mouse and rat using a CRISPR-Cas system. *Nature Biotechnology*, 31(8):681–683.

Liu, H., Sidiropoulos, P., Song, G., Pagliari, L. J., Birrer, M. J., Stein, B., Anrather, J., and Pope, R. M. (2000). TNF-alpha gene expression in macrophages: regulation by NF-kappa B is independent of c-Jun or C/EBP beta. *Journal of immunology (Baltimore, Md. : 1950)*, 164(8):4277–85.

Liu, X., Berry, C. T., Ruthel, G., Madara, J. J., MacGillivray, K., Gray, C. M., Madge, L. A., McCorkell, K. A., Beiting, D. P., Hershberg, U., May, M. J., and Freedman, B. D. (2016). T Cell Receptor-induced Nuclear Factor κB (NF-κB) Signaling and Transcriptional Activation Are Regulated by STIM1- and Orai1-mediated Calcium Entry. *Journal of Biological Chemistry*, 291(16):8440–8452.

Liu, Z., Liu, S., Xie, Z., Pavlovicz, R. E., Wu, J., Chen, P., Aimiuwu, J., Pang, J., Bhasin, D., Neviani, P., Fuchs, J. R., Plass, C., Li, P.-K., Li, C., Huang, T. H.-M., Wu, L.-C., Rush, L., Wang, H., Perrotti, D., Marcucci, G., and Chan, K. K. (2009). Modulation of DNA Methylation by a Sesquiterpene Lactone Parthenolide. *Journal of Pharmacology and Experimental Therapeutics*, 329(2):505–514.

Loo, L. S., Hwang, L.-A., Ong, Y. M., Tay, H. S., Wang, C.-C., and Hong, W. (2009). A role for endobrevin/VAMP8 in CTL lytic granule exocytosis. *European Journal of Immunology*, 39(12):3520–3528.

Lopez, J. A., Jenkins, M. R., Rudd-Schmidt, J. A., Brennan, A. J., Danne, J. C., Mannering, S. I., Trapani, J. A., and Voskoboinik, I. (2013a). Rapid and Unidirectional Perforin Pore Delivery at the Cytotoxic Immune Synapse. *The Journal of Immunology*, 191(5):2328–2334.

Lopez, J. A., Susanto, O., Jenkins, M. R., Lukoyanova, N., Sutton, V. R., Law, R. H. P., Johnston, A., Bird, C. H., Bird, P. I., Whisstock, J. C., Trapani, J. A., Saibil, H. R., and Voskoboinik, I. (2013b). Perforin forms transient pores on the target cell plasma membrane to facilitate rapid access of granzymes during killer cell attack. *Blood*, 121(14):2659–2668.

Love, M. I., Huber, W., and Anders, S. (2014). Moderated estimation of fold change and dispersion for RNA-seq data with DESeq2. *Genome Biology*, 15(12):550.

Lowry, L. E. and Zehring, W. A. (2017). Potentiation of Natural Killer Cells for Cancer Immunotherapy: A Review of Literature. *Frontiers in Immunology*, 8:1061.

Macian, F. (2005). NFAT proteins: key regulators of T-cell development and function. *Nature Reviews Immunology*, 5(6):472–484.

MacIver, N. J., Michalek, R. D., and Rathmell, J. C. (2013). Metabolic Regulation of T Lymphocytes. *Annual Review of Immunology*, 31(1):259–283.

Maher, J., Brentjens, R. J., Gunset, G., Rivière, I., and Sadelain, M. (2002). Human T-lymphocyte cytotoxicity and proliferation directed by a single chimeric TCRζ /CD28 receptor. *Nature Biotechnology*, 20(1):70–75.

Mali, P., Yang, L., Esvelt, K. M., Aach, J., Guell, M., DiCarlo, J. E., Norville, J. E., and Church, G. M. (2013). RNA-guided human genome engineering via Cas9. *Science (New York, N.Y.)*, 339(6121):823–6.

Mandal, A. and Viswanathan, C. (2015). Natural killer cells: In health and disease. *Hematology/Oncology and Stem Cell Therapy*, 8(2):47–55.

Mandal, P., Ferreira, L. M., Collins, R., Meissner, T., Boutwell, C., Friesen, M., Vrbanac, V., Garrison, B., Stortchevoi, A., Bryder, D., Musunuru, K., Brand, H., Tager, A., Allen, T., Talkowski, M., Rossi, D., and Cowan, C. (2014). Efficient Ablation of Genes in Human Hematopoietic Stem and Effector Cells using CRISPR/Cas9. *Cell Stem Cell*, 15(5):643–652.

Marcet-Palacios, M., Odemuyiwa, S. O., Coughlin, J. J., Garofoli, D., Ewen, C., Davidson, C. E., Ghaffari, M., Kane, K. P., Lacy, P., Logan, M. R., Befus, A. D., Bleackley, R. C., and Moqbel, R. (2008). Vesicle-associated membrane protein 7 (VAMP-7) is essential for target cell killing in a natural killer cell line. *Biochemical and Biophysical Research Communications*, 366(3):617–623.

Masson, D. and Tschopp, J. (1987). A family of serine esterases in lytic granules of cytolytic T lymphocytes. *Cell*, 49(5):679–85.

Masson, D., Zamai, M., and Tschopp, J. (1986). Identification of granzyme A isolated from cytotoxic T-lymphocyte-granules as one of the proteases encoded by CTL-specific genes. *FEBS letters*, 208(1):84–8.

Matsumoto, R., Wang, D., Blonska, M., Li, H., Kobayashi, M., Pappu, B., Chen, Y., Wang, D., and Lin, X. (2005). Phosphorylation of CARMA1 Plays a Critical Role in T Cell Receptor-Mediated NF-κB Activation. *Immunity*, 23(6):575–585.

Matti, U., Pattu, V., Halimani, M., Schirra, C., Krause, E., Liu, Y., Weins, L., Fang Chang, H., Guzman, R., Olausson, J., Freichel, M., Schmitz, F., Pasche, M., Becherer, U., Bruns, D., and Rettig, J. (2013). Synaptobrevin2 is the v-SNARE required for cytotoxic T-lymphocyte lytic granule fusion. *Nature Communications*, 4(1):1439.

Maude, S. L., Frey, N., Shaw, P. A., Aplenc, R., Barrett, D. M., Bunin, N. J., Chew, A., Gonzalez, V. E., Zheng, Z., Lacey, S. F., Mahnke, Y. D., Melenhorst, J. J., Rheingold, S. R., Shen, A., Teachey, D. T., Levine, B. L., June, C. H., Porter, D. L., and Grupp, S. A. (2014). Chimeric Antigen Receptor T Cells for Sustained Remissions in Leukemia. *New England Journal of Medicine*, 371(16):1507–1517.

Meister, G. and Tuschl, T. (2004). Mechanisms of gene silencing by double-stranded RNA. *Nature*, 431(7006):343–349.

Ménager, M. M., Ménasché, G., Romao, M., Knapnougel, P., Ho, C.-H., Garfa, M., Raposo, G., Feldmann, J., Fischer, A., and de Saint Basile, G. (2007). Secretory cytotoxic granule maturation and exocytosis require the effector protein hMunc13-4. *Nature Immunology*, 8(3):257–267.

Menasche, G., Feldmann, J., Houdusse, A., Desaymard, C., Fischer, A., Goud, B., and de Saint Basile, G. (2003). Biochemical and functional characterization of Rab27a mutations occurring in Griscelli syndrome patients. *Blood*, 101(7):2736–2742.

Ménasché, G., Ménager, M. M., Lefebvre, J. M., Deutsch, E., Athman, R., Lambert, N., Mahlaoui, N., Court, M., Garin, J., Fischer, A., and de Saint Basile, G. (2008). A newly identified isoform of Slp2a associates with Rab27a in cytotoxic T cells and participates to cytotoxic granule secretion. *Blood*, 112(13):5052–62.

Ménasché, G., Pastural, E., Feldmann, J., Certain, S., Ersoy, F., Dupuis, S., Wulffraat, N., Bianchi, D., Fischer, A., Le Deist, F., and de Saint Basile, G. (2000). Mutations in RAB27A cause Griscelli syndrome associated with haemophagocytic syndrome. *Nature Genetics*, 25(2):173–176.

Mescher, M. F., Curtsinger, J. M., Agarwal, P., Casey, K. A., Gerner, M., Hammerbeck, C. D., Popescu, F., and Xiao, Z. (2006). Signals required for programming effector and memory development by CD8+ T cells. *Immunological Reviews*, 211(1):81–92.

Misura, K. M. S., Scheller, R. H., and Weis, W. I. (2000). Three-dimensional structure of the neuronal-Sec1–syntaxin 1a complex. *Nature*, 404(6776):355–362.

Monks, C. R. F., Freiberg, B. A., Kupfer, H., Sciaky, N., and Kupfer, A. (1998). Three-dimensional segregation of supramolecular activation clusters in T cells. *Nature*, 395(6697):82–86.

Morgan, R. A., Dudley, M. E., Wunderlich, J. R., Hughes, M. S., Yang, J. C., Sherry, R. M., Royal, R. E., Topalian, S. L., Kammula, U. S., Restifo, N. P., Zheng, Z., Nahvi, A., de Vries, C. R., Rogers-Freezer, L. J., Mavroukakis, S. A., and Rosenberg, S. A. (2006). Cancer Regression in Patients After Transfer of Genetically Engineered Lymphocytes. *Science*, 314(5796):126–129.

Munafó, D., Johnson, J., Ellis, B., Rutschmann, S., Beutler, B., and Catz, S. (2007). Rab27a is a key component of the secretory machinery of azurophilic granules in granulocytes. *Biochemical Journal*, 402(2):229–239.

Nagashima, K., Torii, S., Yi, Z., Igarashi, M., Okamoto, K., Takeuchi, T., and Izumi, T. (2002). Melanophilin directly links Rab27a and myosin Va through its distinct coiled-coil regions. *FEBS letters*, 517(1-3):233–8.

Nagle, D. L., Karim, M. A., Woolf, E. A., Holmgren, L., Bork, P., Misumi, D. J., McGrail, S. H., Dussault, B. J., Perou, C. M., Boissy, R. E., Duyk, G. M., Spritz, R. A., and Moore, K. J. (1996). Identification and mutation analysis of the complete gene for Chediak–Higashi syndrome. *Nature Genetics*, 14(3):307–311.

Nakamura, H., Makino, Y., Okamoto, K., Poellinger, L., Ohnuma, K., Morimoto, C., and Tanaka, H. (2005). TCR engagement increases hypoxia-inducible factor-1 alpha protein synthesis via rapamycin-sensitive pathway under hypoxic conditions in human peripheral T cells. *Journal of immunology (Baltimore, Md. : 1950)*, 174(12):7592–9.

Navarro, M. N. and Cantrell, D. A. (2014). Serine-threonine kinases in TCR signaling. *Nature Immunology*, 15(9):808–814.

Neefjes, J., Jongsma, M. L. M., Paul, P., and Bakke, O. (2011). Towards a systems understanding of MHC class I and MHC class II antigen presentation. *Nature Reviews Immunology*, 11(12):823–836.

Neeft, M., Wieffer, M., de Jong, A. S., Negroiu, G., Metz, C. H., van Loon, A., Griffith, J., Krijgsveld, J., Wulffraat, N., Koch, H., Heck, A. J., Brose, N., Kleijmeer, M., and van der Sluijs, P. (2005). Munc13-4 Is an Effector of Rab27a and Controls Secretion of Lysosomes in Hematopoietic Cells. *Molecular Biology of the Cell*, 16(2):731–741.

Ogino, S., Gulley, M. L., den Dunnen, J. T., Wilson, R. B., and Association for Molecular Patholpogy Training and Education Committtee (2007). Standard Mutation Nomenclature in Molecular Diagnostics. *The Journal of Molecular Diagnostics*, 9(1):1–6.

Oh, H. and Ghosh, S. (2013). NF-κB: roles and regulation in different CD4+ T-cell subsets. *Immunological Reviews*, 252(1):41–51.

Ohadi, M., Lalloz, M. R., Sham, P., Zhao, J., Dearlove, A. M., Shiach, C., Kinsey, S., Rhodes, M., and Layton, D. M. (1999). Localization of a Gene for Familial Hemophagocytic Lymphohistiocytosis at Chromosome 9q21.3-22 by Homozygosity Mapping. *The American Journal of Human Genetics*, 64(1):165–171.

Okazaki, T., Chikuma, S., Iwai, Y., Fagarasan, S., and Honjo, T. (2013). A rheostat for immune responses: the unique properties of PD-1 and their advantages for clinical application. *Nature Immunology*, 14(12):1212–1218.

Pahl, H. L. (1999). Activators and target genes of Rel/NF-κB transcription factors. *Oncogene*, 18(49):6853–6866.

Palazon, A., Tyrakis, P. A., Macias, D., Veliça, P., Rundqvist, H., Fitzpatrick, S., Vojnovic, N., Phan, A. T., Loman, N., Hedenfalk, I., Hatschek, T., Lövrot, J., Foukakis, T., Goldrath, A. W., Bergh, J., and Johnson, R. S. (2017). An HIF-1α/VEGF-A Axis in Cytotoxic T Cells Regulates Tumor Progression. *Cancer cell*, 32(5):669–683.e5.

Pan, D., Kobayashi, A., Jiang, P., Ferrari de Andrade, L., Tay, R. E., Luoma, A. M., Tsoucas, D., Qiu, X., Lim, K., Rao, P., Long, H. W., Yuan, G.-C., Doench, J., Brown, M., Liu, X. S., and Wucherpfennig, K. W. (2018). A major chromatin regulator determines resistance of tumor cells to T cell-mediated killing. *Science (New York, N.Y.)*, 359(6377):770–775.

Parish, I. A. and Kaech, S. M. (2009). Diversity in CD8+ T cell differentiation. *Current Opinion in Immunology*, 21(3):291–297.

Park, R. J., Wang, T., Koundakjian, D., Hultquist, J. F., Lamothe-Molina, P., Monel, B., Schumann, K., Yu, H., Krupzcak, K. M., Garcia-Beltran, W., Piechocka-Trocha, A., Krogan, N. J., Marson, A., Sabatini, D. M., Lander, E. S., Hacohen, N., and Walker, B. D. (2017). A genome-wide CRISPR screen identifies a restricted set of HIV host dependency factors. *Nature Genetics*, 49(2):193–203.

Patel, S. J., Sanjana, N. E., Kishton, R. J., Eidizadeh, A., Vodnala, S. K., Cam, M., Gartner, J. J., Jia, L., Steinberg, S. M., Yamamoto, T. N., Merchant, A. S., Mehta, G. U., Chichura, A., Shalem, O., Tran, E., Eil, R., Sukumar, M., Guijarro, E. P., Day, C.-P., Robbins, P., Feldman, S., Merlino, G., Zhang, F., and Restifo, N. P. (2017). Identification of essential genes for cancer immunotherapy. *Nature*, 548(7669):537–542.

Paul, S. and Schaefer, B. C. (2013). A new look at T cell receptor signaling to nuclear factor-κB. *Trends in immunology*, 34(6):269–81.

Peña, S. V., Hanson, D. A., Carr, B. A., Goralski, T. J., and Krensky, A. M. (1997). Processing, subcellular localization, and function of 519 (granulysin), a human late T cell activation molecule with homology to small, lytic, granule proteins. *Journal of immunology (Baltimore, Md. : 1950)*, 158(6):2680–8.

Peña, S. V. and Krensky, A. M. (1997). Granulysin, a new human cytolytic granule-associated protein with possible involvement in cell-mediated cytotoxicity. *Seminars in Immunology*, 9(2):117–125.

Pennock, N. D., White, J. T., Cross, E. W., Cheney, E. E., Tamburini, B. A., and Kedl, R. M. (2013). T cell responses: naïve to memory and everything in between. *Advances in Physiology Education*, 37(4):273–283.

Pereira-Leal, J. B., Hume, A. N., and Seabra, M. C. (2001). Prenylation of Rab GTPases: molecular mechanisms and involvement in genetic disease. *FEBS letters*, 498(2-3):197–200.

Perou, C. M., Moore, K. J., Nagle, D. L., Misumi, D. J., Woolf, E. A., McGrail, S. H., Holmgren, L., Brody, T. H., Dussault, B. J., Monroe, C. A., Duyk, G. M., Pryor, R. J., Li, L., Justice, M. J., and Kaplan, J. (1996). Identification of the murine beige gene by YAC complementation and positional cloning. *Nature Genetics*, 13(3):303–308.

Peters, P. J., Borst, J., Oorschot, V., Fukuda, M., Krähenbühl, O., Tschopp, J., Slot, J. W., and Geuze, H. J. (1991). Cytotoxic T lymphocyte granules are secretory lysosomes, containing both perforin and granzymes. *The Journal of experimental medicine*, 173(5):1099–109.

Platt, R., Chen, S., Zhou, Y., Yim, M., Swiech, L., Kempton, H., Dahlman, J., Parnas, O., Eisenhaure, T., Jovanovic, M., Graham, D., Jhunjhunwala, S., Heidenreich, M., Xavier, R., Langer, R., Anderson, D., Hacohen, N., Regev, A., Feng, G., Sharp, P., and Zhang, F. (2014). CRISPR-Cas9 Knockin Mice for Genome Editing and Cancer Modeling. *Cell*, 159(2):440–455.

Postow, M. A., Chesney, J., Pavlick, A. C., Robert, C., Grossmann, K., McDermott, D., Linette, G. P., Meyer, N., Giguere, J. K., Agarwala, S. S., Shaheen, M., Ernstoff, M. S., Minor, D., Salama, A. K., Taylor, M., Ott, P. A., Rollin, L. M., Horak, C., Gagnier, P., Wolchok, J. D., and Hodi, F. S. (2015). Nivolumab and Ipilimumab versus Ipilimumab in Untreated Melanoma. *New England Journal of Medicine*, 372(21):2006–2017.

Potter, T. A., Grebe, K., Freiberg, B., and Kupfer, A. (2001). Formation of supramolecular activation clusters on fresh ex vivo CD8+ T cells after engagement of the T cell antigen receptor and CD8 by antigen-presenting cells. *Proceedings of the National Academy of Sciences*, 98(22):12624–12629.

Qasim, W., Zhan, H., Samarasinghe, S., Adams, S., Amrolia, P., Stafford, S., Butler, K., Rivat, C., Wright, G., Somana, K., Ghorashian, S., Pinner, D., Ahsan, G., Gilmour, K., Lucchini, G., Inglott, S., Mifsud, W., Chiesa, R., Peggs, K. S., Chan, L., Farzaneh, F., Thrasher, A. J., Vora, A., Pule, M., and Veys, P. (2017). Molecular remission of infant B-ALL after infusion of universal TALEN gene-edited CAR T cells. *Science Translational Medicine*, 9(374):eaaj2013.

Quann, E. J., Merino, E., Furuta, T., and Huse, M. (2009). Localized diacylglycerol drives the polarization of the microtubule-organizing center in T cells. *Nature Immunology*, 10(6):627–635.

Ramezani, A. and Hawley, R. G. (2002). Overview of the HIV-1 Lentiviral Vector System. In *Current Protocols in Molecular Biology*, volume Chapter 16, page Unit 16.21. John Wiley & Sons, Inc., Hoboken, NJ, USA.

Ran, F. A., Hsu, P. D., Wright, J., Agarwala, V., Scott, D. A., and Zhang, F. (2013). Genome engineering using the CRISPR-Cas9 system. *Nature Protocols*, 8(11):2281–2308.

Ren, J., Liu, X., Fang, C., Jiang, S., June, C. H., and Zhao, Y. (2017a). Multiplex Genome Editing to Generate Universal CAR T Cells Resistant to PD1 Inhibition. *Clinical Cancer Research*, 23(9):2255–2266.

Ren, J., Zhang, X., Liu, X., Fang, C., Jiang, S., June, C. H., and Zhao, Y. (2017b). A versatile system for rapid multiplex genome-edited CAR T cell generation. *Oncotarget*, 8(10):17002–17011.

Ricote, M. and Glass, C. K. (2007). PPARs and molecular mechanisms of transrepression. *Biochimica et biophysica acta*, 1771(8):926–35.

Ritter, A. T., Asano, Y., Stinchcombe, J. C., Dieckmann, N. M. G., Chen, B.-C., Gawden-Bone, C., van Engelenburg, S., Legant, W., Gao, L., Davidson, M. W., Betzig, E., Lippincott-Schwartz, J., and Griffiths, G. M. (2015). Actin depletion initiates events leading to granule secretion at the immunological synapse. *Immunity*, 42(5):864–76.

Ritter, A. T., Kapnick, S. M., Murugesan, S., Schwartzberg, P. L., Griffiths, G. M., and Lippincott-Schwartz, J. (2017). Cortical actin recovery at the immunological synapse leads to termination of lytic granule secretion in cytotoxic T lymphocytes. *Proceedings of the National Academy of Sciences*, 114(32):E6585–E6594.

Robert, C., Thomas, L., Bondarenko, I., O'Day, S., Weber, J., Garbe, C., Lebbe, C., Baurain, J.-F., Testori, A., Grob, J.-J., Davidson, N., Richards, J., Maio, M., Hauschild, A., Miller, W. H., Gascon, P., Lotem, M., Harmankaya, K., Ibrahim, R., Francis, S., Chen, T.-T., Humphrey, R., Hoos, A., and Wolchok, J. D. (2011). Ipilimumab plus Dacarbazine for Previously Untreated Metastatic Melanoma. *New England Journal of Medicine*, 364(26):2517–2526.

Rollings, C. M., Sinclair, L. V., Brady, H. J. M., Cantrell, D. A., and Ross, S. H. (2018). Interleukin-2 shapes the cytotoxic T cell proteome and immune environment-sensing programs. *Science signaling*, 11(526):eaap8112.

Rosenberg, S. A., Restifo, N. P., Yang, J. C., Morgan, R. A., and Dudley, M. E. (2008). Adoptive cell transfer: a clinical path to effective cancer immunotherapy. *Nature Reviews Cancer*, 8(4):299–308.

Rosenberg, S. A., Yang, J. C., Sherry, R. M., Kammula, U. S., Hughes, M. S., Phan, G. Q., Citrin, D. E., Restifo, N. P., Robbins, P. F., Wunderlich, J. R., Morton, K. E., Laurencot, C. M., Steinberg, S. M., White, D. E., and Dudley, M. E. (2011). Durable Complete Responses in Heavily Pretreated Patients with Metastatic Melanoma Using T-Cell Transfer Immunotherapy. *Clinical Cancer Research*, 17(13):4550–4557.

Roth, T. L., Puig-Saus, C., Yu, R., Shifrut, E., Carnevale, J., Li, P. J., Hiatt, J., Saco, J., Krystofinski, P., Li, H., Tobin, V., Nguyen, D. N., Lee, M. R., Putnam, A. L., Ferris, A. L., Chen, J. W., Schickel, J.-N., Pellerin, L., Carmody, D., Alkorta-Aranburu, G., del Gaudio, D., Matsumoto, H., Morell, M., Mao, Y., Cho, M., Quadros, R. M., Gurumurthy, C. B., Smith, B., Haugwitz, M., Hughes, S. H., Weissman, J. S., Schumann, K., Esensten, J. H., May, A. P., Ashworth, A., Kupfer, G. M., Greeley, S. A. W., Bacchetta, R., Meffre, E., Roncarolo, M. G., Romberg, N., Herold, K. C., Ribas, A., Leonetti, M. D., and Marson, A. (2018). Reprogramming human T cell function and specificity with non-viral genome targeting. *Nature*, 559(7714):405–409.

Rubio, V., Stuge, T. B., Singh, N., Betts, M. R., Weber, J. S., Roederer, M., and Lee, P. P. (2003). Ex vivo identification, isolation and analysis of tumor-cytolytic T cells. *Nature Medicine*, 9(11):1377–1382.

Rupp, L. J., Schumann, K., Roybal, K. T., Gate, R. E., Ye, C. J., Lim, W. A., and Marson, A. (2017). CRISPR/Cas9-mediated PD-1 disruption enhances anti-tumor efficacy of human chimeric antigen receptor T cells. *Scientific Reports*, 7(1):737.

Ruprecht, C. R., Gattorno, M., Ferlito, F., Gregorio, A., Martini, A., Lanzavecchia, A., and Sallusto, F. (2005). Coexpression of CD25 and CD27 identifies FoxP3+ regulatory T cells in inflamed synovia. *The Journal of Experimental Medicine*, 201(11):1793–1803.

Russell, J. H. and Ley, T. J. (2002). Lymphocyte-mediated cytotoxicity. *Annual Review of Immunology*, 20(1):323–370.

Sadelain, M. (2016). Chimeric antigen receptors: driving immunology towards synthetic biology. *Current Opinion in Immunology*, 41:68–76.

Sadelain, M., Brentjens, R., and Rivière, I. (2013). The Basic Principles of Chimeric Antigen Receptor Design. *Cancer Discovery*, 3(4):388–398.

Sanjana, N. E., Shalem, O., and Zhang, F. (2014). Improved vectors and genome-wide libraries for CRISPR screening. *Nature Methods*, 11(8):783–784.

Schroeder, A., Mueller, O., Stocker, S., Salowsky, R., Leiber, M., Gassmann, M., Lightfoot, S., Menzel, W., Granzow, M., and Ragg, T. (2006). The RIN: an RNA integrity number for assigning integrity values to RNA measurements. *BMC Molecular Biology*, 7(1):3.

Schulze-Luehrmann, J. and Ghosh, S. (2006). Antigen-Receptor Signaling to Nuclear Factor κB. *Immunity*, 25(5):701–715.

Schumann, K., Lin, S., Boyer, E., Simeonov, D. R., Subramaniam, M., Gate, R. E., Haliburton, G. E., Ye, C. J., Bluestone, J. A., Doudna, J. A., and Marson, A. (2015). Generation of knock-in primary human T cells using Cas9 ribonucleoproteins. *Proceedings of the National Academy of Sciences*, 112(33):10437–10442.

Seki, A. and Rutz, S. (2018). Optimized RNP transfection for highly efficient CRISPR/Cas9-mediated gene knockout in primary T cells. *The Journal of Experimental Medicine*, 215(3):985–997.

Shalem, O., Sanjana, N. E., Hartenian, E., Shi, X., Scott, D. A., Mikkelsen, T. S., Heckl, D., Ebert, B. L., Root, D. E., Doench, J. G., and Zhang, F. (2014). Genome-Scale CRISPR-Cas9 Knockout Screening in Human Cells. *Science*, 343(6166):84–87.

Shang, W., Jiang, Y., Boettcher, M., Ding, K., Mollenauer, M., Liu, Z., Wen, X., Liu, C., Hao, P., Zhao, S., McManus, M. T., Wei, L., Weiss, A., and Wang, H. (2018). Genome-wide CRISPR screen identifies FAM49B as a key regulator of actin dynamics and T cell activation. *Proceedings of the National Academy of Sciences*, 115(17):E4051–E4060.

Sharma, P., Hu-Lieskovan, S., Wargo, J. A., and Ribas, A. (2017). Primary, Adaptive, and Acquired Resistance to Cancer Immunotherapy. *Cell*, 168(4):707–723.

Shifrut, E., Carnevale, J., Tobin, V., Roth, T. L., Woo, J. M., Bui, C. T., Li, P. J., Diolaiti, M. E., Ashworth, A., and Marson, A. (2018). Genome-wide CRISPR Screens in Primary Human T Cells Reveal Key Regulators of Immune Function. *Cell*, 175(7):1958–1971.e15.

Shirakawa, R., Higashi, T., Tabuchi, A., Yoshioka, A., Nishioka, H., Fukuda, M., Kita, T., and Horiuchi, H. (2004). Munc13-4 Is a GTP-Rab27-binding Protein Regulating Dense Core Granule Secretion in Platelets. *Journal of Biological Chemistry*, 279(11):10730–10737.

Sinclair, L. V., Rolf, J., Emslie, E., Shi, Y.-B., Taylor, P. M., and Cantrell, D. A. (2013). Control of amino-acid transport by antigen receptors coordinates the metabolic reprogramming essential for T cell differentiation. *Nature Immunology*, 14(5):500–508.

Smith-Garvin, J. E., Koretzky, G. A., and Jordan, M. S. (2009). T Cell Activation. *Annual Review of Immunology*, 27(1):591–619.

Snow, K. and Judd, W. (1987). Heterogeneity of a human T-lymphoblastoid cell line. *Experimental cell research*, 171(2):389–403.

Spessott, W. A., Sanmillan, M. L., McCormick, M. E., Kulkarni, V. V., and Giraudo, C. G. (2017). SM protein Munc18-2 facilitates transition of Syntaxin 11-mediated lipid mixing to complete fusion for T-lymphocyte cytotoxicity. *Proceedings of the National Academy of Sciences*, 114(11):E2176–E2185.

Spessott, W. A., Sanmillan, M. L., McCormick, M. E., Patel, N., Villanueva, J., Zhang, K., Nichols, K. E., and Giraudo, C. G. (2015). Hemophagocytic lymphohistiocytosis caused by dominant-negative mutations in STXBP2 that inhibit SNARE-mediated membrane fusion. *Blood*, 125(10):1566–1577.

Stepp, S. E., Dufourcq-Lagelouse, R., Le Deist, F., Bhawan, S., Certain, S., Mathew, P. A., Henter, J. I., Bennett, M., Fischer, A., de Saint Basile, G., and Kumar, V. (1999). Perforin gene defects in familial hemophagocytic lymphohistiocytosis. *Science (New York, N.Y.)*, 286(5446):1957–9.

Sternberg, S. H., Redding, S., Jinek, M., Greene, E. C., and Doudna, J. A. (2014). DNA interrogation by the CRISPR RNA-guided endonuclease Cas9. *Nature*, 507(7490):62–67.

Stinchcombe, J., Bossi, G., and Griffiths, G. M. (2004). Linking Albinism and Immunity: The Secrets of Secretory Lysosomes. *Science*, 305(5680):55–59.

Stinchcombe, J. C., Barral, D. C., Mules, E. H., Booth, S., Hume, A. N., Machesky, L. M., Seabra, M. C., and Griffiths, G. M. (2001a). Rab27a is required for regulated secretion in cytotoxic T lymphocytes. *The Journal of cell biology*, 152(4):825–34.

Stinchcombe, J. C., Bossi, G., Booth, S., and Griffiths, G. M. (2001b). The immunological synapse of CTL contains a secretory domain and membrane bridges. *Immunity*, 15(5):751–61.

Stinchcombe, J. C. and Griffiths, G. M. (2003). The role of the secretory immunological synapse in killing by CD8+ CTL. *Seminars in Immunology*, 15(6):301–305.

Stinchcombe, J. C. and Griffiths, G. M. (2007). Secretory Mechanisms in Cell-Mediated Cytotoxicity. *Annual Review of Cell and Developmental Biology*, 23(1):495–517.

Stinchcombe, J. C., Majorovits, E., Bossi, G., Fuller, S., and Griffiths, G. M. (2006). Centrosome polarization delivers secretory granules to the immunological synapse. *Nature*, 443(7110):462–465.

Stinchcombe, J. C., Randzavola, L. O., Angus, K. L., Mantell, J. M., Verkade, P., and Griffiths, G. M. (2015). Mother Centriole Distal Appendages Mediate Centrosome Docking at the Immunological Synapse and Reveal Mechanistic Parallels with Ciliogenesis. *Current Biology*, 25(24):3239–3244.

Strasser, A., Jost, P. J., and Nagata, S. (2009). The Many Roles of FAS Receptor Signaling in the Immune System. *Immunity*, 30(2):180–192.

Sucker, A., Zhao, F., Real, B., Heeke, C., Bielefeld, N., Massen, S., Horn, S., Moll, I., Maltaner, R., Horn, P. A., Schilling, B., Sabbatino, F., Lennerz, V., Kloor, M., Ferrone, S., Schadendorf, D., Falk, C. S., Griewank, K., and Paschen, A. (2014). Genetic Evolution of T-cell Resistance in the Course of Melanoma Progression. *Clinical Cancer Research*, 20(24):6593–6604.

Südhof, T. C. and Rothman, J. E. (2009). Membrane fusion: grappling with SNARE and SM proteins. *Science (New York, N.Y.)*, 323(5913):474–7.

Tang, B. L., Low, D. Y., and Hong, W. (1998). Syntaxin 11: A Member of the Syntaxin Family without a Carboxyl Terminal Transmembrane Domain. *Biochemical and Biophysical Research Communications*, 245(2):627–632.

Tanos, B. E., Yang, H.-J., Soni, R., Wang, W.-J., Macaluso, F. P., Asara, J. M., and Tsou, M.-F. B. (2013). Centriole distal appendages promote membrane docking, leading to cilia initiation. *Genes & development*, 27(2):163–8.

Tebas, P., Stein, D., Tang, W. W., Frank, I., Wang, S. Q., Lee, G., Spratt, S. K., Surosky, R. T., Giedlin, M. A., Nichol, G., Holmes, M. C., Gregory, P. D., Ando, D. G., Kalos, M., Collman, R. G., Binder-Scholl, G., Plesa, G., Hwang, W.-T., Levine, B. L., and June, C. H. (2014). Gene Editing of CCR5 in Autologous CD4 T Cells of Persons Infected with HIV. *New England Journal of Medicine*, 370(10):901–910.

Topalian, S., Drake, C., and Pardoll, D. (2015). Immune Checkpoint Blockade: A Common Denominator Approach to Cancer Therapy. *Cancer Cell*, 27(4):450–461.

Topham, N. J. and Hewitt, E. W. (2009). Natural killer cell cytotoxicity: how do they pull the trigger? *Immunology*, 128(1):7–15.

Trapani, J. A. (2001). Granzymes: a family of lymphocyte granule serine proteases. *Genome biology*, 2(12):REVIEWS3014.

Trapani, J. A. and Sutton, V. R. (2003). Granzyme B: pro-apoptotic, antiviral and antitumor functions. *Current opinion in immunology*, 15(5):533–43.

Tschopp, J. and Nabholz, M. (1990). Perforin-Mediated Target Cell Lysis by Cytolytic T Lymphocytes. *Annual Review of Immunology*, 8(1):279–302.

Tzelepis, K., Koike-Yusa, H., De Braekeleer, E., Li, Y., Metzakopian, E., Dovey, O., Mupo, A., Grinkevich, V., Li, M., Mazan, M., Gozdecka, M., Ohnishi, S., Cooper, J., Patel, M., McKerrell, T., Chen, B., Domingues, A., Gallipoli, P., Teichmann, S., Ponstingl, H., McDermott, U., Saez-Rodriguez, J., Huntly, B., Iorio, F., Pina, C., Vassiliou, G., and Yusa, K. (2016). A CRISPR Dropout Screen Identifies Genetic Vulnerabilities and Therapeutic Targets in Acute Myeloid Leukemia. *Cell Reports*, 17(4):1193–1205.

Uellner, R., Zvelebil, M. J., Hopkins, J., Jones, J., MacDougall, L. K., Morgan, B. P., Podack, E., Waterfield, M. D., and Griffiths, G. M. (1997). Perforin is activated by a proteolytic cleavage during biosynthesis which reveals a phospholipid-binding C2 domain. *The EMBO Journal*, 16(24):7287–7296.

Valdez, A. C., Cabaniols, J. P., Brown, M. J., and Roche, P. A. (1999). Syntaxin 11 is associated with SNAP-23 on late endosomes and the trans-Golgi network. *Journal of cell science*, 112 (Pt 6):845–54.

Vallabhapurapu, S. and Karin, M. (2009). Regulation and Function of NF-κB Transcription Factors in the Immune System. *Annual Review of Immunology*, 27(1):693–733.

Walsh, C. M., Matloubian, M., Liu, C. C., Ueda, R., Kurahara, C. G., Christensen, J. L., Huang, M. T., Young, J. D., Ahmed, R., and Clark, W. R. (1994). Immune function in mice lacking the perforin gene. *Proceedings of the National Academy of Sciences of the United States of America*, 91(23):10854–8.

Wang, T., Wei, J. J., Sabatini, D. M., and Lander, E. S. (2014a). Genetic Screens in Human Cells Using the CRISPR-Cas9 System. *Science*, 343(6166):80–84.

Wang, W., Ye, C., Liu, J., Zhang, D., Kimata, J. T., and Zhou, P. (2014b). CCR5 Gene Disruption via Lentiviral Vectors Expressing Cas9 and Single Guided RNA Renders Cells Resistant to HIV-1 Infection. *PLoS ONE*, 9(12):e115987.

Wang, Z., Gerstein, M., and Snyder, M. (2009). RNA-Seq: a revolutionary tool for transcriptomics. *Nature Reviews Genetics*, 10(1):57–63.

Ward, D. M., Griffiths, G. M., Stinchcombe, J. C., and Kaplan, J. (2000). Analysis of the lysosomal storage disease Chediak-Higashi syndrome. *Traffic (Copenhagen, Denmark)*, 1(11):816–22.

Wardyn, J. D., Ponsford, A. H., and Sanderson, C. M. (2015). Dissecting molecular cross-talk between Nrf2 and NF-κB response pathways. *Biochemical Society transactions*, 43(4):621–6.

Wennerberg, K., Rossman, K. L., and Der, C. J. (2005). The Ras superfamily at a glance. *Journal of Cell Science*, 118(5):843–846.

Williams, M. A. and Bevan, M. J. (2007). Effector and Memory CTL Differentiation. *Annual Review of Immunology*, 25(1):171–192.

Wilson, S. M., Yip, R., Swing, D. A., O'Sullivan, T. N., Zhang, Y., Novak, E. K., Swank, R. T., Russell, L. B., Copeland, N. G., and Jenkins, N. A. (2000). A mutation in Rab27a causes the vesicle transport defects observed in ashen mice. *Proceedings of the National Academy of Sciences of the United States of America*, 97(14):7933–8.

Wolchok, J. D., Kluger, H., Callahan, M. K., Postow, M. A., Rizvi, N. A., Lesokhin, A. M., Segal, N. H., Ariyan, C. E., Gordon, R.-A., Reed, K., Burke, M. M., Caldwell, A., Kronenberg, S. A., Agunwamba, B. U., Zhang, X., Lowy, I., Inzunza, H. D., Feely, W., Horak, C. E., Hong, Q., Korman, A. J., Wigginton, J. M., Gupta, A., and Sznol, M. (2013). Nivolumab plus Ipilimumab in Advanced Melanoma. *New England Journal of Medicine*, 369(2):122–133.

Wu, X., Rao, K., Bowers, M. B., Copeland, N. G., Jenkins, N. A., and Hammer, J. A. (2001). Rab27a enables myosin Va-dependent melanosome capture by recruiting the myosin to the organelle. *Journal of cell science*, 114(Pt 6):1091–100.

Wu, X. S., Rao, K., Zhang, H., Wang, F., Sellers, J. R., Matesic, L. E., Copeland, N. G., Jenkins, N. A., and Hammer, J. A. (2002). Identification of an organelle receptor for myosin-Va. *Nature Cell Biology*, 4(4):271–278.

Wucherpfennig, K. W., Gagnon, E., Call, M. J., Huseby, E. S., and Call, M. E. (2010). Structural Biology of the T-cell Receptor: Insights into Receptor Assembly, Ligand Recognition, and Initiation of Signaling. *Cold Spring Harbor Perspectives in Biology*, 2(4):a005140–a005140.

Ye, S., Karim, Z. A., Al Hawas, R., Pessin, J. E., Filipovich, A. H., and Whiteheart, S. W. (2012). Syntaxin-11, but not syntaxin-2 or syntaxin-4, is required for platelet secretion. *Blood*, 120(12):2484–2492.

Young, J. D., Damiano, A., DiNome, M. A., Leong, L. G., and Cohn, Z. A. (1987). Dissociation of membrane binding and lytic activities of the lymphocyte pore-forming protein (perforin). *The Journal of experimental medicine*, 165(5):1371–82.

Yu, H., Rathore, S. S., Lopez, J. A., Davis, E. M., James, D. E., Martin, J. L., and Shen, J. (2013). Comparative studies of Munc18c and Munc18-1 reveal conserved and divergent mechanisms of Sec1/Munc18 proteins. *Proceedings of the National Academy of Sciences*, 110(35):E3271–E3280.

Yu, Z., Chen, Y., Wang, S., Li, P., Zhou, G., and Yuan, Y. (2018). Inhibition of NF-κB results in anti-glioma activity and reduces temozolomide-induced chemoresistance by down-regulating MGMT gene expression. *Cancer Letters*, 428:77–89.

Zhang, N. and Bevan, M. J. (2011). CD8(+) T cells: foot soldiers of the immune system. *Immunity*, 35(2):161–8.

Zou, W., Wolchok, J. D., and Chen, L. (2016). PD-L1 (B7-H1) and PD-1 pathway blockade for cancer therapy: Mechanisms, response biomarkers, and combinations. *Science Translational Medicine*, 8(328):328rv4–328rv4.

zur Stadt, U., Rohr, J., Seifert, W., Koch, F., Grieve, S., Pagel, J., Strauß, J., Kasper, B., Nürnberg, G., Becker, C., Maul-Pavicic, A., Beutel, K., Janka, G., Griffiths, G., Ehl, S., and Hennies, H. C. (2009). Familial Hemophagocytic Lymphohistiocytosis Type 5 (FHL-5) Is Caused by Mutations in Munc18-2 and Impaired Binding to Syntaxin 11. *The American Journal of Human Genetics*, 85(4):482–492.

zur Stadt, U., Schmidt, S., Kasper, B., Beutel, K., Diler, A. S., Henter, J.-I., Kabisch, H., Schneppenheim, R., Nürnberg, P., Janka, G., and Hennies, H. C. (2005). Linkage of familial hemophagocytic lymphohistiocytosis (FHL) type-4 to chromosome 6q24 and identification of mutations in syntaxin 11. *Human Molecular Genetics*, 14(6):827–834.

Appendix A

Plasmid maps

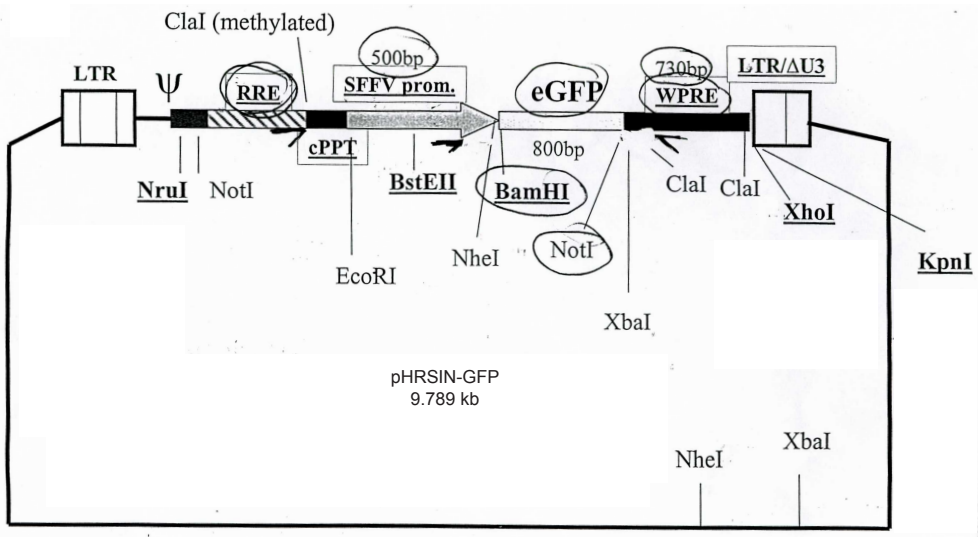

Fig. A.1 ***pHRSIN-GFP plasmid used for lentivirus production.***

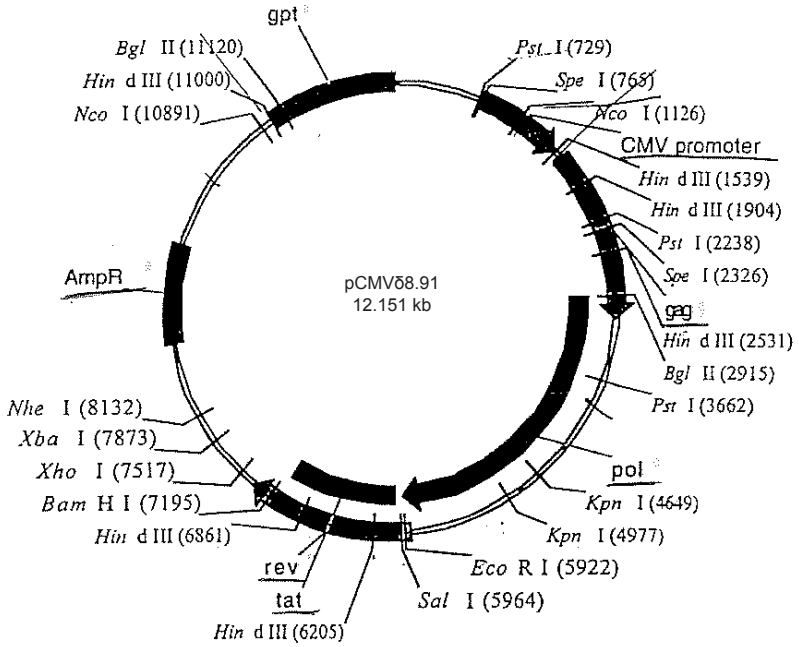

Fig. A.2 ***pCMVδ8.91 packaging plasmid used for lentivirus production.***

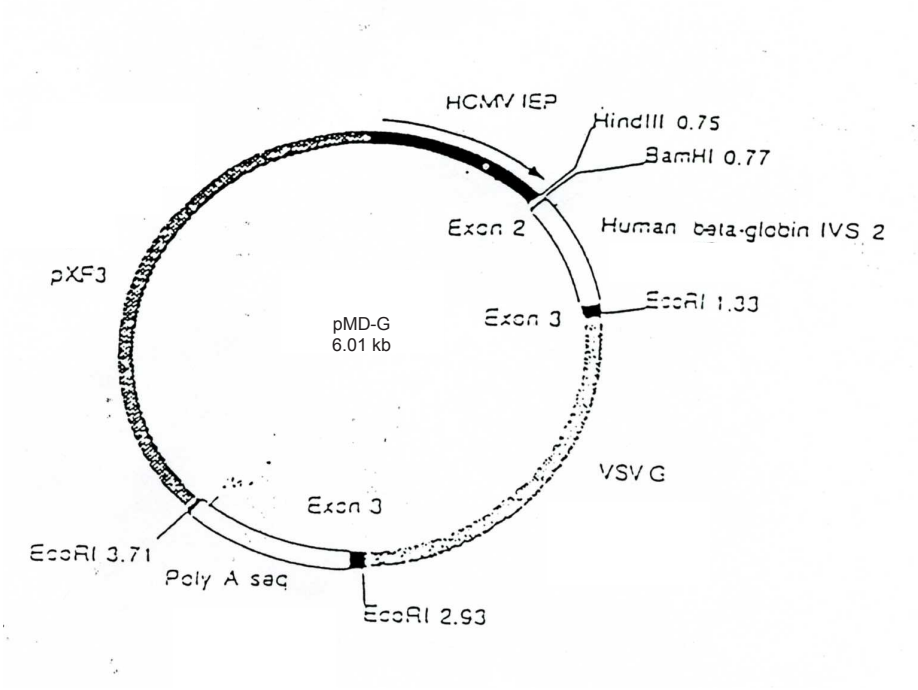

Fig. A.3 ***pMD-G VSV-G envelope plasmid used for lentivirus production.***

Appendix B

Differentially expressed genes in effector and naive CD8 T cells

As outlined in chapter 4, 1803 significantly activated differentially expressed genes with padj<0.01 and log2(fold change)>2 were identified when comparing the transcriptome of effector (day 7 post activation) and naive (day 0) CD8 T cells. The full list of all 1803 genes is included digitally on a CD.

Appendix C

NF-kB signalling compound library toxicity test

Table C.1 ***NF-κB signalling compound library toxicity test.*** *The NF-κB signalling compound library was acquired from MedChem express. Drugs were labelled according to their position in the rack (position 1 - 64). The information given in this table was obtained from Medchem express, except for the highest non-toxic concentrations (HNTC), which were determined using the Celltitre96 AQueous One Solution Cell Proliferation Assay (Promega) as described in chapter 5.*

Drug #	Official name	Molecular target	HNTC
1	Sodium Salicylate	Autophagy, NF-κB	25 μM
2	LY2409881	IKK	25 μM
3	Dimethyl fumarate	Keap1-Nrf2	25 μM
4	Bardoxolone	Keap1-Nrf2	0.9 μM
5	IKK 16	IKK	0.9 μM
6	Pyrrolidinedithiocarbamate (ammonium)	NF-κB	8.3 μM
7	BMS-345541 (free base)	IKK	0.9 μM
8	MRT67307	Autophagy, IKK	0.9 μM
9	Wy-14643	PPAR	25 μM
10	Didox	NF-κB	25 μM
11	Cyclo(his-pro)	NF-κB	25 μM
12	Pioglitazone (hydrochloride)	PPAR	25 μM
13	MLN120B	IKK	8.3 μM
14	MI 2 (MALT1 inhibitor)	MALT1	0.9 μM

Table C.1 continued from previous page

Drug	Official name	Target	HNTC
15	GW1929	PPAR	8.3 μM
16	T0070907	PPAR, RAD51	8.3 μM
17	Adjudin	NF-κB	25 μM
18	L-165041	PPAR	25 μM
19	Parthenolide	Autophagy, DNA Methyltransferase HDAC, NF-κB	8.3 μM
20	Andrographolide	NF-κB	8.3 μM
21	Stachydrine	NF-κB	25 μM
22	Tomatidine	Akt, ERK, NF-κB	25 μM
23	PS-1145	IKK	0.1 μM
24	BMS-345541	IKK	0.9 μM
25	Fenofibrate	Autophagy, PPAR Cytochrome P450	2.8 μM
26	TPCA-1	IKK	0.1 μM
27	Benzafibrate	PPAR	8.3 μM
28	ACHP (Hydrochloride)	IKK	8.3 μM
29	BAY 11-7082	Autophagy, Deubiquitinase, NF-κB	8.3 μM
30	Bardoxolone (methyl)	Autophagy, Keap1-Nrf2	0.9 μM
31	IMD-0354	IKK	0.3 μM
32	SC-514	IKK	0.9 μM
33	Retinoic acid	PPAR, RAR/RXR	0.9 μM
34	BAY 11-7085	NF-κB	0.3 μM
35	GSK0660	PPAR	8.3 μM
36	GW 501516	Autophagy, PPAR	8.3 μM
37	QNZ	NF-κB	8.3 μM
38	BMS-687453	PPAR	8.3 μM
39	RTA-408	Keap1-Nrf2, NF-κB	0.1 μM
40	GSK583	RIP kinase	0.1 μM
41	Ezetimibe	Autophagy, Keap1-Nrf2	8.3 μM
42	GSK3787	PPAR	8.3 μM
43	DG172 (dihydrochloride)	PPAR	0.9 μM

Table C.1 continued from previous page

Drug	Official name	Target	HNTC
44	Amlexanox	IKK	8.3 μM
45	JSH-23	NF-κB	2.8 μM
46	Resveratrol	Autophagy, IKK	2.8 μM
47	Rosiglitazone	Autophagy, PPAR, TRP Channel	8.3 μM
48	Balaglitazone	PPAR	0.9 μM
49	Clofibrate	PPAR	8.3 μM
50	Daidzein	PPAR	8.3 μM
51	GW0742	PPAR	8.3 μM
52	FH535	PPAR, Wnt, β-catenin	0.9 μM
53	Ciprofibrate	PPAR	8.3 μM
54	Gemfibrozil	PPAR	8.3 μM
55	Curcumin	Autophagy, Keap1-Nrf2	2.8 μM
56	Polydatin	Autophagy, NF-κB	0.3 μM
57	GW9662	PPAR	0.3 μM
58	Elafibranor	PPAR	0.9 μM
59	Necrostatin-1	Autophagy, RIP kinase	0.3 μM
60	Rosiglitazone (maleate)	Autophagy, PPAR	8.3 μM
61	NK-252	Keap1-Nrf2	0.9 μM
62	Lipoic acid	NF-κB	8.3 μM
63	JW74	PPAR, Wnt	2.8 μM
64	Troglitazone	Autophagy, PPAR	8.3 μM